Technical University of Denmark

DTU

Development of supported biomimetic membranes for insertion of aquaporin protein water channels for novel water filtration applications

Hansen, Jesper Søndergaard; Emnéus, Jenny; Hélix-Nielsen, Claus

Publication date:
2011

Document Version
Publisher's PDF, also known as Version of record

[Link back to DTU Orbit](#)

Citation (APA):
Hansen, J. S., Emnéus, J., & Helix Nielsen, C. (2011). *Development of supported biomimetic membranes for insertion of aquaporin protein water channels for novel water filtration applications*. Kgs. Lyngby, Denmark: Technical University of Denmark (DTU).

DTU Library
Technical Information Center of Denmark

DTU Nanotech
Department of Micro- and Nanotechnology

Development of supported biomimetic membranes for insertion of aquaporin protein water channels for novel water filtration applications

PhD Thesis

Jesper Søndergaard Hansen

The Biomedical Microsystems Section
DTU Nanotech
Technical University of Denmark
October 2010

Abstract

Aquaporins represent a class of membrane protein channels found in all living organisms that selectively transport water molecules across biological membranes. The work presented in this thesis was motivated by the conceptual idea of incorporating aquaporin water channels into biomimetic membranes to develop novel water separation technologies. To accomplish this, it is necessary to construct an efficient platform to handle biomimetic membranes. Moreover, general methods are required to reliable and controllable reconstitute membrane proteins into artificially made model membranes. These are the topics of this thesis, and are divided into three main chapters.

Chapter 2 reviews recent advances in the design and construction of biomimetic membrane arrays. Moreover, current and novel strategies for the reconstitution of membrane proteins into biomimetic membranes are reviewed.

Chapter 3 presents the development of biomimetic membrane devices suitable of supporting the establishment of functional biomimetic membrane arrays. Furthermore, scaling up the effective membrane area from rectangular 8×8 arrays (64 membranes) to rectangular 24×24 (576 membranes) or hexagonal 24×27 (648 membranes) is demonstrated in a horizontal chamber design.

Chapter 4 characterizes reconstitution and folding of *E. coli* Aquaporin–Z (AqpZ) and the spinach plasma integral protein 2;1 (SoPIP2;1) aquaporins into model membranes. A central part of this chapter is the development of a method for formation of giant protein vesicles (≥10 μm). This constitutes a new methodology to correctly and functionally reconstitute membrane proteins in controllable amounts into giant vesicles. The method for formation of giant protein vesicles subsequently led to the first functional prototype of an aquaporin-membrane water filtration device.

Resumé

Aquaporiner repræsenterer en klasse af membranproteinkanaler der findes i alle levende organismer, og som selektivt transportere vandmolekyler over biologiske membraner. Arbejdet der præsenteres i denne afhandling var motiveret af den konceptuelle ide at inkorporere aquaporin vandkanaler i biomimetiske membraner med henblik på at udvikle nye vandseparations teknologier. For at opnå dette, er det nødvendigt at konstruere en effektiv platform til at håndtere biomimetiske membraner. Generelle metoder er desuden påkrævet til pålideligt og kontrollerbart at rekonstituere membranproteiner ind i kunstigt fremstillede membraner. Dette er emnerne for denne afhandling, og er inddelt i tre hovedkapitler.

Kapitel 2 opsummerer de seneste fremskridt indenfor design og etablering af biomimetiske membran arrays. Derudover opsummeres aktuelle og nye strategier til inkorporering af membranproteiner i biomimetiske membraner.

Kapitel 3 præsenterer udviklingen af biomimetiske membransystemer, der understøtter etablering af funktionelle biomimetiske membraner i arrays. Desuden demonstreres en opskalering af det effektive membran område fra rektangulære 8×8 arrays (64 membraner) til rektangulære 24×24 (576 membraner) eller heksagonale 24×27 (648 membraner).

Kapitel 4 karakteriserer rekonstituering og foldning af *E. coli* Aquaporin-Z (AqpZ) og spinat plasma integrerende protein 2;1 (SoPIP2; 1) aquaporiner i model membraner. En central del af dette kapitel er udviklingen af en metode til fremstilling af *giant protein vesicles (GPV)*/gigantiske protein vesikler (≥10 µm). Dette udgør en ny metode til korrekt og funktionel inkorporing af membranproteiner i kontrollerbare mængder i GPV. Metoden til fremstilling af GPV har ført til den første funktionelle prototype af en aquaporin-membran vandfiltrerings enhed.

Table of contents

Acknowledgements

My contributions to publications included in this thesis

This PhD thesis contains six scientific publications. I have decided to only present first authored papers and manuscripts. A list of patents and co-authored publications is to be found in the Appendix. Below I have listed the papers in the order they appear in the thesis and beneath each publication or manuscript I state my contributions.

1. Book chapter: Creating Scalable and Addressable Biomimetic Membrane Arrays in Biomedicine. J S Hansen and C H Nielsen. Advances in Biomimetics. INTECH Open Access Publisher. Book series editor: Ivana Lorkovic. (Accepted, 6. October 2010).

- I planned the overall contents, themes and subsection headings. I wrote the book chapter, except for subsection 4. Biomedical application of biomimetic membranes.

2. Book chapter: Strategies for integrating membrane proteins in biomembranes. J S Hansen, I Plasencia, K Pszon-Bartosz. Biomimetic Membranes for Sensor and Separation Applications. Springer Verlag. (Accepted, 1. September 2010).

- I planned the overall contents, themes and subsection headings. I wrote the book chapter, except for subsection 13.2 Reconstitution in vesicles

3. Original paper: Development of an automation technique for the establishment of functional lipid bilayer arrays (2009). J S Hansen, M Perry, J Vogel, T Vissing, C R Hansen, O Geschke, J Emnéus and C H Nielsen. Journal Micromech. Microeng. **19**: 025014 (11pp).

- M Perry and I designed the research, did equal amount of experimental laboratory work and we analyzed the data together. I planned and wrote the paper.

4. Original paper: Large scale biomimetic membrane arrays (2009). J S Hansen, M Perry, J Vogel, J S Groth, T Vissing , M S Larsen, O Geschke, J Emneús, H Bohr & C H Nielsen. Anal Bioanal Chem. **395**: 719–727.

- I designed the horizontal biomimetic membrane chamber, designed the research, carried out the majority of experimental work and did the data analysis. I wrote the paper.

5. Manuscript: Sodium dodecyl sulfate does not unfold membrane reconstituted aquaporins SoPIP2;1 and AqpZ. J S Hansen, A Vararattanavech, I Plasencia, P Greisen Jr, J Bomholt, J Torres, J Emnéus, C H Nielsen. Submitted to Proceedings of the National Academy of Sciences (PNAS), 21. October 2010.

- I designed the research, carried out all experimental work except for protein expression and purification of aquaporins. I analyzed the data and wrote the manuscript.

6. Manuscript: Solvent formation of giant protein vesicles and visualization of membrane protein partitioning. J S Hansen, A Vararattanavech, T Vissing, J Torres, J Emnéus, C H Nielsen. Submitted to Journal of the American Chemical Society (JACS), 23. October 2010.

- I designed the research, carried out all experimental work except for protein expression and purification of aquaporins. I analyzed the data and wrote the manuscript.

List of abbreviations

AFM	Atomic force microscopy	DOPS	1,2-dioleoyl-*sn*glycero-3-phospho-L-serine
α-HL	α-Hemolysin		
Ar/R	Aromatic/arginine	DPhPC	1,2-diphytanoyl-sn-glycero-3-phosphocholine
Aqp	Aquaporin		
AqpZ	Aquaporin-Z from *E. coli*	EDTA	Ethylenediaminetetraacetic acid
Badan	6-bromoacetyl-2-dimethylaminonaphthalene	ETFE	Ethylene tetrafluoroethylene
		FomA	*Fusobacterium nucleatum* outer membrane porin A
BLM	Black lipid membrane		
BPM	Black polymer membranes	gA	Gramicidin A
BR	Bacteriorhodopsin	GLV	Giant lipid vesicles
CD	Circular dichroism	GP	Generalized polarization
CHAPS	3-[(3-cholamidopropyl) dimethylammonio]-1-propanesulfonate	GPCR	G-protein coupled receptor
		GPV	Giant protein vesicles
		GlpF	Glycerol facilitator protein
Chol	Cholesterol	GUV	Giant unilamellar vesicles
CMC	Critical micelle concentration	HR	Halorhodopsin
C12E8	Dodecyl octaethylene glycol ether	HTS	High-throughput screening
		HPLC	High pressure liquid chromatography
COX	Cytochrome c oxidase		
CTAB	Hexadecyltrimethylammonium bromide	IRAS	Infrared absorption spectroscopy
		LB	Luria Broth
DDM	*n*-Dodecyl β-D-maltoside	LDAO	N-lauryl-N,N-dimethylammonium-N-oxide
DGK	Diacylglycerol kinase		
DM	Decylmaltoside	LOC	Laboratory-on-a-chip
DMPC	L-a-1,2-dimyristoyl-phosphatidylcholine	LPR	Lipid–to–protein ratio
		LUV	Large unilamellar vesicles
DOPC	1,2-dioleoyl-sn-glycero-3-phosphocholine	nAchR	Nicotinic acetylcholine receptor
		MD	Molecular dynamics
DOPE	1,2-dioleoyl-*sn*-glycero-3-phosphoethanolamine	mdeg	Millidegrees
		MLV	Multilamellar vesicles

MRE	Mean residual ellipicity	PMMA	Poly(methyl methacrylate)
MWCO	Molecular weight cut-off	μTAS	Micrototal-analysis systems
NBD-PC	1-Oleoyl-2-[6-[(7-nitro-2–1,3-benzoxadiazol-4-yl)amino]hexanoyl]-*sn*glycero-3-phosphocholine	ROI	Region of interest
		SDS	Sodium dodecyl sulfate
		SEB	*Staphylococcus* enterotoxin B
		SEM	Scanning electron microscopy
N/E	Nystatin/ergosterol	SIP	Small basic intrinsic protein
NF	Nanofiltration	SNARE	Soluble N-ethylmaleimide sensitive factor attachment receptor
NIP	NOD26-like intrinsic protein		
NPA	Aspargine-proline-alanine		
OD	Optical density	SoPIP2;1	*Spinacea oleracea* plasma integral protein 2;1
OmpA	Outer membrane porin A		
OmpF	Outer membrane porin F	SPR	Surface plasmon resonance
OG	Octyl-β-D-glycopyranoside	SUV	Small unilamellar vesicles
OTG	Octyl β-D-thioglucopyranoside	TEA	Tetraethylammonium
PAGE	Polyacrylamide gel electrophoresis	TEV	Tobacco etch virus
		TIP	Tonoplast intrinsic protein
PBS	Phosphate buffered saline	TM	Transmembrane
PDB	Protein data base	UF	Ultrafiltration
PDI	Polydispersity index	VDAC	Voltage dependent anion channel
PEG	Polyethylene-glycol		
PIP	Plasma membrane intrinsic protein		

Chapter 1

General introduction

The general project aim was to explore novel ways of creating reproducible and scalable biomimetic membranes and new strategies for incorporating correctly folded and fully functional transmembrane proteins into model membranes. The specific commercial objective is to produce composite biomimetic membranes incorporated with aquaporin water channel proteins for industrial water filtration applications.

This thesis is divided into three main chapters and each chapter comprises two separate publications (e.g. book chapters, original research papers or submitted manuscripts). Chapter 2 gives the project background to the practical work of this thesis. Recent advances in biomimetic membrane design are being reviewed as well as strategies for incorporating membrane proteins into biomimetic membranes. These topics are central to the practical work of this PhD project. The experimental work is presented in chapter 3 and 4. The complete study is ended by an overall conclusion and future perspectives.

This part of the thesis gives a general introduction to the work that was carried out throughout this PhD project. It is intended to provide a framework for the separate experimental sections of this thesis. Since my PhD work was motivated by the concept of incorporating aquaporin water channels into biomimetic membranes to develop a protein based water filtration technology, I will begin by presenting basic properties of aquaporin water channels, followed by brief descriptions of the practical work of this project.

1.1 Aquaporin proteins and the basis of a novel water filtration technology

Water transport across biological membranes is central to a myriad of physiological processes in living cells. Although, water molecules can passively diffuse across biological membranes, certain cells such as red blood cells and proximal tubules of the kidney facilitate rapid and selective water

transport across the membranes which cannot be explained by simple diffusion (Preston *et al.*, 1992). This led to the discovery of aquaporin-1 (Aqp1), acting as a water selective protein channel in red blood cells (Preston *et al.*, 1992). Since then, more than 450 members of the aquaporin family have been identified in Achaea, Eubacteria and Eukaryotes (Sasaki, 2008). In mammals 13 members of the aquaporin family have so far been identified (Aqp0-Aqp12), *E. coli* contains 2 members (AqpZ and glycerol facilitator protein (GlpF)), whereas 35 members have been identified in the plant *Arabidopsis thaliana* (Gonen & Walz, 2006; Johanson *et al.*, 2001). Generally, the aquaporin family distinguishes members into two broad categories based on water selectivity; the aquaporins that exclusively allow water molecules to pass and the aquaglyceroporins which, in addition to water, also facilitate the passage of small solutes such as glycerol, urea, arsenite and carbon dioxide (Heymann & Engel, 1999; Tornroth-Horsefield *et al.*, 2010). In plants the aquaporin members are further divided into four subfamilies based on phylogenetic sequence similarities. The four subfamilies comprise the plasma membrane intrinsic proteins (PIPs), tonoplast intrinsic proteins (TIPs), NOD26-like intrinsic proteins (NIPs) and the small basic intrinsic proteins (SIPs) (Johanson *et al.*, 2001).

Unique for members of the aquaporin family is that they very efficiently facilitate the movement of water molecules through the pore with flux rates of up to around 10^9 water molecules per second per channel (Borgnia *et al.*, 1999; Zeidel *et al.*, 1992), while at the same time strictly preventing the transport of protons (Zeidel *et al.*, 1992). Structural studies combined with molecular dynamics (MD) simulations have gained insight into the function and selectivity of aquaporins. Although, only around 19 to 52% of the amino acid sequence is identical among aquaporin members, the overall secondary structures of aquaporins are remarkably similar (Verkman & Mitra, 2000). Aquaporins reside in the membrane as a tetramer and each of the four monomers comprise a channel that folds from 6 transmenbrane α-helices (helix 1-6) connected through 5 loops (loop A-E) (Fig. 1). Loop B and E form half transmembrane helices that fold into the membrane from opposite sides of the membrane, effectively creating a seventh transmembrane helix. Each of the half transmembrane helices contain the highly conserved aspargine-proline-alanine (NPA)-motif (Fig. 1) (Tornroth-Horsefield *et al.*, 2010).
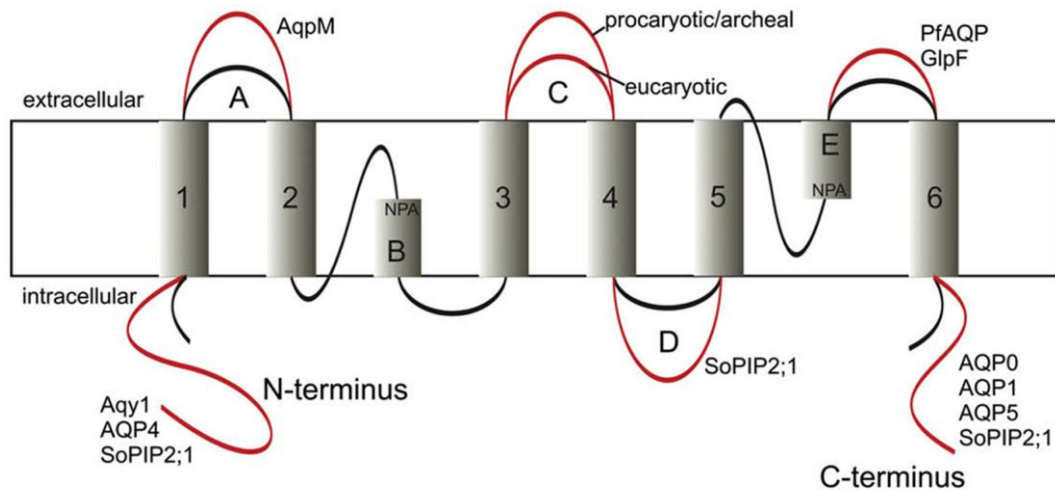
Fig. 1. Topology map of the basic aquaporin fold. Aquaporins consist of 6 transmembrane helices connected through loops. The length of the loops vary among prokaryotic, eukaryotic or plant aquaporin members. The illustration is adapted from (Tornroth-Horsefield *et al.*, 2010).

According to MD simulations, the NPA-motifs are responsible for the ability of aquaporins to allow high rates of water molecules to pass through the channel, whilst excluding protons (Jensen & Mouritsen, 2006; Murata *et al.*, 2000). The proton exclusion mechanism is explained by the Grotthuss mechanism, where a continuous line of water molecules can efficiently transfer protons from one side to the other along the line of water molecules (reviewed in (Cukierman, 2006)). This mechanism is based on hydrogen bonding rearrangements taking place between the proton and the water molecule through the lone pair on oxygen (Fig. 2A). The Grotthuss mechanism of proton transport is prevented in aquaporins by virtue of the conserved NPA-motifs. In aquaporins the two aspargine residues of each NPA-motif form hydrogen bonds with the oxygen lone pairs of the water molecules as they pass through this site of the water channel (Murata *et al.*, 2000) (Fig. 2B). This orchestrates the orientation of the water molecules in such a way that protons are excluded from passage through the aquaporin channel while at the same time having a concerted movement of water molecules through the channel (Murata *et al.*, 2000).

The aromatic/arginine (Ar/R) region is a second conserved aquaporin constriction site that has been identified to be responsible for aquaporin water selectivity. This constriction region forms the narrowest part of the channel and is located just above the NPA-motif to the extracellular side of the channel. Tuning of the pore selectivity is achieved by differences in the residues of the Ar/R region among the aquaporin family members, causing the constriction region to vary in diameter and hydrophobicity (Hub & de Groot, 2008). The Ar/R region is therefore believed to confer water

selectivity to aquaporins by virtue of being both a hydrophobicity filter and a size exclusion filter (Hub & de Groot, 2008). In aquaglyceroporins the Ar/R region is wider and more hydrophobic compared to the corresponding Ar/R region of aquaporins. This allows, as opposed to aquaporins, permeation of small solutes such as glycerol, carbon dioxide, ammonia and oxygen through the aquaglyceroporin channels (Hub & de Groot, 2008).
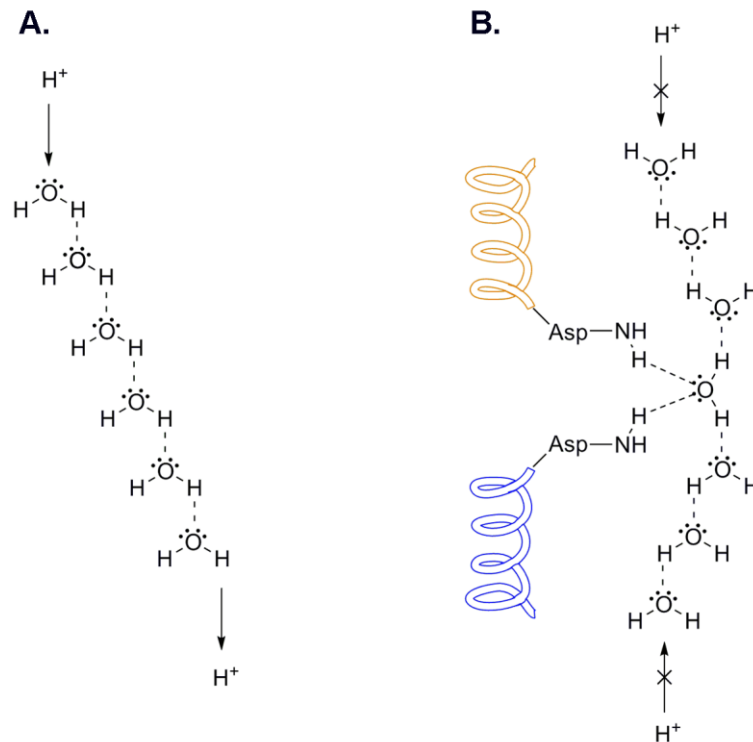
Fig. 2. The Grotthuss mechanism and the suggested proton exclusion mechanism of aquaporins. A) Shows the Grotthuss mechanism for proton transport along a water wire. B) Shows how the two aspargines of the NPA-motif of the two half helices in the aquaporin structure form hydrogen bonds to the central water molecule, thereby preventing proton transport along the line of water molecules in the channel. This allows passage of water molecules through the channel while simultaneously preventing proton transport. Illustration (B) was inspired by (Gonen & Walz, 2006).

Clearly, structural and functional studies of aquaporins have provided increased scientific understanding of water regulation in physiology. Besides the interesting aspects of studying the nature of aquaporins, the high water selectivity and rapid turn-over of water molecules per se of aquaporins, has also inspired the suggestion that aquaporins may be applied for industrial water filtration applications (Kumar *et al.*, 2007; Nielsen, 2009). The basis for this does not solely rely on

the functional aspects of aquaporins, but also on the properties of the biological membranes wherein membrane proteins naturally reside. While the biological membrane is permeable to neutral gasses and to some extent water molecules, the diffusion of electrolytes, such as monovalent and divalent ions, across the biological membrane is negligible (Nielsen, 2010). The water flux and selectivity of aquaporins combined with the natural barrier properties of biological membranes makes the concept of using aquaporins in a water purification technology feasible (Nielsen, 2009; Nielsen, 2010).

In any case, *in situ* studies of aquaporin or implementation of aquaporins in a water purification technology require aquaporin proteins to be embedded into a matrix that sufficiently mimic the biological membrane environment.

1.2 Biomimetic membranes

Artificially made membranes that mimic the naturally occurring properties of biological membranes (e.g. barrier properties) have been coined biomimetic membranes (Martin, 2007). In order to create a biomimetic membrane-based technology (e.g. aquaporin purification technology), it is necessary to construct an efficient platform to handle biomimetic membranes. Prerequisite for an aquaporin-membrane water filtration technology is that the effective membrane area can be scaled up sufficiently. However, while creation of a single biomimetic membrane across a Teflon aperture (typically sub-millimetre in diameter) is a well-established technique, the creation of biomimetic membranes in arrays is not straightforward (discussed further in chapter 2 of this thesis).

The initial practical work of this PhD project focused on creating a biomimetic membrane design for establishing biomimetic membranes in arrays. A comprehensive study of critical parameters for reproducibly creating arrays of biomimetic membranes, such as chamber design, aperture scaffold geometries and membrane-scaffold interactions, led to the development of a vertical chamber design that supported simultaneous establishment of 8×8 membranes in arrays. The membrane formation strategy comprises a novel membrane formation technique, which we termed the automation technique for the establishment of membrane arrays. Electrophysiological recordings across the membrane demonstrated that functional membrane arrays could be successfully created in this design. The detailed description of the development of the automation technique for the establishment of biomimetic membranes in arrays is given in chapter 3.1 comprising the original paper "Development of an automation technique for the establishment of functional lipid bilayer arrays".

To complement our electrophysiological data obtained from vertically positioned membranes, we designed a horizontal chamber design practical for visual inspection of established membranes. With this chamber design we demonstrated that the effective membrane area could conveniently be scaled up from 8×8 membrane arrays to 24×24 (576 apertures) rectangular and 24×27 (648 apertures) hexagonal membrane arrays with averaged diameters of 300 μm (Fig. 3).
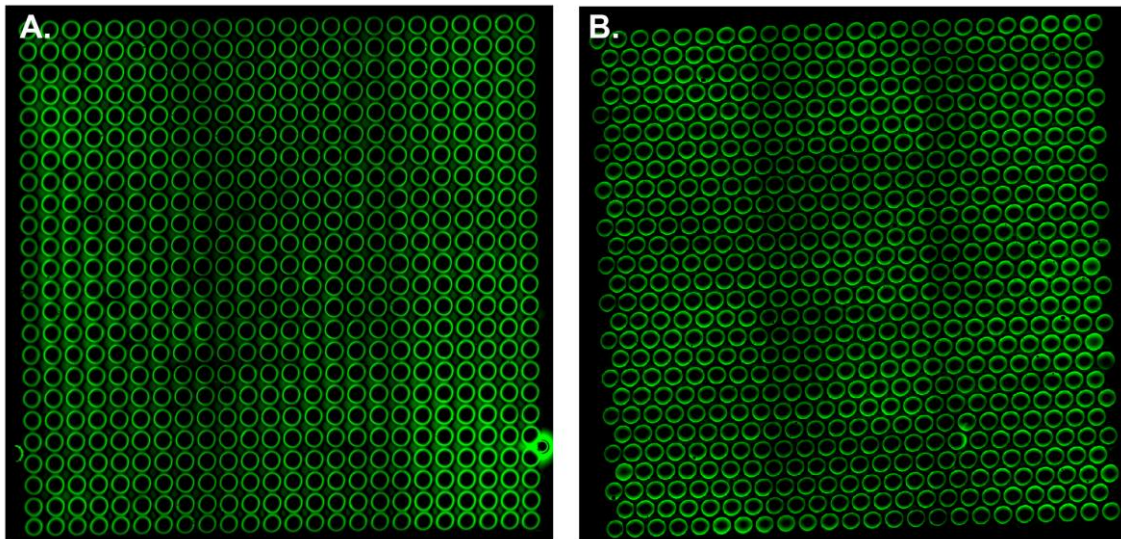
Fig. 3. Biomimetic membrane arrays created in a horizontal biomimetic membrane chamber design. A) Shows a 24×24 rectangular membrane array. B) Shows a 24×27 hexagonal membrane array with averaged aperture diameters of 300 μm. Lipid bilayers were doped with a green fluorescent dye (NBD-PC). See (Hansen *et al.*, 2009) for further details (chapter 3.2).

Scaling up the membrane area unexpectedly also led to increased membrane lifetimes with membranes lasting around 16 h in comparison to an average lifetime of 1 h for the 8×8 membrane arrays. The original paper "Large scale biomimetic membrane arrays" is enclosed as chapter 3.2, which describes the development of the horizontal optical–electrical chamber design and subsequent characterization of biomimetic membranes established in this design.

1.3 Fluorescent assay of transmembrane hydrophobic interactions of aquaporins

While functional insertion of ion channels into biomimetic membranes is relatively easy detectable using standard voltage-clamp electrophysiological methods (Martin, 2007; Nielsen, 2010), measurements of aquaporin incorporations are less straightforward since only water molecules passes through the channel pores. Although, voltage-clamp measurements can be applied to confirm

overall membrane integrity upon aquaporin reconstitution into planar membranes, other techniques are required to address the insertion of aquaporins. It would be advantageous to create an assay that could be applied to characterize aquaporin incorporation into biomimetic membranes; one which preferably could tell something about the reconstituted state of the protein.

Fluorescent probes that are environmentally sensitive to their location and solvent surroundings are useful for creating sensitive protein folding and enzyme activity assays (Hansen *et al.*, 2006; Heuck & Johnson, 2002; Johnson, 2005; Valeva *et al.*, 2008). The fluorescent thiol-reactive probe 6-bromoacetyl-2-dimethylaminonaphthalene (Badan) has fluorescence emission peak and intensity that are particularly sensitive to polarity changes in the environment around the probe (Hansen *et al.*, 2006). Besides the polarity sensitivity of Badan, the probe when conjugated to a thiol (under substitution of bromide) has a molecular size comparable to a tryptophan residue (Fig. 4). This reduces the likelihood, that probe conjugation will affect protein structure or function (Hansen *et al.*, 2008).
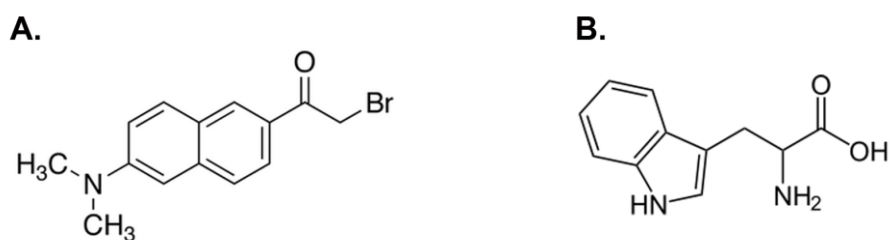
Fig. 4. Molecular structures of the fluorescent dye Badan and tryptophan. A) The structure of Badan. B) The structure of tryptophan. When Badan is conjugated to a thiol it has a molecular size comparable to a tryptophan residue.

On the basis of the crystal structures of aquaporins, we found that several aquaporins contain surface accessible cysteines being strategically positioned in the protein transmembrane (TM) region. Badan conjugation reaction experiments with aquaporins led to the successful development of fluorescently labelled aquaporin SoPIP2;1 and later also a fluorescent version of the *E. coli* AqpZ. This mean that besides being able to carry out electrophysiological measurements across established biomimetic membranes, we also have the possibility to visualize aquaporins reconstituted into artificially made membranes.

Fluorescent spectroscopy measurements of the fluorescently labelled aquaporins in the presence of sodium dodecyl sulfate (SDS) demonstrated that the conjugated Badan group of each protein (Badan-SoPIP2;1 and Badan-AqpZ) was very sensitive to changes in the polarity of the

environment around the probe. This meant that we, by virtue of measuring Badan polarity, could characterize hydrophobic interactions of SDS with the aquaporin TM regions. To explore the relationship between Badan-aquaporin fluorescence spectra and aquaporin secondary structure in the presence of SDS, series of measurements using circular dichroism spectroscopy were carried out in combination with fluorescence spectroscopy measurements. The outcome of this work is presented in chapter 4.1 in the manuscript "Sodium dodecyl sulfate does not unfold membrane reconstituted aquaporins SoPIP2;1 and AqpZ".

1.4 Giant protein vesicles

Exploring novel strategies for controllable and reliable reconstitution of membrane proteins into artificially made membranes resulted in the development of a method to create giant protein vesicles (GPV). Although, giant unilamellar vesicles (≥10 µm) may be visualized directly by microscope techniques and have been extensively applied to study biophysical membrane phase properties and spatial lipid distributions of mixed lipid bilayers (Bagatolli & Gratton, 2000; de Almeida *et al.*, 2007; Fidorra *et al.*, 2006; Fidorra *et al.*, 2009a; Fidorra, Heimburg & Bagatolli, 2009b; Kahya *et al.*, 2004), assembly procedures of giant unilamellar vesicles preclude protein reconstitution (Kahya *et al.*, 2001).

With Badan labelled aquaporins reconstituted into GPV, a visual assay for characterizing hydrophobic interactions with protein TM regions measured by Badan fluorescence polarity was established. Membrane protein functionality was also demonstrated in these GPV using the membrane protein Bacteriorhodopsin, a light–activated proton–pump. The work with establishing the GPV formation method and visual assay for aquaporin hydrophobic interactions using Badan is presented in chapter 4.2 in the manuscript "Solvent formation of giant protein vesicles and visualization of membrane protein partitioning".

1.5 The aquaporin-membrane forward osmosis prototype

The advantages of the GPV formation method are, among others, that GPV can be formed in high densities and the amount of protein incorporated into the GPV can be controlled. The high densities of which GPV could be formed led to the speculation whether the density of GPV was sufficient to constitute a bulk liquid membrane that could be used for separation applications (Fig. 5A). The definition of a bulk liquid membrane is a bulk organic, water-immiscible liquid phase that can act as

a semi-permeable phase separator between an aqueous feed solution and a receiving aqueous solution (Kislik, 2010). The phases may be separated by microporous supports (Kislik, 2010).

In our case, aquaporin GPV would constitute the bulk organic, water-immiscible liquid phase which in principle should be permeable only to water molecules due to the function of aquaporins combined with the barrier properties of biomimetic membranes. Separation of water with a bulk liquid membrane may be achieved by forward osmosis, where the driving force is an osmotic pressure difference between a receiving solution of high osmolarity relative to the feed solution (Kislik, 2010).

In a proof-of-concept study we redesigned the horizontal chamber design presented in chapter 3.2 into a closed chamber design where the aquaporin GPV (bulk liquid membrane) would be encapsulated between a top chamber and a bottom chamber by microporous or nanoporous commercially available filtration membranes (e.g. ultrafiltration (UF) or nanofiltration (NF) membranes). The chamber design is shown in Fig. 5B. In this design, the net movement of water from the feed (tap water) across the aquaporin-membranes to the bottom receiving chamber (10% NaCl) could be measured by reading the water level in a water column connected to the bottom receiving chamber (Fig. 5B).

Fig. 5C shows the very first aquaporin-membrane forward osmosis experiments, demonstrating that it was indeed possible to obtain a net water transport across SoPIP2;1 GPV encapsulated with two NF commercial filter membranes (NF/NF) and also with an UF membrane to the feed side and a NF membrane to the receiving solution side (UF/NF). In contrast, we observed no detectable water transport using giant lipid vesicles (GLV) (Fig. 5C).
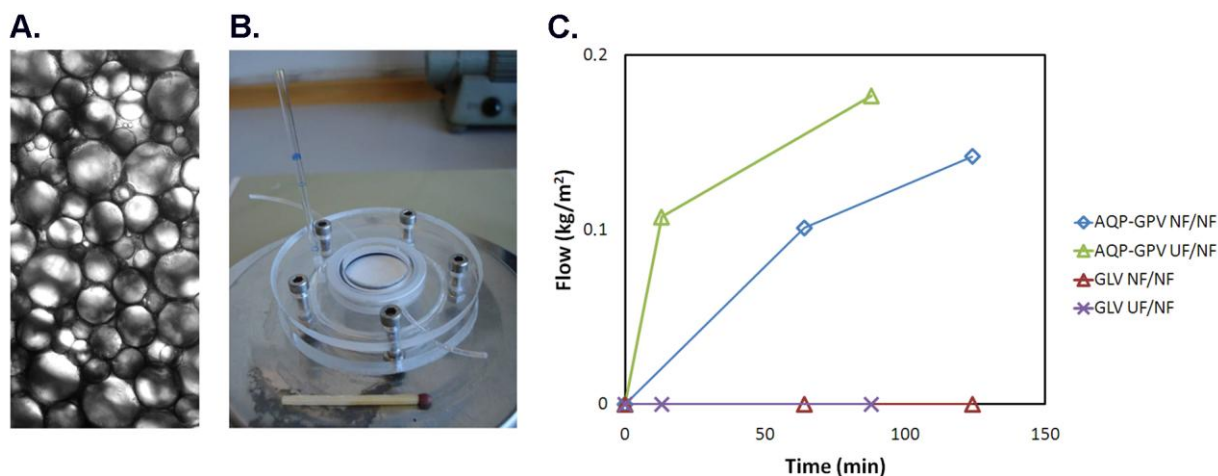
Fig. 5. Forward osmosis based on aquaporin-membranes. A) SoPIP2;1 GPV made from DOPC and squalene. B) The designed forward osmosis chamber design. C) Results of forward osmosis experiments across SoPIP2;1 GPV (bulk liquid membrane). GLV refers to giant lipid vesicles (control vesicles). See text for details.

Although, I was involved in the early work with forward osmosis across aquaporin bulk liquid membranes, it was eventually handed over to other researchers in Aquaporin A/S dedicated to carry out materials testing and design optimization. For my part, I continued aquaporin protein reconstitution characterization and working with protein formulations of GPV. Therefore, besides the general introduction, bulk liquid membranes will not be dealt with further in this thesis. The description of aquaporin bulk liquid membranes is meant to place my practical work during my PhD project into the context of the overall objective of producing composite biomimetic membranes incorporated with aquaporin water channel proteins for industrial water filtration applications.

References

Bagatolli, L.A. & Gratton, E. (2000): Two photon fluorescence microscopy of coexisting lipid domains in giant unilamellar vesicles of binary phospholipid mixtures *Biophys J* 78(1): 290-305.

Borgnia, M.J., Kozono, D., Calamita, G., Maloney, P.C. & Agre, P. (1999): Functional reconstitution and characterization of AqpZ, the E. coli water channel protein *J Mol Biol* 291(5): 1169-79.

Cukierman, S. (2006): Et tu, Grotthuss! and other unfinished stories *Biochimica et Biophysica Acta (BBA) - Bioenergetics* 1757(8): 876-885.

de Almeida, R.F., Borst, J., Fedorov, A., Prieto, M. & Visser, A.J. (2007): Complexity of lipid domains and rafts in giant unilamellar vesicles revealed by combining imaging and microscopic and macroscopic time-resolved fluorescence *Biophys J* 93(2): 539-53.

Fidorra, M., Duelund, L., Leidy, C., Simonsen, A.C. & Bagatolli, L.A. (2006): Absence of fluid-ordered/fluid-disordered phase coexistence in ceramide/POPC mixtures containing cholesterol *Biophys J* 90(12): 4437-51.

Fidorra, M., Garcia, A., Ipsen, J.H., Hartel, S. & Bagatolli, L.A. (2009a): Lipid domains in giant unilamellar vesicles and their correspondence with equilibrium thermodynamic phases: a quantitative fluorescence microscopy imaging approach *Biochim Biophys Acta* 1788(10): 2142-9.

Fidorra, M., Heimburg, T. & Bagatolli, L.A. (2009b): Direct visualization of the lateral structure of porcine brain cerebrosides/POPC mixtures in presence and absence of cholesterol *Biophys J* 97(1): 142-54.

Gonen, T. & Walz, T. (2006): The structure of aquaporins *Q Rev Biophys* 39(4): 361-96.

Hansen, J.S., Faergeman, N.J., Kragelund, B.B. & Knudsen, J. (2008): Acyl-CoA-binding protein (ACBP) localizes to the endoplasmic reticulum and Golgi in a ligand-dependent manner in mammalian cells *Biochem J* 410(3): 463-72.

Hansen, J.S., Perry, M., Vogel, J., Groth, J.S., Vissing, T., Larsen, M.S., Geschke, O., Emneus, J., Bohr, H. & Nielsen, C.H. (2009): Large scale biomimetic membrane arrays *Anal Bioanal Chem* 395(3): 719-27.

Hansen, J.S., Villadsen, J.K., Gaster, M., Faergeman, N.J. & Knudsen, J. (2006): Micro method for determination of nonesterified fatty acid in whole blood obtained by fingertip puncture *Anal Biochem* 355(1): 29-38.

Heuck, A.P. & Johnson, A.E. (2002): Pore-forming protein structure analysis in membranes using multiple independent fluorescence techniques *Cell Biochem Biophys* 36(1): 89-101.

Heymann, J.B. & Engel, A. (1999): Aquaporins: Phylogeny, Structure, and Physiology of Water Channels *News Physiol Sci* 14: 187-193.

Hub, J.S. & de Groot, B.L. (2008): Mechanism of selectivity in aquaporins and aquaglyceroporins *Proc Natl Acad Sci U S A* 105(4): 1198-203.

Jensen, M.O. & Mouritsen, O.G. (2006): Single-channel water permeabilities of Escherichia coli aquaporins AqpZ and GlpF *Biophys J* 90(7): 2270-84.

Johanson, U., Karlsson, M., Johansson, I., Gustavsson, S., Sjovall, S., Fraysse, L., Weig, A.R. & Kjellbom, P. (2001): The Complete Set of Genes Encoding Major Intrinsic Proteins in Arabidopsis Provides a Framework for a New Nomenclature for Major Intrinsic Proteins in Plants *Plant Physiol.* 126(4): 1358-1369.

Johnson, A.E. (2005): Fluorescence approaches for determining protein conformations, interactions and mechanisms at membranes *Traffic* 6(12): 1078-92.

Kahya, N., Pecheur, E.I., de Boeij, W.P., Wiersma, D.A. & Hoekstra, D. (2001): Reconstitution of membrane proteins into giant unilamellar vesicles via peptide-induced fusion *Biophys J* 81(3): 1464-74.

Kahya, N., Scherfeld, D., Bacia, K. & Schwille, P. (2004): Lipid domain formation and dynamics in giant unilamellar vesicles explored by fluorescence correlation spectroscopy *J Struct Biol* 147(1): 77-89.

Kislik, V.S. (2010): *Liquid Membranes - Principles and Applications in Chemical Separations and Wastewater Treatment*, 1 edition. Elsevier.

Kumar, M., Grzelakowski, M., Zilles, J., Clark, M. & Meier, W. (2007): Highly permeable polymeric membranes based on the incorporation of the functional water channel protein Aquaporin Z *Proc Natl Acad Sci U S A* 104(52): 20719-24.

Martin, D.K. (2007): *Nanobiotechnology of Biomimetic Membranes*. Springer

Murata, K., Mitsuoka, K., Hirai, T., Walz, T., Agre, P., Heymann, J.B., Engel, A. & Fujiyoshi, Y. (2000): Structural determinants of water permeation through aquaporin-1 *Nature* 407(6804): 599-605.

Nielsen, C.H. (2009): Biomimetic membranes for sensor and separation applications *Anal Bioanal Chem* 395(3): 697-718.

Nielsen, C.H. (2010): Major intrinsic proteins in biomimetic membranes *Adv Exp Med Biol* 679: 127-42.

Preston, G.M., Carroll, T.P., Guggino, W.B. & Agre, P. (1992): Appearance of water channels in Xenopus oocytes expressing red cell CHIP28 protein *Science* 256(5055): 385-7.

Sasaki, S. (2008): Introduction for Special issue for Aquaporin *Pflügers Archiv European Journal of Physiology* 456(4): 647-649.

Tornroth-Horsefield, S., Hedfalk, K., Fischer, G., Lindkvist-Petersson, K. & Neutze, R. (2010): Structural insights into eukaryotic aquaporin regulation *FEBS Lett* 584(12): 2580-8.

Valeva, A., Siegel, I., Wylenzek, M., Wassenaar, T.M., Weis, S., Heinz, N., Schmitt, R., Fischer, C., Reinartz, R., Bhakdi, S. & Walev, I. (2008): Putative identification of an amphipathic alpha-helical sequence in hemolysin of Escherichia coli (HlyA) involved in transmembrane pore formation *Biol Chem* 389(9): 1201-7.

Verkman, A.S. & Mitra, A.K. (2000): Structure and function of aquaporin water channels *Am J Physiol Renal Physiol* 278(1): F13-28.

Zeidel, M.L., Ambudkar, S.V., Smith, B.L. & Agre, P. (1992): Reconstitution of functional water channels in liposomes containing purified red cell CHIP28 protein *Biochemistry* 31(33): 7436-40.

Chapter 2

Introduction to biomimetic membrane arrays and strategies for incorporation of membrane proteins

Contents

2.1 Creating scalable and addressable biomimetic membrane arrays in biomedicine

Chapter Number

Creating scalable and addressable biomimetic membrane arrays in biomedicine

Jesper Søndergaard Hansen & Claus Hélix Nielsen
Technical University of Denmark and Aquaporin A/S
Denmark

1. Introduction

Biomimetic membrane arrays that mimic biological cell membranes, with the ability to support membrane protein or peptide reconstitutions, are increasingly being recognised as an important platform for biomedical applications. High-throughput screening (HTS) systems based on membrane arrays may become an important alternative to cell-based screening of potential drug candidates on membrane protein targets (Fang *et al.*, 2006). The advantages of such membrane arrays are the ability to address specific drug-on-target interactions and to identify potential unintended effects on cell membrane properties or interactions with secondary unwanted proteins. The transport properties of channel proteins or peptides may also be utilized in novel sensor based platforms such as stochastic sensors for detection of organic molecules in solutions for use in medicine or environmental monitoring (Ashkenasy *et al.*, 2005; Capone *et al.*, 2007; Gu *et al.*, 1999; Nikolelis & Siontorou, 1996).

Provided that the effective membrane area can be scaled sufficiently, protein channel-based membrane arrays may be applied in larger scale biomedical applications. An example is aquaporins, which are water selective proteins that function to filter water, for example in the mammalian kidney. Aquaporin-based large scale biomembranes may be envisaged as the new generation hemodialysis systems for kidney patients, or be applied in general water purification systems.

Biomimetic membrane peptide or protein based arrays are however not currently applied in commercial biomedical or biotechnological applications. While creation of a single lipid bilayer membrane across a Teflon aperture is a well-established technique, the creation of biomembrane arrays comprises a relatively new concept in the scientific field of biomimetics. The reasons are amongst others associated with the inherent difficulties of reproducible creating planar suspended membranes and a generally low stability of established biomembranes. Moreover, amongst the general challenges in biomimetic membrane design is scale up of membrane effective areas to create stable and addressable membrane arrays with long lifetimes (> days).

This chapter will give an overview of recent advances in the development of planar biomimetic membrane arrays, and will discuss strategies and general challenges for creating stable and scalable biomembranes for use in biomedical applications.

2. Biomimetic membrane design

Current planar membrane designs include vertical and horizontal positioned arrays in a chamber or device, which typically relies on membrane arrays being established either by manual, robotics or microfluidic techniques. The choice of design may depend on the nature of the membrane molecule to be incorporated (peptide or protein) and the biomedical application in question.

2.1 Membrane array scaffolds

The fabrication method as well as membrane array geometries are important parameters to consider when designing chambers and devices for sensor and separation applications based on biomimetic membrane arrays.

Membrane proteins function among others to facilitate passive-mediated or active transport of small molecules and substances across the membrane, or function as receptors mediating intracellular signal transduction pathways upon extracellular ligand binding to the receptor. To utilize membrane protein function in model membrane designs, suspended membranes may be created that allow for transport processes to take place across the artificially made membranes. A membrane scaffold supporting planar suspended membrane array formations is illustrated in Fig. 1A.

To create medical screening platforms or microarray assays, the multi aperture scaffold may further be embedded in a polymer-matrix to create individually well-defined wells as is known from microtiter plates or immobilized soluble protein dot-blot microarrays. The design illustrated in Fig. 1B shows a composite half-sandwich scaffold design with well-defined wells. The matrix may be designed to be porous to maintain ion and solute diffusion across the established membranes. This is necessary if electrophysiological measurements of receptor or protein channel properties are included in the design as a read-out parameter.

To support applications that depend on applying a hydrostatic or an osmotic pressure across the membrane, separation applications based on protein channel properties require that the established biomimetic membrane arrays are stabilized by a complete sandwich composite structure (Fig. 1C). As illustrated in Fig. 1, the membrane array scaffold can be created as a modular design based on the actual aperture scaffold and from this design multi composite/encapsulated scaffolds may be created depending on the design criteria.

Fig 1. Biomimetic membrane array designs using micro-structured ethylene tetrafluoroethylene (ETFE) as scaffold. A) ETFE membrane scaffold for freely suspended planar membrane arrays. B) Composite half-sandwich membrane scaffold consisting of an ETFE partition partly embedded in a porous support structure to create individually well-defined wells (grey). C) Complete composite scaffold sandwich structure. Shown in the illustrations are the ETFE membrane scaffold (green), surface modifications of the ETFE scaffold (yellow), biomimetic membranes (red), proteins (white), aqueous layers or hydrogel polymers (transparent) and porous supportive structures (grey).

Single aperture partitions can be created by various mechanical methods such as micro drilling, needle puncturing (Ginsburg & Noble, 1974), heated wire (Benz *et al.*, 1975; Montal & Mueller, 1972; Wonderlin, Finkel & French, 1990) or electrical sparks (Minami *et al.*, 1991). However, common for these methods are that they are generally not suitable for fabricating scaffolds comprising an array of apertures. The reasons are that these methods cannot produce consistent aperture sizes and position the produced apertures closely and precisely, and moreover these techniques have tendencies to create groin and burr edges that do not support stable membrane formations.

Methods described suitable for the fabrication of membrane scaffold arrays include hot embossing of silicon wafers (Heyderman *et al.*, 2003), lithography techniques (Le Pioufle *et al.*, 2008; Mayer *et al.*, 2003; Suzuki, Le Pioufle & Takeuchi, 2009), UV excimer laser ablation (O'Shaughnessy *et al.*, 2007; Sandison & Morgan, 2005) and CO_2-laser ablation (Vogel *et al.*, 2009). The ability to produce consistently sized and closely positioned apertures are important parameters to enable successful formation of stable membranes in array. Of the three mentioned techniques for creating highly defined aperture arrays, the CO_2 laser ablation technique is likely the most versatile and cost efficient technique. It has the ability to ablate Teflon films with different thicknesses (micrometers to >1 mm), enable fast scaffold production times (milliseconds-seconds) and support easy scale up. Fig. 2 shows rectangular and hexagonal aperture scaffolds, respectively, micro-structured with the CO_2 laser ablation technique.
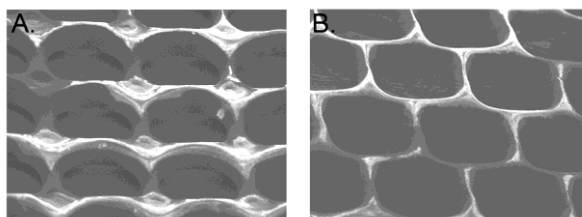
Fig. 2. Scanning electron microscopy images of CO_2 laser fabricated ETFE multi-aperture scaffolds. Images show middle sections of A) Rectangular 8×8 aperture array and B) Hexagonal 8×8 aperture array. EFTE micro structuring was performed as described by Vogel *et al.* (Vogel *et al.*, 2009).

2.2 Chamber designs for membrane array formation

There exist numerous chamber designs to encompass a membrane array scaffold, albeit there are common features relating to the strategy of membrane formation. Fig. 3 schematically illustrates some of the chamber design strategies recently developed in our laboratory, and we will discuss current trends and common features in chamber designs from these examples.

The vertical chamber design strategy (Fig. 3A, D) is a classical chamber design approach originally described for painting or folding a lipid bilayer across a Teflon partition aperture (Montal & Mueller, 1972; Mueller & Rudin, 1969). This design provides easy access to the chambers via wells from the top of the chamber and to each side of the established membranes. This allows for addition of solutes (e.g. creation of osmotic gradients), substances (e.g. ligands), transmembrane peptides, membrane proteins, liposomes or proteoliposomes close to established membranes. At the same time it allows for sample collecting via the accessible top chamber wells. In this manner, the vertical chamber design has, among others, been applied to characterize vesicle fusion events with planar artificially made membranes (Kendall & MacDonald, 1982; Perin & MacDonald, 1989; Woodbury & Hall, 1988a; Woodbury & Hall, 1988b; Zimmerberg, Cohen & Finkelstein, 1980b). The hydrophilic dye calcein was used as a traceable marker that was encapsulated into lipid synaptic vesicles and added to one side of the membrane (Zimmerberg, Cohen & Finkelstein, 1980a). Membrane fusion events with the established planar membrane resulted in calcein release to the other side of the membrane, which could subsequently be sampled and the fluorescent calcein content quantified (Zimmerberg *et al.*, 1980a).
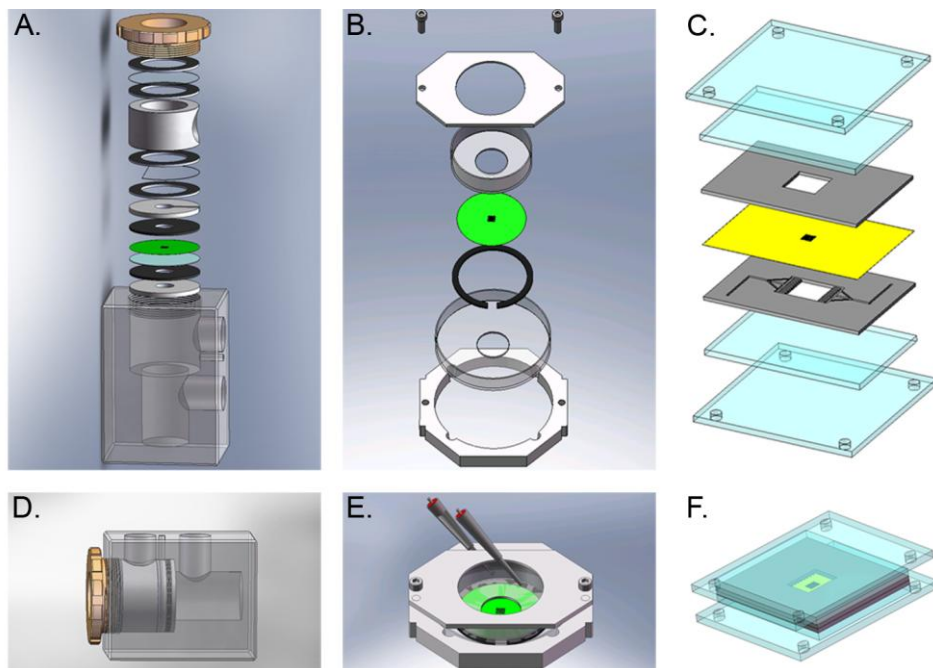
Fig. 3. Chamber designs for creating biomimetic membrane arrays A), D) Automation technique chamber design strategy for establishing vertically oriented membrane arrays (Hansen *et al.*, 2009b). B), E) Horizontal chamber design that supports combined optical–electrical measurements of established biomimetic membranes (Hansen *et al.*, 2009a). C), F) Automated microfluidic chamber design for microfluidic filling and establishment of biomembrane arrays (Kamila Pszon-Bartosz *et al.*, manuscript in submission).

We recently developed a vertical chamber based on the classical design (Fig 3A, D), where the membrane formation strategy was modified to comprise a novel membrane array formation technique; the so called automation technique for the establishment of vertically positioned membrane arrays (Hansen *et al.*, 2009b). Electrophysiological recordings across the membrane demonstrated that functionally membrane arrays were created in this design. Moreover, this technique supported membrane formations of 5×5, 8×8 and 30×21 arrays having average aperture diameters of 300 μm (Hansen *et al.*, 2009b).

In general, the vertical chamber design allows for electrophysiological recordings across the membrane, but the simultaneous visualization of established membranes by surface sensitive techniques such as fluorescence microscopy is not straightforward in this design. Therefore, the current trends in chamber design are directed towards the development of horizontal chambers that fit, or can be adapted, into modern array scanners (Le Pioufle *et al.*, 2008; Suzuki *et al.*, 2009) or fluorescent microscope stages (Hemmler *et al.*, 2005; Wilburn, Wright & Cliffel, 2006). Such designs are typically created to support more than one read-out parameter such as having voltage-clamp read-outs combined with optical imaging.

Membrane array formation in horizontal chambers is typically carried out manually by painting the membrane array across the scaffold or by applying microfluidic techniques to establish fully automated membrane formations. The rationale behind manually painting membranes onto scaffold arrays is that it may be adapted to robotic-based membrane deposition techniques, such as robotic array spotters or printers, or be re-designed to include microfluidic membrane formation techniques.

The chamber fabrication time and the material costs are important parameters to ensure that biomimetic membrane based arrays are made economically feasible for the pharmaceutical industry or creating commercially available medical point-of-care microdevices. Therefore, preferred biomimetic membrane designs comprise single-use chambers or microarray devices that are based on low-cost materials, easy to produce and which are easy and efficient to handle. Our suggestions of how to meet these design criteria are illustrated in Fig 3B-F. Fig 3B, 3E illustrate a single-use chamber design based on clamping membrane scaffold arrays between 35-mm and 50-mm culture dishes, whereas Fig. 3C, 3F show a fully automated and closed microfluidic device based on poly(methyl methacrylate) (PMMA), in which all materials are cut and micro structured by CO_2 laser ablation.

2.3 Considerations of membrane design criteria

Membrane design criteria should preferably be defined on the basis of the biotechnological application in question. A commonly accepted membrane quality criterion is that established membranes should exhibit >1 Giga-Ohm sealing resistance in order to achieve low ion leakage. (Reimhult & Kumar, 2008). This is however a somewhat misleading membrane quality criterion. Ohmic sealing that may be obtained for a given membrane is inversely related to the effective membrane area, meaning that >1 Giga-Ohm seals cannot practically be achieved with large membrane arrays. Instead, for large biomimetic membrane arrays it makes more sense to define membrane quality as membranes having a large effective area as evidenced by a large value for the electrical capacitance and low ionic permeability as evidenced by a low value for the electrical conductance compared to the effective membrane area.

Another important design criterion for biotechnological/pharmacological applications may be peptide or protein reconstitution yield, because this likely depend on the application. Less peptides or proteins are likely needed to create a sensitive screening platform in drug discovery compared to creating a membrane based separation technology. Thus when setting up design criteria, strategies and goals for the peptide or protein reconstitution yield need to be taken into consideration.

Additional design criteria for HTS systems or mass transfer flow applications may include a high perforation level of the membrane scaffold material so that the artificial membrane platform is scalable to meet various requirements for individual technical applications (Hansen *et al.*, 2009b). For example functional membrane units can be arranged in arrays to facilitate rapid screening (e.g. by microplate readers).

Membrane stability is a key parameter to be considered for biomimetic membrane based devices. There is a general consensus that biomimetic membranes should have lifetimes for > 1 day (Reimhult & Kumar, 2008). This will also depend on the application in question and on whether a membrane-based assay relies on the end user to create the membrane arrays as a step in the assay protocol, or if the membranes will be fully assembled in ready-to-use

devices before reaching the end user. In addition, the membranes or precursor membrane solutions should exhibit transportation robustness and be storable for defined time periods. The methodology for membrane formation should be considered during the design of novel biomimetic sensor and separation platforms. This may also relate to cost efficiency and feasibility to enter a competitive market. Membrane formations by robotic spotting techniques is likely more expensive than microfluidic-based membrane formations, but robotic deposition techniques may be designed for an application where the total cost would still allow for a competitive product. Thus biomimetic membrane device fabrication processes and materials costs should be considered as a whole during product development.

3. Formation of functionally stable and scalable membrane arrays

Although, it is straightforward to set up specific design criteria for a given biomimetic based platform technology, there are several inherent challenges of biomimetic membrane formations that tend to make it difficult or challenging to meet defined design criteria in practice. Challenges with poor membrane stability, limited scalability and low membrane formation reproducibility must be solved in order to create a general commercially available biomimetic membrane based platform technology.

3.1 Biomimetic membrane stability

Poor membrane stability is a recognized challenge with artificially made membranes. This is an even more pronounced general challenge when working with arrays of biomimetic membranes. To understand why poor membrane stability is a general challenge, it is necessary to realize the properties and dimensions that apply for artificial biomimetic membranes.

The lipid bilayer is only a few nanometers thick and varies with the acyl chain length from 4-10 nm for natural occurring phospholipid species (Lewis & Engelman, 1983; White & Thompson, 1973). The partition scaffold is typically in the range of 20 to 50 micrometers in thickness, meaning that the aperture scaffold is thousand times thicker than the lipid bilayer. Lipid bilayers established across partition apertures are therefore surrounded by an annulus of thick parent lipid solution to compensate for the dimension differences between scaffold and bilayer thickness (White, 1972) (Fig. 4). Solvents such as alkanes (e.g. *n*-decane) are typically used to precondition the scaffold to membrane formations; so called partition prepainting. It is believed that the solvent of the preconditioning step and/or the solvent present in the lipid bilayer slowly diffuses from the annulus, resulting in membrane destabilization and eventually membrane collapse (Malmstadt, Jeon & Schmidt, 2008).
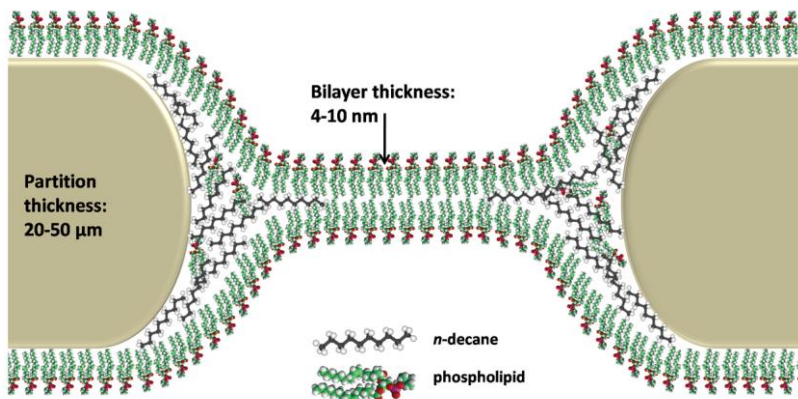
Fig. 4. Schematic illustration of typical dimensions of a lipid bilayer and partition aperture. Typical lipid bilayer thicknesses are 4-10 nanometers (nm), whereas partition thicknesses generally range from 20 to 50 micrometers (μm). The figure is not drawn to scale.

Malmstadt *et al.* showed that membrane stability may be significantly increased (> days) by stabilizing the membrane surroundings by hydrogel encapsulation, which was explained to result from a slowing down of the solvent diffusion out of the annulus, thereby prolonging the membrane lifespan (Malmstadt *et al.*, 2008). This approach is promising and may also be crucial for creating stable and portable devices.

We noticed that the typical partition preconditioning step resulted in inhomogeneous coverage of the preconditioning solution on the partition. Since the membrane stability is dependent on sufficient hydrophobic interactions between the bilayer forming solution and the partition scaffold we speculated that a more homogenous surface pretreatment coverage could result in increased membrane stability (Hansen *et al.*, 2009b). To investigate this, we developed an airbrush technique to homogenously cover the partition with preconditioning solution. This resulted in a markedly increased reproducibility in membrane formation, but did not increase the membrane lifetimes correspondingly (Hansen *et al.*, 2009b).

Ries *et al.* showed that the membrane electrical characteristics, dynamics of membrane formation and the membrane stability are strongly dependent on the partition substrate (Ries *et al.*, 2004). Inspired by this, we studied the effect of covalently modifying the partition substrate using surface plasma polymerization (Perry *et al.*, submitted). By this technique we were able to increase the membrane stability significantly. Using double-sided *n*-hexene partition surface modifications we were able to increase membrane lifetimes from an average of 100 min (Hansen *et al.*, 2009b) to average membrane lifetimes of approx. 70 hours, while 20% of established membranes lasted 140 hours (Perry *et al.*, submitted). These results underline that long term stability of established biomimetic membranes is critically dependent on a sufficient interaction with the hydrophobic surface of the partition and the bilayer forming solution.

Another approach to increase membrane stability has been based on biomimetic membranes consisting of semi-synthetic or synthetic biomimetic polymers. It was recently demonstrated that 8×8 arrays of triblock copolymers could successfully be established by the automation technique for creating biomimetic membrane arrays (Gonzalez-Perez *et al.*, 2009). Membrane

stability could be achieved with lifetimes up to 23 hours. Also cross-linkable lipids have been suggested to being able to increase membrane stability (Benz, Praß & Ringsdorf, 1982; Daly *et al.*, 2006; Shenoy *et al.*, 2005), but more work is needed to show if this strategy may sufficiently increase membrane lifetimes.

Besides the membrane annulus and the biomimetic membrane composition, the aperture diameter is also a crucial determining factor for membrane stability. The membrane stability generally increases with decreasing aperture diameters. This has motivated designs based on nano-sized biomimetic membrane arrays (Han *et al.*, 2007; Hemmler *et al.*, 2005; Studer & Tiefenauer, 2007). The nano-sized aperture diameters should in principle favour long lived membranes, but they may also increase the risk of creating non-functional membranes, because the nanoscale aperture diameter may preclude sufficient membrane thinning.

An impressive silicone nitride chip array comprising 960,000 nano-membranes has been developed (Han *et al.*, 2007). The membrane lifetimes achieved using this technique was up to 144 hours. These lifetimes are comparable to our best membrane array lifetimes using plasma polymerization as pretreatment. In comparison the total membrane effective area of 0.045 cm² for the previously described 8×8 arrays is about 150 times larger than the total membrane area in the silicon nano-membrane chip array. Practical uses of small nano-sized chip arrays could be in microelectronic devices or novel nanotechnology applications.

While membrane stabilities of > 1 day can be achieved with recent advances in biomimetic membrane research, it is still difficult to create storable and transportable biomimetic membrane devices. However, recent developments in membrane encapsulation strategies suggest that robust portable biomimetic membranes may be created (Jeon, Malmstadt & Schmidt, 2006; Kang *et al.*, 2007; Malmstadt *et al.*, 2008; Oliver *et al.*, 2008; Uto *et al.*, 1994). Efforts are none the less still required to create a general stable and transportable biomimetic membrane design.

3.2 Membrane array scalability

A general biomimetic membrane platform supporting different biotechnological applications would preferably be scalable to meet various application requirements. Fig. 5 illustrates scalability in biomimetic design. Biomimetic membrane scalability is not straightforward, and also represents a new concept in formation of biomimetic membrane arrays. The tendency in biomimetic membrane work has actually been to scale down the designs. The reason is likely related to the inherent membrane instability, but recent advances in membrane stability (as discussed in section 3.1) have led to the acceptance that scaling up the arrays may indeed be practically feasible. In this relation, we recently demonstrated that scaling up from rectangular 8×8 arrays (64 membranes) to rectangular 24×24 (576 membranes) or hexagonal 24×27 (648 membranes) arrays may actually provide an overall higher membrane stability evidenced by significant longer lifetimes (Hansen *et al.*, 2009a).
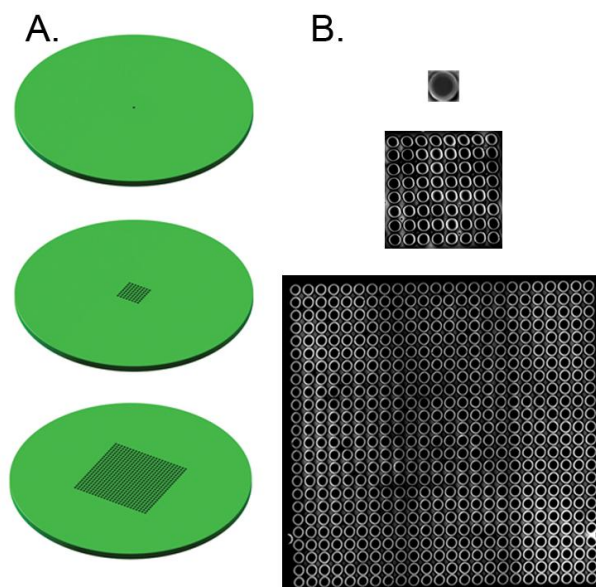
Fig. 5. Illustration of scalability of biomimetic membranes A) Schematic presentation of scalable aperture scaffolds with 300 μm diameter apertures supporting establishment of suspended biomembranes. B) Fluorescent images of established membranes in ETFE microstructured scaffolds corresponding to panel A). Established lipid membranes of 1,2-diphytanoyl-*sn*-glycero-3-phosphocholine were doped with the fluorescent lipid analogue 1-oleoyl-2- [6-[(7-nitro-2-1, 3-benzoxadiazol-4-yl) amino]hexanoyl]-*sn*-glycero-3-phosphocholine (NBD-PC) for visualization. Membranes shown in panel B) were established in the chamber design depicted in Fig. 3B and 3E. The membranes of panel B) are not shown to scale.

An emerging concept, relying on a high degree of membrane scalability, is novel separation technologies based on reconstitution of functional membrane protein channels. A study of the solute transport characteristics and permeability of aquaporin water selective channels incorporated into polymer vesicles indicated that the water permeability and salt rejection of aquaporin based biomimetic membranes would potentially represent a novel separation technology that would be able to exceed current reverse osmosis and forward osmosis membranes in performance (flux and salt-rejection) (Kumar *et al.*, 2007). Novel membrane protein based separation technologies may be explored, provided that the biomimetic membrane effective area can be scaled sufficiently. Extended research activities in biomimetic membrane scalability is therefore required to produce first generation biomimetic membrane based separation technologies.

3.3. Membrane addressability in membrane arrays

Biomimetic membrane arrays offer a platform for generating large membrane protein arrays, where a lot of information can be achieved with extremely low sample volumes

(Suzuki & Takeuchi, 2008). A unique feature of biomimetic membrane arrays is that it offers the opportunity of multiplexed measurements on several levels within the same technology platform.

The trend in biomimetic membrane design is to create chambers that support electrical recordings of membrane, protein or peptide electrical properties combined with fluorescence microscopy. The most straightforward designs include voltage-clamp measurements of an entire array to ensure that functional membranes are established (Hansen *et al.*, 2009a; Hemmler *et al.*, 2005; Wilburn *et al.*, 2006). In principle the electrical voltage clamp recordings could be adapted to individually address the membrane electrical properties of a membrane array. The concept of multiplexed electrical recordings was explored in a proof-of-concept study by Suzuki *et al.*, demonstrating that each well of a 96-wells microplate format could be electrically addressed (Suzuki *et al.*, 2009). Each well of the 96-wells plate however comprised a membrane array of 3×3 membranes, and individually membrane addressability was not addressed in this study, but would in principle be achievable in the presented design.

A solution to enable individual addressability of membranes of a biomimetic membrane array could be achieved by creating a microelectrode array that would be positioned beneath the membrane scaffold. A microelectrode array has been successfully created for electrochemical detection of soluble enzyme activities (Lin *et al.*, 2008). Although the microelectrode array was demonstrated using immobilized soluble proteins, there is no principal hindrance in adapting this concept to biomimetic membrane array designs. Fig. 6 schematically illustrates how such microelectrode arrays may be envisaged to be adapted in biomimetic membrane designs in order to create individually addressable membranes.

Electrical membrane array multiplexing using microelectrode arrays combined with *in situ* fluorescence assays would offer results read-out on two levels. The latter has been demonstrated on solid supported protein immobilized G-protein coupled receptor (GPCR) microarrays, where receptor-ligand interactions could be detected using fluorescently-labelled ligands (Fang, Frutos & Lahiri, 2002; Fang, Lahiri & Picard, 2003).

A third level of biomimetic membrane readouts could be created by detection of small solutes, ions or other substances transported across the membrane facilitated by proteins or peptides reconstituted into the biomimetic membrane arrays. Hemmler *et al.* demonstrated this principle in practice by visualizing transport of the aqueous calcein fluorescent dye across individual membranes reconstituted with α-hemolysin membrane protein pores (Hemmler *et al.*, 2005). Next generation of individually addressable membrane arrays could be envisaged to comprise ligand-receptor assays, where extracellular binding of ligand to receptors would lead to a secondary signaling pathway on the other side that subsequently would lead to a fluorescent or colorimetric signal, which could be quantified. For microfluidic devices the chamber outlets could be connected in line with fluorescence or absorbance detection, or alternatively connected to HPLC instruments for quantifying solutes or molecules. Functional demonstration of such novel conceptual ideas are however still to be proven in practice.
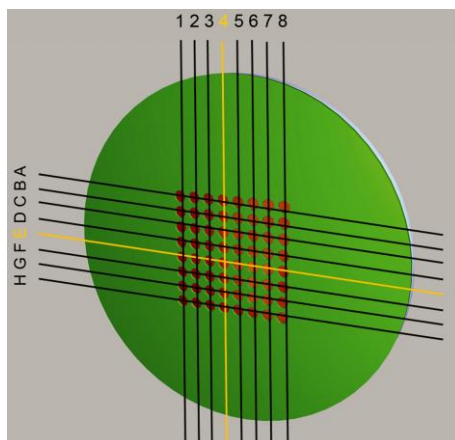
Fig. 6. Schematic illustration of how electrical multiplexing of biomimetic membrane arrays may be designed. Shown are the aperture partition (green), biomimetic membranes (red), electronic grid (black and yellow lines). The yellow lines show the individually addressed membrane of the array (where line E crosses line 4).

To sum up, a lot of information may be achieved with extremely low sample volumes from a single biomimetic membrane array by designing platforms that enable multiple results read-out. Such design strategies may aim at combining microelectrode multiplexing, *in situ* fluorescence assays and quantification of transport processes across the membranes by sample collecting followed by solute determination or concentration measurements.

3.4 Incorporation of membrane peptides and proteins into membrane arrays

Functional incorporation of membrane molecules into biomimetic membranes is essential to create peptide or membrane protein based sensor or separation applications using biomimetic membrane arrays.

Small fusiogenic membrane spanning depsipeptides or peptides generally insert spontaneously into established membranes, and may in many instances be dissolved in aqueous buffers, or other solvents (e.g. alcohols), that can be added directly to established membranes (Zagnoni *et al.*, 2007). The ease of incorporation is one of the main reasons why they are often used to demonstrate that functional biomimetic membranes have been successfully established. In this sense incorporation of small fusiogenic peptides constitute a quality control parameter for functional biomimetic membrane formation. Moreover, some fusiogenic peptides may be relevant in biotechnological and biomedical applications such as for creation of ion-sensing electrodes or biosensors for detection of small solutes and analyte molecules (Borisenko, Zhang & Woolley, 2002; Capone *et al.*, 2007; Frant & Ross, 1970; Nikolelis & Siontorou, 1996; Schar-Zammaretti *et al.*, 2002).

In contrast, medium to large membrane proteins (35-500 kDa), especially α-helical membrane proteins, do generally not readily self-insert into pre-established membranes (Zagnoni *et al.*, 2007). Although, the light-driven α-helical proton-pump bacteriorhodopsin (BR) as well as several *E. coli* outer membrane (β-barrel) porins (e.g. OmpA, OmpF and

FomA) may be reconstituted into planar membranes directly from a detergent solubilized state (Arora *et al.*, 2000; Pocanschi *et al.*, 2006; Schmitt, Vrouenraets & Steinem, 2006), this is general not applicable for most membrane proteins. Therefore, a general reconstitution methodology is required for incorporation of membrane proteins into biomimetic membranes preserving correct protein function (e.g. ensuring correct orientation in the membrane).

Another, largely unresolved challenge is how to reconstitute different proteins into individual membranes to create large membrane protein microarrays, as is known from commercially available DNA microarrays or immobilized protein dot-blot arrays.

4. Biomedical application of biomimetic membranes

The function of a biomimetic membrane array depends not only of successful reconstitution of membrane proteins in stable host lipid/polymer membranes. Also the sensitivity or signal-to-noise ratio in the output-signal of the device must be high in order to allow for detection of analyte concentrations down to the single-molecule level. Thus sufficient amplification of the signal is vital for biomedical application of biomimetic membrane devices. This amplification generally arises as an intrinsic amplification in the biomimetic membrane material per se combined with external amplification.

Due to the relative ease by which pA currents can be resolved many biomimetic membrane based sensor platforms have built on incorporation of ion channels (Nielsen, 2009). The linear gramicidins present a versatile system that can be easily engineered. The preferred conformation of gramicidin in lipid bilayers is a $\beta^{6.3}$ helical fold of the pentadecapeptide. Upon dimerization of two gramicidin monomers from each opposing lipid monolayers an ion conducting dimer permeable to monovalent cations is formed. This system has revealed many basal features of ion channel function, for reviews see (Andersen & Koeppe, 2007; Koeppe & Andersen, 1996). In a free-standing bilayer gramicidin monomers diffuse randomly in each monolayer leaflet and dimerization is a random process. When a transmembrane potential is applied over a membrane separating two aqueous electrolyte compartments dimerization is evident as discrete amplitude changes in the recorded current-trace corresponding to appearance and disappearance of ion conducting dimers.

Sensors based on matrices with engineered gramicidin channels have been presented (Cornell *et al.*, 1997; Wiess-Wichert *et al.*, 1997). These sensors operate by changing the conformational equilibrium between gramicidin monomers and dimers. Concretely the sensors are built with a lower lipid monolayer tethered to an electrode and a mobile upper lipid monolayer where each monolayer leaflet contains engineered gramicidins. The gramicidins in the lower monolayer are covalently tethered to the electrode substrate whereas the upper monolayer gramicidins are covalently linked to specific antibodies moieties which can recognize specific analyte molecules. Another set of antibodies are covalently linked to the upper headgroup of bilayer spanning bolalipids with the lower bolalipid headgroup linked to the electrode substrate. This arrangement effectively anchors the bolalipid-linked antibodies relative to the gramicidin monomer-linked antibodies in the upper monolayer.

If no analyte molecules are present, the conformational equilibrium between monomers and dimers results in a randomly fluctuating current with a mean value effectively dependent on the total gramicidin concentration. When an analyte is present it may cross-link

antibodies attached to the mobile outer layer channels with those attached to membrane spanning bolalipid-based tethers. The result is a decreased mean value of the fluctuating current as the outer monomers now are 'captured' by the analyte mediated crosslinking and therefore not available for dimerization with their immobilized lower monolayer channel partners. The increase in the effective transmembrane resistance (equivalent to a decrease of membrane admittance) with time provides a means to estimate the concentration of the analyte.

Gramicidin channels are low molecular weight peptides and unique in the sense that channel function (i.e. transfer of ions across the membrane) depends on dimerization of two (identical) monomers. In general membrane spanning ion channels are high molecular weight oligomeric structures with large hydrophilic moieties where the oligomeric interactions may depend only on weak interactions. However, recently the voltage-gated HERG potassium channel has been successfully reconstituted in biomimetic membranes tethered on mercury showing that large 'bulky' channel forming oligomeric proteins can be functional in a confined cushion geometry (Becucci *et al.*, 2008).

Ion channel gating (i.e. opening and closing of the ion conducting pathway) is a result of complex conformational changes in the protein. Although our structural understanding of ion channel gating is still limited, sensing devices based on detecting ion channel gating has been proposed. For example the ligand-gated nicotinic acetylcholine receptor (nAchR) ion channel (with acetylcholine as the 'natural' ligand) has been reconstituted in free-standing lipid bilayers (Boheim *et al.*, 1981; Eray *et al.*, 1995) as well as in lipopetide supported biomimetic membranes (Schmidt *et al.*, 1998). Using nAchR modified with two bispecific antibodies the channel remains open until both antibodies bind to the same antigen (Eray *et al.*, 1995).

Also the rectifying voltage gated Kv1.5 potassium channel has been reconstituted in free standing and solid supported membranes (Dhoke *et al.*, 2005; Matsuno *et al.*, 2004). The current/voltage relations display symmetric sigmoidal shapes. This highlights one of the major challenges in biomimetic membrane design based on reconstituted ion channels. The sigmoidal I/V relationship indicates that approximately half of the channels are inserted so they are rectifying the ionic current in one direction and the other half is rectifying currents in the opposite direction. For some application orientational randomness is problematic as membrane proteins generally have distinct intracellular and extracellular binding sites – thus for a sensor based on ligand detection directional control over protein insertion is imperative. However by careful optimization reconstitution procedures a more or less pronounced unidirectionality may be achieved.

The application of gated ion channels in biosensors exemplifies how signal amplification occurs both intrinsically (e.g. the binding of a single ligand gives rise to currents with 10^6 ions/second per channel) and externally though e.g. the I/V conversion and amplification of the current signal in voltage-clamp amplifiers. As we gain more insight into channel gating through more high-resolution structures of ion channel proteins in various conformational states the use of complex ion channel proteins in biomimetic membrane sensors may evolve from an 'all-or-nothing' type of response to more complex read-outs based on detecting ion channel sub-conductance states.

Ion channels represent one important class of biomedical 'targets'. Another important class is comprised of GPCRs. GPCRs generally detect molecules outside the cell and initiate downstream signalling in the form of a cascade of biochemical reactions leading to changes

in cellular function. Since GPCRs are targets for more than 50% of all medicinal drugs there is a huge interest in understanding GPCR mediated signalling. Although the signalling process is generally well-described it is also very complex because it can involve several GPCRs simultaneously and the signalling may also occur by other pathways not requiring G-proteins. Also different ligands can result in different signals from the same GPCR depending on the cell type and *vice versa:* the same ligand can result in different signals in different cells. This complexity presents a major obstacle in our understanding of GPCRs but recently an elegant biosensing method has pointed to a way of overcoming some of the complexities. The sensor is based on coupling ion channels with GPCRs. Thus when the GPCR binds an agonist, its conformation changes, and this changes the structure of the coupled ion channel. (Moreau *et al.*, 2008). The conformational change in the GPCR is thus transduced into a change in ion channel current. In order to make this (and other ion channel based methods) technologically feasible electrical measurements must be integrated with membrane array designs allowing for parallel current recordings.

Another strategy is to take advantage of the electrical properties of bilayers and use them as insulating surfaces. Any defect in this surface is easily detectable as a change in impedance and as the defect locations create strong non-specific binding sites the sensitivity of such a device is high (Steltze, 1993). Impedance analysis on supported lipid bilayers can also be used to dissect the action of channel forming peptides e.g. the bee venom melittin (Becucci *et al.*, 2006a), the potassium specific valinomycin (Becucci *et al.*, 2005), and channel forming proteins e.g. the bacterial outer membrane porin Omp F (Becucci, Moncelli & Guidelli, 2006b) on the bilayer. This approach has also been used in black polymer membranes (BPMs) where protein driven energy transduction was realized by incorporation of cytochrome c oxidase (COX) (Ho *et al.*, 2004).

Light driven transport across membranes constitutes a particular interesting biosensing mechanism behind the design of membranes for energy conversion and advanced photoresponsive/optical devices (LaVan & Cha, 2006). BR and halorhodopsin (HR) are examples of light-driven ion pumps for protons (Oesterhelt & Stoeckenius, 1973) and chloride (and other halide) ions respectively (Essen, 2002; Schobert & Lanyi, 1982). BR occurs natually in highly ordered two-dimensional arrays (purple membranes) in *Halobacterium salinarium* (Oesterhelt & Stoeckenius, 1973). BR may be reconstituted in proteoliposomes (Kayushin & Skulachev, 1974; Oesterhelt & Schuhmann, 1974) but direct adsorption of purple membrane fractions onto suitable substrates takes direct advantage of the natural two-dimensional layout of BR in the native membrane (Ganea *et al.*, 1998). This approach has been refined by forming lipid membranes on a porous alumina substrate and then adsorbing purple membrane patches onto the membrane (Horn & Steinem, 2005). Also HR (Essen, 2002; Varo, 2000) has been reconstituted in proteoliposomes (Duschl, McCloskey & Lanyi, 1988) and lipid bilayer membranes (Bamberg, Hegemann & Oesterhelt, 1984).

Biomimetic sensing with reconstituted rhodopsins rely on an optical input, but changes in optical properties of supported biomimetic membranes may also be used as output signal. For example the application of supported membranes in the design of biosensors mounted on electro-optical devices is attracting considerable interest. Using surface plasmon resonance (SPR) allows for real-time measurements of ligand binding to immobilized proteins (Löfås & Johnsson, 1990) and thus opens for the possibility to detect ligand binding to membrane spanning proteins. Immunosensing can be seen as a special case of ligand binding sensing and detection of *Staphylococcus* enterotoxin B (SEB) in milk has been

demonstrated in a microfluidic system with supported bilayer membranes with biotinylated anti-SEB IgG (Dong, Scott Phillips & Chen, 2006).

Although most work on biomimetic membrane sensors is based on incorporating membranes proteins, some sensor designs may also be realized in protein free systems. A recent example is a membrane supported by nanoporous aluminium oxide providing a high surface area and a protective environment against dewetting (Largueze, Kirat & Morandat, 2010). The membrane contains polyethylene-glycol (PEG) conjugated lipids as hydrating, protective and tethering agents and ubiquinone which is a naturally occurring redox lipophilic mediator embedded within the acyl chains of the lipid bilayer. The sensing system is based on cyclic voltammetry and can detect alterations of lipid membranes that are induced by the addition of surfactants (exemplified by the commonly used non-ionic detergent: Triton X-100). Biomedical application of this system could for example be screening of pulmonary surfactant candidates, monitoring enzymatic degradation by lipases, and studying peptide bilayer insertion.

Another method relies in the use of infrared absorption spectroscopy (IRAS) measurements. A recent study combining IRAS and voltage-clamp has demonstrated changes in specific regions in spectra obtained with solvent containing biomimetic membranes formed with D_2O in the electrolyte solutions providing insight into membrane formation (Hirano-Iwata *et al.*, 2009). An OD stretching peak (arising from D_2O) appeared immediately after lipid application (painting). The band intensity increased with time with a concomitant decrease in bandwidth which could reflect gradual changes in the ordering of interfacial water molecules. Also specific bands could be assigned to CHx stretching modes of acyl chains. The intensity of these bands was about ten times higher than that of the C=O modes of PC. Thus these CHx bands likely arose from *n*-decane rather than from phospholipid acyl chains. The band intensities decreased with time, suggesting that *n*-decane was slowly expelled. These results demonstrate that IRAS can detect self-thinning of the lipid solution to form biomimetic membranes, the resulting expulsion of the *n*-decane solvent, and reordering of interfacial D_2O. By extending this methodology combined IRAS-voltage-clamp may be used to detect spectroscopic signals due to specific conformational changes in lipid acyl chains induced by pharmaceutical compounds as well as a biomedical screening assay for investigating the properties of naturally occurring (antioxidant) membrane residing solvents e.g. ubiquinone.

5. Future research

By virtue of mimicking cellular membranes, model systems based on one or few lipid species and reconstituted proteins have attracted considerable interest in biomedical research since the first appearance of black lipid membranes in the 1960ties. With the recent advances in nanotechnology over the last two decades this interest has now manifested itself in laboratory model devices with multiparameter detection of membrane dynamics and protein function. Recent developments in membrane design have led to the concept of biomimetic membrane arrays that may provide powerful HTS assays in drug discovery and in creation of novel separation technologies based on membrane peptide and protein function.

A reason that biomimetic membrane array devices are not already commercially available is related to the difficulty of creating stable and transportable devices. Although, major efforts

have resulted in increased biomimetic membrane stability and lifetimes (several days to weeks), further improvements are still required. Especially transportation robustness needs further attention. With further developments in multi composite materials, sandwich structuring and encapsulation strategies storable and transportable biomimetic membrane based biomedical devices appear feasible.

While general protocols for reconstitution small fusiogenic membrane-spanning depsipeptides and peptides are relatively well-established, general reconstitution strategies are urgently required for controlled and reliable incorporating medium to large membrane proteins (35-500 kDa) that do not reliable self-insert into established biomimetic membrane arrays. Moreover, designs that support reconstitution of different membrane proteins into individual membranes would enable fabrication of membrane peptide or protein microarrays similar to current DNA microarrays and protein dot-blot arrays.

With the recent advances in biomimetic membrane array design and with further developments of biomimetic designs to comprise laboratory-on-a-chip (LOC) and micro-total-analysis systems (µTAS) the ultimate goal of industrially fabricated devices for drug-discovery, toxicologial testing, and other biomedical/pharmaceutical applications based on biomembrane function seem within reach.

References

Andersen, O.S. & Koeppe, R.E., 2nd (2007): Bilayer thickness and membrane protein function: an energetic perspective *Annu Rev Biophys Biomol Struct* 36: 107-30.

Arora, A., Rinehart, D., Szabo, G. & Tamm, L.K. (2000): Refolded outer membrane protein A of Escherichia coli forms ion channels with two conductance states in planar lipid bilayers *J Biol Chem* 275(3): 1594-600.

Ashkenasy, N., Sanchez-Quesada, J., Bayley, H. & Ghadiri, M.R. (2005): Recognizing a single base in an individual DNA strand: a step toward DNA sequencing in nanopores *Angew Chem Int Ed Engl* 44(9): 1401-4.

Bamberg, E., Hegemann, P. & Oesterhelt, D. (1984): Reconstitution of halorhodopsin in black lipid membranes *Prog Clin Biol Res* 164: 73-9.

Becucci, L., Carbone, M.V., Biagiotti, T., D'Amico, M., Olivotto, M. & Guidelli, R. (2008): Incorporation of the HERG potassium channel in a mercury supported lipid bilayer *J Phys Chem B* 112(4): 1315-9.

Becucci, L., Leon, R.R., Moncelli, M.R., Rovero, P. & Guidelli, R. (2006a): Electrochemical investigation of melittin reconstituted into a mercury-supported lipid bilayer *Langmuir* 22(15): 6644-50.

Becucci, L., Moncelli, M.R. & Guidelli, R. (2006b): Impedance spectroscopy of OmpF porin reconstituted into a mercury-supported lipid bilayer *Langmuir* 22(3): 1341-6.

Becucci, L., Moncelli, M.R., Naumann, R. & Guidelli, R. (2005): Potassium ion transport by valinomycin across a Hg-supported lipid bilayer *J Am Chem Soc* 127(38): 13316-23.

Benz, R., Frohlich, O., Lauger, P. & Montal, M. (1975): Electrical capacity of black lipid films and of lipid bilayers made from monolayers *Biochim Biophys Acta* 394(3): 323-34.

Benz, R., Praß, W. & Ringsdorf, H. (1982): Black Lipid Membranes from Polymerizable Lipids *Angewandte Chemie International Edition in English* 21(S5): 869-880.

Boheim, G., Hanke, W., Barrantes, F.J., Eibl, H., Sakmann, B., Fels, G. & Maelicke, A. (1981): Agonist-activated ionic channels in acetylcholine receptor reconstituted into planar lipid bilayers *Proc Natl Acad Sci U S A* 78(6): 3586-90.

Borisenko, V., Zhang, Z. & Woolley, G.A. (2002): Gramicidin derivatives as membrane-based pH sensors *Biochim Biophys Acta* 1558(1): 26-33.

Capone, R., Blake, S., Restrepo, M.R., Yang, J. & Mayer, M. (2007): Designing nanosensors based on charged derivatives of gramicidin A *J Am Chem Soc* 129(31): 9737-45.

Cornell, B.A., Braach-Maksvytis, V.L., King, L.G., Osman, P.D., Raguse, B., Wieczorek, L. & Pace, R.J. (1997): A biosensor that uses ion-channel switches *Nature* 387(6633): 580-3.

Daly, S.M., Heffernan, L.A., Barger, W.R. & Shenoy, D.K. (2006): Photopolymerization of mixed monolayers and black lipid membranes containing gramicidin A and diacetylenic phospholipids *Langmuir* 22(3): 1215-22.

Dhoke, M.A., Ladha, P.J., Boerio, F.J., Lessard, L.B., Malinowska, D.H., Cuppoletti, J. & Wieczorek, D.S. (2005): Porous membranes for reconstitution of ion channels *Biochim Biophys Acta* 1716(2): 117-25.

Dong, Y., Scott Phillips, K. & Chen, Q. (2006): Immunosensing of Staphylococcus enterotoxin B (SEB) in milk with PDMS microfluidic systems using reinforced supported bilayer membranes *Lab on a Chip* 6: 675-681.

Duschl, A., McCloskey, M.A. & Lanyi, J.K. (1988): Functional reconstitution of halorhodopsin. Properties of halorhodopsin-containing proteoliposomes *J Biol Chem* 263(32): 17016-22.

Eray, M., Dogan, N.S., Reiken, S.R., Sutisna, H., Van Wie, B.J., Koch, A.R., Moffett, D.F., Silber, M. & Davis, W.C. (1995): A highly stable and selective biosensor using modified nicotinic acetylcholine receptor (nAChR) *Biosystems* 35(2-3): 183-8.

Essen, L.O. (2002): Halorhodopsin: light-driven ion pumping made simple? *Curr Opin Struct Biol* 12(4): 516-22.

Fang, Y., Frutos, A.G. & Lahiri, J. (2002): Membrane protein microarrays *J Am Chem Soc* 124(11): 2394-5.

Fang, Y., Hong, Y., Webb, B. & Lahiri, J. (2006): Applications of biomembranes in drug discovery *MRS bulletin* 31(7): 5.

Fang, Y., Lahiri, J. & Picard, L. (2003): G protein-coupled receptor microarrays for drug discovery *Drug Discov Today* 8(16): 755-61.

Frant, M.S. & Ross, J.W., Jr. (1970): Potassium ion specific electrode with high selectivity for potassium over sodium *Science* 167(920): 987-8.

Ganea, C., Tittor, J., Bamberg, E. & Oesterhelt, D. (1998): Chloride- and pH-dependent proton transport by BR mutant D85N *Biochim Biophys Acta* 1368(1): 84-96.

Ginsburg, S. & Noble, D. (1974): The activation enthalpies for ion conductance systems in lipid bilayer membranes *Journal of Membrane Biology* 18(1): 163-176.

Gonzalez-Perez, A., Stibius, K.B., Vissing, T., Nielsen, C.H. & Mouritsen, O.G. (2009): Biomimetic Triblock Copolymer Membrane Arrays: A Stable Template for Functional Membrane Proteins *Langmuir* 25(18): 10447-10450.

Gu, L.Q., Braha, O., Conlan, S., Cheley, S. & Bayley, H. (1999): Stochastic sensing of organic analytes by a pore-forming protein containing a molecular adapter *Nature* 398(6729): 686-90.

Han, X., Studer, A., Sehr, H., Geissbühler, I., Di Berardino, M., Winkler, F.K. & Tiefenauer, L.X. (2007): Nanopore Arrays for Stable and Functional Free-Standing Lipid Bilayers *Advanced Materials* 19(24): 4466-4470.

Hansen, J.S., Perry, M., Vogel, J., Groth, J.S., Vissing, T., Larsen, M.S., Geschke, O., Emneus, J., Bohr, H. & Nielsen, C.H. (2009a): Large scale biomimetic membrane arrays *Anal Bioanal Chem* 395(3): 719-27.

Hansen, J.S., Perry, M., Vogel, J., Vissing, T., Hansen, C.R., Geschke, O., Emneus, J. & Nielsen, C.H. (2009b): Development of an automation technique for the establishment of functional lipid bilayer arrays *Journal of Micromechanics and Microengineering* 19(2): 025014.

Hemmler, R., Bose, G., Wagner, R. & Peters, R. (2005): Nanopore unitary permeability measured by electrochemical and optical single transporter recording *Biophys J* 88(6): 4000-7.

Heyderman, L.J., Ketterer, B., Bächle, D., Glaus, F., Haas, B., Schift, H., Vogelsang, K., Gobrecht, J., Tiefenauer, L., Dubochet, O., Surbled, P. & Hessler, T. (2003): High volume fabrication of customised nanopore membrane chips *Microelectronic Engineering* 67-68: 208-213.

Hirano-Iwata, A., Oshima, A., Onodera, K., Aoto, K., Taira, T., Yamaguchi, R., Kimura, Y. & Niwano, M. (2009): Self-formation of bilayer lipid membranes on agarose-coated silicon surfaces studied by simultaneous electrophysiological and surface infrared spectroscopic measurements *Applied Physics Letters* 94.

Ho, D., Chu, B., Lee, H. & Montemagno, C. (2004): Protein-driven energy tranduction across polymeric biomembranes *Nanotechnology* 15: 1084-1094.

Horn, C. & Steinem, C. (2005): Photocurrents generated by bacteriorhodopsin adsorbed on nano-black lipid membranes *Biophys J* 89(2): 1046-54.

Jeon, T.J., Malmstadt, N. & Schmidt, J.J. (2006): Hydrogel-encapsulated lipid membranes *J Am Chem Soc* 128(1): 42-3.

Kang, X.F., Cheley, S., Rice-Ficht, A.C. & Bayley, H. (2007): A storable encapsulated bilayer chip containing a single protein nanopore *J Am Chem Soc* 129(15): 4701-5.

Kayushin, L.P. & Skulachev, V.P. (1974): Bacteriorhodopsin as an electrogenic proton pump: reconstitution of bacteriorhodopsin proteoliposomes generating delta psi and delta pH *FEBS Lett* 39(1): 39-42.

Kendall, D.A. & MacDonald, R.C. (1982): A fluorescence assay to monitor vesicle fusion and lysis *J Biol Chem* 257(23): 13892-5.

Koeppe, R.E., II & Andersen, O.S. (1996): Engineering the gramicidin channel *Annu. Rev. Biophys. Biomol. Struct.* 25: 231-258.

Kumar, M., Grzelakowski, M., Zilles, J., Clark, M. & Meier, W. (2007): Highly permeable polymeric membranes based on the incorporation of the functional water channel protein Aquaporin Z *Proc Natl Acad Sci U S A* 104(52): 20719-24.

Largueze, J.-B., Kirat, K.E. & Morandat, S. (2010): Preparation of an electrochemical biosensor based on lipid membranes in nanoporous alumina *Colloids and Surfaces B: Biointerfaces* 79: 33-40.

LaVan, D.A. & Cha, J.N. (2006): Approaches for biological and biomimetic energy conversion *Proc Natl Acad Sci U S A* 103(14): 5251-5.

Le Pioufle, B., Suzuki, H., Tabata, K.V., Noji, H. & Takeuchi, S. (2008): Lipid bilayer microarray for parallel recording of transmembrane ion currents *Anal Chem* 80(1): 328-32.

Lewis, B.A. & Engelman, D.M. (1983): Lipid bilayer thickness varies linearly with acyl chain length in fluid phosphatidylcholine vesicles *Journal of Molecular Biology* 166(2): 211-217.

Lin, Z., Takahashi, Y., Kitagawa, Y., Umemura, T., Shiku, H. & Matsue, T. (2008): An addressable microelectrode array for electrochemical detection *Anal Chem* 80(17): 6830-3.

Löfås, S. & Johnsson, B.J. (1990): A novel hydrogel matrix on gold surfaces in surface plasmon resonance sensors for fast and efficient covalent immobilization of ligands *Chem. Soc. Chem. Commun.*: 1526-1528.

Malmstadt, N., Jeon, J. & Schmidt, J. (2008): Long-Lived Planar Lipid Bilayer Membranes Anchored to an In Situ Polymerized Hydrogel *Advanced Materials* 20(1): 84-89.

Matsuno, N., Murawsky, M., Ridgeway, J. & Cuppoletti, J. (2004): Solid support membranes for ion channel arrays and sensors: application to rapid screening of pharmacological compounds *Biochim Biophys Acta* 1665(1-2): 184-90.

Mayer, M., Kriebel, J.K., Tosteson, M.T. & Whitesides, G.M. (2003): Microfabricated teflon membranes for low-noise recordings of ion channels in planar lipid bilayers *Biophys J* 85(4): 2684-95.

Minami, H., Sugawara, M., Odashima, K., Umezawa, Y., Uto, M., Michaelis, E.K. & Kuwana, T. (1991): Ion channel sensors for glutamic acid *Anal Chem* 63(23): 2787-95.

Montal, M. & Mueller, P. (1972): Formation of bimolecular membranes from lipid monolayers and a study of their electrical properties *Proc Natl Acad Sci U S A* 69(12): 3561-6.

Moreau, C.J., Dupuis, J.P., Revilloud, J., Arumugam, K. & Vivaudou, M. (2008): Coupling ion channels to receptors for biomolecule sensing *Nat Nanotechnol* 3(10): 620-5.

Mueller, P. & Rudin, D.O. (1969): Translocators in bimolecular lipid membranes: their role in dissipative and conservative bioenergetic transduction *Curr Topics Bioenergetics* 3: 157–249.

Nielsen, C.H. (2009): Biomimetic membranes for sensor and separation applications *Anal Bioanal Chem* 395: 697-718.

Nikolelis, D.P. & Siontorou, C.G. (1996): Ammonium ion minisensors form self-assembled bilayer lipid membranes using gramicidin as an ionophore. Modulation of ammonium selectivity by platelet-activating factor *Anal Chem* 68(10): 1735-41.

O'Shaughnessy, T.J., Hu, J.E., Kulp, J.L., 3rd, Daly, S.M. & Ligler, F.S. (2007): Laser ablation of micropores for formation of artificial planar lipid bilayers *Biomed Microdevices* 9(6): 863-8.

Oesterhelt, D. & Schuhmann, L. (1974): Reconstitution of bacteriorhodopsin *FEBS Lett* 44(3): 262-5.

Oesterhelt, D. & Stoeckenius, W. (1973): Functions of a new photoreceptor membrane *Proc Natl Acad Sci U S A* 70(10): 2853-7.

Oliver, A.E., Kendall, E.L., Howland, M.C., Sanii, B., Shreve, A.P. & Parikh, A.N. (2008): Protecting, patterning, and scaffolding supported lipid membranes using carbohydrate glasses *Lab Chip* 8(6): 892-7.

Perin, M.S. & MacDonald, R.C. (1989): Fusion of synaptic vesicle membranes with planar bilayer membranes *Biophys J* 55(5): 973-86.

Pocanschi, C.L., Apell, H.J., Puntervoll, P., Hogh, B., Jensen, H.B., Welte, W. & Kleinschmidt, J.H. (2006): The major outer membrane protein of Fusobacterium nucleatum (FomA) folds and inserts into lipid bilayers via parallel folding pathways *J Mol Biol* 355(3): 548-61.

Reimhult, E. & Kumar, K. (2008): Membrane biosensor platforms using nano- and microporous supports *Trends Biotechnol* 26(2): 82-9.

Ries, R.S., Choi, H., Blunck, R., Bezanilla, F. & Heath, J.R. (2004): Black Lipid Membranes: Visualizing the Structure, Dynamics, and Substrate Dependence of Membranes *Journal of Physical Chemistry B* 108(41): 16040-16049.

Sandison, M.E. & Morgan, H. (2005): Rapid fabrication of polymer microfluidic systems for the production of artificial lipid bilayers *Journal of Micromechanics and Microengineering* 15(S139-S144).

Schar-Zammaretti, P., Ziegler, U., Forster, I., Groscurth, P. & Spichiger-Keller, U.E. (2002): Potassium-selective atomic force microscopy on ion-releasing substrates and living cells *Anal Chem* 74(16): 4269-74.

Schmidt, E.K., Liebermann, T., Kreiter, M., Jonczyk, A., Naumann, R., Offenhausser, A., Neumann, E., Kukol, A., Maelicke, A. & Knoll, W. (1998): Incorporation of the acetylcholine receptor dimer from Torpedo californica in a peptide supported lipid membrane investigated by surface plasmon and fluorescence spectroscopy *Biosens Bioelectron* 13(6): 585-91.

Schmitt, E.K., Vrouenraets, M. & Steinem, C. (2006): Channel activity of OmpF monitored in nano-BLMs *Biophys J* 91(6): 2163-71.

Schobert, B. & Lanyi, J.K. (1982): Halorhodopsin is a light-driven chloride pump *J Biol Chem* 257(17): 10306-13.

Shenoy, D.K., Barger, W.R., Singh, A., Panchal, R.G., Misakian, M., Stanford, V.M. & Kasianowicz, J.J. (2005): Functional reconstitution of protein ion channels into planar polymerizable phospholipid membranes *Nano Lett* 5(6): 1181-5.

Steltze, M. (1993): On the application of supported bilayers as receptive layers for biosensors with electrical detection *J. Phys. Chem.* 97: 2974-2981.

Studer, A. & Tiefenauer, L. (2007): Stable planar lipid bilayers in nanopores *European Cells and Materials* 14(Suppl. 3): 33.

Suzuki, H., Le Pioufle, B. & Takeuchi, S. (2009): Ninety-six-well planar lipid bilayer chip for ion channel recording fabricated by hybrid stereolithography *Biomed Microdevices* 11(1): 17-22.

Suzuki, H. & Takeuchi, S. (2008): Microtechnologies for membrane protein studies *Anal Bioanal Chem* 391(8): 2695-702.

Uto, M., Araki, M., Taniguchi, T., Hoshi, S. & Inoue, S. (1994): Stability of an Agar-Supported Bilayer Lipid Membrane and Its Application to a Chemical Sensor *Analytical Sciences* 10(6): 943-946.

Varo, G. (2000): Analogies between halorhodopsin and bacteriorhodopsin *Biochim Biophys Acta* 1460(1): 220-9.

Vogel, J., Perry, M., Hansen, J.S., Bolinger, P.Y., Nielsen, C.H. & Geschke, O. (2009): A support structure for biomimetic applications *Journal of Micromechanics and Microengineering* 19(2): 025026.

White, S.H. (1972): Analysis of the torus surrounding planar lipid bilayer membranes *Biophys J* 12(4): 432-45.

White, S.H. & Thompson, T.E. (1973): Capacitance, area, and thickness variations in thin lipid films *Biochim Biophys Acta* 323(1): 7-22.

Wiess-Wichert, C., Smetazko, M., Valina-Saba, M. & Schalkhammer, T. (1997): A new analytical device based on gated ion channels: A peptide-channel biosensor *J. Biol. Screening* 2: 11-18.

Wilburn, J.P., Wright, D.W. & Cliffel, D.E. (2006): Imaging of voltage-gated alamethicin pores in a reconstituted bilayer lipid membrane via scanning electrochemical microscopy *Analyst* 131(2): 311-6.

Wonderlin, W.F., Finkel, A. & French, R.J. (1990): Optimizing planar lipid bilayer single-channel recordings for high resolution with rapid voltage steps *Biophys J* 58(2): 289-97.

Woodbury, D.J. & Hall, J.E. (1988a): Role of channels in the fusion of vesicles with a planar bilayer *Biophys J* 54(6): 1053-63.

Woodbury, D.J. & Hall, J.E. (1988b): Vesicle-membrane fusion. Observation of simultaneous membrane incorporation and content release *Biophys J* 54(2): 345-9.

Zagnoni, M., Sandison, M.E., Marius, P., Lee, A.G. & Morgan, H. (2007): Controlled delivery of proteins into bilayer lipid membranes on chip *Lab Chip* 7(9): 1176-83.

Zimmerberg, J., Cohen, F.S. & Finkelstein, A. (1980a): Fusion of phospholipid vesicles with planar phospholipid bilayer membranes. I. Discharge of vesicular contents across the planar membrane *J Gen Physiol* 75(3): 241-50.

Zimmerberg, J., Cohen, F.S. & Finkelstein, A. (1980b): Micromolar Ca^{2+} Stimulates Fusion of Lipid Vesicles with Planar Bilayers Containing a Calcium-Binding Protein *Science* 210(4472): 906-908.

2.2 Strategies for integrating membrane proteins in biomembranes

13. Strategies for integrating membrane proteins in biomembranes

Jesper S. Hansen[†,§,*], Inés Plasencia[‡], Kamila Pszon-Bartosz[†,§]

[†]Aquaporin A/S, DK-2200 Copenhagen, Denmark. [§]DTU Nanotech, Technical University of Denmark, DK-2800 Kgs. Lyngby, Denmark. [‡]MEMPHYS-Center for Biomembrane Physics. Department of Physics and Chemistry. University of Southern Denmark. DK-5230 Odense, Denmark. [*]E-mail address: jsh@aquaporin.dk

Abstract   Correct integration of membrane proteins with biomimetic membranes is crucial for designing novel sensor and separation technologies based on the functionality of membrane proteins. Membrane proteins are generally delicate molecules and care need to be taken in order to retain protein structure and function during handling and reconstitution into model membranes. This chapter will give a detailed overview of available and novel membrane protein reconstitution strategies in both vesicular and planar model membrane designs.

13.1 Protein reconstitution

Membrane proteins function among others as receptors, ion channels, transporters and pore formers. They carry out important cellular functions in many physiologic processes in normal physiology, and may cause or contribute to several disease states. For the same reason membrane proteins are key targets for therapeutic intervention (Fang et al. 2003). Membrane proteins can moreover be chemically modified or genetically engineered, giving unprecedented control over membrane binding and transport properties (Castellana and Cremer 2006). Therefore, membrane proteins, either in native forms or modified versions, may give rise to the creation of novel protein-based biosensors, biomedical screening platforms and novel separation technologies.

   Reconstitution of membrane proteins into artificially made lipid bilayers represent a powerful technique to study and functionally work with membrane proteins under controlled experimental conditions (Woodbury 1999). However, membrane protein reconstitution is not a trivial process. Here we will give a practical approach to the strategies and considerations for functionally reconstituting membrane proteins into vesicular and planar model membranes. The requirements for protein reconstitution yield in sensor or separation applications may not be the same. Reconstitution approaches and considerations to meet the requirements of reconstitution yield in sensor or separation technologies are also discussed here.

13.2 Reconstitution in vesicles

Vesicles are spherical shells of lipid bilayers and represent one of the most widely used methods for reconstituting membrane proteins into biomimetic model membranes. When lipids are the principal component of the vesicles, they may also be called liposomes. Polymerosomes on the other hand refers to vesicles formed by synthetic polymers (Lorenceau et al. 2005; Rastogi et al. 2009; Rosenkranz et al. 2009).

There are presently several methods available for reconstituting membrane proteins into vesicles. The protein purification conditions will be an initial parameter defining the reconstitution methodology to choose. Although few membranes proteins can be extracted by organic solvents, e.g. pulmonary surfactant proteins SP–B and SP–C (Curstedt et al. 1988; Johansson et al. 1988), most membrane protein purification protocols rely on solubilizing the cell membrane to obtain an aqueous detergent–solubilized protein state that subsequently may be reconstituted into model membranes.

13.2.1 Preparation of liposomes and proteoliposomes

Various techniques exist for preparing liposomes, and the method of choice may result in different types of liposomes. The types of liposomes may be classified on the basis of size and number of bilayers forming the vesicles (Szoka and Papahadjopoulos 1980; Deamer and Uster 1983). The classifications used for the different types of liposomes are often divided into:

1. *Multilamellar vesicles (MLV).* This type of vesicles contains multiple lipid bilayer vesicles inside each other. They vary in size, internal volume (Singer et al. 1990) and osmotic activity (Yoshikawa et al. 1983). This can make liposome analysis and result interpretation difficult.
2. *Small unilamellar vesicles (SUV).* SUVs consist of a single lipid bilayer and the vesicle sizes are between 4 –20 nm. These vesicles are very small, resembling the sizes of biological vesicles carrying neurotransmitters in the nerve synapses.
3. *Large unilamellar vesicles (LUV).* These vesicles also consist of a single lipid bilayer and are defined by having sizes between 50 nm and up to 10 μm. These vesicles are often the preferred type for protein reconstitution.
4. *Giant Unilamellar vesicles (GUV).* They are also known as cell-size unilamellar vesicles, because their size approximately mimics biological living cell sizes. GUVs are defined by having a size of ≥10 μm.

Vesicle size will not be the only parameter influenced by the preparation method, the polydispersity, surface potential, degree of ionization, thermotropic phase behavior, permeability and physical stability will also be affected (Szoka and Papahadjopoulos 1980; Angelova et al. 1992; Joannic et al. 1997; Feitosa et al. 2000). Many applications of vesicles rely on a narrow size distribution and a concomitant high stability during a long time period (Fendler 1987). When natural or synthetic long–tailed phospholipids are dispersed in aqueous solution, they form large multilamellar structures (Gabriel and Roberts 1984).

There are several methods to form unilamellar vesicles from multilamellar. This is relevant for creating vesicles suitable for reliable and reproducible protein reconstitution and may also be of importance in many analytical techniques. A straightforward method to create unilamellar vesicles from multilamellar vesicles is sonication. However, it does not produce a uniform size distribution and moreover the method may potentially cause metal contamination, lipid degradation and generation of heat and aerosols (Maguire et al. 2003). Another method is mechanical extrusion of multilammelar vesicles through a filter membrane with a defined pore size, resulting in unilamellar vesicles with a narrow size distribution. Vesicle extrusion may be carried out by small inexpensive hand–held extruders or with nitrogen pressurized barrel extruders. The latter can range in capacities from 1 ml, 10 ml and up to industrial scale (many liters). Generally, we have good experience with both hand–held and pressurized barrel extruders. However, hand–held extruders tend to produce a slightly more polydisperse vesicle solution and vesicles produced in this manner also tend to be slightly more instable compared to the barrel extruded vesicles (higher tendency of vesicle–vesicle fusions).

An important consideration in protein reconstitution is which strategy to choose for delivering membrane proteins into model membranes. As mentioned the majority of membrane protein reconstitution procedures involve the use of a detergent. The detergent play a dual role for membrane proteins in solution: i) the solubilization of the native membrane to release the contained membrane spanning protein into solution and ii) maintain the protein folded and soluble in an aqueous state (le Maire et al. 2000). Moreover, the physio-chemical properties of the detergent may be important for the integrity and activity of the protein upon reconstitution into model membranes (Paternostre et al. 1988; Rigaud et al. 1988).

To produce protein reconstituted liposomes (proteoliposomes) removal of the detergent is necessary in order to transfer the proteins from an aqueous detergent stabilized state and into the model membrane lipid bilayer. Conventional techniques for removing the detergent include among others dialysis, gel exclusion chromatography and adsorption onto polymeric materials. A detailed description and comparison of the various techniques for detergent removal is reviewed in (Silvius 1992; Ollivon et al. 2000). Generally the choice of detergent removal technique is often a choice between using dialysis or adsorption onto polymeric

4

materials such as hydrophobic Bio–Beads or a combination of both these techniques. Both methods are straightforward and do not require costly technical equipment. The decision of which method to use for detergent removal is typically based on the nature of the detergent. Detergents with a high critical micelle concentration (CMC) and with low to moderate molecular weight micelles can be dialyzed away, whereas dialysis is not an appropriate technique for detergent removal if the opposite is the case (Table 1). Table 1 gives a brief overview of some of the more commonly used non-denaturing detergents for membrane protein reconstitution and also indicates whether the detergent is dialyzable.

Table 1. Non-denaturing detergents commonly used for membrane protein reconstitution.

Type	Detergent	Mw micelle (Da)	CMC (mM)	Dialyzable
Anionic	Sodium cholate	900-1,300	9-15	Yes
	Sodium deoxycholate	1,200-5,000	2-6	Yes
Cationic	CTAB	62,000	1	Yes
Zwitterionic	CHAPS	6,150	6-10	Yes
	CHAPSO	7,000	8	Yes
	LDAO	ND	1	Yes
Nonionic	OG	25,000	20-25	Yes
	OTG	ND	9	Yes
	Triton X-100	90,000	0.24	No
	C12E8	65,000	0.09	No
	DDM	50,000	0.15	No
	Digitonin	70,000	0.5	No
	MEGA-9	ND	6-7	Yes
	MEGA-10	ND	19-25	Yes

[1]Abbreviations: CTAB: Hexadecyltrimethylammonium bromide; LDAO: Lauryldimethylamine N-oxide; OG: Octyl-β-glycopyranoside; OTG: Octyl β-D-thioglucopyranoside; C12E8: Dodecyl octaethylene glycol ether; DDM: *n*-Dodecyl β-D-maltoside.
[2]ND indicates that the detergent molecular weight micelles have not or cannot be determined.
[3]Notice: CMC changes with temperature and salt concentration. Given values are 20°C –25°C.

Another parameter to consider before carrying out the protein reconstitution process is the lipid–to–protein ratio (LPR). The LPR is the mol of lipids per mol protein to be reconstituted into the vesicles. There is an upper limit of how much protein that physically can be incorporated into a defined amount of lipid (or polymer). This limit depends on the surface area of the protein and the area of the lipid. The area per lipid of phosphatidylcholines has for example been characterized by NMR spectroscopy and may provide useful information in LPR calculations (Petrache et al. 2000). Since the lipid membrane exists as a bimolecular structure, lipid molecules are needed in both bilayers to cover a single transmembrane protein. Similarly the crystal structure has been determined for various membrane

proteins from which the protein monomer surface has been published. The spinach aquaporin SoPIP2;1 is just one example (Tornroth-Horsefield et al. 2006). Thus, based on the area values of the lipid and protein a minimum mol/mol ratio of lipid molecules to protein may be estimated. It is often necessary to test different LPRs (e.g. LPR 200, 100, 50, etc) to find the optimal protein reconstitution conditions.

In our laboratory we work with aquaporins which are tetrameric α-helical water channel forming membrane proteins. We have good experience with octyl–β–D–glycopyranoside (OG) and generally use this detergent for protein solubilization and reconstitution. Since OG is dialyzable the preferred detergent removal technique is dialysis (Table 1). To ensure complete detergent removal a second (optional) Bio–Beads step may be included. Our scheme for protein reconstitution into liposomes to produce proteoliposomes is:

1. *Preparation of detergent containing MLVs.* The MLVs are prepared either by drying down the lipid from a chloroform phase or directly dissolving lyophilized lipids in lipid hydration buffer. The lipid hydration buffer is usually matched to be comparable to the buffer of the protein (note: it also contains detergent).
2. *Formation of detergent containing LUVs*. LUVs are prepared from MLVs typically by extrusion using a pressurized barrel extruder with 100, 200 or 400 nm filters depending on the desired proteoliposomes size.
3. *Mixing of detergent LUVs with detergent solubilized protein.* Detergent solubilized protein is mixed with the formed detergent containing LUVs to the desired LPR (e.g. 200, 100, 50, etc).
4. *Detergent removal.* To remove the detergent dialysis is applied. An efficient way is to use dynamic dialysis where a continuous flow of the detergent-free dialysate buffer passes the dialysis tubing containing the lipid-protein-detergent sample (with flow rates of 2–10 ml dialysate/min).
5. *Optionally second detergent removal step.* To ensure that all detergent has been removed from the formed proteoliposomes absorption Bio-Beads may be added to the proteoliposomes sample. This may be relevant for carrying out stopped–flow permeability measurements of aquaporin function, where the presence of residual detergent can hamper the result interpretation of aquaporin permeability. Following the additional detergent removal step the supernatant is collected and used (the proteoliposomes).

The simplified scheme represented above for reconstitution aquaporins into model membrane vesicles is in many aspects a general methodology and may be followed as a flow chart for preparing proteoliposomes using a dialyzable detergent. Parameters such as the detergent, detergent concentration, dialysis times, the optimal LPR and buffer composition may vary from protein to protein. Moreover, various protein isoforms may often require different buffer conditions.

13.2.2 How lipid composition may affect protein folding

A stable integration of a protein into a lipid membrane will be affected among other factors by the hydrophobic interactions of the hydrophobic protein segment(s) with the acyl chains of the lipids. The difference between the hydrophobic length of a membrane integral protein and the hydrophobic thickness of the membrane is known as hydrophobic mismatch. In order to avoid unfavorable exposition of the protein to the hydrophilic environment the length of the hydrophobic thickness of the membrane and the hydrophobic segment of the protein are expected to be matched so they are approximately equal.

Elastic properties of the lipid bilayer are vital to the folding and function of membrane proteins (Booth 2005). Membrane proteins have a percentage of apolar residues that is much higher than for their water soluble counterparts (Samatey et al. 1995; Hong et al. 2009). However, membrane proteins cannot bury all the hydrophobic residues in a hydrophobic core. Therefore, the membrane proteins associate with lipid bilayers both *in vivo* (Van den Berg et al. 2004; Osborne et al. 2005) and *in vitro* (Seddon et al. 2004) and tend to aggregate in aqueous solutions in order to escape the hydrophilic environments. The bilayer thickness is determined by several factors, where some of them for example are the lipid chain length and the degree of saturation of the lipid acyl chains (Rawicz et al. 2000), cholesterol content (Mouritsen and Zuckermann 2004) and the membrane proteins themselves (Mitra et al. 2004). When the lipids forming the model membrane constitute a hydrophobic environment shorter than the hydrophobic protein segment the protein tend to aggregate or oligomerize to minimize the exposed hydrophobic areas. Alternatively they can change the conformation or induce a tilt of the protein in the membrane. In the opposite situation, where the protein chain length is longer than the hydrophobic protein segment the mismatch can also result in protein aggregation.

Membrane proteins may also have specific requirements for phospholipids and sterols which may be essential for folding, oligomerization and/or activity. Moreover, the lipid composition of biological membranes varies, so it may be a good idea to consider what the origin of the protein in question is and in which host organism the protein have been expressed and purified from. A detailed review of specific lipid requirements of selected membrane proteins as well as the lipid composition of various biological membranes are given by Opekarová and Tanner (Opekarova and Tanner 2003). A good starting point, however, for membrane protein reconstitution is to use total lipid extracts such as soybean asolectin or *E. coli* total lipid extract. These lipid mixtures are total lipid membrane extracts and therefore contain all the natural constituents of a biological membrane. They also generally tend to result in good protein reconstitution yield.

13.3 Reconstitution in planar membranes

Planar biomimetic membranes constitute an important platform for studying membrane protein function and protein-lipid interactions. The planar membrane design creates a possibility to study the transport processes of a membrane protein across the lipid bilayer (Janshoff and Steinem 2006). Techniques available to study processes across planar artificially made membranes include among others electrophysiological measurements (Mueller and Rudin 1969; Montal and Mueller 1972) and optical techniques such a fluorescence microscopy or a combination (Hemmler et al. 2005; Wilburn et al. 2006; Hansen et al. 2009a). The structural and dynamic processes of proteins in the membrane may also be studied by surface sensitive techniques (Goennenwein et al. 2003; Buzhynskyy et al. 2007a; Buzhynskyy et al. 2007b).

The potential biotechnological applications of planar membrane designs are large and include both sensor and separation technologies. The creation of membrane protein microarrays for high-throughput screening of protein-drug interactions has attracted much attention (Fang et al. 2002; Majd and Mayer 2008). Designs that fit into modern plate readers are attractive in the development of high-throughput membrane protein assays for the pharmaceutical industry (Fang et al. 2006; Le Pioufle et al. 2008; Suzuki et al. 2009). Provided that the effective functional membrane area can be scaled up sufficiently, planar biomimetic membranes may also be suitable for novel separation technologies using membrane protein channels (Nielsen 2009).

Small fusiogenic pepsipeptides or peptides such as valinomycin, gramicidin or alamethicin, respectively, spontaneously self-insert into pre-established membranes (Zagnoni et al. 2007). These membrane spanning molecules are therefore well-characterized and due to the ease of reconstitution they are often applied to demonstrate the functionality of artificially made lipid membranes (Hansen, Perry et al. 2009a; Hansen et al. 2009b). In contrast, medium to large membrane proteins (35-500 kDa) do generally not reliable self-insert into pre-established membranes (Zagnoni, Sandison et al. 2007). An exception is the heptameric α-hemolysin channel pore from *S. aureus* (Suzuki et al. 2007). In addition, several *E. coli* outer membrane porins such as OmpA, OmpF and FomA may be reconstituted into planar membranes directly from a detergent solubilized state (Arora et al. 2000; Pocanschi et al. 2006; Schmitt et al. 2006). It should be noted, however, that although the detergent solubilized proteins can be added in a few microliter aliquots to the lipid bilayer chamber, the detergent present tends to make the established membrane(s) unstable.

8

In order to study most membrane proteins, reliable and controllable reconstitution methods are required for the delivery of functionally active membrane proteins into planar membranes.

13.3.1 Vesicle fusion with planar lipid bilayers

The conventional technique to deliver membrane proteins to pre-established planar lipid bilayers is by vesicle fusion. The methodology can be viewed as a biomimicry of the ubiquitous biological phenomena of exocytosis. In exocytosis intracellular vesicles fuse with the plasma membrane and subsequently release the extracellular content (Zimmerberg et al. 1980a). Exocytosis is involved in important biological processes such as neurotransmitter release from nerve synapses and the release of hormones and messenger substances from endocrine and exocrine glands (Zimmerberg, Cohen et al. 1980a). Vesicles fusion with artificially made membranes is inspired by these elegant biological processes in nature, albeit *in vitro* model systems of vesicle fusion with model membranes are greatly simplified compared to the naturally occurring processes.

The approach of vesicle fusion with model membrane systems can be simplified to four discrete steps:

1. *Preparation of proteoliposomes.* Reconstitute the membrane protein of interest into vesicles, usually LUVs, resulting in formation of proteoliposomes (see section 13.2).
2. *Establishment of a planar model membrane*. Planar lipid bilayers are typically created across a Teflon aperture and commonly by using the Müller-Rudin (Mueller and Rudin 1969) or the Montal-Müller technique (Montal and Mueller 1972).
3. *Addition of the proteoliposomes to the planar model membrane.* Aliquots of the prepared proteoliposomes are added (usually) to the *cis* side of the chamber design, which per definition consist of a *cis* and a *trans* side separated by the established membrane (Mueller and Rudin 1969; Montal and Mueller 1972).
4. *Induction of fusion of the proteoliposomes with the membrane.* There are various means to stimulate vesicles fusion with the established lipid bilayers, including creating an osmotic gradient, magnetic stirring, addition Ca^{2+}, vesicle buoyancy, LPR. This will be discussed in details below.

The reality is often more nuanced than simplified schemes and vesicle fusion with planar membranes is no exception. The fusion efficiency is often influenced by several factors that may be difficult to pinpoint. These may both be related to the applied biomimetic membrane chamber design, the stability of

the established biomimetic membrane and the specific nature of the membrane protein in question.

In general, adding proteoliposomes to a pre-established lipid model membrane results in a low basal rate of fusion. Efficient reconstitution of membrane proteins into the planar membrane thus requires stimulation of the fusion rate. An efficient way to induce fusion events of vesicles to planar membranes is by creating an osmotic gradient across the membrane (Cohen et al. 1980). Creation of an osmotic gradient across the membrane may be established by addition of an osmolyte (i.e. salt or sugar) to the same side of the membrane as the vesicles (*cis* side). An effective way to do this is to add a 3 M KCl solution to the *cis* chamber side to a final concentration in the chamber of around 800-900 mM KCl (Woodbury 1999). The established osmotic gradient across the membrane is believed to result in osmotic swelling of the vesicles which eventually causes them to burst and subsequently fuse to the planar bilayer membrane (Zimmerberg et al. 1980b; Cohen et al. 1982).

In exocytosis calcium ions play a crucial role for biological membrane fusion (Furber et al. 2009). For *in vitro* vesicle fusion to planar membranes divalent cations (i.e. Ca^{2+}, Mg^{2+}, Ba^{2+}) in millimolar concentrations have been described to enhance vesicle fusion to planar lipid bilayers in the presence of an osmotic gradient (Cohen, Zimmerberg et al. 1980). In contrast, with vesicles derived from brain synapses or proteoliposomes reconstituted with Ca^{2+} binding proteins, only Ca^{2+} specifically stimulates fusion events (not Mg^{2+} or Ba^{2+}) and it does so in micromolar concentrations (Zimmerberg, Cohen et al. 1980b). This indicates that the effect of calcium ions on vesicle fusion events arise from protein interactions rather than lipid interactions. This also fits well with the mechanism of biological exocytosis, where the soluble *N*-ethylmaleimide sensitive factor attachment receptor (SNARE) protein complexes dock the vesicles to the plasma membrane, and a subsequent influx of Ca^{2+} triggers vesicle fusion (Jeremic et al. 2004; Ungermann and Langosch 2005; Carr and Munson 2007). However, although Ca^{2+} has an important role in biological membrane fusion, it may not necessarily be beneficial to include Ca^{2+}, or other divalent cations, for that matter in model membrane systems. In this relation, Woodbury (1999) describes that the vesicles may clump or fuse together prior to reaching the planar membrane, leading to suboptimal fusion conditions (Woodbury 1999). Indeed, we also noticed in our laboratory that Ca^{2+} does not necessarily stimulate vesicle fusion to planar membranes. In support of Woodbury (1999) we also find that Ca^{2+} appears to result in vesicle-vesicle fusions and formation of vesicle aggregation before reaching the planar membrane. That this is the case may be evidenced by dynamic light scattering measurements (Table 2). It is likely that these larger fused vesicle or vesicle aggregates looses the ability to fuse with the established planar membrane. Therefore, it is recommended to carefully test and evaluate whether including Ca^{2+} in model membrane systems are beneficial for stimulating fusion events of the model membrane system in question.

10

Poly(ethylene gycol) (PEG) has been described to stimulate vesicle-vesicle fusion (Lentz 1994; Lee and Lentz 1997). Stimulation of vesicle-bilayer fusion events have not been described in the literature. Like $CaCl_2$ we observed that the presence of PEG in the buffer stimulated vesicle–vesicle fusion events (Table 2). Again, it is likely that these larger fused vesicle or vesicle aggregates looses the ability to fuse with the established planar membrane. In relation to this it has been described that PEG–mediated vesicle fusion is favored by lipid bilayer curvature (Lentz 1994). Moreover, in vesicle–lipid bilayer fusions the buffer viscosity due to the high PEG concentration (17.5 wt%) may pose a problem.

Table 2. Dynamic light scattering measurements of initially 200 nm extruded lipid vesicles under various buffer conditions.

Solution outside vesicles	Vesicle size	PDI
Phosphate buffered saline (PBS)	137 ± 2	0.11
300 mM KCl, PBS	134 ± 0	0.09
10 mM $CaCl_2$, PBS	8253 ± 469	0.63
10 mM $CaCl_2$, 300 mM KCl, PBS	4952 ± 2097	1.00
17.5 wt% PEG(6000), PBS	1015 ± 79	0.28

Vesicles consisted of POPE:POPC:POPS:Ergosterol (2:1:1:1). Results are n = 3 measurements ± standard deviation. PDI is the polydispersity index, where in this case a value of 0 represents a monodisperse, while a value of 1 indicates a completely polydisperse solution. (Ibragimova and Rein unpublished results).

Magnetic stirring of the model membrane system may be important to keep a continuous motion of the vesicles in the chamber (Woodbury 1999). This may increase the likelihood that vesicles come so close to the planar membrane that they can interact and fuse with the planar membrane.

The buoyancy of vesicles may possess a problem for obtaining optimal fusion efficiency with the planar membrane. In biological exocytosis docking of the vesicles to the plasma membrane is a crucial step for fusion, which is mediated by SNARE proteins (Carr and Munson 2007). In model membrane systems, we usually do not have SNAREs, but what we can do is altering the vesicle density. The vesicle density may be increased to ensure that the vesicles sink down on to the planar membrane, thereby ensuring close proximity of the vesicles with the membrane. In principle this should be able to increase the likelihood for membrane fusion. In practice, increasing the density of vesicles may be created by encapsulating 200–300 mM of a sugar, preferably a membrane impermeant sugar such as sorbitol or mannitol, inside the vesicles. This may be done by i) creating the vesicles in a sugar containing buffer and ii) removing the sugar outside the vesicles. Removal of sugar outside the vesicles may essentially be done by the techniques briefly mentioned in section 13.2.1 for removal of detergent during protein reconstitution into vesicles.

A factor that may also be considered for optimizing the fusion efficiency of proteoliposomes with planar membranes is the LPR of the proteoliposomes. We have found that the LPR may affect the fusion efficiency of *F. nucleatum* outer membrane porin A (FomA) with planar membranes in a LPR dependent manner. Our results demonstrate that fusion events with planar membranes are significantly increased with decreasing LPR (200 to 50) with maximal fusion efficiency at LPR 50 (Fig. 1). However, with LPR 25 fusion events ceases and become comparable to LPR 200. The theoretical proteoliposome coverage with FomA porins is 18% to 31%, 47% and 68% for LPR values 200, 100, 50 and 25, respectively. Clearly something happens with fusion efficiency between LPR 50 and 25, but exactly what causes the fusion efficiency to decrease is difficult to address. It may be that 68% protein coverage in the proteoliposomes is too high and this may cause or stimulate protein aggregation rather than functional protein reconstitution.
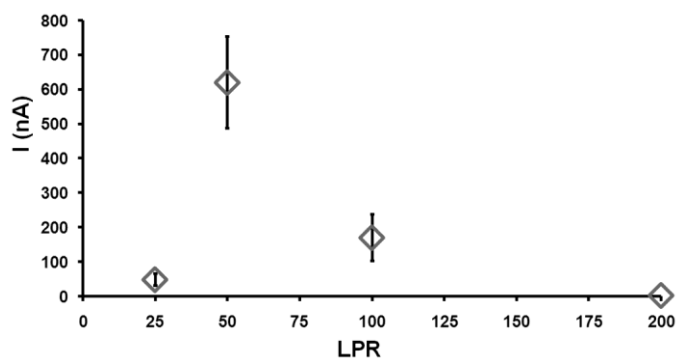
Fig. 1. Dependence of LPR on FomA proteoliposomes fusion with planar lipid membrane arryas. Planar lipid bilayers arrays were established as described by (Hansen, Perry et al. 2009a).

The fusion efficiency of vesicles with planar membranes is influenced by numerous factors as discussed in this section. Clearly creating an osmotic gradient across the established lipid bilayers and having magnetic stirring in the model membrane chamber design are likely the most important parameters for getting started with model membrane vesicle fusion experiments. Subsequently, factors such as including divalent cations in the model membrane buffers, increase vesicle density or adjusting the LPR may be considered to achieve optimal vesicle fusion efficiency.

13.3.2 Addressing vesicle fusion events with planar membranes

How do we address the vesicle fusion efficiency in our model membrane system? Vesicle fusion with planar membranes is characterized by i) the transfer of vesicular contents across the planar membrane to the *trans* chamber side and ii) the incorporation of vesicular membrane with the planar membrane (Zimmerberg, Cohen et al. 1980b). These two criteria may be utilized to create sensor systems for assessing the degree of vesicle fusion events with planar membranes.

To utilize i) vesicles may be loaded with a fluorescent dye, which upon fusion with the planar membrane is released to the *trans* chamber and following may be quantified (e.g. by fluorescence spectroscopy or microscopy). The water soluble impermeant dye calcein is often used for these purposes. A good feature of calcein is that its fluorescence emission can be quenched, either by self–quenching at high concentrations ($\geq$ 6 mM) or by cobalt ions. Self–quenching may be utilized by encapsulating millimolar calcein concentrations in vesicles, resulting in a low fluorescence emission yield. Upon fusion with the planar membrane calcein is released and diluted, resulting in a high fluorescence emission yield (Perin and MacDonald 1989). To utilize calcein quenching by cobalt ions, the vesicles may be encapsulated with a micromolar calcein concentration, while having cobalt ions in the *trans* chamber buffer. Upon fusion of the calcein–cobalt loaded vesicles the vesicular content is released. Cobalt effectively chelates the released calcein and quenches the fluorescence signal (Niles and Cohen 1987; Woodbury and Hall 1988a; Woodbury and Hall 1988b). Alternatively, ethylenediaminetetraacetic acid (EDTA) which is a divalent cation chelating agent may be applied to chelate cobalt. The assay could then be designed to encapsulate saturating amounts of cobalt with calcein to create fluorescently quenched calcein–cobalt complexes in vesicles (Kendall and MacDonald 1982). Having included EDTA in the *trans* chamber buffer, results in chelation of cobalt upon release of the calcein–cobalt complexes by vesicle fusion, yielding fluorescent calcein (Kendall and MacDonald 1982).

There are several ways to utilize ii) the incorporation of vesicular membrane with the planar membrane upon membrane fusion:

- *Fluorescent tracer fusion assay*. Fluorescence may be used to label the receiving planar lipid membrane, say green fluorescence, while having a different fluorescence label, say red fluorescence, of the lipid vesicles or a labeled protein reconstituted into the fusiogenic vesicles. In this case vesicle fusion will result in incorporation of the red fluorescent dye of the vesicles or of the labeled proteins reconstituted in the vesicles, respectively, into the planar fluorescently green membrane (Ganesan and Boxer 2009).

- *Nystatin/ergosterol fusion activity assay*. The Nystatin/ergosterol (N/E) fusion activity assay is a very neat way to assess vesicle fusion activity (Woodbury and Miller 1990). Nystatin is a pore–forming antibiotic, which binds to ergosterol and when the ergosterol concentration is high enough, 10 nystatin monomers associate to form a membrane pore (Woodbury 1999). If vesicles are prepared to include both nystatin and ergosterol, the nystatin molecules form functional pores in the lipid vesicles. When the N/E vesicles fuse with the planar membrane functional nystatin pores is being transferred to the planar membrane. The nystatin pore conductance can be measured shortly, because the ergosterol will diffuse into the planar membrane, which in turn causes the nystatin to dissociate into monomers and the nystatin becomes nonfunctional (Woodbury and Miller 1990). In conductance measurements the fusion event of N/E vesicles will be seen as a "current spike" in voltage clamp measurements (Fig 2A). The number of "spikes" per time can be seen a measure of fusion efficiency. The advantage of this assay is that it can co-include a membrane protein of interest (Woodbury 1999; Zagnoni, Sandison et al. 2007). Since the nystatin becomes nonfunctional upon fusion to the planar membrane most measurements of reconstituted membrane protein using N/E vesicles will not be affected by the presence of nystatin. A disadvantage may be that care has to be taken for interpretation of the N/E fusion events, since it can be hampered by air bubbles that may arise during formation of the planar membrane. If an entrapped air bubble burst in the membrane this may be misinterpreted as a fusion event (our unpublished data). Another disadvantage may also be that the amount of molecules loaded into the planar membrane cannot be directly determined – it only shows if fusion has taken place. To get started with the vesicle N/E fusion activity assay we recommend reading the review by Dixon J. Woodbury (1999) on this topic (Woodbury 1999)

- *Outer membrane porin fusion efficiency assay*. A reporter membrane protein may be used to address the amount of protein that can be reconstituted into a model membrane system with vesicle fusion. As stated in the beginning of section 13.3 several *E. coli* outer membrane porins may be reconstituted into planar membranes directly from a detergent solubilized state. However, they may also be reconstituted into vesicles. Many of these β–barrel proteins have a specific conductance that is well–characterized. Thus, outer membrane porin proteoliposomes may conveniently be used to address fusion efficiency with a model membrane system. The voltage dependent anion channel (VDAC) has in the literature been used as a reporter for vesicle fusion activity with planar membranes (Cohen, Zimmerberg et al. 1980). In our laboratory we use the trimeric *Fusobacterium nucleatum* outer membrane protein A (FomA) as reporter for vesicle fusion efficiency with planar membranes (Fig 2B). In the following we use FomA as example. In voltage clamp measurements FomA porin has a single channel current value of approximately 15 pA in 1.0 M KCl saline solution with an applied potential of ±60 mV (Kleivdal et al. 1995; Pocanschi, Apell et al. 2006). Thus, reconstitution of a single functional FomA porin gives rise to a current increase of approximately 15 pA (Fig 3B). Incorporation of multiple FomA porins is seen as a "lad-

der–like" increase in the current trace (Fig 2B). Since the current value for a single functional FomA porin is known (15 pA) we can calculate how many porins that reconstituted with the planar model membrane during vesicle fusion. For further details about voltage clamp measurements we refer to Perry *et al.* 2009 (Perry et al. 2009).
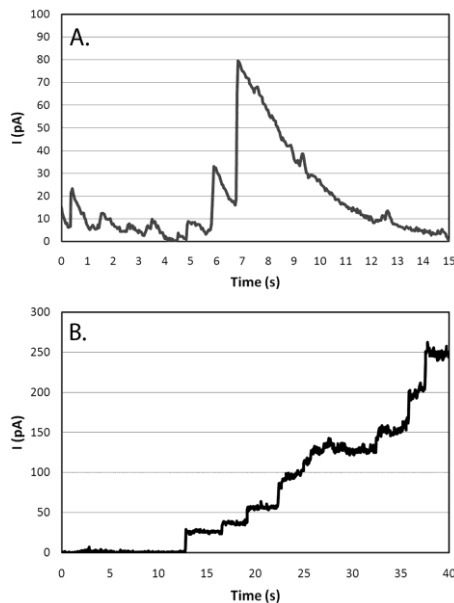

Fig. 2. Vesicle fusion with N/E vesicles and FomA proteoliposomes. A) Current trace of N/E vesicle fusion activity. B) Current trace of FomA proteoliposomes vesicle fusion. Measurements were carried out using voltage clamp technique.

In summary, transfer of vesicular content following vesicle fusion may be used a measure of whether vesicle fusion takes place. The fluorescence calcein assay is an example of a way to address vesicle fusion by measuring the amount of fluorescent molecules released to the *trans* chamber side. Fluorescence may also be utilized to address transfer of vesicular membrane to the planar membrane, which occurs during membrane fusion. Fluorescent labels may be positioned in the membranes and/or on the membrane protein of interest. Voltage clamp measurements of fusion of N/E vesicles with planar membranes may be utilized to address vesicle fusion activity, whereas reconstitution of outer membrane porin may be used to address vesicle fusion efficiency.

13.3.3 Direct incorporation into planar membranes

A novel strategy for reconstituting membrane proteins into planar membranes is by direct incorporation, which refers to reconstitution of membrane proteins simultaneously with establishing the planar model membrane. Although, a general methodology for direct reconstitution would potentially revolutionize the field of biomimetic membrane research, only a few reports have dealt with the topic of direct reconstitution. Here we will describe the practical approach of direct incorporation described for bacteriorhodopsin (BR) and the nicotinic acetylcholine receptor, respectively, and use these examples to discuss some of the considerations and concerns of this strategy of reconstituting membrane proteins.

A clear advantage of the direct incorporation approach is that the LPR, and thereby also the amount of the protein reconstituted into the model membrane, may be precisely controlled. The ability to incorporate large quantities of protein into model membranes may especially be important for using planar protein-based biomimetic membranes for separation techniques, such as water purification through aquaporin water channel-based biomimetic membranes (Nielsen 2009).

Bamberg *et al.* (1981) reported successful direct reconstitution of the proton-pump BR from a proteo–lipid solvent–containing solution (Bamberg et al. 1981). The approach was to solubilize BR purple membranes in an aqueous solution and then transfer the protein into an asolectin/n–alkane (e.g. n–decane) lipid bilayer forming solution. The methodology was to add 100 μL of the BR solution (10 mg/ml) to a 1 mL asolectin/n–decane solution (50 mg/mL). The sample was then sonicated and the suspension was subsequently added successive aliquots of $CaCl_2$ (100 μL, 0.1 M) until a clear purple BR apolar phase developed. The clear purple apolar phase was then used to successfully create a BR–based lipid bilayer membrane while maintaining the functionality of the protein (Bamberg, Dencher et al. 1981). It should be noted however, that BR as lyophilized purple membranes can be solubilized in aqueous solutions without the use of detergent. This makes BR a somewhat special case that is not general for most other membrane proteins.

Beddow *et al.* (2004) reported a similar approach to functionally reconstitute nicotinic acetylcholine receptors into lipid bilayer model membranes (Beddow et al. 2004). The main differences were that the bilayer forming solution consisted of glycerol monooleate and n–hexane, the receptor extracts were prepared as vesicles and the bilayer forming solution was emulsified with receptor extract without using $CaCl_2$ (Beddow, Peterson et al. 2004).

Membrane proteins are generally delicate structures, especially α–helical proteins whereas β–barrel proteins often are somewhat more stable (Bowie 2001). A concern for the transfer of membrane protein to a solvent containing lipid phase is

that the protein structure and function will be affected by the solvent. Several reports have described that membrane proteins can be extracted in a functional state by harsh solvents such as diethyl ether, toluene or chloroform/methanol/water mixtures (Ayala et al. 1985; Ayala et al. 1986; Reiken et al. 1996; Dmitriev et al. 2004). However, it is difficult to predict the long term effects of solvent exposure on protein structure and function. In this context protein functionality has been shown to be affected considerably by solvent exposure and to decrease in a time-dependent manner (Ayala, Nascimento et al. 1985; Beddow, Peterson et al. 2004).

To circumvent the potential deleterious effects of solvent on membrane protein structure and function it may be considered to use a less harmful solvent in the bilayer forming solution. Solventless bilayer forming solutions using squalene, a naturally derived oil, as substitute for *n*-alkanes have been described for formation of planar lipid bilayers (White 1978).

A major issue to be solved for creating a successful general formulation for direct protein incorporation is to make an amphiphilic bilayer forming solution that is sufficiently polar to shield and protect the hydrophilic residues of membrane proteins, while at the same time being hydrophobic enough to make a homogeneous solution that can shield the hydrophobic membrane protein regions and that can support lipid bilayer formation (Fig. 3). In section 13.2.2 we discussed considerations of hydrophobic matching lipid species to the protein hydrophobic regions for protein reconstitution in vesicles. The same considerations also apply for matching the hydrophobic regions of the protein in a direct protein incorporation formulation.

A likely more demanding challenge is to create an amphiphilic bilayer forming solution that sufficient shield the hydrophilic protein regions, since the extent of the hydrophilic regions varies considerably among membrane proteins (Fig. 3).

For direct protein incorporation it would be advantageous to be able to transfer the protein directly from a detergent–solublized state to the bilayer forming solution. This may be carried out by the use of hydrophobic absorption polymer beads (such as Bio–Beads SM absorbents or similar). In this approach an appropriate amount of the absorption beads (e.g. matching the amount of detergent to be removed) is included to the protein/lipid/solvent dispersion. By placing the protein-lipid dispersion with bio–beads end–over–end rotation at 4°C over night the protein is transferred to the apolar phase while removing the detergent. Using this approach we have been able to create lipid bilayers reconstituted with spinach aquaporin SoPIP2;1 (our unpublished results). If the detergent was not sufficiently removed during the described procedure it would not be possible to create sealed lipid bilayers.

Direct protein incorporation would be a powerful tool to reconstitute large quantities of membrane protein into model membranes. In this light it is surprising that there are still very limited reports on this subject. Major contributions to biomimetic membrane research may be envisaged provided that attention is directed towards the topic of direct protein incorporation.
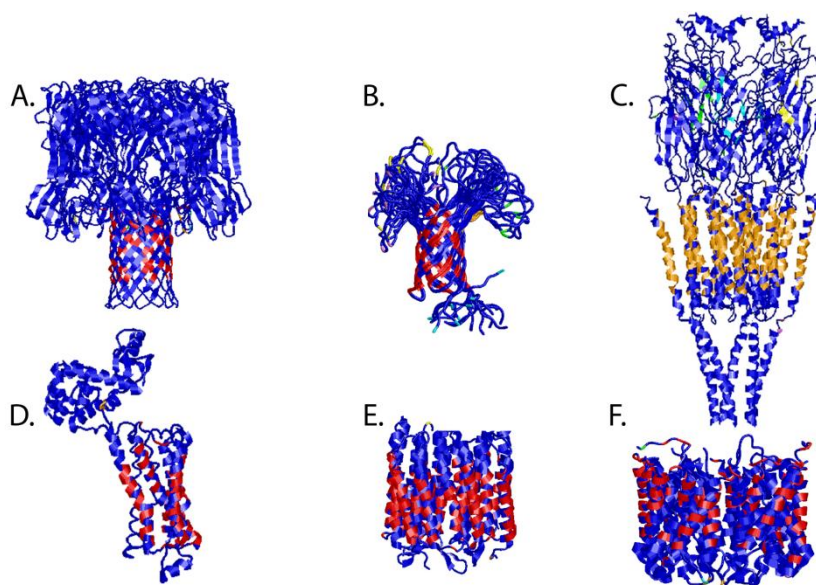
Fig. 3. Hydrophobic and hydrophilic regions of membrane protein surfaces. The extracellular domains of membrane proteins vary. Examples shown are A. α-hemolysin, B. outer membrane porin A (OmpA), C. Nicotinic acetylcholine receptor, D. human B$_2$-adrenergic G-protein coupled receptor, E. Bacteriorhodopsin and F. Spinach aquaporin SoPIP2;1. Analysis of lipid interaction patches (hydrophobicity) was carried out using HotPatch statistical analysis. It is an algorithm-based program for the analysis of protein surface patches (Pettit et al. 2007). Identified (individual) hydrophobic protein surface patches are shown as red, orange, yellow and green, respectively, while blue correspond to hydrophilic surface regions.

13.4 Requirements for protein reconstitution yield

The planar membrane design for protein reconstitution may be suitable for sensor and separation technologies. The protein reconstitution yield into model membrane is almost never addressed, but it makes good sense to include protein reconstitution yield as a biomimetic membrane design criteria. The requirements of the amount of protein to be reconstituted for the different applications may not be the same. Considerations of the protein reconstitution methodology to apply may therefore be of importance in the design criteria for the biomimetic

membrane application in question. For sensor applications the reconstitution yield may not be that important per se, instead it may be more important to have an optimized reliable and reproducible protein reconstitution protocol. Sensitive sensor designs may be created with a reasonable low amount of functionally reconstituted protein. Here vesicle fusion with planar membranes may be considered as a first choice reconstitution method.

The maximum protein reconstitution yield that can be reached with vesicle fusion is rather low. Using the outer membrane porin fusion efficiency assay, Cohen *et al*. (1980) showed that the fusion efficiency that could be reached was approximately 513 porin insertions in 10 min into a single bilayer suspended across a $1–mm^2$ aperture (Cohen, Zimmerberg et al. 1980). We have addressed the maximum vesicle fusion efficiency of a membrane array consisting of 8×8 apertures with an average aperture diameter of 300 μm. Here the maximal fusion efficiency was approx. 147,600 porin insertions during the vesicle fusion experiment. Although this sounds as a high number of protein insertions it only corresponds to approximately 0.003 ‰ of the total effective membrane area. While this protein reconstitution yield may be sufficient for designing sensor based assays, it is clearly insufficient to create novel separation technologies based on membrane proteins. Alternative methods for reconstitution membrane proteins in high yield need to be sought. Direct protein reconstitution may be the novel strategy to consider for obtaining a high protein reconstitution yield into biomimetic membranes. Since the protein and lipid are simultaneously included in a combined bilayer forming solution prior to establishing the biomimetic membranes it may be possible to control the LPR. Thereby it should also be possible to control the amount of protein reconstituted into biomimetic membranes per se.

13.5 Perspectives

To summarize, the following key elements in protein reconstitution should be considered to create novel sensor and separation technologies based on membrane proteins:

- Protein reconstitution into vesicles is the conventional strategy in membrane protein biomimetic designs.
- Proteoliposomes may be applied directly in protein analytical methods or may be further used to reconstitute membrane proteins into planar membrane designs.
- Fluorescence assays, N/E vesicle fusion activity assay or outer membrane porin fusion efficiency assay may be applied to evaluate and optimize protein reconstitution into planar model membranes.
- Direct membrane protein reconstitution may represent a novel strategy to reconstitute large amounts of protein into planar model membranes.

- In both conventional and novel protein reconstitution strategies the LPR and hydrophobic matching of the protein hydrohopbic regions to the model membrane hydrophobic regions are crucial considerations for optimal and functional protein reconstitution.
- Reconstitution yield should be included as a biomimetic membrane design criteria.
- Proteoliposomes fusion with planar membrane may be applied for the creation of novel protein biosensor and drug–screening applications.
- Proteoliposomes fusion efficiency is likely insufficient to support fabrication of large scale separation technologies based on membrane protein function. Here alternative protein reconstitution strategies need to be explored. Direct protein reconstitution may be a promising approach; albeit technical advances in this protein reconstitution strategy is required.

20

References

Angelova, M. I., et al. (1992). "Preparation of giant vesicles by external AC electric fields. Kinetics and applications." <u>Prog. Colloid. Polym. Sci.</u> **89**: 127-131.

Arora, A., et al. (2000). "Refolded outer membrane protein A of Escherichia coli forms ion channels with two conductance states in planar lipid bilayers." <u>J Biol Chem</u> **275**(3): 1594-600.

Ayala, G., et al. (1986). "Thermostability of membrane systems in organic solvents." <u>FEBS Lett</u> **203**(1): 41-3.

Ayala, G., et al. (1985). "Extraction of mitochondrial membrane proteins into organic solvents in a functional state." <u>Biochim Biophys Acta</u> **810**(2): 115-22.

Bamberg, E., et al. (1981). "Transmembranous incorporation of photoelectrically active bacteriorhodopsin in planar lipid bilayers." <u>Proc Natl Acad Sci U S A</u> **78**(12): 7502-6.

Beddow, J. A., et al. (2004). "Reconstitution of nicotinic acetylcholine receptors into gel-protected lipid membranes." <u>Anal Chem</u> **76**(8): 2261-5.

Booth, P. J. (2005). "Sane in the membrane: designing systems to modulate membrane proteins." <u>Curr Opin Struct Biol</u> **15**(4): 435-40.

Buzhynskyy, N., et al. (2007a). "Human cataract lens membrane at subnanometer resolution." <u>J Mol Biol</u> **374**(1): 162-9.

Buzhynskyy, N., et al. (2007b). "The supramolecular architecture of junctional microdomains in native lens membranes." <u>EMBO Rep</u> **8**(1): 51-5.

Carr, C. M. and M. Munson (2007). "Tag team action at the synapse." <u>EMBO Rep</u> **8**(9): 834-8.

Castellana, E. T. and P. S. Cremer (2006). "Solid supported lipid bilayers: From biophysical studies to sensor design." <u>Surface Science Reports</u> **61**(10): 429-444.

Cohen, F. S., et al. (1982). "Osmotic swelling of phospholipid vesicles causes them to fuse with a planar phospholipid bilayer membrane." <u>Science</u> **217**(4558): 458-60.

Cohen, F. S., et al. (1980). "Fusion of phospholipid vesicles with planar phospholipid bilayer membranes. II. Incorporation of a vesicular membrane marker into the planar membrane." J Gen Physiol **75**(3): 251-70.

Curstedt, T., et al. (1988). "Low-molecular-mass surfactant protein type 1. The primary structure of a hydrophobic 8-kDa polypeptide with eight half-cystine residues." Eur J Biochem **172**(3): 521-5.

Deamer, D. W. and P. S. Uster (1983). Liposome Preparation: Methods and Mechanism. . Liposomes. E. M.J. Ostro. New York, Marcel Dekker**:** 27-51.

Dmitriev, O. Y., et al. (2004). "Subunit A of the E. coli ATP synthase: reconstitution and high resolution NMR with protein purified in a mixed polarity solvent." FEBS Lett **556**(1-3): 35-8.

Fang, Y., et al. (2002). "Membrane protein microarrays." J Am Chem Soc **124**(11): 2394-5.

Fang, Y., et al. (2006). "Applications of biomembranes in drug discovery." MRS bulletin **31**(7): 5.

Fang, Y., et al. (2003). "G protein-coupled receptor microarrays for drug discovery." Drug Discov Today **8**(16): 755-61.

Feitosa, E., et al. (2000). "Phase transition in dioctadecyldimethylammonium bromide and chloride vesicles prepared by different methods." Chem Phys Lipids **105**(2): 201-13.

Fendler, H. (1987). "Atomic and molecular clusters in membrane mimetic chemistry." Chem. Rev. **87**: 877-899.

Furber, K. L., et al. (2009). "Identifying critical components of native Ca2+-triggered membrane fusion. Integrating studies of proteins and lipids." Ann N Y Acad Sci **1152**: 121-34.

Gabriel, N. E. and M. F. Roberts (1984). "Spontaneous formation of stable unilamellar vesicles." Biochemistry **23**(18): 4011-5.

Ganesan, P. V. and S. G. Boxer (2009). "A membrane interferometer." Proc Natl Acad Sci U S A **106**(14): 5627-32.

22

Goennenwein, S., et al. (2003). "Functional incorporation of integrins into solid supported membranes on ultrathin films of cellulose: impact on adhesion." Biophys J **85**(1): 646-55.

Hansen, J. S., et al. (2009a). "Large scale biomimetic membrane arrays." Anal Bioanal Chem **395**(3): 719-27.

Hansen, J. S., et al. (2009b). "Development of an automation technique for the establishment of functional lipid bilayer arrays." Journal of Micromechanics and Microengineering **19**(2): 025014.

Hemmler, R., et al. (2005). "Nanopore unitary permeability measured by electrochemical and optical single transporter recording." Biophys J **88**(6): 4000-7.

Hong, H., et al. (2009). "Methods for measuring the thermodynamic stability of membrane proteins." Methods Enzymol **455**: 213-36.

Janshoff, A. and C. Steinem (2006). "Transport across artificial membranes-an analytical perspective." Anal Bioanal Chem **385**(3): 433-51.

Jeremic, A., et al. (2004). "Calcium drives fusion of SNARE-apposed bilayers." Cell Biol Int **28**(1): 19-31.

Joannic, R., et al. (1997). "Monodisperse Vesicles Stabilized by Grafted Polymers." Phys. Rev. Lett. **78**: 3402-3405.

Johansson, J., et al. (1988). "Size and structure of the hydrophobic low molecular weight surfactant-associated polypeptide." Biochemistry **27**(10): 3544-7.

Kendall, D. A. and R. C. MacDonald (1982). "A fluorescence assay to monitor vesicle fusion and lysis." J Biol Chem **257**(23): 13892-5.

Kleivdal, H., et al. (1995). "The Fusobacterium nucleatum major outer-membrane protein (FomA) forms trimeric, water-filled channels in lipid bilayer membranes." Eur J Biochem **233**(1): 310-6.

le Maire, M., et al. (2000). "Interaction of membrane proteins and lipids with solubilizing detergents. ." Biochim. Biophys. Acta Reviews on Biomembranes **1508**: 86-111.

Le Pioufle, B., et al. (2008). "Lipid bilayer microarray for parallel recording of transmembrane ion currents." Anal Chem **80**(1): 328-32.

Lee, J. and B. R. Lentz (1997). "Evolution of lipidic structures during model membrane fusion and the relation of this process to cell membrane fusion." Biochemistry **36**(21): 6251-9.

Lentz, B. R. (1994). "Polymer-induced membrane fusion: potential mechanism and relation to cell fusion events." Chem Phys Lipids **73**(1-2): 91-106.

Lorenceau, E., et al. (2005). "Generation of polymerosomes from double-emulsions." Langmuir **21**(20): 9183-6.

Maguire, L. A., et al. (2003). "Preparation of small unilamellar vesicles (SUV) and biophysical characterization of their complexes with poly-l-lysine-condensed plasmid DNA." Biotechnol Appl Biochem **37**(Pt 1): 73-81.

Majd, S. and M. Mayer (2008). "Generating arrays with high content and minimal consumption of functional membrane proteins." J Am Chem Soc **130**(47): 16060-4.

Mitra, K., et al. (2004). "Modulation of the bilayer thickness of exocytic pathway membranes by membrane proteins rather than cholesterol." Proc Natl Acad Sci U S A **101**(12): 4083-8.

Montal, M. and P. Mueller (1972). "Formation of bimolecular membranes from lipid monolayers and a study of their electrical properties." Proc Natl Acad Sci U S A **69**(12): 3561-6.

Mouritsen, O. G. and M. J. Zuckermann (2004). "What's so special about cholesterol?" Lipids **39**(11): 1101-13.

Mueller, P. and D. O. Rudin (1969). "Translocators in bimolecular lipid membranes: their role in dissipative and conservative bioenergetic transduction." Curr Topics Bioenergetics **3**: 157–249.

Nielsen, C. H. (2009). "Biomimetic membranes for sensor and separation applications." Anal Bioanal Chem **395**(3): 697-718.

24

Niles, W. D. and F. S. Cohen (1987). "Video fluorescence microscopy studies of phospholipid vesicle fusion with a planar phospholipid membrane. Nature of membrane-membrane interactions and detection of release of contents." J Gen Physiol **90**(5): 703-35.

Ollivon, M., et al. (2000). "Vesicle reconstitution from lipid-detergent mixed micelles." Biochim Biophys Acta **1508**(1-2): 34-50.

Opekarova, M. and W. Tanner (2003). "Specific lipid requirements of membrane proteins--a putative bottleneck in heterologous expression." Biochim Biophys Acta **1610**(1): 11-22.

Osborne, A. R., et al. (2005). "Protein translocation by the Sec61/SecY channel." Annu Rev Cell Dev Biol **21**: 529-50.

Paternostre, M. T., et al. (1988). "Mechanisms of membrane protein insertion into liposomes during reconstitution procedures involving the use of detergents. 1. Solubilization of large unilamellar liposomes (prepared by reverse-phase evaporation) by triton X-100, octyl glucoside, and sodium cholate." Biochemistry **27**(8): 2668-77.

Perin, M. S. and R. C. MacDonald (1989). "Fusion of synaptic vesicle membranes with planar bilayer membranes." Biophys J **55**(5): 973-86.

Perry, M., et al. (2009). "Automated sampling and data processing derived from biomimetic membranes." Bioinspir Biomim **4**(4): 044001.

Petrache, H. I., et al. (2000). "Area per lipid and acyl length distributions in fluid phosphatidylcholines determined by (2)H NMR spectroscopy." Biophys J **79**(6): 3172-92.

Pettit, F. K., et al. (2007). "HotPatch: a statistical approach to finding biologically relevant features on protein surfaces." J Mol Biol **369**(3): 863-79.

Pocanschi, C. L., et al. (2006). "The major outer membrane protein of Fusobacterium nucleatum (FomA) folds and inserts into lipid bilayers via parallel folding pathways." J Mol Biol **355**(3): 548-61.

Rastogi, R., et al. (2009). "Flexible polymerosomes--an alternative vehicle for topical delivery." Colloids Surf B Biointerfaces **72**(1): 161-6.

Rawicz, W., et al. (2000). "Effect of chain length and unsaturation on elasticity of lipid bilayers." Biophys J **79**(1): 328-39.

Reiken, S. R., et al. (1996). "Bispecific antibody modification of nicotinic acetylcholine receptors for biosensing." Biosens Bioelectron **11**(1-2): 91-102.

Rigaud, J. L., et al. (1988). "Mechanisms of membrane protein insertion into liposomes during reconstitution procedures involving the use of detergents. 2. Incorporation of the light-driven proton pump bacteriorhodopsin." Biochemistry **27**: 2677-2688.

Rosenkranz, T., et al. (2009). "Observing proteins as single molecules encapsulated in surface-tethered polymeric nanocontainers." Chembiochem **10**(4): 702-9.

Samatey, F. A., et al. (1995). "On the distribution of amino acid residues in transmembrane alpha-helix bundles." Proc Natl Acad Sci U S A **92**(10): 4577-81.

Schmitt, E. K., et al. (2006). "Channel activity of OmpF monitored in nano-BLMs." Biophys J **91**(6): 2163-71.

Seddon, A. M., et al. (2004). "Membrane proteins, lipids and detergents: not just a soap opera." Biochim Biophys Acta **1666**(1-2): 105-17.

Silvius, J. R. (1992). "Solubilization and functional reconstitution of biomembrane components." Annu Rev Biophys Biomol Struct **21**: 323-48.

Singer, M. A., et al. (1990). "The formation of multilamellar vesicles from saturated phosphatidylcholines and phosphatidylethanolamines: morphology and quasi-elastic light scattering measurements." Chem Phys Lipids **54**(2): 131-46.

Suzuki, H., et al. (2009). "Ninety-six-well planar lipid bilayer chip for ion channel recording fabricated by hybrid stereolithography." Biomed Microdevices **11**(1): 17-22.

Suzuki, H., et al. (2007). "Electrophysiological recordings of single ion channels in planar lipid bilayers using a polymethyl methacrylate microfluidic chip." Biosens Bioelectron **22**(6): 1111-5.

26

Szoka, F., Jr. and D. Papahadjopoulos (1980). "Comparative properties and methods of preparation of lipid vesicles (liposomes)." Annu Rev Biophys Bioeng **9**: 467-508.

Tornroth-Horsefield, S., et al. (2006). "Structural mechanism of plant aquaporin gating." Nature **439**(7077): 688-94.

Ungermann, C. and D. Langosch (2005). "Functions of SNAREs in intracellular membrane fusion and lipid bilayer mixing." J Cell Sci **118**(Pt 17): 3819-28.

Van den Berg, B., et al. (2004). "X-ray structure of a protein-conducting channel." Nature **427**(6969): 36-44.

White, S. H. (1978). "Formation of "solvent-free" black lipid bilayer membranes from glyceryl monooleate dispersed in squalene." Biophys J **23**(3): 337-47.

Wilburn, J. P., et al. (2006). "Imaging of voltage-gated alamethicin pores in a reconstituted bilayer lipid membrane via scanning electrochemical microscopy." Analyst **131**(2): 311-6.

Woodbury, D. J. (1999). "Nystatin/ergosterol method for reconstituting ion channels into planar lipid bilayers." Methods Enzymol **294**: 319-39.

Woodbury, D. J. and J. E. Hall (1988a). "Role of channels in the fusion of vesicles with a planar bilayer." Biophys J **54**(6): 1053-63.

Woodbury, D. J. and J. E. Hall (1988b). "Vesicle-membrane fusion. Observation of simultaneous membrane incorporation and content release." Biophys J **54**(2): 345-9.

Woodbury, D. J. and C. Miller (1990). "Nystatin-induced liposome fusion. A versatile approach to ion channel reconstitution into planar bilayers." Biophys J **58**(4): 833-9.

Yoshikawa, W., et al. (1983). "Light-scaterring properties of osmotically active liposomes." Biochim. Biophys. Acta **735**: 397-406.

Zagnoni, M., et al. (2007). "Controlled delivery of proteins into bilayer lipid membranes on chip." Lab Chip **7**(9): 1176-83.

Zimmerberg, J., et al. (1980a). "Fusion of phospholipid vesicles with planar phospholipid bilayer membranes. I. Discharge of vesicular contents across the planar membrane." J Gen Physiol **75**(3): 241-50.

Zimmerberg, J., et al. (1980b). "Micromolar Ca^{2+} Stimulates Fusion of Lipid Vesicles with Planar Bilayers Containing a Calcium-Binding Protein." Science **210**(4472): 906-908.

Chapter 3

Biomimetic membrane arrays

Contents

3.1 Development of an automation technique for the establishment of functional lipid bilayer arrays

Development of an automation technique for the establishment of functional lipid bilayer arrays

J S Hansen[1,2,5]**, M Perry**[2,5]**, J Vogel**[1,2]**, T Vissing**[2]**, C R Hansen**[2,3]**,
O Geschke**[1]**, J Emnéus**[1] **and C H Nielsen**[1,4,6]

[1] DTU Nanotech, Technical University of Denmark, DK-2800 Kgs. Lyngby, Denmark
[2] Aquaporin A/S, Diplomvej 377, DK-2800 Kgs. Lyngby, Denmark
[3] Nano-Science Center, Copenhagen University, DK-2100, Copenhagen, Denmark
[4] Quantum Protein Centre, Technical University of Denmark, DK-2800 Kgs. Lyngby, Denmark

E-mail: Claus.Nielsen@fysik.dtu.dk

Abstract

In the present work, a technique for establishing multiple black lipid membranes (BLMs) in arrays of micro structured ethylene tetrafluoroethylene (ETFE) films, and supported by a micro porous material was developed. Rectangular 8×8 arrays with apertures having diameters of $301 \pm 5\ \mu$m were fabricated in ETFE Teflon film by laser ablation using a carbon dioxide laser. Multiple lipid membranes could be formed across the micro structured 8×8 array ETFE partitions. Success rates for the establishment of cellulose-supported BLMs across the multiple aperture arrays were above 95%. However, the time course of the membrane thinning process was found to vary considerably between multiple aperture bilayer experiments. An airbrush partition pretreatment technique was developed to increase the reproducibility of the multiple lipid bilayers formation during the time course from the establishment of the lipid membranes to the formation of bilayers. The results showed that multiple lipid bilayers could be reproducible formed across the airbrush-pretreated 8×8 rectangular arrays. The ionophoric peptide valinomycin was incorporated into established membrane arrays, resulting in ionic currents that could be effectively blocked by tetraethylammonium. This shows that functional bimolecular lipid membranes were established, and furthermore outlines that the established lipid membrane arrays could host functional membrane-spanning molecules.

(Some figures in this article are in colour only in the electronic version)

Abbreviations

AFM	atomic force microscopy
BLM	black lipid membrane
DPhPC	1,2-diphytanoyl-*sn*-glycero-3-phosphocholine
ETFE	ethylene tetrafluoroethylene;
NBD-PC	1-Oleoyl-2-[6-[(7-nitro-2–1,3-benzoxadiazol-4-yl)amino]hexanoyl]-*sn*glycero-3-phosphocholine
ROI	region of interest
SEM	scanning electron microscopy
TEA	tetraethylammonium

[5] Shared first authorship.
[6] Author to whom any correspondence should be addressed.

1. Introduction

Artificially made lipid bilayers suited for the insertion of functional molecules, such as ion channel peptides or membrane proteins, have potentials in a diverse range of technical applications, including cell adhesion and ligand–receptor interaction studies [5], screening platforms for drug discovery [9], development of nanobiosensor devices [3, 18], immuno-assays [16] and bioremediation platforms in environmental biology.

1

BLMs are typically formed by painting a solvent containing lipid solution across a hydrophobic partition material (typically Teflon) with an aperture of up to 1 mm in diameter [17], or by the folding technique where solvent-free lipid monolayers of each side of a partition aperture are spread and raised across the aperture (diameters of 50–100 μm) to produce a BLM [15]. Both methods for producing artificial lipid membranes are commonly produced in a single aperture partition separating two Teflon compartments each containing a saline solution.

Although multiple aperture partitions in a hydrophobic partition material can be produced, both the painting and the folding techniques are only useful in the preparation of a BLM in a single aperture or a small number of apertures [11, 19], and they are not straightforward to scale into large aperture arrays. Establishing a folded membrane often requires multiple lowering and raisings of the aqueous solutions, which may compromise the simultaneous formation of membranes across multiple apertures. Formation of painted membranes requires manual painting of the single partition aperture and for this reason the membrane painting technique is not easy to scale into multi-aperture partitions.

Various mechanical fabrication methods for producing a partition having a single aperture have been described previously including micro drilling [4], puncturing the scaffold film with a needle [12], a heated wire [29, 2, 15], or an electrical spark [14]. Of these mechanical aperture production methods, only micro drilling could be suitable for scale up into aperture arrays. However, it is difficult to produce consistently sized and closely positioned apertures using micro drilling. Moreover, micro machined apertures commonly exhibit microscopic burr and groin edges resulting in poor experimental reproducibility.

A soft lithography technique based on casting of amorphous Teflon to create partitions with multiple apertures (up to 15) was described by Mayer *et al* [11]. This technique has the ability to produce precisely positioned and sized (2–800 μm) apertures, but the technique is time intensive with the casting time for the partition being between 4 and 24 h [11].

Recently, UV excimer laser ablation has been described for the fabrication of multiple apertures in thin polycarbonate films (20 μm) and polymethyl methacrylate with aperture diameters of 4–105 μm and 50–100 μm, respectively [23, 19]. Common for the UV excimer laser ablation technique for fabricating multi-array apertures is that the technique is highly reproducible, apertures are precisely positioned, but the UV excimer laser technology is costly and a major drawback is the inability to use Teflon films [19] with this technology. Moreover, excimer lasers are in general slow due to the pulse lasing technique and for this reason are not suited for the fabrication of large aperture arrays.

In the current work, laser ablation was applied to produce ETFE partitions with aperture diameters of 301 $\pm$ 5 μm as 8 $\times$ 8 multiple aperture arrays using a CO_2 laser. Three main criteria made this method to be preferred for the production of a support structure. First, the CO_2 laser is able to ablate Teflon films with different thicknesses (25 μm to above 1 mm) by varying the lasing parameters. Second, the apertures can

be positioned in a precise and controlled manner giving high reproducibility. Third, the CO_2 laser offers a cost efficient and fast production with fabrication times in the range of milliseconds–seconds. Moreover, this technique supports easy scale up [24].

To enable the simultaneous formation of cellulose-supported multiple lipid bilayers in an array, a novel modified painting method was established. We show by voltage clamp experiments that multiple BLMs can be reproducible formed across 64 aperture arrays by this method, and that established membrane arrays are suited for the functional insertion of membrane-spanning molecules.

Our results are discussed in the context of current developments in free-spanning artificial membrane platform technologies.

2. Material and methods

2.1. Materials

Tefzel ethylene tetrafluoroethylene (ETFE) LZ200 for the fabrication of multi-aperture partitions, and Viton A fluoroelastomer for production of rubber chamber sealing O-rings were from DuPont Fluopolymers (Detroit, U.S.A.). Solid Teflon (polytetrafluoroethylene) blocks to the manufacture of the lipid bilayer chambers were supplied by Vink A/S (Randers, Denmark). Sheets of regenerated cellulose (DSS-RC70PP) were purchased from Alfa Laval (Nakskov, Denmark). Round glass cover slips (30 mm) were from VWR—Bie & Berntsen (Herlev, Denmark). The lipids 1,2-diphytanoyl-*sn*-glycero-3-phosphocholine and 1-oleoyl-2- [6-[(7-nitro-2–1, 3-benzoxadiazol-4-yl) amino]hexanoyl]-*sn*-glycero-3-phosphocholine were from Avanti Polar Lipids Inc. (Alabaster, AL, USA). The potassium ion-selective cyclodepsipeptide valinomycin (SIGMA), the channel blocker tetraethylammonium (Fluka) and *n*-decane (Fluka) were purchased from Sigma-Aldrich Denmark (Brøndby, Denmark). All other chemicals were purchased from commercial sources.

2.2. Micro structuring of ETFE membrane scaffold arrays

A Synrad Duo 48–5 S Duo Lase carbon dioxide laser with a specified power output of 50 W (Mulkiteo, WA, USA) and equipped with a 200 mm focal length lens was used to fabricate partitions with rectangular arrayed apertures in ETFE LZ200 film (50.8 μm thickness). The EFTE film was laser ablated into 29 mm diameter discs, where the aperture array was placed in the middle hereof. The apertures within the structure had a distance from center to center of 400 μm. The apertures were produced with an intensity of 4.4 W, a spot lase time (impact time of the beam) of 4 ms and an off vector delay of 1 ms, respectively. The ETFE film was placed in a custom-produced sample holder made of polymethyl methacrylate. A clearance was situated in the middle of this fixture where the lasers beam impact on the sample. Thereby, it was assured that no underlying material interfered with the production process.

2

2.3. Scanning electron microscopy of produced Teflon partitions

The scanning electron microscope (SEM) used was a Jeol JSM 5500 LV SEM from GN Nettest. It is capable of a lateral resolution down to 30–50 nm and a magnification up to ×300 000. The acceleration voltage can be set between 1 and 30 kV. The SEM used has a reproducibility and accuracy in lateral distance measurements better than 5%.

2.4. Atomic force microscopy of produced Teflon partitions

Topographic measurements of the laser-ablated aperture arrays were carried out using atomic force microscopy (AFM). The equipment used was a model: MFP-3D, atomic force microscope (Asylum Research) with an Olympus Silicon Nitride tip (AC240, k ∼2 N m^{-1}) used in tapping mode. The sample used for AFM was an ETFE LZ200 partition with a rectangular 3×3 partition array with 300 μm diameter apertures having a center-to-center distance of 400 μm. The average surface roughness of a region of interest (ROI) was calculated using

$$\mathrm{SD}_{\mathrm{average}} = \frac{1}{V_{\mathrm{ntp}}} \sum_{i=0}^{V_{\mathrm{ntp}-1}} |Y_i - \overline{Y}|,$$

where $\mathrm{SD}_{\mathrm{average}}$ is the average surface deviation of the ROI, V_{ntp} is the total number of pixels of the ROI, Y_i is the height of each pixel and $\overline{Y}$ is the average pixel height.

2.5. The lipid bilayer chamber design

The lipid bilayer chamber design is depicted in figure 1. The complete chamber setup consists of a main Teflon chamber with two axisymmetrically drilled holes having diameters of 20 and 30 mm respectively, a 30 mm diameter cylindrical Teflon tube (5 mm thickness), two 30 mm circular Teflon inter spacers where one has a 2 mm slit, six Viton O-ring seals, two cover slip glasses where one is cut and a brass screw to tighten the bilayer chamber (figure 1(A)). The inner elements consisting of porous regenerated cellulose, micro structured ETFE partition array, Teflon spacers, circular glass cover slips and Viton O-rings (figure 1(B)) fit into the cylindrical 30 mm diameter tube of the *cis* chamber, and rest upon the ledge created by the interface of the *trans* chamber and the cylindrical 20 mm diameter tube of the *cis* chamber (figures 1(A) and (B)). The 5 mm thick cylindrical Teflon tube provides the link to the annular brass screw (perimeter thickness 7 mm) generating sufficient pressure from the exterior of the chamber to obtain a water tight sealing (figure 1(C)). Thus the *cis* and *trans* chambers have identical volumes. A circular, 2 mm thick Teflon spacer with a 2 mm slit is positioned with the opening at the top of the chamber that allows bilayer-forming solutions to enter into the lipid bilayer chamber with a Hamilton syringe (figures 1(A) and (B)).

2.6. Preparation of lipid solution for BLM experiments

The lipid solution for the pre-treatment of ETFE LZ200 partitions (prepainting) and for the bilayer formation consisted
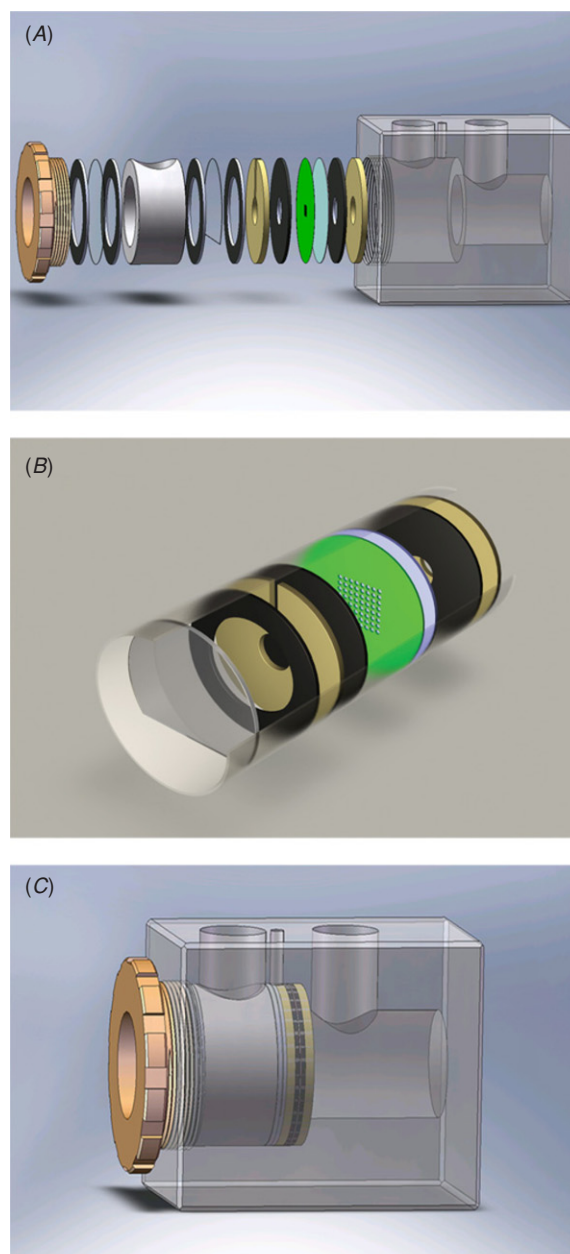
Figure 1. Lipid bilayer chamber design and assembly. (*A*) The assembly of the main Teflon chamber. The component order of the assembly into the main Teflon chamber (grey) is from right to left: a Teflon spacer (tawny), a Viton O-ring (black), a circular cellulose sheet (light blue), an ETFE LZ200 partition (green), a Viton O-ring (black), a Teflon spacer with a slit (tawny), a Viton O-ring (black), a cut glass cover slip (transparent) and another Viton O-ring (black). Following this, a cylindrical Teflon tube (grey) is placed onto the inserted components, and a glass cover slip (transparent) is clamped between two Viton O-rings (black) to create a window for visual inspections into the assembled chamber. Finally, an annular brass screw is used to clamp all of the components to ensure a tight chamber. (*B*) The inner elements of the *cis* chamber. Indicated are the cut glass cover slip (transparent grey), the Teflon spacers (tawny), the Viton O-rings (black), the cellulose support (light blue) and the ETFE partition (green). (*C*) The lipid bilayer chamber fully assembled.

of 1,2-diphytanoyl-*sn*-glycero-3-phosphocholine (DPhPC) in *n*-decane (50 mg ml^{-1}). DPhPC (2 ml) in chloroform

3

(10 mg ml^{-1} stock) was evaporated under nitrogen gas and the dry lipid was resuspended in 400 μL *n*-decane. For fluorescent microscopy the lipid solutions were added 1 mol% of 1-oleoyl-2-[6-[(7-nitro-2–1,3-benzoxadiazol-4-yl)amino]hexanoyl]-*sn*-glycero-3-phosphocholine (NBD-PC). The lipid solutions were prepared the day before, and stored at −20 °C until use.

2.7. Partition pretreatment

The prepainting of ETFE partitions was carried out by the addition of approximately 2 μL of prepainting solution using a glass Pasteur pipette to both sides of the ETFE partition. The ETFE partitions were left to dry for 10 min followed by applying a gentle stream of nitrogen gas to both sides of the partition to ensure that the apertures were not clogged. The prepainting step was repeated five times, and the pretreated ETFE partitions were stored in a vacuum desiccator for 30 min before use.

Another prepainting strategy was developed to provide a more controlled and uniform deposition of the prepainting solution (50 mg ml^{-1} DPhC in *n*-decane) to the ETFE partition aperture arrays. This was based on airbrushing the prepainting solution onto the ETFE partition sides. The airbrush setup consisted of an airbrush (type: MAS G41, TCPGlobal) pressurized by a nitrogen gas flask, and mounted onto an aluminium track with a ruler. The airbrush was positioned at a distance of 45 mm from the airbrush nozzle to the ETFE partition. The partition was mounted on a perforated brass housing connected to a low-capacity vacuum pump. Partitions were placed on the brass housing and the vacuum applied keeping the partition in position during the prepainting procedure.

The 0.6 ml gravity-fed cup of the airbrush was filled with the prepainting solution (100 μl) and the prepainting solution was deposited onto the ETFE partitions as a fine mist using a nitrogen pressure of 1 bar. The partitions were applied on the prepainting solution on each side for 20 times with 30 s intervals to give a thin uniform coverage of the prepainting solution on the ETFE partitions.

2.8. Fluorescence microscopy

Fluorescent imaging was performed on a Zeiss Axiovert 200 M epifluorescence microscope (Carl Zeiss, Jena, Germany) equipped with a monochrome Deltapix DP450 CCD camera (Deltapix, Maalov, Denmark). The images were acquired using Deltapix DpxView Pro acquisition software (Deltapix, Maalov, Denmark). The objectives used were air corrected Plan-Neofluar 2.5 ×/0.075 Numerical Aperture (NA), 10 ×/0.25 NA and 20 ×/0.40 NA, respectively.

2.9. Formation of BLMs across multi-aperture ETFE partitions

The lipid bilayer chamber was assembled with a 8 × 8 multi-aperture ETFE partition (300 μm diameter apertures, center-to-center distance of 400 μm) and a circular regenerated cellulose sheet (DSS-RC70PP, Alfa Laval). Once assembled,

the ETFE partition was by design located at the center of the circular interface between the *trans* and *cis* chambers (figure 1).

The *trans* and *cis* chambers were filled with 7.5 ml of a saline solution (0.2 M KCl), and the lipid bilayer chamber was then placed in a Faraday cage and the silver/silver chloride electrodes were placed in the electrode wells.

The level in the *cis* chamber was lowered to the beginning of the cut glass cover slip by aspiration of approximately 7 ml of the aqueous electrolyte solution using a plastic Pasteur pipette (figure 2(*A*)). A Hamilton pipette was filled with 100 μl of DPhC in *n*-decane (50 mg/ml), and the bilayer forming solution was applied to the space between the cut cover slip glass and the ETFE partition of the *cis* chamber through the 2 mm slit in the circular Teflon spacer (figure 2(*B*)). The level of the aqueous electrolyte solution in the *cis* chamber was slowly raised by re-adding approximately 7 ml of the saline solution using a plastic Pasteur pipette (figures 2(*C*) and (*D*)). During the raising of the saline solution the formation of BLMs in the partition aperture arrays was recorded by measurements of the capacitance and conductance signals.

2.10. Data acquisition

The experimental setup consisted of a Model 2400 Patch Clamp Amplifier with a head stage containing 10 G/10 M feedback resistors (A–M Systems, Inc., WA, USA) and a Thurlby Thandar Instruments model TG2000 20 MHz DDS function generator (RS Components Ltd, Northants, UK). The electrodes were placed in the *trans* and *cis* compartments of the bilayer formation chamber with the ground electrode positioned in the *trans* compartment. Data acquisition was done with a combined oscilloscope/analog–digital converter (ADC-212/50, Pico Technology, Cambridgeshire, UK) connected to a laptop computer. The sampling frequency was 50 Hz.

Capacitance and conductance measurements were performed by applying 1 Hz triangular (2 Vpp) and rectangular (20 mVpp) voltage clamp wave forms, respectively. Reference measurements of the combined regenerated cellulose and perforated ETFE partition were made prior to the formation of the multiple BLMs. Membrane capacitance ($C = 1/I \cdot dU/dt$) was determined by measuring the peak-to-peak amplitude of the square-shaped response signal, while the membrane conductance ($G = I/U$) was determined from the post-transient steady-state amplitudes. The capacitance and conductance amplitudes were converted into currents using the appropriate head stage conversion factor. The results are given as mean ± SD of a minimum of five experiments for each measurement.

2.11. Incorporation of valinomycin

Valinomycin was dissolved in 96% ethanol to yield a 1.8 mM working solution, which was stored at 4 °C until use. Tetraethylammonium (TEA) working solution (16 mM) was prepared in 0.2 M KCl immediately before use. Valinomycin (1.8 mM) was added (10 μl) to the small chamber volume between the ETFE partition and the first glass cover slip
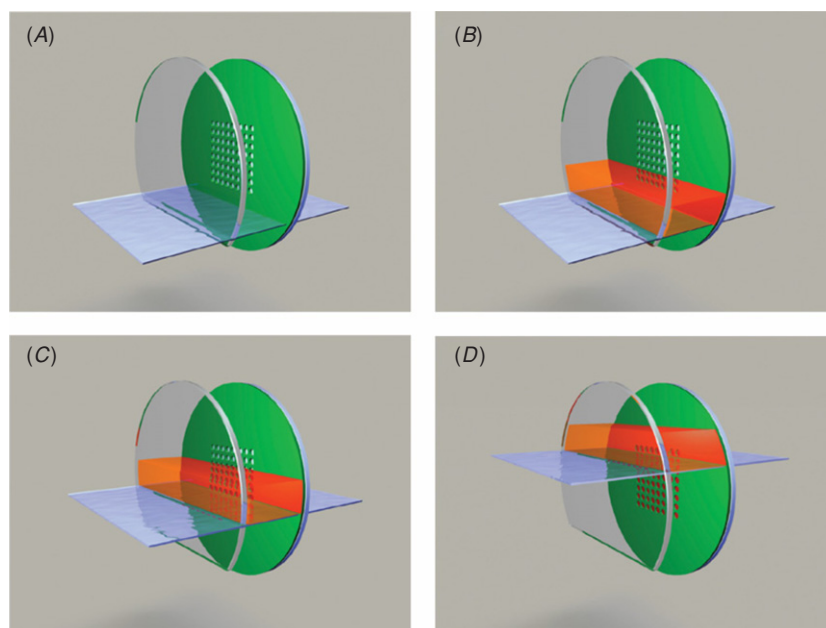
Figure 2. Principle of the automation technique for the establishment of multiple bilayers in the array. The aqueous electrolyte solution (0.2 M KCl) is filled up to the cut glass cover slip (*A*) and the bilayer forming solution (50 mg ml^{-1} DPhPC in *n*-decane) is applied from the top through the slit in the front Teflon spacer (*B*). The aqueous electrolyte solution is then slowly applied to the *cis* chamber thereby raising the bilayer-forming solution across the multiple aperture partition to form an array of lipid bilayers (*C*)–(*D*).

in the chamber setup (volume 0.5 ml). This corresponds to an estimated valinomycin concentration of about 36 μM in close proximity to the membrane array, provided that no diffusion occurs from the small chamber to the rest of the *cis* chamber. Valinomycin incorporation was only performed on multiple BLMs displaying constant membrane characteristics for more than 60 min. To reverse the valinomycin-induced conductance, a TEA working solution was added (200 μl) to the small chamber volume, corresponding to an estimated final concentration of 4.5 mM TEA close to the membrane array.

3. Results

In the following, the development of an automation technique to enable reproducible establishment of multiple bilayers across micro structured membrane scaffolds will be presented.

3.1. CO$_2$ laser-ablated multi-array ETFE partitions

ETFE LZ200 films having a thickness of 50.8 μm were micro structured into partition aperture arrays using a carbon dioxide laser. The arrays consisted of 8×8 apertures with an average diameter of 301 ± 5 μm (number of experiments, $n = 5$), which were positioned in a rectangular array with an aperture center-to-center spacing of 400 μm (figure 3). SEM images of the ETFE partition arrays showed that the apertures were symmetrically positioned with slight elliptical apertures that exhibited nicely rounded edges (figure 3).

To further investigate the topography of the edge of the aperture rims, AFM topographical measurements were carried out (figure 4). In order to calculate the topographic roughness around the rim edge, a 470×470 nm^2 ROI without artifacts

such as scan lines was selected (figure 4). On this basis, the average surface roughness of the aperture edge was determined to be approximately 3.5 nm. The micro structured apertures were expected to be suited for accommodation of lipid bilayers, based on the overall geometries obtained by the combination of SEM and AFM imaging, respectively, of the fabricated partition apertures [28].

3.2. Automation technique for simultaneous formation of multiple lipid bilayers

Current methods for lipid bilayer formation are not straightforward to scale up to simultaneous establishment of multiple lipid bilayers in arrays. Therefore, the aim was to develop an automation technique for the establishment of functional lipid bilayers in rectangular arrays.

The bilayer formation strategy chosen was the formation of lipid bilayers from hydrocarbon containing bilayer-forming solutions, which was essentially based on the ease of lipid bilayer formation, membrane thickness and stability (reviewed in [13]). On this basis a two-cell Teflon chamber was designed to accommodate the micro structured partition arrays (figure 1). In this design the cut glass cover slip and the Teflon spacer with the 2 mm slit provide a small accessible chamber within the *cis* chamber that functions to contain the bilayer-forming solution (figures 1(*A*) and (*B*)). This prevents spreading of the bilayer-forming solution to the rest of the *cis* chamber and minimizes the volume required to establish multiple aperture membranes. The Viton fluoroelastomer was custom fabricated into sealing O-rings, thereby removing the need for silicone grease (figure 1).

Regenerated cellulose was included in the multiple bilayer formation technique to provide a micro porous support
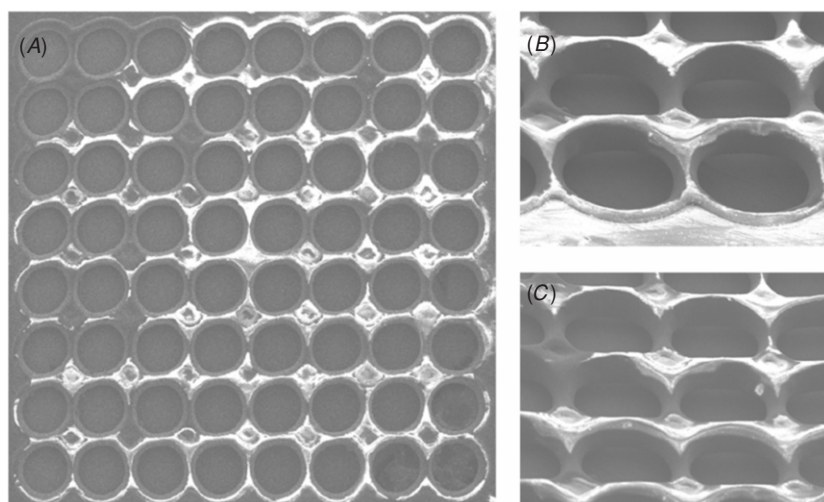
Figure 3. SEM images of CO_2 laser ablated multi-array aperture partitions. (*A*) SEM image of 8×8 apertures in a rectangular array with average aperture diameters of 303 ± 5 μm. The center-to-center spacing of the micro structured apertures is 400 μm. The same multi-aperture partition is tilted at a $55°$ angle to show (*B*) the intermediate stage from the unmodified ETFE film to the CO_2 laser ablated apertures and (*C*) the mid section of the partition array.
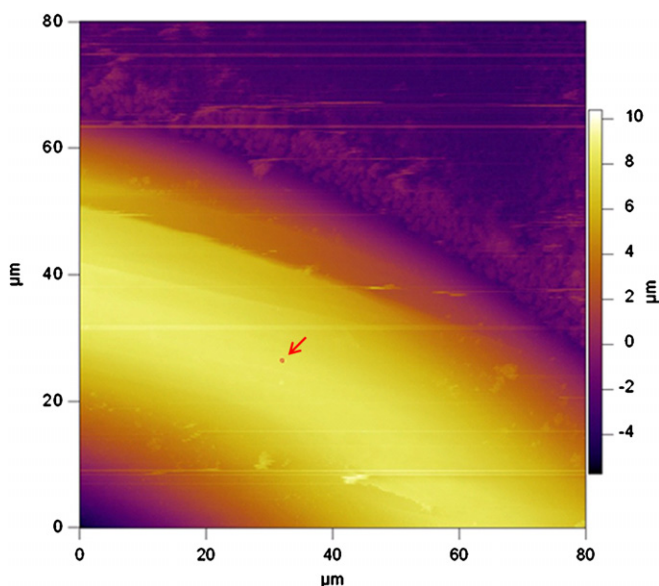
Figure 4. AFM image of the edge topography of an aperture rim in a partition array. The ROI (red square) indicated by the red arrow was used for the surface roughness calculation. The left lower corner of the image is the edge nearest to the aperture.

structure for bilayer formation (figures 1(*A*) and (*B*)). This semi-supported bilayer formation strategy was chosen to prevent fluid flow through the apertures from the *trans* to the *cis* chamber upon establishment of lipid bilayers (figure 2).

The technique for multiple bilayer formation was based on raising the aqueous electrolyte solution in the *cis* chamber in front of the glass cover slip leading to the raising of the bilayer-forming solutions between the cut glass cover slip and the multi-aperture partition (figure 2). The process of multiple bilayer formations could in this manner be established automatically by raising the bilayer-forming solution across the partition aperture array (figure 2).

3.3. Formation of planar lipid bilayers across multiple aperture ETFE partitions

We evaluated the capacitance and conductance contributions of the regenerated cellulose, and of ETFE film without apertures plus the regenerated cellulose mounted in the bilayer chamber, respectively. The regenerated cellulose had a conductance of 9165.9 ± 23.0 nS and no measurable capacitance ($n = 5$), whereas the non-perforated ETFE film plus cellulose had a conductance of 127.0 ± 1.6 nS and a capacitance of 2336.4 ± 19.0 pF ($n = 5$). Thus the values for ETFE film and cellulose are regarded as the background. In line with this multiple aperture bilayer experiments had initial conductance values in the range of 250–900 nS and capacitance values in the range of 2000–6000 pF. The fluctuations in the initial conductance and capacitance values were found to be variations in chamber assembly (e.g., tightening of the brass screw).

Following lipid membrane sealing across the apertures, lipid bilayers start to form and expand inside the apertures. The thinning of lipid membranes into bilayers gives rise to an increase in capacitance values above the background (figure 5(*A*)). The time-dependent increase in capacitance above the background values is interpreted as thinning of lipid membranes into lipid bilayers [27], and is thus also taken as evidence for the establishment of functional bilayers. Conversely, an increase in conductance is observed when the sealing properties of the BLMs start to fail (figure 5(*B*)).

Although multi-array membranes could consistently be formed, the membrane thinning curves varied considerably for the membranes established across Pasteur pipette prepainted ETFE partition apertures. Average capacitance and conductance values were $31\,600 \pm 13\,400$ pF and 2950 ± 2900 nS ($n = 5$) at 250 min (figures 5(*A*) and (*B*)).

A subset of membranes (~10%) exhibited a capacitative discharge and recharge cycling behavior with a time course of approximately 500 min, which is also reflected in the time course of the conductance. This behavior of BLMs

6
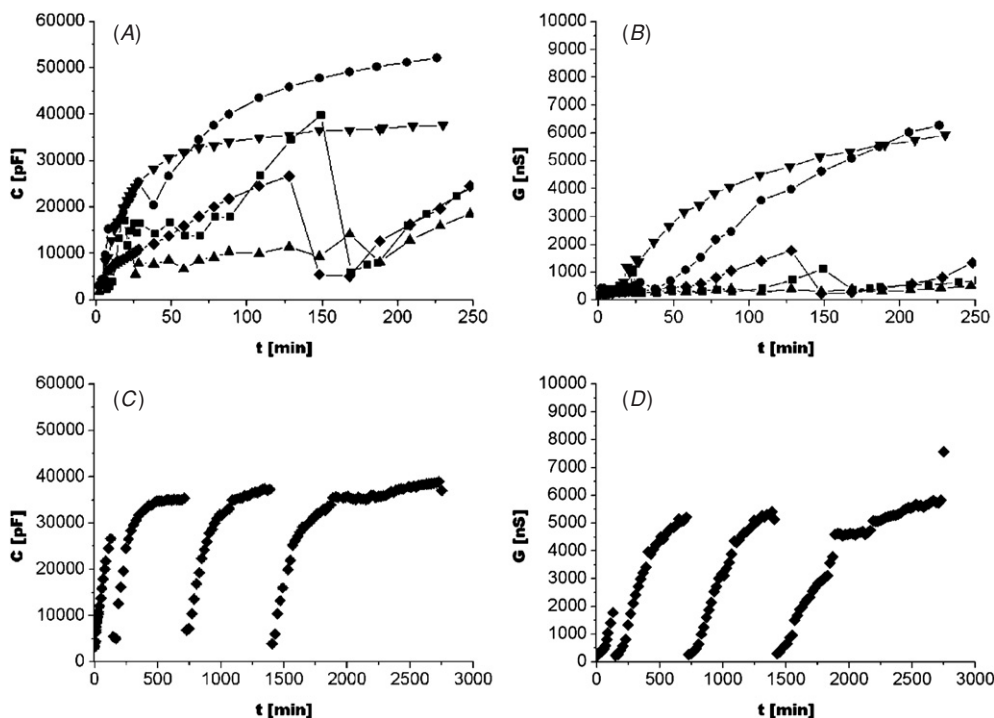
Figure 5. Time course characteristics of bilayers formed across multiple apertures. Bilayers were formed across Pasteur pipette pretreated ETFE partition arrays. (*A*) Capacitance and (*B*) conductance time course characteristics (250 min) of the bilayer formation across ETFE partitions with an 8 × 8 rectangular array of averaged 300 μm diameter apertures. The individual symbols represent independent experiments carried out under the same conditions. (*C*) Capacitance and (*D*) conductance of multi-aperture array BLMs exhibiting membrane discharge and recharge behavior during a time course of 50 h.

formed across multiple aperture partitions was observed as a repetitive cycling in capacitance and conductance values from the initial lipid bilayer formation values of around 2000–6000 pF and 250–900 nS, and to the lipid bilayer values of 26 000–38 000 pF and 2500–5800 nS, respectively (figures 5(*C*) and (*D*)).

3.4. Improved membrane reproducibility by controlled partition pretreatment

In order to improve membrane reproducibility, the deposition of prepainting solution onto the ETFE aperture arrays was assessed. Fluorescent images were acquired of 8 × 8 array ETFE partitions following prepainting using the traditional Pasteur pipette application method with DPhPC in *n*-decane (50 mg ml^{-1}) added 1 mol% of the fluorescent lipid NBD-PC. The results showed that the prepainting solution was inhomogeneously deposited on the partition surface, and several apertures were consistently partial or completely occluded by the prepainting solution in spite of the applied nitrogen to open the apertures (figure 6).

To circumvent this inhomogeneous lipid deposition and to improve reproducibility, an airbrushing pretreatment technique was developed. Fluorescent images of the airbrush pretreated partitions showed that this technique was able to deposit lipids onto the ETFE partition in a homogeneous and controlled manner (figure 6).

Following a short lag phase (~2–10 min) multiple formed lipid membranes established across airbrush pretreated ETFE

partition arrays thinned in a time-dependent manner reaching the maximum capacitance values of 28500 ± 1400 pF at around 250 min (*n* = 5) (figure 7(*A*)). The conductance values were relatively stable (541 ± 128 nS) during the time course of 100 min at which point the conductance increased during the time course from 100 min to 250 min to values of 2300 ± 461 nS (figure 7(*B*)).

Compared with the bilayer characteristics obtained with the traditional prepainting method, a significantly increased reproducibility could be achieved by applying the prepainting solution to the ETFE arrays in a controlled manner (figure 8).

3.5. Incorporation of valinomycin into multiple formed lipid bilayers

To ensure that bilayers were formed across the aperture arrays the potassium ion-selective cyclodepsipeptide valinomycin was added (10 μl, 1.8 mM stock solution) to lipid bilayers displaying stable membrane properties for more than 60 min [25]. Following the addition of valinomycin to the chamber an abrupt increase in conductance was immediately observed indicating a functional reconstition of valinomycin cyclodepsipeptides into the bilayers formed across the array of 8 × 8 apertures (figure 9(*A*)). The effect of valinomycin could effectively be reversed by the addition of the channel blocker TEA (200 μl, 16 mM stock solution) (figure 9(*A*)). Before valinomycin incorporation the near-square response to the triangular wave form reflects the capacitative properties of the bilayers. The capacitance response signal becomes

7
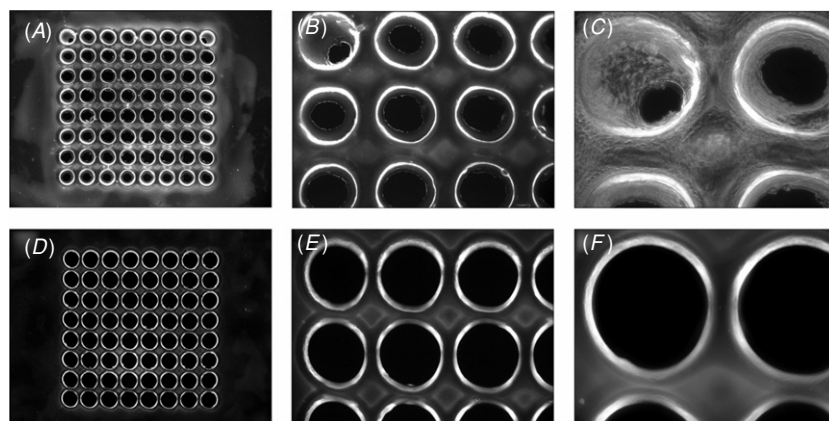
Figure 6. Fluorescent images of Pasteur pipette and airbrush-applied prepainting solution onto ETFE partition arrays. (*A*), (*B*) and (*C*) Pretreatment of ETFE partitions by the traditional prepainting method using a glass Pasteur pipette for five times on both sides. Objectives used were (*A*) 2.5×, (*B*) 10× and (*C*) 20×. (*D*), (*E*) and (*F*) Pretreatment of ETFE partitions by the airbrushing technique. The prepainting solution was airbrushed onto both sides of the ETFE partition array for 20 times with 30 s intervals. The objectives used were (*D*) 2.5×, (*E*) 10× and (*F*) 20×. The prepainting solution consisted of 50 mg ml^{-1} DPhPC in *n*-decane with 1 mol% of NBD-PC. The ETFE partition aperture diameters are 301 ± 5 μm.
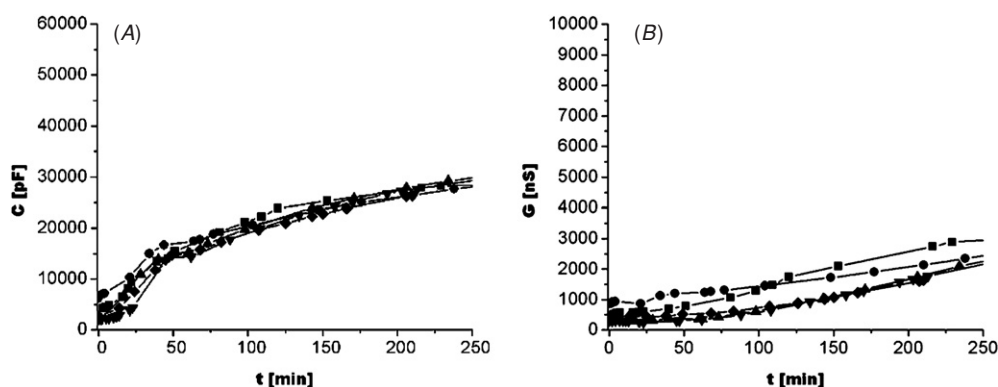
Figure 7. Time course characteristics of bilayers formed across airbrush pretreated ETFE partition arrays. (*A*) Capacitance and (*B*) conductance time course characteristics (250 min) of bilayer formation across ETFE partitions with 8 × 8 rectangular array pretreated for 20 times with prepainting solution (50 mg ml^{-1} DPhPC in *n*-decane) using the airbrush prepainting technique. The individual symbols represent independent experiments carried out under the same conditions.

more triangular upon functional valinomycin incorporation into established bilayers reflecting ionic currents through the bilayers and reverts following the channel blockage by TEA (figure 9(*B*)). In contrast, the addition of ethanol or TEA alone to preformed lipid bilayers to final chamber concentrations of up to 1% and 5.9 mM, respectively, did not significantly affect the membrane characteristics (data not shown).

Combined, these results strongly indicate that stable lipid bilayers are in fact formed across the multi-array aperture partitions, and that lipid bilayer spanning channels can be functionally inserted into the formed lipid bilayers.

4. Discussion

Current design criteria for free-spanning biomimetic membrane platform technologies are low leak currents (i.e., good membrane sealing); long-lasting membranes (i.e., lifetimes > 1 day); absolute reproducibility with a high success rate; a scaffold consisting of multiple functional units for effective up-scaling; the ability to reconstitute membrane spanning proteins/peptides; robustness (i.e., stable during transportation/handling); and cost effective in production [21]. For mass transfer flow and high throughput screening applications additional design criteria must be met. These include a high perforation level of the membrane scaffold material, the functional membrane units are arranged in arrays to facilitate a screening platform (e.g., for microplate readers) and the artificial membrane platform is scalable to meet various requirements for individual technical applications.

The criteria of a high perforation level of the membrane scaffold material and the fabrication of functional membrane units were in this study achieved by micro structuring ETFE films using a carbon dioxide laser. The positioning of averaged 300 μm diameter apertures in 8 × 8 rectangular arrays with a center-to-center distance of 400 μm yielded a perforation level of 43.6%, and created a total aperture area of 0.045 cm^2. This area is about 150 times larger compared to a recently published silicon nitride nano-structured array chip which had impressive 960 000 nanometer-sized apertures [6].

8
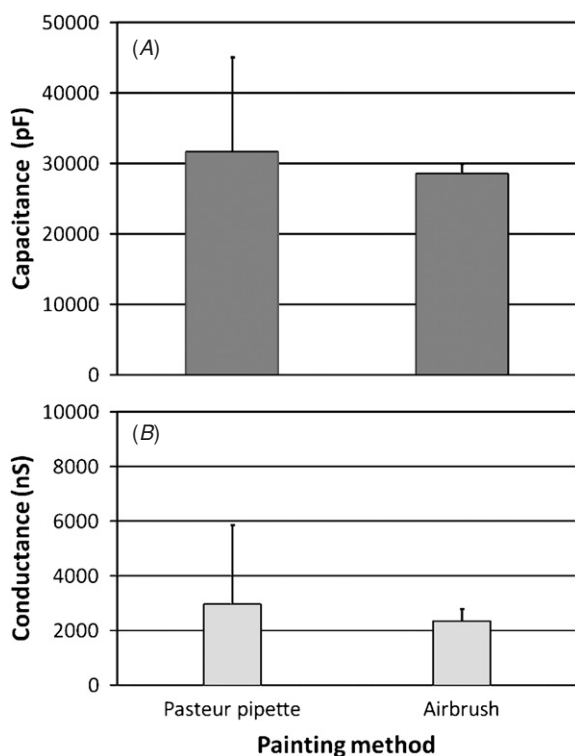
Figure 8. Comparison of bilayer characteristics between prepainting techniques. (*A*) Capacitance and (*B*) conductance values at 250 min for bilayers established on Pasteur pipette or airbrush prepainted ETFE arrays. Standard deviations are indicated.

The automation technique for multiple bilayer formations was created to meet the above-mentioned design criteria of stable, scalable and reproducible membranes for establishing planar artificially made membranes in arrays (figures 1 and 2). Generally, the 8×8 arrayed lipid bilayers were established by a single lowering and raising of the aqueous electrolyte solution in the chamber design (figure 2). The success rates for multi-array bilayer experiments exceeded 95%. Moreover, the technique is easy to scale and the bilayers have been created in single aperture, 5×5, 8×8 and 30×21 arrays having average aperture diameters of 300 μm. Multi-array lipid bilayers were in general stable for 200–300 min before breakdown, while 40% of the established bilayer membranes lasted for 1–3 days when left with voltage potentials $\leqslant \pm$ 100 mV. A few membranes lasted for more than a week and up to 14 days.

Reproducible multiple aperture bilayer experiments were achieved by the development of an airbrush partition pretreatment technique for controlled surface pre-coatings of the aperture arrays (figures 7 and 8). Our results indicate that the substrate for the establishment of lipid bilayers is very important in order to achieve highly reproducible biomimetic membrane platforms. This notion is supported by Ries *et al* who showed that the reproducibility of bilayer formations was strongly influenced by the substrate material, e.g., delrin, polyethylene or silicon wafers, respectively [22].

Although a high reproducibility was achieved in the automation technique for the establishment of multi-array bilayers, the life span of bilayers was not increased

correspondingly. The low leak currents of established multiple bilayers across partition arrays could only be maintained for approximately 100 min. Following a gradual decrease in the overall membrane sealing properties until membrane rupture was observed (figure 7(*B*)). Therefore, the membrane stability issue needs to be further addressed.

Evidence for the formation of functional bilayers in the multiple aperture bilayer experiments was provided by the obtained capacitance values of 28 500 $\pm$ 1400 pF (figure 7(*A*)). Giving a total aperture area of 0.045 cm^2 for 64 apertures with average diameters of 300 μm and literature values of the specific capacitance of 0.4–0.6 μF cm^{-2} for the solvent containing lipid bilayers [2], the capacitance for multiple formed lipid bilayers was expected to be in the range of 18 100–27 100 pF. Therefore, the capacitance values could indicate that the total lipid bilayer area is somewhat 4.9–36.6% larger than expected with a specific bilayer capacitance of 0.4–0.6 μF cm^{-2}. This discrepancy is however regarded as a technical capacitance measurement artifact. The membrane capacitances were consistently determined by measuring the peak-to-peak amplitude of the square-shaped signal in response to applying a triangular pulse. Any leak current in the setup (e.g., if individual bilayers start to fail) will therefore give rise to an ohmic contribution to the square capacitance response signal, and thus an overestimation of the obtained capacitance values. Therefore, it is reasonable to assume that the specific capacitance values of thinned lipid bilayers in our multiple aperture experiments lie within the range of 0.4–0.6 μF cm^{-2} for solvent-containing lipid bilayers.

Further evidence for the establishment of lipid bilayers was the functional reconstitution of valinomycin into formed bilayers, and the blockage of ionic currents by the addition of TEA (figure 9). These results showed that the established bilayers in array were accessible to the reconstitution of transmembrane spanning molecules, which is also an important design criterion for the construction of a free-spanning artificial membrane platform. In this regard experimental results have recently shown that there is no practical hindrances in the use of hydrocarbon containing lipid bilayers compared with the solvent-free folded membranes regarding the reconstitution of transmembrane proteins through proteoliposome vesicle fusion events [1].

The transportation robustness of the presented method has not been addressed here. However, recent advantages in bilayer encapsulation methods suggest that a robust portable artificial membrane platform can be produced [7, 8, 10, 20, 26].

An unresolved issue is to understand the cycling membrane characteristic behavior exhibited in roughly 1 out of 10 membranes, where repeated events of gradual decreases in membrane tightness followed by sudden resealing were observed (figures 5(*C*) and (*D*)). We were however not able to record the actual membrane failure events where the overall conductance increases to background levels (in this case $\sim$8000 nS, figure 5(*D*)) due to our 20 min intervals between samplings. One explanation is that a gradual increase in membrane conductance in a small subset of apertures occurs, most likely a single aperture, followed by membrane failure and subsequent resealing of a single or several apertures.

9
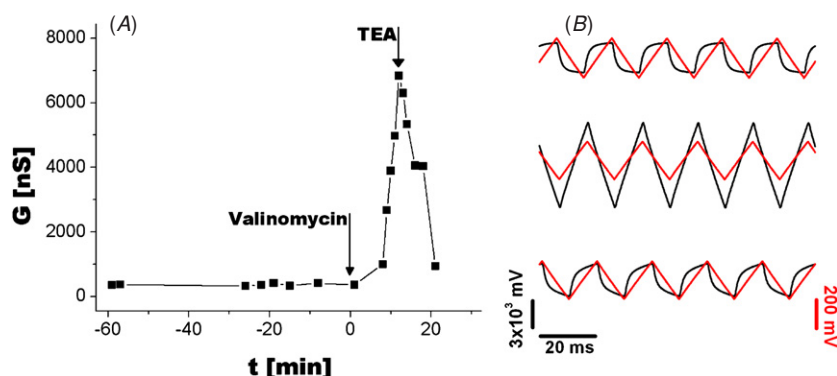
Figure 9. Reconstitution of valinomycin and channel blocking in multiple lipid bilayers. (*A*) Time course of conductance values for a bilayer array (8 × 8) alone, reconstituted with valinomycin and subsequently blocked by TEA. (*B*) Capacitative signals of lipid bilayers in the array (top panel), reconstituted with valinomycin (middle panel), and valinomycin blockage by TEA (lower panel). Capacitance signals correspond to $t = -10$, 15 and 20 min in (*A*). Red lines represent the triangular applied voltage clamp wave forms to obtain the membrane capacitance response signals (black lines).

The single aperture failure notion is based on the observation that the cycling behavior of both the capacitance and the conductance displays a high degree of regularity (figures 5(*C*) and (*D*)). If all 64 aperture bilayers went through a membrane failure and resealing event, the observable regular behavior would require that all of the individual membrane events to take place more or less in phase. Therefore, a single (or small subset) aperture event is more probable. Upon the single membrane failure, the electric field across the entire membrane system breaks down causing a global discharge leading to the overall system capacitance dropping to zero in phase with the drop in conductance. The electric field breakdown may subsequently trigger a global membrane thickening event caused by a backflow of bilayer forming solution into the aperture areas from reservoirs (Plateau-Gibbs) present in the surrounding partition landscape. This would explain the gradual increase in membrane capacitance on a global scale following the abrupt single membrane failure and resealing event. If the system as a whole remained unchanged after the resealing event, the increase in capacitance would be solely due to recharging of the system and take place with a considerable smaller time constant compared to what was observed.

Recently, a platform for the individual production of BLMs in 4 × 4 aperture arrays has been described, where each BLM should be established manually. In this method a success rate of 50% could be achieved, and the authors suggested a robotic injection approach to obtain better and more reproducible rates of the BLM formation [30]. We do not see any major obstacles in converting our current automation technique from establishing vertical BLMs to form horizontal BLMs thus enabling a modular design allowing for individual BLM measurements.

In this study we demonstrated that large BLM arrays can reproducible be fabricated with high success rates (above 95%) by an automation technique that does not require sophisticated and expensive robots. We conclude, based on the large capacitance values relative to the background and the reconstitution of valinomycin and subsequent blockage by TEA, that functional multi-array bilayers were established

with the presented automation technique. The low leak sealing properties of the established functional bilayers are ideally suited for the design of mass transfer devices based on mass transport through highly selective membrane transport peptides and proteins (e.g., biomimetic filters based on incorporated aquaporins or ion channels).

Acknowledgments

References

[1] Anzai K, Ogawa K, Ozawa T and Yamamoto H 2001 Quantitative comparison of two types of planar lipid bilayers—folded and painted—with respect to fusion with vesicles *J. Biochem. Biophys. Methods* **48** 283–91

[2] Benz R, Frohlich O, Lauger P and Montal M 1975 Electrical capacity of black lipid films and of lipid bilayers made from monolayers *Biochim. Biophys. Acta* **394** 323–34

[3] Eray M, Dogan N S, Reiken S R, Sutisna H, Van Wie B J, Koch A R, Moffett D F, Silber M and Davis W C 1995 A highly stable and selective biosensor using modified nicotinic acetylcholine receptor (nAChR) *Biosystems* **35** 183–8

[4] Ginsburg S and Noble D 1974 The activation enthalpies for ion conductance systems in lipid bilayer membranes *J. Membr. Biol.* **18** 163–76

[5] Goennenwein S, Tanaka M, Hu B, Moroder L and Sackmann E 2003 Functional incorporation of integrins into solid supported membranes on ultrathin films of cellulose: impact on adhesion *Biophys. J* **85** 646–55

[6] Han X, Studer A, Sehr H, Geissbühler I, Di Berardino M, Winkler F K and Tiefenauer L X 2007 Nanopore arrays for stable and functional free-standing lipid bilayers *Adv. Mater.* **19** 4466–70

[7] Jeon T J, Malmstadt N and Schmidt J J 2006 Hydrogel-encapsulated lipid membranes *J. Am. Chem. Soc.* **128** 42–3

10

[8] Kang X F, Cheley S, Rice-Ficht A C and Bayley H 2007 A storable encapsulated bilayer chip containing a single protein nanopore *J. Am. Chem. Soc.* **129** 4701–5

[9] Kelety B, Diekert K, Tobien J, Watzke N, Dorner W, Obrdlik P and Fendler K 2006 Transporter assays using solid supported membranes: a novel screening platform for drug discovery *Assay Drug. Dev. Technol.* **4** 575–82

[10] Malmstadt N, Jeon J and Schmidt J 2008 Long-lived planar lipid bilayer membranes anchored to an *in situ* polymerized hydrogel *Adv. Mater.* **20** 84–9

[11] Mayer M, Kriebel J K, Tosteson M T and Whitesides G M 2003 Microfabricated teflon membranes for low-noise recordings of ion channels in planar lipid bilayers *Biophys. J.* **85** 2684–95

[12] Melikov K C, Frolov V A, Shcherbakov A, Samsonov A V, Chizmadzhev Y A and Chernomordik L V 2001 Voltage-induced nonconductive pre-pores and metastable single pores in unmodified planar lipid bilayer *Biophys. J.* **80** 1829–36

[13] Miller C 1986 *Ion Channel Reconstitution* (New York: Plenum)

[14] Minami H, Sugawara M, Odashima K, Umezawa Y, Uto M, Michaelis E K and Kuwana T 1991 Ion channel sensors for glutamic acid *Anal. Chem.* **63** 2787–95

[15] Montal M and Mueller P 1972 Formation of bimolecular membranes from lipid monolayers and a study of their electrical properties *Proc. Natl. Acad. Sci. USA* **69** 3561–6

[16] Moran-Mirabal J M, Edel J B, Meyer G D, Throckmorton D, Singh A K and Craighead H G 2005 Micrometer-sized supported lipid bilayer arrays for bacterial toxin binding studies through total internal reflection fluorescence microscopy *Biophys. J.* **89** 296–305

[17] Mueller P and Rudin D O 1969 Translocators in bimolecular lipid membranes: their role in dissipative and conservative bioenergetic transduction *Curr. Top. Bioenerg.* **3** 157–249

[18] Nikolelis D P and Siontorou C G 1995 Bilayer lipid membranes for flow injection monitoring of acetylcholine, urea, and penicillin *Anal. Chem.* **67** 936–44

[19] O'Shaughnessy T J, Hu J E, Kulp J L 3rd, Daly S M and Ligler F S 2007 Laser ablation of micropores for formation of artificial planar lipid bilayers *Biomed. Microdevices* **9** 863–8

[20] Oliver A E, Kendall E L, Howland M C, Sanii B, Shreve A P and Parikh A N 2008 Protecting, patterning, and scaffolding supported lipid membranes using carbohydrate glasses *Lab. Chip.* **8** 892–7

[21] Reimhult E and Kumar K 2008 Membrane biosensor platforms using nano- and microporous supports *Trends Biotechnol.* **26** 82–9

[22] Ries R S, Choi H, Blunck R, Bezanilla F and Heath J R 2004 Black lipid membranes: visualizing the structure, dynamics, and substrate dependence of membranes *J. Phys. Chem* B **108** 16040–9

[23] Sandison M E and Morgan H 2005 Rapid fabrication of polymer microfluidic systems for the production of artificial lipid bilayers *J. Micromech. Microeng.* **15** S139–44

[24] Snakenborg D, Klank H and Kutter J P 2004 Microstructure fabrication with a CO2 laser system *J. Micromech. Microeng.* **14** 182–9

[25] Stark G, Benz R, Pohl G W and Janko K 1972 Valinomycin as a probe for the study of structural changes of black lipid membranes *Biochim. Biophys. Acta* **266** 603–12

[26] Uto M, Araki M, Taniguchi T, Hoshi S and Inoue S 1994 Stability of an agar-supported bilayer lipid membrane and its application to a chemical sensor *Anal. Sci.* **10** 943–6

[27] White S H 1970 A study of lipid bilayer membrane stability using precise measurements of specific capacitance *Biophys. J.* **10** 1127–48

[28] White S H 1972 Analysis of the torus surrounding planar lipid bilayer membranes *Biophys. J.* **12** 432–45

[29] Wonderlin W F, Finkel A and French R J 1990 Optimizing planar lipid bilayer single-channel recordings for high resolution with rapid voltage steps *Biophys. J.* **58** 289–97

[30] Zagnoni M, Sandison M E and Morgan H Microfluidic array platform for simultaneous lipid bilayer membrane formation *Biosens. Bioelectron.* at press

3.2 Large scale biomimetic membrane arrays

ORIGINAL PAPER

Large scale biomimetic membrane arrays

Jesper S. Hansen · Mark Perry · Jörg Vogel · Jesper S. Groth · Thomas Vissing ·
Marianne S. Larsen · Oliver Geschke · Jenny Emneús · Henrik Bohr ·
Claus H. Nielsen

Abstract To establish planar biomimetic membranes
across large scale partition aperture arrays, we created a
disposable single-use horizontal chamber design that sup-
ports combined optical–electrical measurements. Functional
lipid bilayers could easily and efficiently be established
across CO_2 laser micro-structured 8×8 aperture partition
arrays with average aperture diameters of 301 ± 5 μm. We
addressed the electro-physical properties of the lipid
bilayers established across the micro-structured scaffold
arrays by controllable reconstition of biotechnological
and physiological relevant membrane peptides and proteins.
Next, we tested the scalability of the biomimetic membrane
design by establishing lipid bilayers in rectangular 24×24
and hexagonal 24×27 aperture arrays, respectively. The
results presented show that the design is suitable for further
developments of sensitive biosensor assays, and further-
more demonstrate that the design can conveniently be
scaled up to support planar lipid bilayers in large square-
centimeter partition arrays.

Abbreviations

α-HL	α-Hemolysin
BLM	Black lipid membrane
DPhPC	1,2-Diphytanoyl-*sn*-Glycero-3-Phosphocholine
ETFE	Ethylene tetrafluoroethylene
FomA	*Fusobacterium nucleatum* outer membrane protein A
gA	Gramicidin A
LDAO	*N*-lauryl-*N,N*-dimethylammonium-*N*-oxide
NBD-PC	1-Oleoyl-2-[6-[(7-nitro-2-1, 3-benzoxadiazol-4-yl)amino]hexanoyl]-*sn*-glycero-3-phosphocholine
TEA	Tetraethylammonium

J. S. Hansen · J. Vogel · O. Geschke · J. Emneús
DTU Nanotech, Technical University of Denmark,
2800 Lyngby, Denmark

J. S. Hansen
e-mail: jsh@aquaporin.dk

J. S. Hansen · M. Perry · J. Vogel · J. S. Groth · T. Vissing ·
M. S. Larsen · C. H. Nielsen
Aquaporin A/S, Scion DTU,
Diplomvej 377,
2800 Lyngby, Denmark

H. Bohr · C. H. Nielsen (✉)
DTU Physics, Quantum Protein Center,
Technical University of Denmark,
2800 Lyngby, Denmark
e-mail: claus.nielsen@fysik.dtu.dk

Introduction

To create a device that utilizes membrane-spanning mole-
cules, it is necessary to construct an efficient platform to
handle biomimetic membranes [1]. The advantages of
biomimetic membrane-based applications are, among others,
that a lot of information can be achieved with extremely low
sample volumes, specific drug interactions with a single
target (protein or peptide) can be assessed, and the
experimental conditions can be exactly controlled (e.g.,
buffer, protein amount, and membrane composition) [1].

Biomimetic membrane-based biosensing devices may
provide a powerful tool in the early stage of identifying
promising drug candidates for a specific membrane protein
or peptide [2–5]. Moreover, a reduction in drug candidates

Springer

failing at later stages may be expected. The reason for this is the ability to exactly address the specific effects of a drug candidate on a single target, as well as the potential unintended effects that may occur due to the physio-chemical properties of the lipid membrane [6]. This reduces the potential of obtaining unintended interactions with secondary receptors or proteins, or potentially indirect effects on the lipid membrane, which may otherwise occur in living-cell-based systems.

Recently, we described a fast and cost efficient method to produce large scale aperture partitions by micro-structuring ethylene tetrafluoroethylene (ETFE) films using CO_2 laser ablation [7]. In a parallel study, we constructed a vertical automation technique for the simultaneous establishment of functional bilayers in 8×8 partition arrays [8].

In this study, we created a horizontal biomimetic membrane design supporting optical–electrical measurements of lipid bilayers established across the CO_2 laser-ablated ETFE LZ200 partition arrays. The chamber design was created to constitute a low-cost disposable single-use system. Lipid bilayers could efficiently be established across the partition arrays in the chamber design by employing a modified painting method [9]. The success rate for establishing lipid bilayers across the partition array in the presented design was ≥98%. To demonstrate the functionality of the biomimetic membrane design, controllable reconstitution of the biotech-nological and physiological relevant peptides valinomycin and gramicidin A (gA), together with the membrane proteins α-hemolysin and FomA was carried out. We show that the design supports low-current (high sensitivity) recordings of membrane peptides and proteins by incorporating gA, α-hemolysin, and FomA into the established lipid bilayers.

Finally, we demonstrate that the design can conveniently be scaled up to 24×24 (576 apertures) rectangular and 24×27 (648 apertures) hexagonal membrane arrays with averaged diameters of 300 μm. The two different geome-tries of the micro-structured aperture arrays seem to support stable membrane arrays, however, with somewhat different electrical properties.

Our results are discussed in the context of improving the design to create a multifunctional biomimetic platform suitable for the development of biosensing devices.

Experimental

Reagent and materials

Tefzel ETFE LZ200 fluoropolymer for the fabrication of multi-aperture partitions, and Viton A fluoroelastomer for the production of rubber chamber sealing rings were from DuPont Fluoropolymers (Detroit, U.S.A.). Uncoated 35- and 50-mm glass-bottom culture dishes were purchased from MatTek

Corporation (Ashland, MA, U.S.A.). The lipids 1, 2-diphytanoyl-sn-glycero-3-phosphocholine and 1-oleoyl-2-[6-[(7-nitro-2-1, 3-benzoxadiazol-4-yl)amino]hexanoyl]-sn-glycero-3-phosphocholine were from Avanti Polar Lipids Inc. (Alabaster, U.S.A.). The potassium ion-selective cyclo-depsipeptide valinomycin (Sigma), *Bacillus brevis* gramici-din A (Sigma), *Staphylococcus aureus* α-Hemolysin (Sigma), tetraethylammonium (Fluka), *n*-heptane and *n*-decane (Fluka) were purchased from Sigma-Aldrich Denmark (Brøndby, Denmark). All other chemicals were of analytical grade and purchased from commercial sources.

Micro-structuring and surface modification of ETFE scaffold arrays

ETFE LZ200 film (50.8 μm thickness) was laser-structured to produce partition aperture arrays as previously described [7]. Partitions produced were rectangular 8×8 and 24×24, and hexagonal 24×27 arrays, respectively. The apertures within the partition structure had average diameters of 301 ± 5 μm and with a nominal distance from center-to-center of 400 μm.

The ETFE surfaces were covalently modified by plasma treatment with lower-carbon-chain-length alkanes, predominantly hexanes, resulting in a hydrophobic surface coating as described by Inagaki et al. [10] and by Park and Inagaki [11]. This surface modification was applied to provide a molecular anchoring for establishing the lipid membranes across the micro-structured arrays.

Disposable single-use horizontal biomimetic membrane chamber design

A horizontal lipid bilayer chamber was designed for optical imaging that at the same time enabled recording of the electrical membrane properties by voltage clamp. The assembly of the chamber design is schematically depicted in Fig. 1a. The design was inspired from previous work by Hemmler et al. [12] and Wilburn et al. [13], respectively. Our chamber was, however, made from commercially available 35- and 50-mm MatTek glass-bottom culture dishes, where the 35-mm dish constituted the upper and the 50-mm dish the lower compartments, respectively (Fig. 1). The glass cover slip of the 35-mm MatTek glass-bottom dishes was replaced with the ETFE LZ200 partition by first removing the cover slip by adding 0.5 ml *n*-heptane to the dishes for 10 min, and then gluing the ETFE LZ200 partition array on the dish using silicone-based glue (Dow Corning). A reusable aluminum microscope sample holder was designed to clamp the upper and lower compartments (Fig. 1b and c). A 34-mm cut Viton ring was placed between the two Petri dishes to create two independently accessible compartments (Fig. 1c). By design, the chamber components were made of low-cost, commercially available
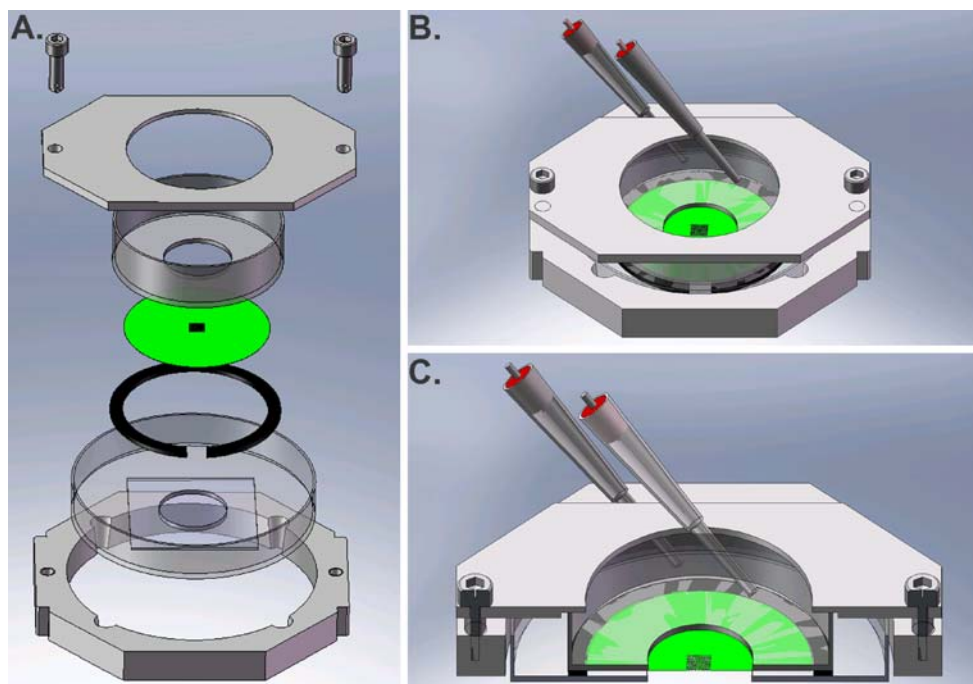
Fig. 1 The horizontal lipid chamber design. **a** Assembly of the bilayer chamber. The chamber is assembled sequentially from the bottom and up. The upper *cis* compartment consists of a MatTek 35 mm culture dish (transparent) with a micro-structured ETFE LZ200 partition (*green*) glued onto the bottom across the center hole. A MatTek 50-mm-diameter glass-bottom culture dish constitutes the lower *trans* compartment (*transparent*). A cut Viton ring (*black*) is placed between the dishes to create two independently accessible compartments. A custom-designed aluminum sample holder clamps the chamber elements together (*gray*). **b** The assembled lipid chamber. **c** Cross-sectional view of the assembled chamber. The position of the Ag/AgCl electrodes connected to the voltage-clamp setup is indicated in **b** and **c**

components that constituted a convenient disposable single-use chamber design.

Preparation of lipid solutions for BLM experiments

The lipid solution for bilayer formation consisted of 1, 2-diphytanoyl-*sn*-glycero-3-phosphocholine (DPhPC) in *n*-decane (25 mg/ml) doped with 1 mol% 1-oleoyl-2-[6-[(7-nitro-2-1, 3-benzoxadiazol-4-yl)amino]hexanoyl]-*sn*-glycero-3-phosphocholine (NBD-PC). The lipid solution for bilayer formation is henceforth referred to as the bilayer-forming solution (BFS). The lipid solutions were prepared the day before, and stored at −20°C until use.

Formation of BLMs across multi-aperture ETFE partitions

Planar lipid bilayers were established across the micro-structured ETFE partition arrays by the lipid bilayer painting technique [9], which was modified essentially, as previously described [12]. Briefly, ~0.5–5 μl (depending on the array size) of the BFS was deposited onto the partition array. To thin the membranes into bilayers, a sterile plastic inoculation loop with a 1 μl loop capacity (Sarstedt) was used. The thinning process was carried out by gently sweeping the inoculation loop across the entire ETFE partition array.

Fluorescence microscopy visualization

Fluorescent imaging was performed on a Zeiss Axiovert 200M epifluorescence microscope (Carl Zeiss, Jena, Germany) equipped with a monochrome Deltapix DP450 CCD camera (Deltapix, Maalov, Denmark). Images were acquired using Deltapix DpxView Pro acquisition software (Deltapix, Maalov, Denmark). Objectives used were air-corrected Plan-Neofluar 2.5×/0.075 Numerical Aperture (NA) and 10×/0.25 NA, respectively.

Voltage-clamp data acquisition and processing

The experimental setup consisted of a Model 2400 Patch Clamp Amplifier with a head stage containing 10 GΩ/10 MΩ feedback resistors (A-M Systems, Inc., WA, USA) and a Thurlby Thandar Instruments model TG2000 20 MHz DDS function generator (RS Components Ltd, Northants, UK). The Ag/AgCl electrodes were placed in the *trans* and *cis* compartments of the bilayer formation chamber with the ground electrode positioned in the *trans* compartment. Data acquisition was done with a combined oscilloscope/analog–digital converter (ADC-212/50, Pico Technology, Cambridgeshire, UK) connected to a laptop computer. Sampling frequency was 50 Hz.

Capacitance and conductance measurements were performed as previously described [8]. The results are given as means±S.D. for five individual experiments unless otherwise stated. Off-line analysis was done using custom made software.

To measure channel incorporation electrically, a current potential of +60 mV or +150 mV was applied, and the resulting membrane output current was filtered through 1 kHz on the amplifier and subsequently further filtered through a low-pass Bessel filter with 50 Hz cutoff (Frequency Devices, IL, USA) before data acquisition.

Reconstitution of transmembrane peptides and proteins

Valinomycin dissolved in ethanol (1.8 mM) was added (10 μl) to the top horizontal chamber to yield a final concentration of 12 μM in close proximity to the lipid bilayer array. To reverse the valinomycin-induced current increase, tetraethylammonium (TEA, 16 mM) was added (200 μl) to the top horizontal chamber. The aqueous chamber solution consisted of 0.2 M KCl. The applied potential across the partition arrays was +60 mV.

Incorporation of *B. brevis* gramicidin A (gA) into established membrane arrays was carried out by the addition of 5 μl gA dissolved in ethanol (120 nM) to both the *cis* and *trans* horizontal chambers. The aqueous solution in the bilayer chamber consisted of HCl (1 N) adjusted to pH 1.0, while the potential applied across the bilayers was +150 mV.

S. aureus α-hemolysin (α-HL) was reconstituted into 8× 8 bilayer arrays by adding 10 μl of a 50 μg/ml stock solution to the *cis* chamber, while 20 μl of a 0.5 mg/ml stock solution was used for the large arrays. The aqueous solution in the chamber consisted of 1.0 M KCl for the 8×8 partition arrays, while a 0.2 M KCl saline solution was used for the large partition arrays. The applied potential across the partition arrays was +60 mV.

The *F. nucleatum* outer membrane protein A (FomA) was kindly provided by Dr. Jörg H. Kleinschmidt (Universität Konstanz, Germany). Incorporation of FomA into established lipid bilayer arrays was carried out by adding 2 μl of refolded FomA (9.6 mg/ml) in *N*-lauryl-*N*,*N*-dimethylammonium-*N*-oxide (LDAO) micelles (LDAO/FomA ratio=800 mol/mol) to the *cis* chamber compartment as previously described [14]. The *cis* and *trans* chamber were filled with a saline solution consisting of 1.0 M KCl, and the applied potential across the partition arrays was +60 mV.

Results and discussion

We created a horizontal biomimetic membrane chamber based on commercially available MatTek glass-bottom culture dishes to make an inexpensive and easily assembled design. Thus, the main chamber parts constitute a disposable single-use biomimetic membrane chamber, where only the custom-designed aluminum sample holder is reusable, and which does not require cleaning prior to re-assembly (Fig. 1).

The design allows for combined optical imaging and voltage-clamp recordings of established bilayers across the micro-structured ETFE LZ200 partition arrays (Fig. 1). The pair of Ag/AgCl electrodes is positioned in the *cis* and *trans* chamber, respectively (Fig. 1b and c). The electrodes therefore give an overall electrical readout of the complete set of membranes established across the micro-structured ETFE LZ200 partition arrays.

The electrical properties of the biomimetic membrane chamber, with non-perforated ETFE LZ200 films, were evaluated. The capacitance (C) and conductance (G) contributions of the chamber setup with non-perforated ETFE LZ200 film were 132±13 pF and 2.5±0.5 nS, respectively. These values of the non-perforated ETFE LZ200 film are defined as the baseline values of C and G.

Establishment of horizontal 8×8 lipid bilayer arrays

Lipid bilayers were established across the micro-structured ETFE LZ200 partition arrays in the horizontal biomimetic membrane chamber by spreading ~0.5 μl of the BFS onto the 8×8 partition array. This resulted in complete lipid membrane coverage of all the partition apertures. In contrast to the previously described establishment of lipid bilayer arrays across vertically positioned ETFE LZ200 partitions [8], the lipid membranes did not thin spontaneously to lipid bilayers in the horizontal setup. In this stage, lipid membranes were stable for days, and could be transported without disrupting the membranes. Manual thinning of lipid membranes was therefore necessary to obtain functional lipid bilayers suitable for insertion of membrane-spanning peptides and proteins. Prior to the manual-thinning process, the deposited membranes were equilibrated for 15 min with the micro-structured ETFE partition. The thinning of the membranes was carried out by gently sweeping a sterile plastic inoculation loop (1 μl capacity) across the entire ETFE partition array. This manual-thinning process took approximately 30 s per array. Repetitions of the sweeping motions across the membranes were required if the bilayer in a single or a few individual apertures ruptured, or if excess BFS flowed back from the surroundings into the actual aperture array positioned in the center of the ETFE partition. The fact that bilayers could be easily re-established if they ruptured during the membrane thinning process resulted in a success rate of ≥98% for establishing bilayers across the partition arrays. The establishment of bilayers in the ETFE arrays could

furthermore be carried out by untrained personnel with no previous experience in establishing black lipid membranes following a short instruction behind the principle of the manual-thinning technique.

To adapt the current manual processes of lipid bilayer formation to a fully automated system for industrial scale applications a robotic deposition technique or a micro fluidic system is envisaged.

The fluorescent lipid analog NBD-PC (1 mol%) included in the BFS provided a convenient visual control over the thinning process, and the Plateau–Gibbs border of the individual bilayers could easily be visualized (Fig. 2).

Following the manual-thinning process, the resulting lipid bilayers were equilibrated for another 15 min in order for the established bilayers to stabilize before carrying out experimentation.

The lipid bilayer arrays established under these conditions had average lifetimes of 1 h with voltage potentials less than or equal to ±100 mV, and exhibited C and G values of 9,750±515 pF and 61±11 nS, respectively. This indicated that the bilayer area constituted around 36–54% of the aperture area [15].

To demonstrate that functional lipid bilayers were established across the horizontal 8×8 arrays the potassium-selective cyclodepsipeptide valinomycin was added to the cis chamber to a final concentration of 12 μM [16]. The resulting increase in the current trace recording indicated functional reconstitution of valinomycin, which could effectively be reversed by the addition of the channel blocker TEA (Fig. 3a). This strongly suggested that functional lipid bilayers were established in the horizontal setup.

Sensitivity of current trace recordings of membrane molecules

The current noise increases strongly with the aperture diameters and the recording bandwidth [17]. This could affect the ability to resolve low-conductance events by voltage-clamp recordings in the bilayers established across the horizontal 8×8 partition arrays.

The current noise of the bilayers established in 8×8 arrays was determined to be in the range 3–5 pA peak-to-peak with a frequency bandwidth of 50 Hz. This scale of current noise would be expected to be acceptable for resolving low-conductance events of a wide range of membrane-spanning peptides and proteins, provided that the experimental conditions are optimal (e.g., ionic strength) for the given peptide or protein. We therefore addressed the sensitivity of the bilayers established in the 8×8 partition arrays by incorporating biotechnological or physiological relevant membrane peptides and proteins (Table 1).

The well-characterized peptide gA from *B. brevis* is a cation-selective channel formed by transbilayer association of pentadecapeptide subunits residing in each monolayer of the lipid bilayer [18]. We reconstituted gA into established bilayers by adding gA dissolved in ethanol to both the *cis* and *trans* bilayer chambers. Reconstituted gA peptides exhibited a high channel activity, where multiple gA channel opening and closures could be observed during the current trace (Fig. 3b). The current of single-channel activity with the chosen experimental conditions was expected to be ~20 pA [19]. Channel events with these current values could be distinguished in the current traces

Fig. 2 Fluorescent and bright-field images of established horizontal 8×8 bilayer arrays. **a** Fluorescent image of established 8×8 bilayer array with 25 mg/ml DPhPC in *n*-decane doped with NBD-PC (1 mol%). Image was acquired with a 2.5× air-corrected objective. **b** Fluorescent image acquired with a 10× air-corrected objective, and **c** the corresponding brightfield image. Indicated is the visual appearance of the Plateau–Gibbs border (*black arrow*)
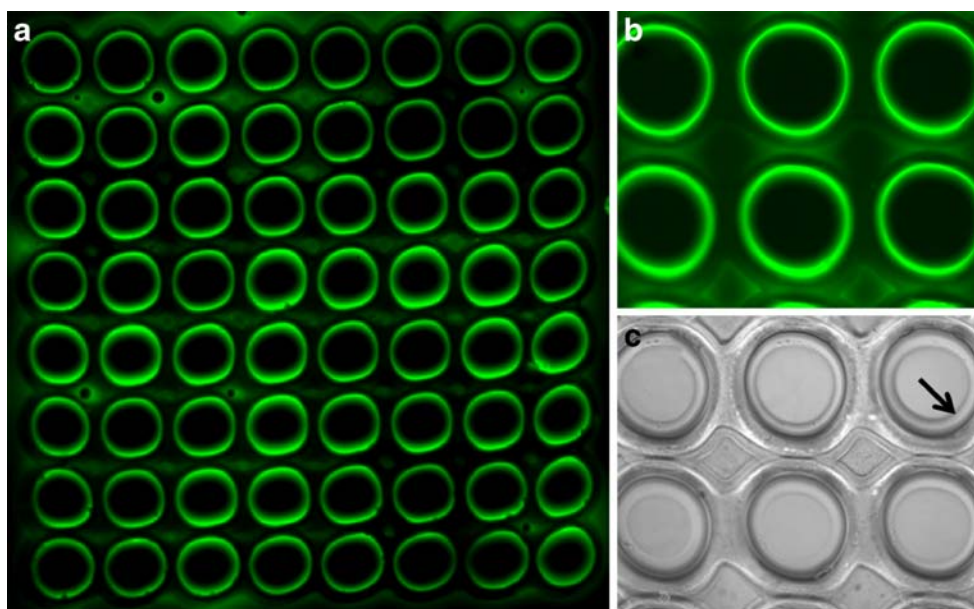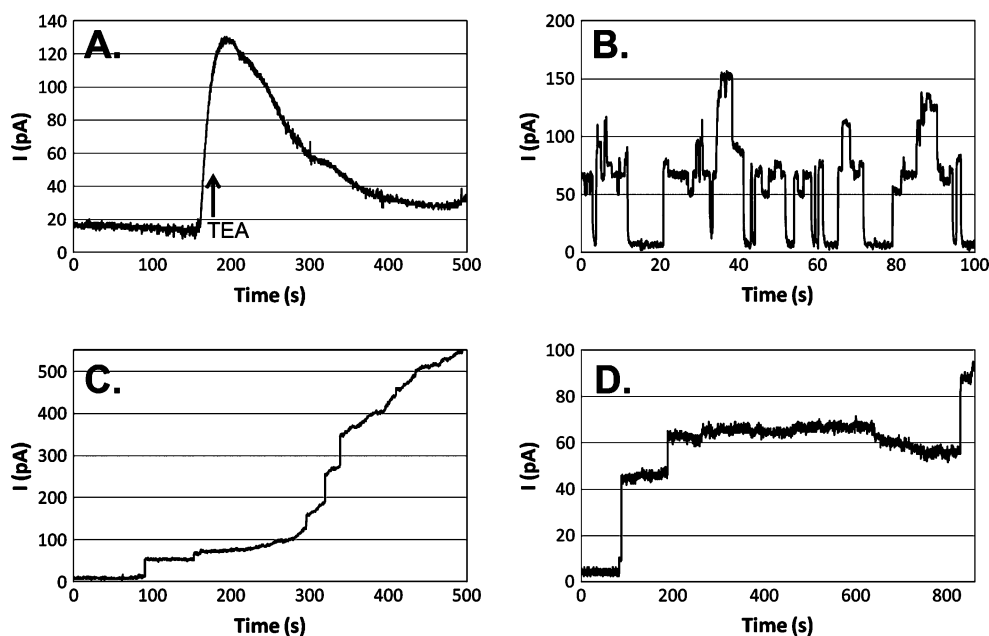
Fig. 3 Current traces of reconstituted membrane peptides and proteins in established 8×8 bilayer arrays. **a** Insertions of valinomycin and blocking by TEA. TEA was added (*t*=180 s) when the current increased as a consequence of functional valinomycin insertions. **b** Traces of gA channel activities. High channel activities are seen during the current trace with simultaneous opening and closure of multiple channels. Single-channel opening and closure could be distinguished with current values of ~20 pA **c** Reconstitution of heptameric α-HL pores. Single-channel incorporations had current values of ~35 pA. **d** Incorporation of trimeric FomA porins. Single-channel events had current values of approximately 15 pA. In the current traces of **b**, **c**, and **d** multiple insertions together with single-channel events could be observed. Applied potentials were +60 mV in **a**, **c**, and **d** and +150 mV in **b**

of incorporated gA peptides, although with some conductance heterogeneity (Fig. 3b).

We next evaluated the compatibility of the horizontal bilayers in the 8×8 arrays to support functional incorporation of membrane proteins, and to further characterize the ability to resolve low-conductance events. The pore-forming heptameric α-HL membrane protein from *S. aureus* and the trimeric outer-membrane-embedded porin FomA from *F. nucleatum*, respectively, were reconstituted into bilayers established across the partition arrays. The α-HL pores incorporated into the membranes with single-channel currents of around 35 pA (Fig. 3c), agreeing with previous reports [12]. The voltage-dependent FomA channel porins inserted into the membrane with a current of approximately 15 pA (Fig. 3d), which also agreed with previously

published current traces [14, 20]. Simultaneous multiple-channel insertions were also observed in the current traces of both reconstituted α-HL pores and FomA channel porins (Fig. 3c and d).

These results show that the bilayers established in the micro-structured 8×8 ETFE LZ200 partitions support low-current (high sensitivity) recordings.

The individual bilayers are, at present, not electrically addressable. Recent approaches have been described that conveniently allow the integration of a membrane scaffold with planar addressable microelectrode arrays [21, 22]. Further developments of the horizontal biomimetic membrane design could therefore be to develop composite membrane scaffolds enabling the electrical readout of individual bilayers. The lipid bilayers are however optically

Table 1 Potential applications of selected membrane peptides and proteins

Name	Type	Biotechnology/pharmacology	References
Valinomycin	Cyclodepsipeptide	Biomedical devices	[30, 31]
gA	Peptide	Sensors for drug-induced toxicity, chemical and biochemical analytes, pH and ammonium	[6, 32–34]
α-HL	Protein	Stochastic sensing techniques	[35, 36]
		Polynucleotide detection and sequencing	[37–41]
FomA	Protein	Drug discovery in Gram-negative bacteria infectious diseases	[42, 43]
		Immunological assays	[44]

individually addressable and fluorescent-based techniques may be combined with the membrane design in order to characterize specific interactions with membrane peptides or proteins [23, 24]. Moreover, the aperture array geometry (diameters of 300 μm and nominal center-to-center distances of 400 μm) provides a platform that may be adapted to modern array scanners and/or automated imaging and image analysis systems.

Lipid bilayers across rectangular 24×24 and hexagonal 24×27 partition arrays

The scalability of the array size is a key feature in the successful development of biotechnological applications based on planar biomimetic membranes. We therefore addressed the scalability of our design by scaling up the partition array size from the 8×8 rectangular arrays to 24×

24 rectangular and 24×27 hexagonal EFTE LZ200 partition arrays. The total aperture areas were 0.41 cm^2 for the 24× 24 rectangular and 0.45 cm^2 for the 24×27 hexagonal arrays, corresponding to a nine- and ten times area increase, respectively, compared to the 8×8 partition arrays (0.045 cm^2).

Lipid bilayers could be established across the large ETFE LZ200 partition arrays in a similar manner as for the 8× 8 partition arrays. Modifications were that 5 μl BFS was needed to cover the large partition arrays and an equilibration period of approximately 1 h were required prior to the membrane thinning to obtain stable membranes. In order to obtain a full view of the bilayers established across the large partition arrays, mosaics of twelve images were assembled for each large array (Fig. 4a and b). The membranes could be evenly thinned across the whole partition array as evidenced by the separate bright appearance of the torus of the
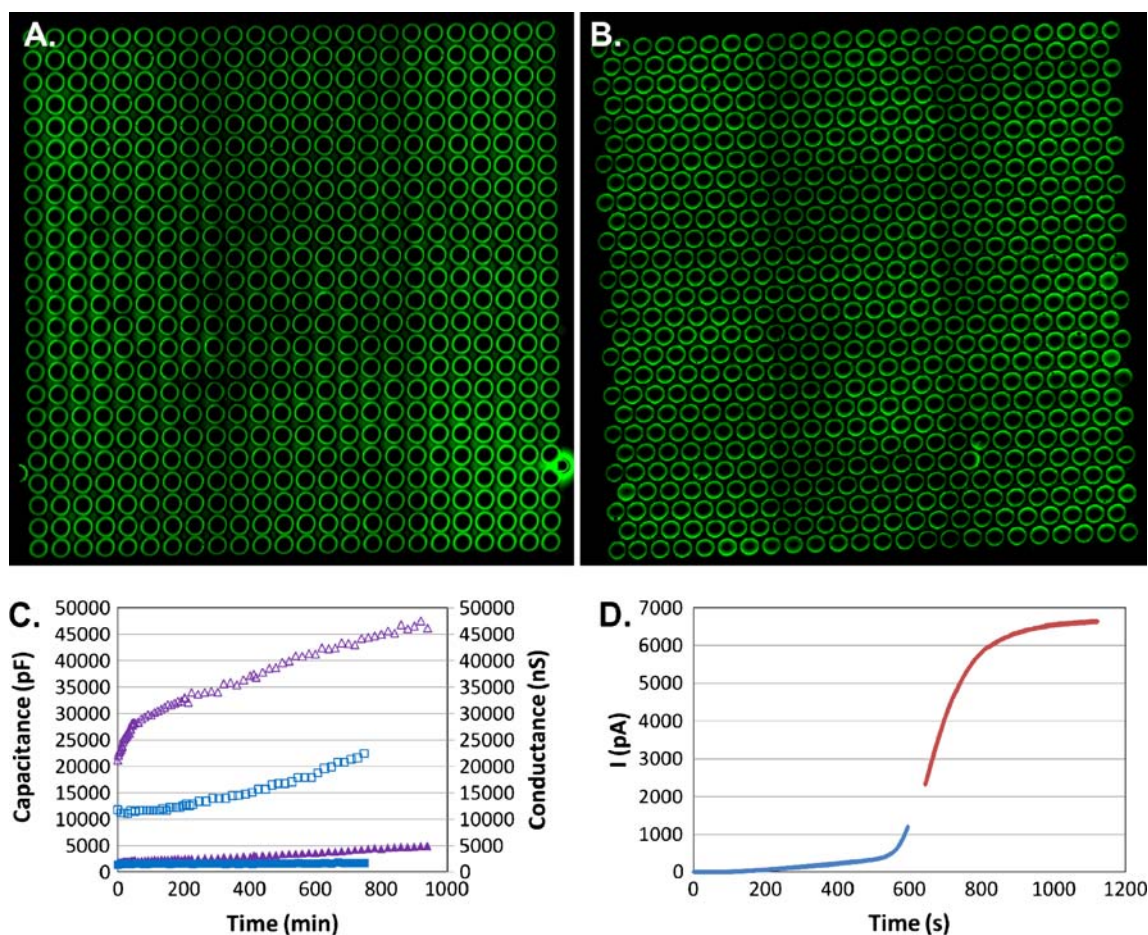
Fig. 4 Comparison of 24×24 rectangular and 24×27 hexagonal bilayer arrays. **a** and **b** Mosaics comprising 12 fluorescent images of the 24×24 rectangular and 24×27 hexagonal bilayer arrays. **c** Capacitance (*open boxes*) and conductance (*filled boxes*) values during the membrane lifetime of the 24×24 rectangular (*purple*) and 24×27 hexagonal (*blue*) arrays. Time=0 is subsequent a 15 min equilibration period after the manual thinning process. **d** Demonstra-

tion of α-HL incorporation into a 24×24 rectangular array. The initial amplifier gain was set to 10× (*blue line*). When the amplifier saturated due to the incorporation of α-HL pores, the gain was adjusted and the trace recording was resumed (*red line*). The aqueous solution in the horizontal bilayer chamber consisted of a 0.2 M KCl. The applied potential was +60 mV

individual bilayers (Fig 4a and b). Although the large arrays also needed initial manual thinning, they spontaneously continued the thinning process (Fig 4c). The maximum capacitance values that could be achieved were around 50,000 pF for the 24×24 rectangular arrays, while considerably lower values were obtainable for the 24×27 hexagonal arrays (Fig. 4c).

The bilayers exhibited relatively stable conductance values ranging between 2,000–5,000 nS, depending on the array type, throughout the bilayer lifetimes, indicating good sealing properties of the large arrays (Fig. 4c).

The current noise of the bilayers established across the large arrays was also assessed, and determined to be in the range of 10–20 pA peak-to-peak for both the 24×24 rectangular and the 24×27 hexagonal arrays, respectively.

Surprisingly, the bilayers established across the large partition arrays were considerably more stable than the bilayers established across the 8×8 partition arrays with membrane lifetimes up to around 16 h for both the rectangular and hexagonal arrays. The reason might be that bilayer breakages often appeared at the edges of the partition array. The percentage of bilayers residing at the edges is ~44% for the 8×8 partition arrays, whereas this fraction only constitutes ~16% for the 24×24 arrays and ~15% for the 24×27 arrays, respectively.

To evaluate the functionality of the large bilayer arrays, α-HL was reconstituted into the large arrays (Fig. 4d). The α-HL incorporated exponentially exhibiting a sigmoid current shape, indicating that α-HL incorporated into the bilayers in a cooperative manner (Fig 4d). The large arrays therefore comprised functional bilayers suitable for incorporation of membrane proteins, preferentially in large scale amounts.

Although evenly thinned bilayers could be consistently obtained across the large partition arrays, the spontaneous thinning process varied between experiments. This could mainly be attributed to the manual handling involved in the establishment of the lipid arrays.

To establish large scale biomimetic membrane arrays in a more reproducible manner, an automation technique needs to be integrated with the current horizontal setup. The automation of bilayer formations can be integrated with the horizontal design by either a robotic-based membrane deposition technique or a micro fluidic-based system.

In this study, we have addressed the electro-physical properties of the micro-structured membrane scaffold and the scalability of the bilayer arrays in the constructed horizontal design.

The transportation robustness of the functional bilayer arrays has not been addressed here. However, the thick precursor membranes could be stored and transported without disrupting the membranes in the stage prior to the manual thinning of membranes to lipid bilayers. Encapsu-lation of the suspended bilayers would be an expected requirement. Recent advantages in bilayer encapsulation methods suggest that a robust portable artificial membrane platform may be produced [25–29].

We conclude that the electro-physical properties of the micro-structured membrane scaffold combined with the scalability of array sizes enable further development of novel biomimetic membrane-based biosensing devices.

References

1. Suzuki H, Takeuchi S (2008) Anal Bioanal Chem 391:2695–2702
2. Fang Y, Frutos AG, Lahiri J (2002) J Am Chem Soc 124:2394–2395
3. Fang Y, Hong Y, Webb B et al (2006) MRS bulletin 31:5
4. Fang Y, Lahiri J, Picard L (2003) Drug Discov Today 8:755–761
5. Kaczorowski GJ, McManus OB, Priest BT et al (2008) J Gen Physiol 131:399–405
6. Lundbaek JA (2008) J Gen Physiol 131:421–429
7. Vogel J, Perry M, Hansen JS et al (2009) J Micromech Microeng 19:025026
8. Hansen JS, Perry M, Vogel J et al (2009) J Micromech Microeng 19:025014
9. Mueller P, Rudin DO (1969) Curr Topics Bioenergetics 3:157–249
10. Inagaki N, Narushima K, Lim SK, Park YW, Ikeda Y (2002) Journal of Polymer Science Part B: Polymer Physics 40:2871–2882
11. Y. W. Park N I (2004) Journal of Applied Polymer Science 93:1012-1020
12. Hemmler R, Bose G, Wagner R et al (2005) Biophys J 88:4000–4007
13. Wilburn JP, Wright DW, Cliffel DE (2006) Analyst 131:311–316
14. Pocanschi CL, Apell HJ, Puntervoll P et al (2006) J Mol Biol 355:548–561
15. Benz R, Frohlich O, Lauger P et al (1975) Biochim Biophys Acta 394:323–334
16. Stark G, Benz R, Pohl GW et al (1972) Biochim Biophys Acta 266:603–612
17. Mayer M, Kriebel JK, Tosteson MT et al (2003) Biophys J 85:2684–2695
18. Andersen OS, Koeppe RE 2nd (2007) Annu Rev Biophys Biomol Struct 36:107–130
19. Mobashery N, Nielsen C, Andersen OS (1997) FEBS Lett 412:15–20
20. Kleivdal H, Benz R, Jensen HB (1995) Eur J Biochem 233:310–316
21. Baaken G, Sondermann M, Schlemmer C et al (2008) Lab Chip 8:938–944
22. Lin Z, Takahashi Y, Kitagawa Y et al (2008) Anal Chem 80:6830–6833
23. Hebert TE, Gales C, Rebois RV (2006) Cell Biochem Biophys 45:85–109
24. Lohse MJ, Bunemann M, Hoffmann C et al (2007) Curr Opin Pharmacol 7:547–553

25. Jeon TJ, Malmstadt N, Schmidt JJ (2006) J Am Chem Soc 128:42–43
26. Kang XF, Cheley S, Rice-Ficht AC et al (2007) J Am Chem Soc 129:4701–4705
27. Malmstadt N, Jeon J, Schmidt J (2008) Advanced Materials 20:84–89
28. Oliver AE, Kendall EL, Howland MC et al (2008) Lab Chip 8:892–897
29. Uto M, Araki M, Taniguchi T et al (1994) Analytical Sciences 10:943–946
30. Frant MS, Ross JW Jr (1970) Science 167:987–988
31. Schar-Zammaretti P, Ziegler U, Forster I et al (2002) Anal Chem 74:4269–4274
32. Capone R, Blake S, Restrepo MR et al (2007) J Am Chem Soc 129:9737–9745
33. Borisenko V, Zhang Z, Woolley GA (2002) Biochim Biophys Acta 1558:26–33
34. Nikolelis DP, Siontorou CG (1996) Anal Chem 68:1735–1741
35. Braha O, Gu LQ, Zhou L et al (2000) Nat Biotechnol 18:1005–1007
36. Gu LQ, Braha O, Conlan S et al (1999) Nature 398:686–690
37. Ashkenasy N, Sanchez-Quesada J, Bayley H et al (2005) Angew Chem Int Ed Engl 44:1401–1404
38. Kasianowicz JJ, Brandin E, Branton D et al (1996) Proc Natl Acad Sci U S A 93:13770–13773
39. Kasianowicz JJ, Henrickson SE, Weetall HH et al (2001) Anal Chem 73:2268–2272
40. Vercoutere WA, Winters-Hilt S, DeGuzman VS et al (2003) Nucleic Acids Res 31:1311–1318
41. Winters-Hilt S, Vercoutere W, DeGuzman VS et al (2003) Biophys J 84:967–976
42. Bolstad AI, Jensen HB, Bakken V (1996) Clin Microbiol Rev 9:55–71
43. Jensen HB, Skeidsvoll J, Fjellbirkeland A et al (1996) Microb Pathog 21:331–342
44. Guo M, Han YW, Sharma A et al (2000) Oral Microbiol Immunol 15:119–123

Chapter 4

Reconstitution and folding of aquaporins

Contents

4.1 Sodium dodecyl sulfate does not unfold membrane reconstituted aquaporins SoPIP2;1 and AqpZ

Sodium dodecyl sulfate does not unfold membrane reconstituted aquaporins SoPIP2;1 and AqpZ

Jesper S. Hansen[a,b], Ardcharaporn Vararattanavech[c], Inés Plasencia[d], Per Greisen Jr[e], Julie Bomholt[b], Jaume Torres[c], Jenny Emnéus[a], Claus Hélix-Nielsen[b,e,1]

[a]The Biomedical Microsystems Section (BIOMICS), DTU Nanotech, Technical University of Denmark, DK-2800 Kgs. Lyngby, Denmark.

[b]Aquaporin A/S, Copenhagen Bio Science Park (COBIS), DK-2200 Copenhagen, Denmark.

[c]Structural & Computational Biology, School of Biological Sciences, Nanyang Technological University, 637551 Singapore.

[d]MEMPHYS – Center for Biomembrane Physics, Department of physics and chemistry, University of Southern Denmark, DK-5230 Odense, Denmark.

[e]Quantum Protein Center, DTU Physics, Technical University of Denmark, DK-2800 Kgs. Lyngby, Denmark.

[1]To whom correspondence should be sent: Claus Hélix-Nielsen, Aquaporin A/S, COBIS, Ole Maaloes Vej 3, DK-2200 Copenhagen N, Denmark. E-mail: chn@aquaporin.dk. Telephone: (+45) 27102076.

Classification. BIOLOGICAL SCIENCES: Biochemistry.

1

Abstract

The canonical picture of the anionic detergent sodium dodecyl sulfate (SDS) is that it potently unfolds soluble proteins. This has nourished the general belief that SDS is also a denaturing agent for membrane proteins. This belief is questionable and here we present evidence that SDS does not induce protein unfolding when SDS is acting on membrane proteins already reconstituted into lipid bilayers. Specifically we studied effects of SDS on the structure of α-helical bundle membrane proteins reconstituted into lipid bilayers of various lipid compositions. We demonstrate that when added to membrane reconstituted SoPIP2;1 aquaporin in concentrations below the SDS critical micelle concentration (CMC, ~8 mM), SDS causes helical rearrangements consistent with a transformation from coiled-coil to single helices, which gradually revert to coiled-coil helical arrangements with increasing SDS concentration (above SDS CMC). In contrast, a threshold value of 30% of SDS CMC promotes an abrupt change in membrane reconstituted AqpZ aquaporin secondary structure from a reconstituted conformation to a structure similar to that of the aqueous octyl-β-D-Glycopyranoside detergent stabilized state. Using a fluorescent polarity sensitive probe (Badan) we show that SDS action on membrane reconstituted SoPIP2;1 as well as AqpZ is associated with initial increased hydrophobic interactions in protein transmembrane (TM) spanning regions up to a concentration of 10% SDS CMC. At higher SDS concentrations TM hydrophobic interactions, as reported by Badan, decrease and reach a plateau from SDS CMC up to $12.5\times$ SDS CMC while preserving overall protein secondary structure.

Keywords: Membrane protein, sodium dodecyl sulfate, folding, reconstitution, lipid membrane

2

Introduction

The paradigm of SDS is that it potently unfolds and denatures proteins, but is this an unequivocal picture? SDS unfolds and denatures most water-soluble proteins with the mechanism of action being relatively well-understood (1). The unfolding and introduction of negative surface charges proportional to the mass of water-soluble proteins induced by SDS has found immense practical applications in molecular biology and biochemistry, among others, by its use in SDS polyacrylamide gel electrophoresis (PAGE) (2, 3). The mechanism of action of SDS on soluble proteins has been directly extrapolated to membrane proteins with the general belief that SDS is also a potent unfolding agent of membrane proteins (4).

Structurally membrane proteins have a much higher percentage of apolar residues than their soluble counterparts. In contrast to water-soluble proteins, membrane proteins cannot shield all their apolar residues by folding around a hydrophobic core (5). As a consequence membrane proteins avidly associate with lipid *in vivo* or *in vitro* or require detergent micelle stabilization in aqueous solutions not to unfold (5). Detergents are therefore generally a prerequisite for studying membrane proteins in aqueous solutions. A pitfall with folding and stability studies of membrane proteins in aqueous solutions is that detergents represent a more dynamic environment than the native bilayer and may alter protein flexibility and promote instability to the solubilized membrane protein (6).

An intriguing issue of SDS is that protein interactions with SDS micelles may promote formation of ordered α-helical protein conformations, also of initially non-helical proteins (7). SDS-induced structures of peptides were amphiphilic (7), and SDS peptide studies have in this perspective recently suggested that SDS micelles are capable of sufficiently mimicking protein-lipid interaction occurring at membrane protein TM regions (6). Anomalous migration of membrane proteins in SDS-PAGE has further nourished speculations of the effect of SDS on membrane protein structure (8).

Although, SDS unfolding of several polytopic membrane proteins in solution including diacylglycerol kinase (DGK) (9), bacteriorhodopsin (BR) (10, 11) and rhodopsin (12, 13) have been described, NMR and X-ray studies of membrane proteins and model TM peptides have reported secondary and tertiary conformations when solubilized in SDS, correlating well with crystal structures obtained without SDS (reviewed in (14)). Addition of SDS to BR, rhodopsin or DGK folded in detergent micelles causes
3

highly cooperative spectroscopic changes which have been interpreted as unfolding, but there is no clear evidence that these spectral changes represent a folding-unfolding equilibrium (14). Recent folding studies of rhodopsin failed to show explanatory correlation between absorbance (12) and circular dichroism (13) at the threshold where SDS induced spectroscopic absorbance changes of rhodopsin.

Circular dichroism (CD) spectroscopy is a commonly applied tool to address secondary structures of peptides and proteins. Model peptide studies of α-helical coil-coils and single helices structural differences revealed that the ratio of ellipicities at 208 nm and 222 nm was important for result interpretation, both for helical content and for helical arrangements (15, 16). A 222/208 nm ellipicity ratio of ≥1 was reported consistent with α-helical coil-coiled arrangement, while a ratio <1 correlated with single helices (17). Decreased ellipicity at 222 nm has been consistently interpreted as unfolding (13, 18-20). However, a decreased ellipicity at 222 nm alone does not necessarily picture protein unfolding, but could depending on the ellipicity at 208 nm rather be consistent with helical rearrangements of membrane protein helices as demonstrated with model peptides.

The discrepancy in the literature of how SDS affects membrane protein conformations may in part be related to the experimental setup commonly applied for membrane protein folding studies. Previous reported SDS unfolding/refolding experiments have exclusively been carried out in aqueous membrane protein solutions, consisting of detergent micelles (e.g. decylmaltoside (DM) or dodecylmaltoside (DDM)) or mixed lipid/detergent bicelle systems (e.g. L-α-1,2-dimyristoylphosphatidylcholine (DMPC)/3-[(3-cholamidopropyl)dimethylammonio]-1-propanesulfonate (CHAPS)) (11, 21-25). Unfolding in detergent micelles or mixed lipid/detergent bicelle solutions therefore rely on efficient displacement by SDS of the detergent and/or lipid molecules that otherwise shields the hydrophobic segments of the membrane protein. Thus, the molecular forces exerted on membrane proteins as well as the structural and molecular interactions of SDS/detergent or SDS/detergent/lipid micelle protein solutions are very complex.

Large unilamellar vesicles represent a more biological relevant biomimetic protein environment compared to protein/detergent micelle or protein/detergent/lipid mixed bicelle solutions. Here we reconstituted the α-helical polytopic aquaporins SoPIP2;1 and AqpZ into large unilamellar vesicles, which were subsequently titrated with SDS. We carried out equilibrium folding studies of the structural protein reorganizations imposed by SDS on membrane reconstituted proteins. We demonstrate that
4

result interpretations give a more detailed picture of the protein folding mechanisms taking place in the membrane and during protein solubilization. Our results show that SDS does not unfold the α-helical polytopic membrane proteins studied here. Moreover, our results give insight to the mechanism of detergent solubilization of membrane proteins from a membrane reconstituted protein state.

Results and discussion

SDS does not unfold reconstituted SoPIP2;1 or AqpZ. To measure the secondary structures of SoPIP2;1 or AqpZ in the presence of SDS, reconstituted or aqueous detergent octyl-β-D-glycopyranoside (OG) stabilized proteins were titrated with increasing concentrations of SDS and the CD spectra recorded at equilibrium conditions for each concentration.

E. coli total lipids consist of all the biological membrane constituents of *E. coli* bacterial membranes, including cholesterol, fatty acids and lysophospholipids. Thus, it represents a genuine cell-mimetic protein environment. The secondary structure of SoPIP2;1 reconstituted into *E. coli* total lipids showed a negative ellipicity band at 222 nm compared to 208 nm (222/208 nm ratio >1). The secondary structure of SoPIP2;1 in aqueous OG solutions showed nearly equal negative ellipicities at 222 nm and 208 nm (208/222 nm ratio ~1), which previously has been described as characteristic of predominantly helical secondary structure of proteins and peptides in solution (Figure S1A) (26). This means that the reconstituted secondary structure of SoPIP2;1 differs from the detergent solubilized structure.

In response to increasing SDS concentrations, the ellipicity profile of SoPIP2;1 reconstituted into *E. coli* total lipid liposomes changed in a concentration dependent manner at 208 nm, while the ellipicity at 222 was virtually unaltered (Figure 2A). The absolute ellipicity value at 208 nm increased from 0.03× SDS CMC (i.e. 0.25 mM SDS) to an ellipicity maximum around 0.63× SDS CMC (i.e. 5 mM SDS), followed by a decrease in the absolute ellipicity value from hereafter and to 1.25× SDS CMC (i.e. 10 mM SDS) where a plateau was reached (Fig. 1A and 2A). Consistent with reported secondary structures of synthetic α-helical coiled-coil peptide models (17), the ellipicity profile of SoPIP2;1 can be interpreted in terms of a gradual transformation of SoPIP2;1 secondary structure from an initial coiled-coil helices arrangement to single helices around 0.63× SDS CMC, which revert to comprise coiled-coil helices with increasing SDS concentrations. This also implies that the solubilization of reconstituted SoPIP2;1 proceed through an intermediate folding state until it is being completely solubilized by the SDS
5

molecules. Although increased SDS concentrations imposed α-helical rearrangements of SoPIP2;1, SDS does not unfold SoPIP2;1 when the protein is reconstituted into a lipid bilayer prior titration with SDS.

Although, the sequence identity of SoPIP2;1 and AqpZ is 25%, structural alignment of the crystal structures of SoPIP2;1 and AqpZ exhibited a root mean square deviation of <1 Å, demonstrating major similarities in secondary structure (Fig. S2). However, the CD spectra of AqpZ reconstituted into *E. coli* total lipid bilayers or in OG detergent solution differed in several aspects from that of SoPIP2;1 (Fig. 1 and Fig. S1). Apparent helical content of reconstituted AqpZ was lower compared to that of reconstituted SoPIP2;1, but the overall shape of the spectrum was similar to SoPIP2;1 and with a 222/208 nm ellipicity ratio >1 (Fig 1). This indicated that the reconstituted protein secondary structure of AqpZ was different from SoPIP2;1, but not unfolded. This was substantiated by our observation that an abrupt change in protein secondary structure of AqpZ *E. coli* lipid proteoliposomes was observed in the presence of SDS at a threshold of $0.31\times$ SDS CMC (i.e. 2.5 mM SDS) (Fig. 1B and 3A). The protein secondary structure changes imposed at this threshold went from the reconstituted protein secondary structure to a structure similar to that of the aqueous OG detergent stabilized state (Fig. S1B).

To gain more insight into the protein secondary structure changes of reconstituted proteins in response to SDS we also reconstituted SoPIP2;1 into 1,2-dioleoyl-*sn*-glycero-3-phosphocholine (DOPC) liposomes, because it comprises a more defined lipid system. With DOPC proteoliposomes the overall ellipicity change of SoPIP2;1 at 208 nm was around 15% larger from the initial protein reconstituted state and to $0.63\times$ SDS CMC compared with *E. coli* total lipids (Fig. 2B). Cholesterol increases the stiffness of the lipid bilayer, which changes the lipid molecules packing around the protein residing in the lipid bilayer (27, 28). A lipid composition of cholesterol:DOPC (3:7) resulted in an overall ellipicity change of SoPIP2;1 at 208 nm that increased around 17% at $0.63\times$ SDS CMC compared to that of pure DOPC and 30% compared to *E. coli* total lipids (Fig. 2A-C).

The influences of lipid species on reconstituted AqpZ secondary structures in presence of SDS was different from SoPIP2;1. For AqpZ reconstituted into DOPC liposomes the ellipicity change at 208 nm with a SDS concentration of $0.31\times$ SDS CMC was 16 % less compared to that of *E. coli* total lipids (Fig. 3A-C). Instead of reconstituting AqpZ into cholesterol:DOPC we reconstituted AqpZ into 1,2-diphytanoyl-*sn*-glycero-3-phosphocholine (DPhPC) liposomes and subsequently titrated the produced proteoliposomes with SDS. DPhPC is a methyl-branched synthetic archaeal lipid species, which exhibit

6

a low ion leakage in lipid bilayers and has fatty acyl packing and dynamics (as evidenced by MD simulations) comparable to that of cholesterol-phospholipids mixtures (29-31). Interestingly, the helical content of AqpZ reconstituted into DPhPC liposomes was increased compared to protein reconstitution into either *E. coli* total lipids or DOPC. Although, the secondary structure also changed from the reconstituted state to a structure similar to the OG stabilized state, the ellipicity changes was more subtle compared to AqpZ reconstituted into *E. coli* total lipids or DOPC (Fig. 3C). The overall ellipicity change at 208 nm was 31% less that of DOPC and 42% less compared with *E. coli* total lipids.

Overall, the solubilization of reconstituted AqpZ by SDS is an all-or-nothing response promoted at a specific SDS concentration threshold ($0.31\times$ SDS CMC) of which the secondary protein change from the reconstituted protein state to a structure similar to the protein of aqueous detergent solutions. Lipid bilayer stiffness affected AqpZ and SoPIP2;1 differently. Helical rearrangements of SoPIP2;1 in response to SDS was more pronounced with increased bilayer stiffness as evidenced with addition of cholesterol to DOPC phospholipids. For AqpZ the secondary structure changes in presence of SDS decreased with increased bilayer stiffness as evidenced with DPhPC. The results combined with the fact that these membrane proteins reside in plant or bacteria, respectively, could imply that although they are similar in secondary structure they have different lipid requirements.

SDS does not unfold AqpZ but partly unfolds SoPIP2;1 in OG detergent solutions. In comparison to reconstituted AqpZ, SDS did not promote notable secondary structure changes with any concentration (from $0.03\times$ to $12.5\times$ CMC) when AqpZ was in the aqueous OG detergent solubilized state (Fig 3D). This is consistent with previous published SDS PAGE experiments with AqpZ, which showed that AqpZ structure was resistant to SDS (32). In contrast, SDS promoted decreased ellipicity profiles of SoPIP2;1 in aqueous detergent solutions around $0.31\times$ SDS CMC reaching a plateau at $1.25\times$ CMC (Fig. 2D). The overall ellipicity decrease were subtle (16% of initial ellipicity value), indicating partial unfolding of SoPIP2;1 in presence of SDS in aqueous detergent solutions (Fig. 2D). Clearly there is a discrepancy between folding data obtained for membrane proteins in aqueous detergent solutions and that of reconstituted proteins. This questions the physiological relevance of obtaining detailed information of free energy changes of protein folding in detergent micelle or detergent/lipid bicelle solutions as has previously been reported.

7

Fluorescent probing of hydrophobic interactions in protein TM regions. To address hydrophobic interactions of protein TM spanning regions in response to SDS, surface exposed cysteines of native SoPIP2;1 or AqpZ were conjugated with the fluorescent polarity sensitive Badan probe. Badan shifts emission spectra upon local environment polarity changes; the emission of Badan is red-shifted followed by a concomitant fluorescence intensity decrease in response to increased polarity, whereas the opposite is the case with decreased polarity (33). The Badan spectral emission wavelength shifts inferred by polarity changes can be up to ~100 nm which compared to the intrinsic tryptophan fluorescence is large. This high degree of polarity sensitivity has been demonstrated suited for detailed examination of protein-lipid interactions at TM regions of membrane proteins (34, 35).

Crystal structures of aquaporin isoforms show that several aquaporins, including SoPIP2;1 and AqpZ, contain surface exposed cysteines that are located in the protein TM region (Table S1). The crystal structure of SoPIP2;1 revealed that Cys127 and Cys132 were both positioned in the acyl-acyl interface, relative to the lipid bilayer membrane, while Cys9 of AqpZ was located at the acyl-phospholipid headgroup interface. The difference in lateral position between SoPIP2;1 Cys127 and Cys132 is very close, meaning that labeling of both or either of the two cysteines would likely result in similar Badan polarity sensitivity. However, it is likely only Cys132 that is available for chemical conjugation reactions, because of dipole and dipole-quadropole interactions between Cys127 and Trp246 and Phe227, respectively (Fig. S3). The superimposition of deduced Badan conjugation of SoPIP2;1 and AqpZ structures are shown in Fig. 4.

The presence of cysteines in the aquaporin membrane TM regions makes it possible to probe lipid-protein interactions without the need of performing site-directed mutagenesis to introduce strategically positioned cysteines. Badan was chosen for labeling reactions due to its polarity sensitivity, but also because it is a very small fluorescent probe not much larger than a tryptophan residue. The latter significantly decreases the likelihood that probe conjugations affect folding or function. Indeed, the Badan group of conjugated SoPIP2;1 or AqpZ did not cause structural alterations compared to the native protein secondary structure (Fig. S4).

Although the dye/monomer ratio would be expected to be ~1, we found a Badan dye labeling degree of around 0.5 mol dye/monomer SoPIP2;1 and 0.4 mol dye/monomer AqpZ, respectively, indicating that not all of the Cys132 of SoPIP2;1 or Cys9 of AqpZ were accessible for the conjugation reactions. A
8

reason for this could of course be due to the presence of disulfide bridges. Shielding of the surface exposed cysteines by detergent could also explain this observation. In support, the 2.5 Å X-ray structure of AqpZ revealed that an OG molecule was bound to hydrophobic TM regions of each monomer of the tetramer structure (36). This was further substantiated by our observation that 20 h labeling times were necessary to obtain the above mentioned dye labeling degrees, a process that for soluble proteins normally proceed to completion within minutes (37, 38).

Polarity changes in TM regions of reconstituted aquaporins in response to SDS. The relative positions of the Badan probe of conjugated SoPIP2;1 and AqpZ reconstituted into lipid bilayers were reflected by the fluorescence emission wavelength maxima. Baseline values for Badan fluorescence emission wavelength maxima are around 440 nm in apolar solvents and 550 nm in water. Reconstituted Badan labeled SoPIP2;1 had fluorescence emission maxima around 447 nm in *E. coli* total lipids and 454 nm in DOPC liposomes (Fig. 5A and 5C), while Badan labeled AqpZ had fluorescence emission maxima around 471 nm or 492 nm, respectively, in the corresponding *E. coli* lipids or DOPC proteoliposomes (Fig. 5B and 5D). This is in line with the expected positioning of the SoPIP2;1 Badan group in the interior of the lipid bilayer compared to the Badan group of AqpZ expected to be located in the phospholipid acyl-phosphate headgroup interface of the lipid bilayer. Moreover, this indicated that the Badan label of reconstituted aquaporins was very sensitive to the changes in the polarity of the micro environment around the Badan group of both proteins.

In presence of SDS, polarity in the protein TM region initially decreased as evidenced by an increased fluorescence emission yield and a blue shifted spectra of Badan labeled SoPIP2;1 as well as AqpZ. The SDS concentration where the environment of the protein TM region became most apolar, as measured by Badan emission, differed between the two proteins (Fig. 5). For reconstituted Badan labeled SoPIP2;1 this occurred at 0.06× SDS CMC (i.e. 0.5 mM SDS), followed by gradually increase in polarity until 0.13× CMC (i.e. 1 mM SDS). At higher SDS pronounced red shifting occurred with 0.3× and 0.6× SDS CMC concentrations (Fig. 5A and 5C). With higher SDS concentrations the TM region polarity reached a plateau around SDS CMC and up to concentrations of 12.5 × CMC (100 mM) (Fig. 5A, 5C and Fig. S5A). For Badan labeled AqpZ the polarity changes at low SDS concentrations were more pronounced than for SoPIP2;1. The most apolar situation occurred with 0.31× SDS CMC. At 0.63× SDS CMC a large red shift occurred, meaning that the polarity of the protein TM regions

9

increased substantially at this concentration. With increased SDS concentrations the polarity increased gradually up to 12.5× SDS CMC (Fig. 5B, 5D and Fig. S5B).

Combined the results demonstrated that the presence of SDS molecules at low concentrations lead to increased hydrophobic interactions in the protein TM regions of reconstituted membrane proteins. SDS detergent solubilization of the lipid membranes appear around 0.63× SDS CMC as evidenced by the concomitant large Badan red shift at this threshold, which was observed for both reconstituted Badan-SoPIP2;1 and Badan-AqpZ (Fig. 5). The Badan fluorescence emission red shifts imposed by SDS are caused by detergent solubilization and not related to protein unfolding per se as evidenced by CD spectroscopy (Fig. 2 and 3).

Hydrophobic interactions in protein TM regions were related to lipid bilayer stiffness. The largest hydrophobicity interactions experienced by SoPIP2;1 TM regions in response to low SDS concentrations occurred with the protein reconstituted into cholesterol:DOPC (3:7) liposomes (Fig. S5A) as compared to *E. coli* lipids or DOPC liposomes. Similarly, AqpZ reconstituted into DPhPC liposomes also experienced the largest TM hydrophobic interactions at the low SDS concentrations (Fig. S5B). This demonstrates that increased lipid bilayer stiffness results in increased packing of molecules (lipid and/or detergent) around the protein TM regions in response to low SDS concentrations (<0.5 SDS CMC). The hydrophobic TM region interactions experienced with low SDS concentrations were much more pronounced for AqpZ with the Badan positioned in the phospholipid headgroup interface compared to SoPIP2;1 where the probe is positioned in the acyl-acyl region. This indicates that the packing of lipid and/or detergent molecules in response to low SDS concentrations is denser in the phospholipid headgroup interfacial region compared to the interior region of the lipid bilayer.

Displacement of OG by SDS at TM regions differs for SoPIP2;1 and AqpZ. SDS interactions with TM regions of OG detergent stabilized Badan-SoPIP2;1 in aqueous solutions led to increased hydrophobicity at low SDS concentrations, which is consistent with the results of reconstituted SoPIP2;1 (Fig. 6A). The largest degree of hydrophobicity was observed around 1× SDS CMC (8 mM), and with increased SDS concentrations gradual Badan spectral red shifting occurred up to 12.5× SDS CMC consistent with gradually increased hydrophilicity. This demonstrated that OG above SDS CMC is being displaced from the protein TM regions by SDS. For AqpZ the interactions of SDS with protein

10

TM regions in aqueous OG solutions were different from SoPIP2;1 (Fig. 6B). This is likely related to a higher binding affinity of AqpZ with OG detergent molecules.

The X-ray crystal structure of AqpZ was resolved with OG molecules bound to the hydrophobic protein TM regions (36). A likely scenario is the persistence of a SDS/OG bicelle interactions around the TM regions of detergent solubilized AqpZ titrated with SDS, which could explain the different fluorescent emission spectra compared to SoPIP2;1 in response to SDS. These results combined with the CD spectroscopy data indicates a difference in lipid requirements between AqpZ and SoPIP2;1.

Conclusions

Biophysical studies of membrane proteins are complicated by generally low yield of recombinant purified protein and by the general requirement of detergents which on one hand are necessary to prevent protein unfolding in aqueous solutions, but on the other hand may also promote protein instability. Hydrophobic interactions in protein TM regions of reconstituted membrane proteins could provide detailed information of molecular lipid-protein interactions taking place in biological membranes. However, previous folding studies of membrane proteins have generally been carried out with proteins in detergent micelles (e.g. DM, DDM and OG) or with mixed micelles such as DMPC/CHAPS bicelle systems with ambiguous results. Combined our results recommend a paradigm shift from folding studies in aqueous solutions to folding studies of reconstituted membrane proteins, representing genuine cell-mimetic.

Acknowledgments

11

Supporting Information Available

Materials and methods, CP spectra of SoPIP2;1 and AqpZ reconstituted in various lipids or OG stabilized aqueous solutions, structural alignment of SoPIP2;1 and AqpZ, identification of surface exposed cysteines of various aquaporin crystal structures, analysis of Cys127 and Cys132 and neighboring residues of SoPIP2;1, CD spectra of non-labeled versus Badan fluorescently labeled aquaporin SoPIP2;1 or AqpZ, fluorescence spectra of Badan labeled SoPIP2;1 or AqpZ reconstituted into cholesterol:DOPC (3:7) or DPhPC liposomes, respectively.

Footnotes

Author contributions: J.S.H. designed research; J.S.H., A.V., I.P., P.G.J. and J.B. performed research; J.S.H., I.P., P.G.J., J.B., J.T., J.E. and C.H.N. analyzed data; J.S.H. and C.H.N. wrote paper.

Conflict of interest statement: A patent application related to this work has been filed for which J.S.H. and C.H.N. are inventors.

12

References

1. Reynolds JA & Tanford C (1970) The Gross Conformation of Protein-Sodium Dodecyl Sulfate Complexes. *Journal of Biological Chemistry* 245(19):5161-5165.
2. Shapiro AL, Viñuela E, & V. Maizel J (1967) Molecular weight estimation of polypeptide chains by electrophoresis in SDS-polyacrylamide gels. *Biochemical and Biophysical Research Communications* 28(5):815-820.
3. Weber K & Osborn M (1969) The Reliability of Molecular Weight Determinations by Dodecyl Sulfate-Polyacrylamide Gel Electrophoresis. *Journal of Biological Chemistry* 244(16):4406-4412.
4. Reynolds JA & Tanford C (1970) Binding of dodecyl sulfate to proteins at high binding ratios. Possible implications for the state of proteins in biological membranes. (Translated from eng) *Proc Natl Acad Sci U S A* 66(3):1002-1007 (in eng).
5. Fiedler S, Broecker J, & Keller S (2010) Protein folding in membranes. (Translated from eng) *Cell Mol Life Sci* 67(11):1779-1798 (in eng).
6. Tulumello DV & Deber CM (2009) SDS micelles as a membrane-mimetic environment for transmembrane segments. (Translated from eng) *Biochemistry* 48(51):12096-12103 (in eng).
7. Parker W & Song PS (1992) Protein structures in SDS micelle-protein complexes. (Translated from eng) *Biophys J* 61(5):1435-1439 (in eng).
8. Rath A, Glibowicka M, Nadeau VG, Chen G, & Deber CM (2009) Detergent binding explains anomalous SDS-PAGE migration of membrane proteins. (Translated from eng) *Proc Natl Acad Sci U S A* 106(6):1760-1765 (in eng).
9. Lau FW & Bowie JU (1997) A Method for Assessing the Stability of a Membrane Protein. *Biochemistry* 36(19):5884-5892.
10. Huang KS, Bayley H, Liao MJ, London E, & Khorana HG (1981) Refolding of an integral membrane protein. Denaturation, renaturation, and reconstitution of intact bacteriorhodopsin and two proteolytic fragments. (Translated from eng) *J Biol Chem* 256(8):3802-3809 (in eng).
11. Curnow P & Booth PJ (2007) Combined kinetic and thermodynamic analysis of alpha-helical membrane protein unfolding. (Translated from eng) *Proc Natl Acad Sci U S A* 104(48):18970-18975 (in eng).
12. Dutta A, *et al.* (2010) Characterization of membrane protein non-native states. 2. The SDS-unfolded states of rhodopsin. (Translated from eng) *Biochemistry* 49(30):6329-6340 (in eng).
13. Dutta A, Tirupula KC, Alexiev U, & Klein-Seetharaman J (2010) Characterization of membrane protein non-native states. 1. Extent of unfolding and aggregation of rhodopsin in the presence of chemical denaturants. (Translated from eng) *Biochemistry* 49(30):6317-6328 (in eng).
14. Renthal R (2006) An unfolding story of helical transmembrane proteins. (Translated from eng) *Biochemistry* 45(49):14559-14566 (in eng).
15. McNamara C, *et al.* (2008) Coiled-coil irregularities and instabilities in group A Streptococcus M1 are required for virulence. (Translated from eng) *Science* 319(5868):1405-1408 (in eng).
16. Monera OD, Zhou NE, Kay CM, & Hodges RS (1993) Comparison of antiparallel and parallel two-stranded alpha-helical coiled-coils. Design, synthesis, and characterization. (Translated from eng) *J Biol Chem* 268(26):19218-19227 (in eng).
17. Lau SY, Taneja AK, & Hodges RS (1984) Synthesis of a model protein of defined secondary and quaternary structure. Effect of chain length on the stabilization and formation of two-stranded alpha-helical coiled-coils. (Translated from eng) *J Biol Chem* 259(21):13253-13261 (in eng).

13

18. Das TK, Mazumdar S, & Mitra S (1998) Characterization of a partially unfolded structure of cytochrome c induced by sodium dodecyl sulphate and the kinetics of its refolding. (Translated from eng) *Eur J Biochem* 254(3):662-670 (in eng).

19. Read MJ & Burkett SL (2003) Asymmetric [alpha]-helicity loss within a peptide adsorbed onto charged colloidal substrates. *Journal of Colloid and Interface Science* 261(2):255-263.

20. Scholtz JM, Qian H, York EJ, Stewart JM, & Baldwin RL (1991) Parameters of helix–coil transition theory for alanine-based peptides of varying chain lengths in water. *Biopolymers* 31(13):1463-1470.

21. Curnow P & Booth PJ (2009) The transition state for integral membrane protein folding. (Translated from eng) *Proc Natl Acad Sci U S A* 106(3):773-778 (in eng).

22. Booth PJ & Curnow P (2009) Folding scene investigation: membrane proteins. (Translated from eng) *Curr Opin Struct Biol* 19(1):8-13 (in eng).

23. Chill JH, Louis JM, Miller C, & Bax A (2006) NMR study of the tetrameric KcsA potassium channel in detergent micelles. (Translated from eng) *Protein Sci* 15(4):684-698 (in eng).

24. Chen GQ & Gouaux E (1999) Probing the folding and unfolding of wild-type and mutant forms of bacteriorhodopsin in micellar solutions: evaluation of reversible unfolding conditions. (Translated from eng) *Biochemistry* 38(46):15380-15387 (in eng).

25. Charalambous K, O'Reilly AO, Bullough PA, & Wallace BA (2009) Thermal and chemical unfolding and refolding of a eukaryotic sodium channel. (Translated from eng) *Biochim Biophys Acta* 1788(6):1279-1286 (in eng).

26. Kelly SM & Price NC (1997) The application of circular dichroism to studies of protein folding and unfolding. (Translated from eng) *Biochim Biophys Acta* 1338(2):161-185 (in eng).

27. Vist MR & Davis JH (1990) Phase equilibria of cholesterol/dipalmitoylphosphatidylcholine mixtures: 2H nuclear magnetic resonance and differential scanning calorimetry. (Translated from eng) *Biochemistry* 29(2):451-464 (in eng).

28. Lundbaek JA, Birn P, Girshman J, Hansen AJ, & Andersen OS (1996) Membrane stiffness and channel function. (Translated from eng) *Biochemistry* 35(12):3825-3830 (in eng).

29. Hsieh CH, Sue SC, Lyu PC, & Wu WG (1997) Membrane packing geometry of diphytanoylphosphatidylcholine is highly sensitive to hydration: phospholipid polymorphism induced by molecular rearrangement in the headgroup region. (Translated from eng) *Biophys J* 73(2):870-877 (in eng).

30. Shinoda W, Mikami M, Baba T, & Hato M (2004) Molecular Dynamics Study on the Effects of Chain Branching on the Physical Properties of Lipid Bilayers: 2. Permeability. *The Journal of Physical Chemistry B* 108(26):9346-9356.

31. Shinoda W, Mikami M, Baba T, & Hato M (2004) Dynamics of a highly branched lipid bilayer: a molecular dynamics study. *Chemical Physics Letters* 390(1-3):35-40.

32. Borgnia MJ, Kozono D, Calamita G, Maloney PC, & Agre P (1999) Functional reconstitution and characterization of AqpZ, the E. coli water channel protein. (Translated from eng) *J Mol Biol* 291(5):1169-1179 (in eng).

33. Kawaski A, Kuklinski B, & Bojarski P (2002) Thermochromic Absorption, Fluorescence Band Shifts and Dipole Moments of BADAN and ACRYLODAN. *Z. Naturforsch* 57a:716–722.

34. Koehorst RB, Spruijt RB, & Hemminga MA (2008) Site-directed fluorescence labeling of a membrane protein with BADAN: probing protein topology and local environment. (Translated from eng) *Biophys J* 94(10):3945-3955 (in eng).

35. Valeva A, *et al.* (2008) Putative identification of an amphipathic alpha-helical sequence in hemolysin of Escherichia coli (HlyA) involved in transmembrane pore formation. (Translated from eng) *Biol Chem* 389(9):1201-1207 (in eng).

14

36.   Savage DF, Egea PF, Robles-Colmenares Y, O'Connell JD, 3rd, & Stroud RM (2003) Architecture and selectivity in aquaporins: 2.5 a X-ray structure of aquaporin Z. (Translated from eng) *PLoS Biol* 1(3):E72 (in eng).

37.   Hansen JS, Villadsen JK, Gaster M, Faergeman NJ, & Knudsen J (2006) Micro method for determination of nonesterified fatty acid in whole blood obtained by fingertip puncture. (Translated from eng) *Anal Biochem* 355(1):29-38 (in eng).

38.   Wadum MC, *et al.* (2002) Fluorescently labelled bovine acyl-CoA-binding protein acting as an acyl-CoA sensor: interaction with CoA and acyl-CoA esters and its use in measuring free acyl-CoA esters and non-esterified fatty acids. (Translated from eng) *Biochem J* 365(Pt 1):165-172 (in eng).

15

Figure legends

Fig. 1. Circular dichroism profiles of SoPIP2;1 and AqpZ *E. coli* lipid proteoliposomes titrated with SDS. SoPIP2;1 from spinach (A) and *E. coli* AqpZ (B) were reconstituted into *E. coli* proteoliposomes and subsequently titrated with SDS. Spectra were recorded at equilibrium conditions proceeding 1 h incubation periods.

Fig. 2. Correlation of mean residual ellipicity and SDS concentration of SoPIP2;1 reconstituted or aqueous detergent solubilized. Mean residual ellipicity (MRE) profiles of SDS titrated into SoPIP2;1 reconstituted into proteoliposomes with lipid compositions: A) *E. coli* total lipids, B) 1,2-dioleoyl-*sn*-glycero-3-phosphocholine (DOPC) proteoliposomes and C) cholesterol:DOPC (3:7 mol/mol). D) Shows the SDS titration MRE profile of the OG detergent solubilized state of SoPIP2;1. Sample protein concentrations were 0.25 mg/ml.

Fig. 3. Correlation of mean residual ellipicity and SDS concentration of AqpZ reconstituted or aqueous detergent solubilized. Mean residual ellipicity (MRE) profiles of SDS titrated into AqpZ reconstituted into proteoliposomes with lipid compositions: A) *E. coli* total lipids, B) DOPC proteoliposomes, or C) 1,2-diphytanoyl-*sn*-glycero-3-phosphocholine (DPhPC). D) Shows the SDS titration MRE profile of the OG detergent solubilized state of AqpZ. Sample protein concentrations were 0.25 mg/ml.

Fig. 4. Superimposition of the fluorescent probe Badan with surface exposed cysteines of the structures of SoPIP2;1 and AqpZ. A) Top view and B) Side view of SoPIP2;1 conjugated with Badan. C) Top view and D) Side view of AqpZ conjugated with Badan. Badan superimposition was performed with PDB structures of the resolved open tetramer structure of SoPIP2;1 (PDB: 2B5F) or the tetrameric crystal structure of AqpZ (PDB: 2ABM).

Fig. 5. SDS induced Badan fluorescence emission changes of reconstituted SoPIP2;1 and AqpZ. Equilibrium measurements of SDS titration with Badan labeled SoPIP2;1 reconstituted into DOPC (A) and *E. coli* total lipids (C) or AqpZ reconstituted into DOPC (B) or *E. coli* total lipids (D). Sample protein concentrations were 0.25 mg/ml. Fluorescence spectra were recorded with excitation at 380 nm and emission collected from 400 to 700 nm.

16

Fig. 6. SDS induced fluorescence changes of Badan labeled SoPIP2;1 and AqpZ in aqueous solutions. SDS equilibrium measurements of Badan labeled SoPIP2;1 (A) and AqpZ (B) in octyl-β-D-glycopyranoside aqueous solution. Sample protein concentrations were 0.25 mg/ml. Fluorescence spectra were recorded with excitation at 380 nm and emission collected from 400 to 700 nm.

17

Figures

Fig. 1

Fig. 2

Fig. 3

Fig. 4

A.

B.

C.

D.

Fig. 5

Fig. 6

23
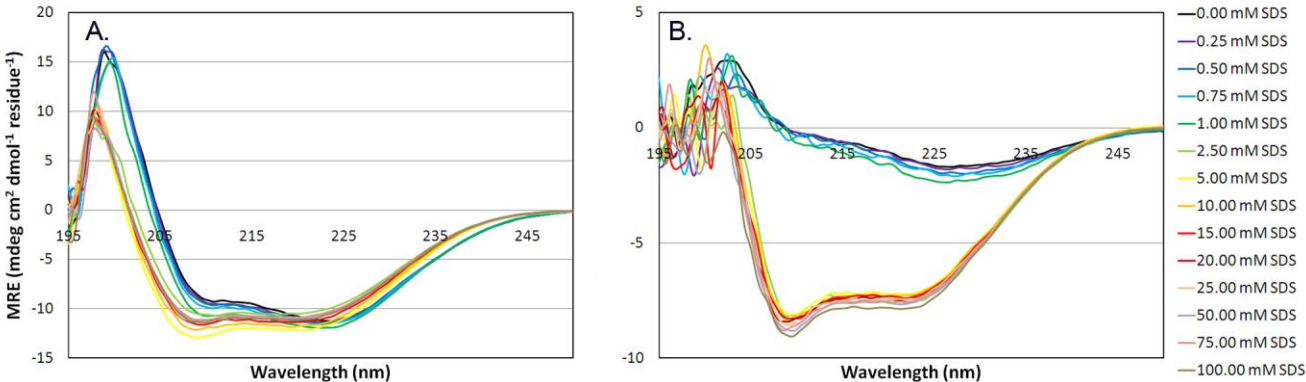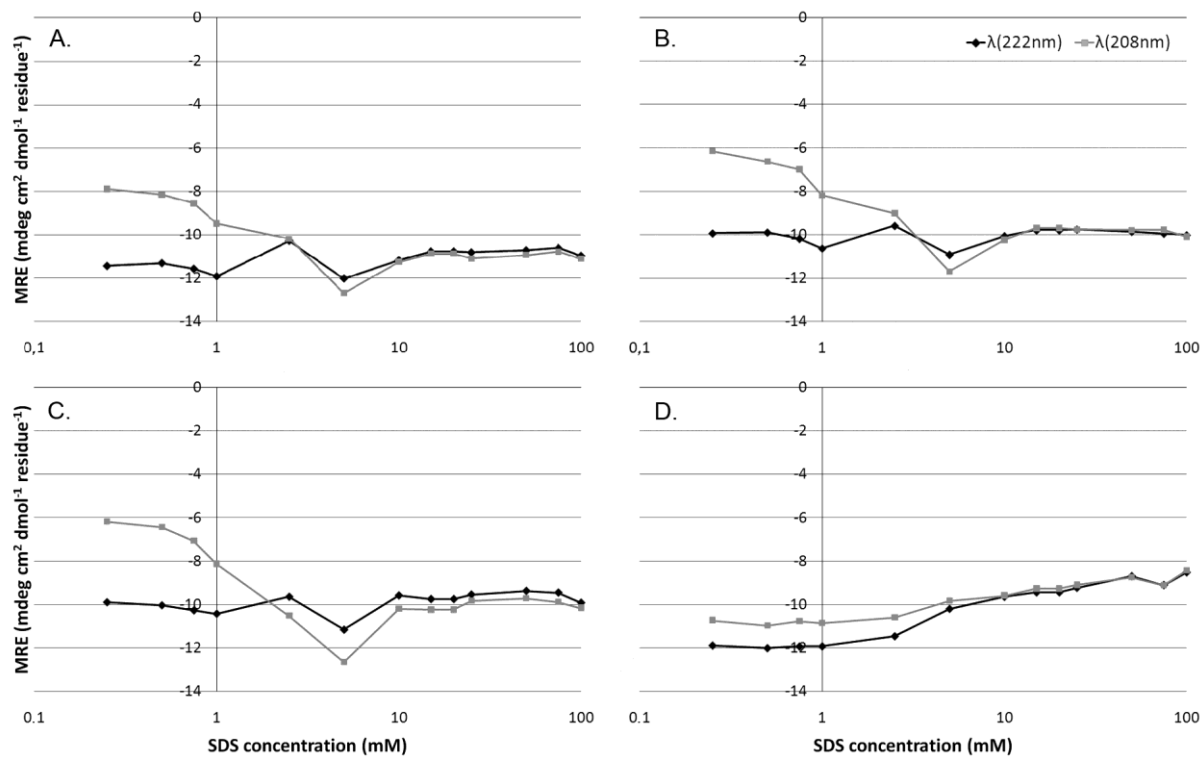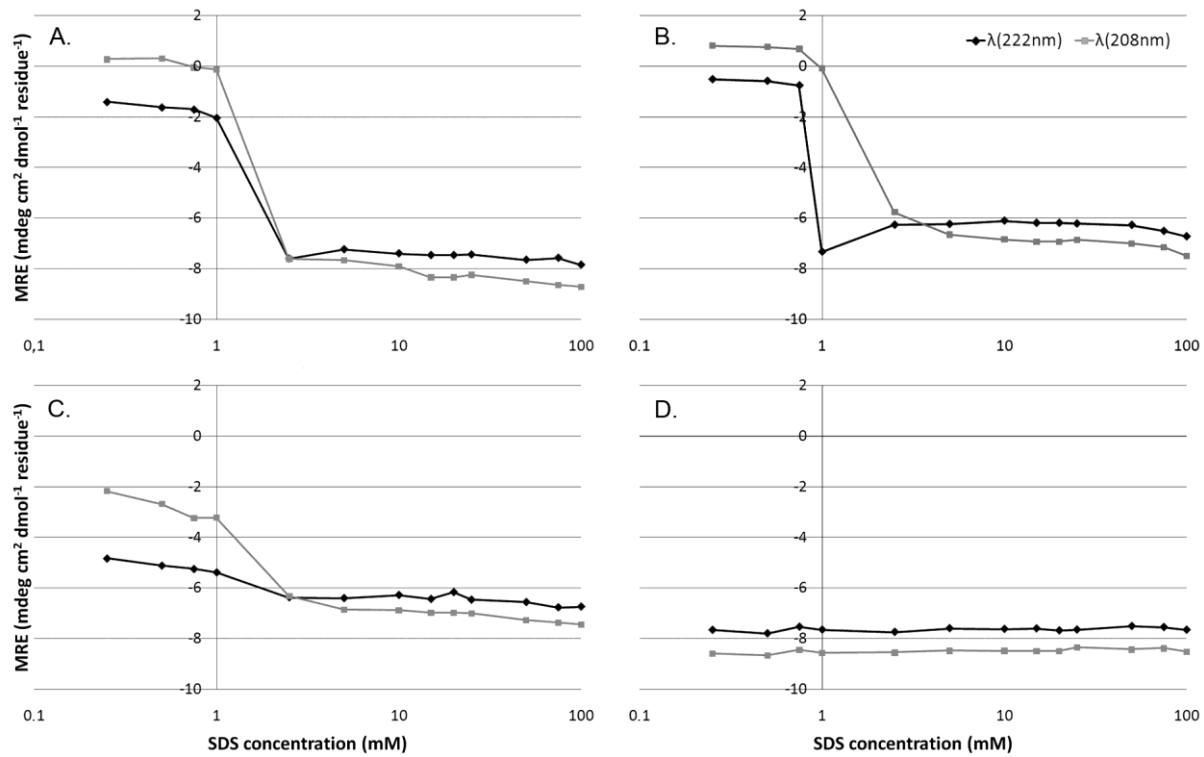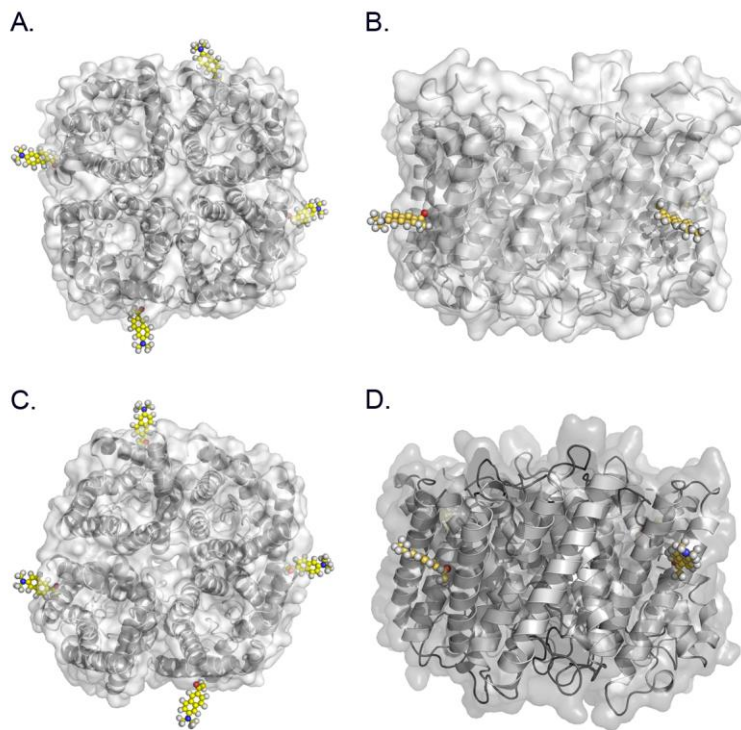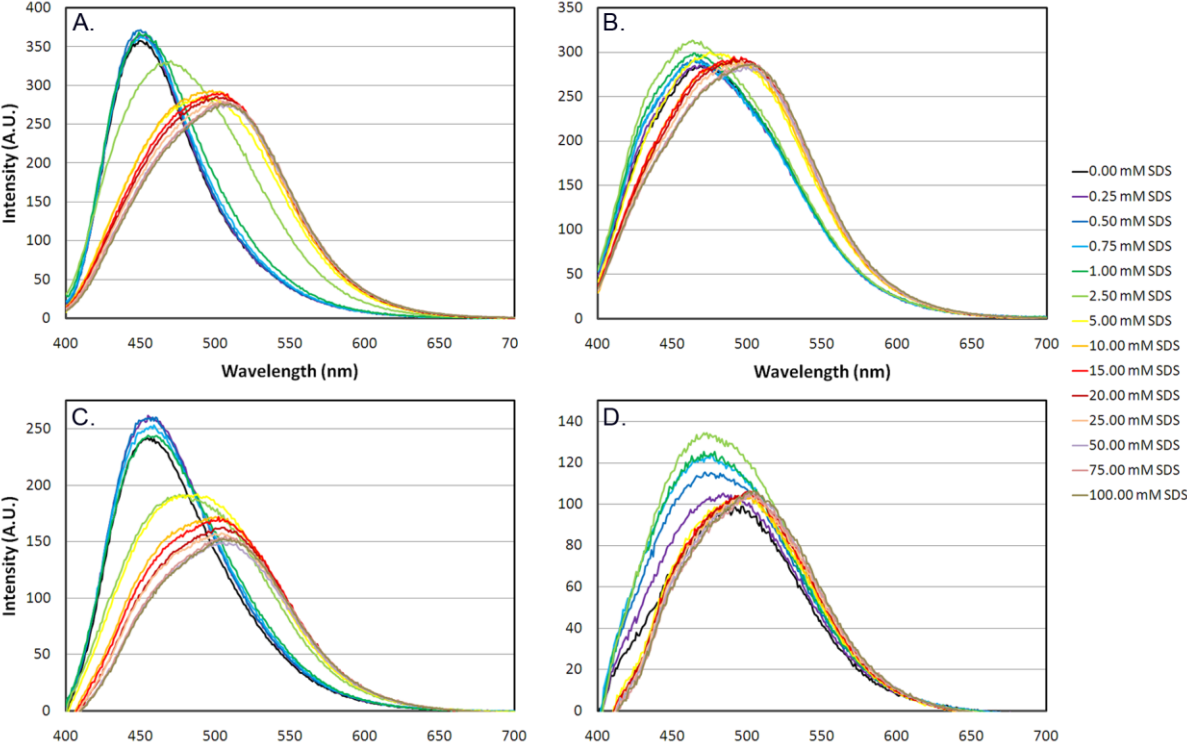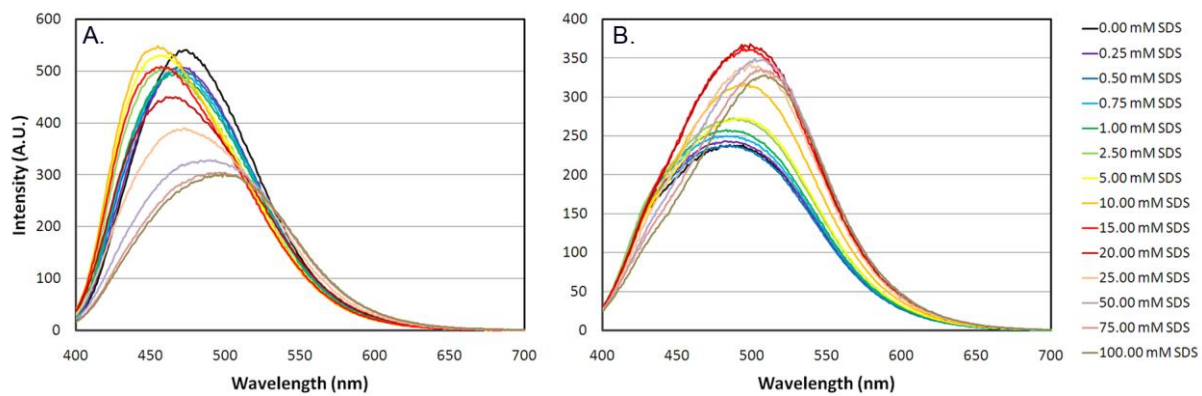
Supporting Information

Sodium dodecyl sulfate does not unfold membrane reconstituted aquaporins SoPIP2;1 and AqpZ

Jesper S. Hansen[a,b], Ardcharaporn Vararattanavech[c], Inés Plasencia[d], Per Greisen Jr[e], Julie Bomholt[b], Jaume Torres[c], Jenny Emnéus[a], Claus Hélix-Nielsen[b,e,1]

[a]The Biomedical Microsystems Section (BIOMICS), DTU Nanotech, Technical University of Denmark, DK-2800 Kgs. Lyngby, Denmark.

[b]Aquaporin A/S, Copenhagen Bio Science Park (COBIS), DK-2200 Copenhagen, Denmark.

[c]Structural & Computational Biology, School of Biological Sciences, Nanyang Technological University, 637551 Singapore.

[d]MEMPHYS – Center for Biomembrane Physics, Department of physics and chemistry, University of Southern Denmark, DK-5230 Odense, Denmark.

[e]Quantum Protein Center, DTU Physics, Technical University of Denmark, DK-2800 Kgs. Lyngby, Denmark.

[1]To whom correspondence should be sent: Claus Hélix-Nielsen, Aquaporin A/S, COBIS, Ole Maaloes Vej 3, DK-2200 Copenhagen N, Denmark. E-mail: chn@aquaporin.dk. Telephone: (+45) 27102076.

Classification. BIOLOGICAL SCIENCES: Biochemistry.

1

Materials and Methods

Reagents. The lipids 1,2-dioleoyl-*sn*-glycero-3-phosphocholine (DOPC), *E. coli* total lipid extract and 1,2-diphytanoyl-*sn*-glycero-3-phosphocholine (DPhPC) were purchased from Avanti Polar Lipids Inc. (Alabaster, AL, USA). The fluorescent dye 6-bromoacetyl-2-dimethylaminonaphthalene (Badan) and polyacrylamide gel Econo-Pac 10DG desalting columns (Bio-Rad) for purification of dye-protein conjugations were obtained from AnaSpec (Fremont, CA, USA). Octyl-β-D-glucopyranoside (OG) was purchased from Anatrace, Inc. (Maumee, OH, USA). Cholesterol, SDS, Tris, phosphate buffered saline (PBS) (10 mM sodium phosphate, 138 mM sodium chloride, 2.7 mM potassium chloride, pH 7.4) and 99.5% glycerol were obtained from Sigma Aldrich Denmark (Brøndby, Denmark). All other chemicals used were of analytical grade and purchased from commercial sources.

Heterologous protein overexpression of spinach SoPIP2;1 and bacterial AqpZ. Spinach aquaporin SoPIP2;1 was kindly provided by Professor Urban Johansson, Department of Biochemistry, Lund University, Sweden. The protein was overproduced in the methylotrophic yeast *Pichia pastoris* as His-tagged protein with a myc epitope, which was subsequently purified using Ni-affinity chromatography as previously described (1). The protein was delivered solubilized in PBS (10 mM sodium phosphate, 138 mM sodium chloride, 2.7 mM potassium chloride, pH 7.4) supplemented with 1% OG and 10% glycerol. The SoPIP2;1 protein was stored at -80°C until use.

Functional AqpZ was overproduced in *E. coli* strain BL21(DE3) bacterial cultures as His-tagged protein with a tobacco etch virus cleavage site. The fusion protein has 264 amino acid and a Mw of 27,234 Da. Genomic DNA from *E. coli* DH5α was used as a source for amplifying the AqpZ gene. The AqpZ gene was amplified using gene specific primers with the addition of a tobacco etch virus cleavage site (TEV); ENLYFQSN at the N-terminus of AqpZ. The amplified AqpZ was digested with the enzyme *Nde*I and *BamH*I and then ligated to the similarly digested 6-His tagged expression pET28b vector DNA. The positive clones were verified by PCR-screening. Then the authenticity of the constructs was confirmed by DNA sequencing. The *E.coli* strain BL21(DE3) was used for expression of the protein. Luria Broth cultures containing 50 µg/ml Kanamycin were incubated for 13-16 hours at 37°C, diluted 100-fold into fresh LB broth and propagated to a density of about 1.2-

2

1.5 (OD at 600 nm). Expression of recombinant protein was induced by addition of 1 mM IPTG for 3 hour at 35°C before centrifugation.

Harvested cell was resuspended in ice cold binding buffer (20 mM Tris pH 8.0, 50 mM NaCl, 2 mM β-mercaptoethanol, 10% glycerol) in the presence of 0.4 mg/ml lysozyme, 50 units Bensonase and 3% OG The sample was subjected to five times lysis cycles in a microfluidizer at 12,000 Pa. Insoluble material was pelleted by 30 minutes centrifugation at 40,000× g. The supernatant was passed through a Q-sepharose fast flow column (Amersham Pharmacia), and the flow through was collected. The flow though fraction was topped up with NaCl to 300 mM before loaded onto a pre-equilibrated Ni-NTA column. The column was washed with 100 column volumes of a wash buffer (20 mM Tris pH 8.0, 300 mM NaCl, 25 mM Imidazole, 2 mM β-mercaptoethanol, 10% glycerol) to remove non-specifically bound material. Ni-NTA agarose bound material was eluted with five bed volumes of elution buffer (20 mM Tris pH 8.0, 300 mM NaCl, 300 mM Imidazole, 2 mM β-mercaptoethanol, 10% glycerol, containing 30 mM OG. AqpZ was further purified with anion exchange chromatography; monoQ column (GE healthcare). The mixture sample was diluted and concentrated to bring the salt and imidazole concentration to approximately 10 mM with Amicon concentrator, membrane cut off 10,000 Da before loading to MonoQ column. The buffer used during anion exchange chromatography were (A) 20 mM Tris pH 8.0, 30 mM OG, 10% glycerol and (B) 20 mM Tris pH 8.0, 1 M NaCl, 30 mM OG, 10% glycerol. The eluted peak fractions containing AqpZ from the ion exchange column was pooled. The purified AqpZ was kept frozen at -80°C.

Fluorescent labeling of spinach SoPIP2;1 and *E. coli* AqpZ aquaporins. Spinach aquaporin SoPIP2;1 and *E. coli* AqpZ were labeled with Badan. Synthesis and handling of Badan-derivatized proteins was carried out under dim light. To carry out the reaction, 10-fold molar excess of Badan to protein from a 20 mM stock solution of Badan (dissolved in dimethylformamide) was added to a 10 mg/ml protein solution. The reaction was allowed to take place for 20 h at 4ºC with end-over-end rotation. The reaction mixture was desalted on a polyacrylamide gel Econo-Pac 10DG desalting column (Bio-Rad) using PBS, 1% OG, 1% glycerol, pH 7.4 as eluent buffer. The resulting fluorescently-labeled aquaporins was stored at 4ºC until use.

3

Preparation of large unilamellar liposomes and proteoliposomes. Liposomes for protein reconstitution were prepared by evaporation of the chloroform by nitrogen gas, drying in under vacuum in a glass desiccator for 2 h followed by rehydration in PBS containing 1.3% OG, pH 7.4 to a lipid concentration of 10 mg/ml. The liposomes were extruded 21 times through a 200 nm polycarbonate filter using a LIPEX barrel extruder (Northern Lipids Inc., Burnaby, BC, Canada).

The SoPIP2;1, or AqpZ or the corresponding fluorescent Badan-SoPIP2;1 or Badan-AqpZ were reconstituted by mixing with the liposomes at a lipid-to-protein ratio (LPR) of 200. Protein concentrations were determined by UV/Vis absorbance spectroscopy using the extinction coefficient at 280 nm of 46,660 M^{-1} cm^{-1} for SoPIP2;1 and 36,370 M^{-1} cm^{-1} for AqpZ. The mixed protein and liposome solutions were dialyzed for 24 h in a dynamic microdialyzer dialysis device (Spectrum Laboratories Europe, Breda, The Netherlands) using a molecular weight cut-off of 10,000 Daltons and a dialysate flow of 3 ml/min. Dialysis was performed against PBS, pH 7.4. Control vesicles were made in the same manner without protein. The resulting proteoliposomes or liposomes were stored at 4°C until use.

Fluorescence spectroscopy. Fluorescence spectroscopy was performed using a Varian Cary Eclipse fluorescence spectrometer (Varian Inc., Palo Alto, CA, USA) with λ_{ex} (excitation wavelength) of 380 nm and emission recorded at 400 to 700 nm. Protein concentrations used were 0.25 mg/ml.

Circular Dichroism (CD) spectroscopy. CD spectra were acquired with a Jasco J-815 spectrometer (Jasco UK, Essex, UK). The sample temperature was controlled by a built-in Peltier device to 25°C. The spectra were collected with 20 nm/min between 250-195 nm with a response time of 0.25 s and a data pitch of 0.1 nm. Baselines were collected in the same manner and spectra were baseline corrected. Cuvettes used were quartz with a 10 mm path length. Results were obtained in millidegrees (mdeg) and subsequently converted to the mean residue ellipticity (MRE) ([θ] × mdeg cm^2 $dmol^{-1}$) based on 303 amino acid residues and a molecular weight (M_w) of 32,511.7 g/mol for SoPIP2;1 or 264 amino acid and a M_w of 27,234 Da for AqpZ. Protein concentrations used were 0.25 mg/ml.

4

References

1.   Karlsson M, *et al.* (2003) Reconstitution of water channel function of an aquaporin overexpressed and purified from Pichia pastoris. (Translated from eng) *FEBS Lett* 537(1-3):68-72 (in eng).

5

SI Table legends

Table S1. Structural alignment of various aquaporins with AqpZ to identify surface exposed cysteines.

6

SI Figure legends

Fig. S1. CD spectra of SoPIP2;1 and AqpZ in OG aqueous solutions reconstituted into lipids. A) CD spectra of SoPIP2;1 in OG (black line) or reconstituted into *E. coli* lipids (green line), DOPC (blue line) or cholesterol:DOPC 3:7 mol/mol (light brown line). B) CD spectra of AqpZ in OG (black line) or reconstituted into *E. coli* lipids (green line), DOPC (blue line) or DPhPC (pink line). Protein concentrations for each sample measured were 0.25 mg/ml. For reconstituted protein samples the lipid-to-protein ratio was 200 in all cases, and the proteins were reconstituted into 200 nm extruded liposomes as described in materials and methods.

Fig. S2. Structural alignment of SoPIP2;1 and AqpZ. Shown are A) top view of the structural alignment and B) side view of the alignment. Crystal structures of the open conformation of 3.9Å resolution of spinach SoPIP2;1 (PDB no.: 2B5F) and the 3.2 Å structural resolution of the *E. coli* AqpZ tetramer (PDB no.: 2ABM) were aligned using molecular visualization software PyMOL. (PyMOL Molecular Graphics System, version 3.2.0, Schrödinger, LLC). For the alignment the E, F, G and H chains of protein 2ABM were excluded as well as any water molecules. Based on the fit of the respective A chains, the proteins were aligned during five cycles and the RMSD value of the alignment were calculated by the software based on the fit of 867 to 867 atoms The RMSD of the alignment was calculated to be <1 Å. The SoPIP2;1 structure is shown in oceanic blue, while the AqpZ structure is shown in light grey.

Fig. S3. The residue environment around Cys127 and Cys132 of SoPIP2;1. Cys127 and Cys132 are surface exposed cysteines and target for Badan labeling. A) Shows the residue environment around Cys127 (C127). Trp246 (W246) and Phe227 (F227) residues are in the vicinity of C127 giving rise to possible dipole and dipole-quadropole interactions between C127 and W246 and F227. B) Shows the residue environment around Cys132 (C132). There appear not to be possible interactions with neighboring aromatic residues that could hamper with dye conjugation reactions.

Fig. S4. Secondary structure of native aquaporins and the Badan labeled counterparts. A) CD spectra of native SoPIP2;1 and Badan labeled SoPIP2;1 in aqueous OG solutions. B) CD spectra of native AqpZ and Badan labeled AqpZ in aqueous OG solutions. Protein concentrations were 0.25

7

mg/ml. The molecular weight of 292.17 g/mol was taking into account for calculations of mean residual ellipicities (MRE) of Badan labeled AqpZ and SoPIP2;1.

Fig. S5. Hydrophobic interactions of reconstituted SoPIP2;1 and AqpZ in response to SDS.. Equilibrium measurements of SDS titration with (A) Badan labeled SoPIP2;1 reconstituted into cholesterol:DOPC 3:7 and (B) Badan labeled AqpZ reconstituted into DPhPC. Sample protein concentrations were 0.25 mg/ml. Fluorescence spectra were recorded with excitation at 380 nm and emission collected from 400 to 700 nm.

8

SI Tables

Table S1

Aquaporin isoforms	PDB-id	Overall RMSD	Total number of cysteines	Overall cystein RMSD	Cys9 best fit RMSD	Best fit cystein residue
AQP0 Bovine lens	1YMG	0.932	4	3.391	0.684	14
AQP0 closed ovine lens	2B6O	1.042	3	4.170	0.203	144
AQP0 Ovine lens junction	3M9I	0.982	2	4.211	0.067	144
AQP1 Bovine red blood cell	1J4N	1.075	4	3.808	0.059	154
AQP1 Human red blood cell	1FQY	1.429	4	5.839	0.661	102
AQP1 Human red blood cell 2	1IH5	2.366	4	2.861	0.519	102
AQP4 Rat glial cell	2D57	1.015	6	0.431	0.619	123
AQP5 Human	3D9S	1.052	3	8.209	0.169	145
AQPM Bacteria	2F2B	0.958	3	3.144	0.469	79
AqpZ e. coli	1RC2	0.330	2	0.239	0.166	9
Aquaporin 4 Human	3GD8	0.922	6	0.599	0.619	87
Aquaporin yeast	2W2E	1.115	2	1.355	0.628	215
Sopipi2;1 closed	1Z98	0.983	4	9.052	0.643	132
Sopipi2;1 open	2B5F	0.990	4	9.117	0.662	132

9

SI Figures

Fig. S1

Fig. S2

Fig. S3

Fig. S4

A.

B.

13
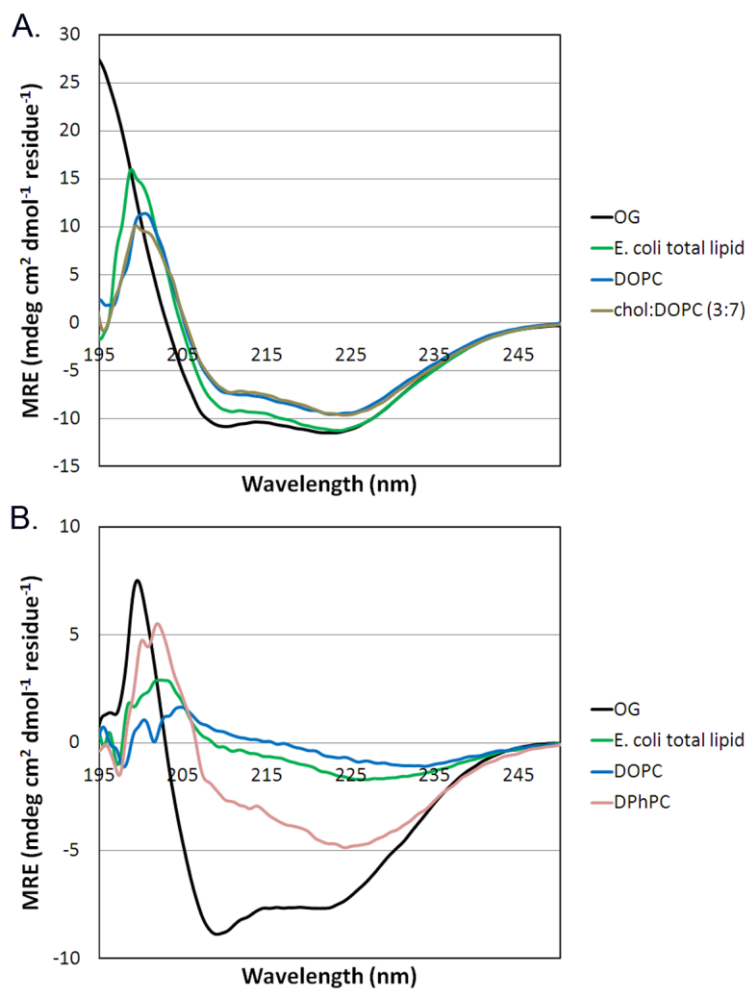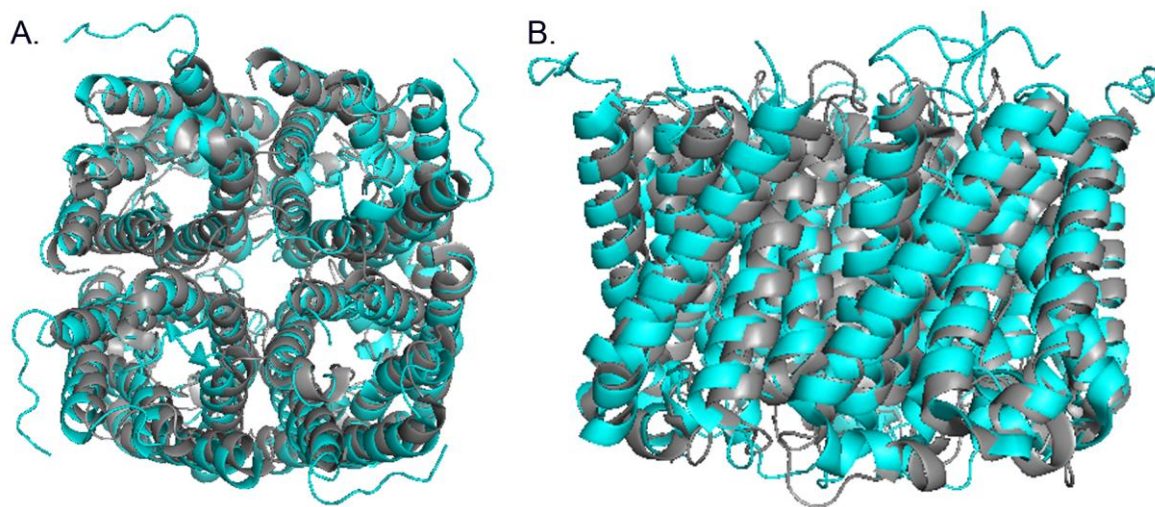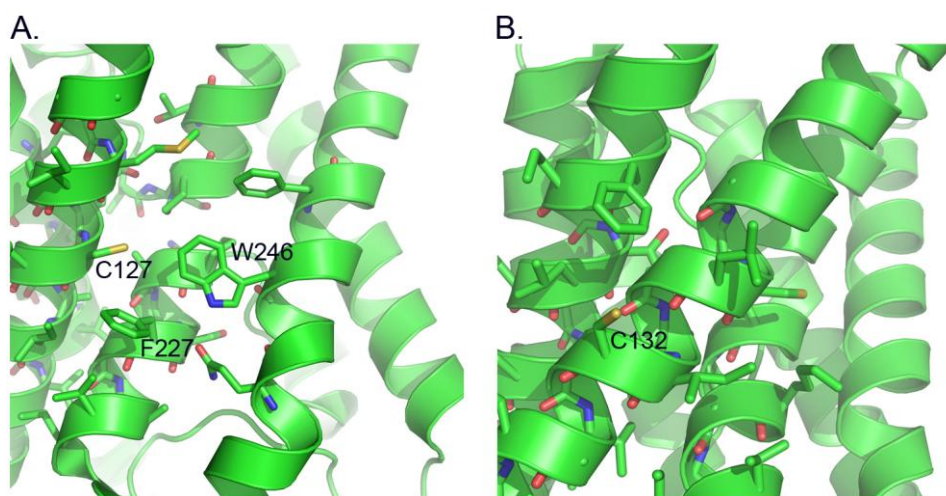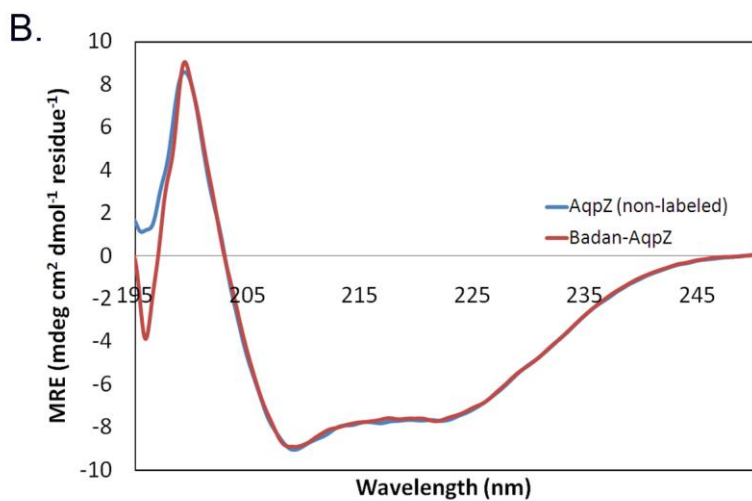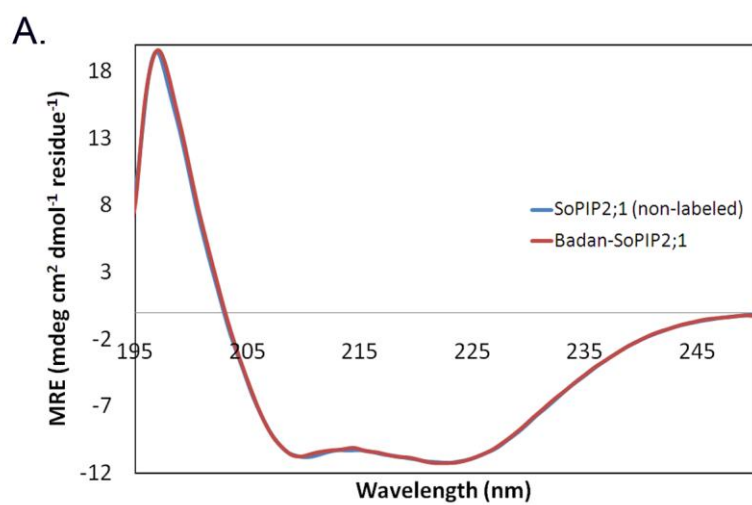
Fig. S5
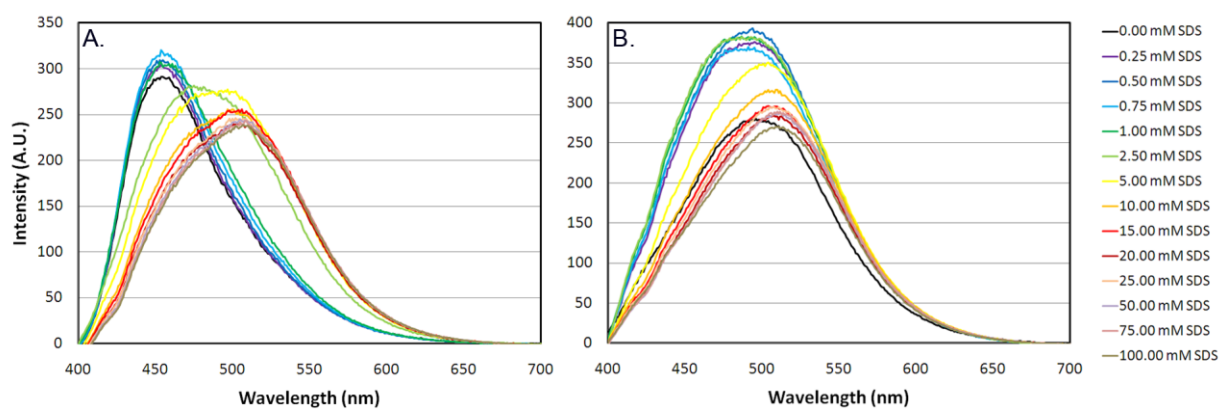
4.2 Solvent formation of giant protein vesicles and visualization of membrane protein partitioning

Solvent formation of giant protein vesicles and visualization of membrane protein partitioning

Jesper S. Hansen[a, b], Ardcharaporn Vararattanavech[c], Thomas Vissing[b], Jaume Torres[c], Jenny Emnéus[a], Claus Helix-Nielsen[d,b,]*

[a]The Biomedical Microsystems Section (BIOMICS), DTU Nanotech, Technical University of Denmark, Kgs. Lyngby, Denmark. [b]Aquaporin A/S, Copenhagen Bio Science Park (COBIS), Copenhagen, Denmark. [c]Structural & Computational Biology, School of Biological Sciences, Nanyang Technological University, Singapore. [d]Quantum Protein Center, DTU Physics, Technical University of Denmark, Kgs. Lyngby, Denmark

TITLE RUNNING HEAD: SOLVENT FORMATION OF GIANT PROTEIN VESICLES

* Corresponding author: Claus Hélix-Nielsen, Technical University of Denmark, DTU Physics, Fysikvej Building 309, Denmark. E–mail: claus.nielsen@dtu.fysik.dk. Telephone: (+45) 27102076.

ABSTRACT   This paper describes a method to form giant protein vesicles (GPV) (≥10 μm) by fusion of large vesicles (0.1– 0.2 μm) triggered by lipid containing solvents. Formation of GPV proceeded from rotational mixing of large protein vesicles with a lipid containing solvent phase consisting of either squalene or *n*–decane. The method supports formation of GPV in physiological ionic strength buffers such as phosphate buffered saline, and does not require specialized equipment, specialized lipids and peptides or a dehydration/rehydration step. Moreover, the amount of reconstituted protein in the GPV may be controlled by the lipid–to–protein ratio of the large vesicles. The water selective aquaporins SoPIP2;1 from spinach and the *E. coli* AqpZ were use as model proteins of α–helical bundle membrane proteins. To address membrane protein reconstitution and partitioning into established GPV we created a novel quantitative visualization assay of membrane protein reconstitution based on fluorescence Badan generalized polarization ratio imaging. With generalized polarization imaging of the created GPV it was possible to differentiate between well, heterogeneous or poorly reconstituted membrane proteins. Functional protein reconstitution into GPV is demonstrated with the light–driven proton pump Bacteriorhodopsin. Moreover, we show that lipid membrane barrier properties may be modulated by the solvent used, while retaining protein function. We suggest that the described method may constitute a general and versatile method for the formation of GPV.

2

Introduction

Giant vesicles offer a great potential as a native like cell–mimetic environment for protein reconstitutions and subsequent protein characterization.[1] These vesicles mimic mammalian cells in size (≥10 μm) and may be visualized directly by microscope techniques.[2, 3] Accordingly, giant vesicles have been extensively used in biophysical characterizations of lipid–lipid interactions, phase separation and lipid domain formations.[4-6] However, protein reconstitution into giant vesicles is not straightforward and the assembly procedures of giant vesicles generally preclude protein reconstitution.[7] This has so far limited the use of these vesicles as a general biomimetic platform for studying membrane proteins and in novel membrane protein–based biotechnological applications.

Several methods produce giant vesicles including controlled hydration of dried (and semi–dried) lipid films by spontaneous swelling or electroformation, transformation of lipids in water–oil or water–oil–water emulsions into giant vesicles, solvent evaporation, microfluidic jetting of planar membranes and fusion of small and large unilamellar vesicles.[8] Methods for forming giant vesicles commonly include evaporation of a volatile organic solvent (such as chloroform) from a lipid–solvent mixture.[9-12] The use of volatile organic solvents is generally not well tolerated by most amphiphilic membrane proteins.[13] The fabrication of giant vesicles is moreover generally limited to solutions of low non–physiological ionic strengths.[11, 14] Specific lipid formulations[15, 16], refined electroformation protocols[14, 17-19] or novel giant vesicle assembly approaches[11, 20] have been developed to circumvent this issue, albeit these approaches often still rely on solvent evaporation. Moreover, limited amounts of detergents are tolerated in order not to solubilize the giant vesicle membranes.[13] Detergent is a requirement to maintain folding of membrane proteins in aqueous solutions[21], and this restricts the amount of protein that can be incorporated directly into preformed giant vesicles.

Only few attempts, and with limited success, have been made to elucidate a general method for controllable reconstitution of membrane proteins into giant vesicles. A method has been presented that consists of creating large unilamellar protein vesicles (0.1 – 0.2 μm), which subsequently are dehydrated and then fabricated into giant vesicles by rehydration and electroformation.[13] The toleration of

3

membrane proteins to a dehydration step is questionable, since this may potentially introduce unwanted adverse effects on protein folding and function. Improvements using sucrose as protein stabilizer during dehydration have been described, but this modified procedure was not used in combination with physiological ionic strength buffers.[22] Another idea was to create large protein vesicles and subsequently fuse these to electroformed giant lipid vesicles using synthetic anchoring lipids and fusiogenic peptides.[7] The drawback of this methodology is the requirements of specialized synthetic lipids and custom designed peptides, the limitations of electroformation still apply and the protein reconstitution yield is limited to the fusion events taking place between the large protein vesicles and the giant lipid vesicles.

Here we present an emulsion based method for the formation of giant vesicles that allows controllable membrane protein reconstitutions and subsequent creation of giant protein vesicles (GPV), without the use of specialized lipids, specialized equipment or a dehydration/rehydration step. Our method originates from the idea that solvents (oils) may induce fusion of large protein vesicles into GPV. We demonstrate that GPV can be created in this manner in low ionic strength as well as at physiological ionic strength in e.g. phosphate buffered saline (PBS).

The *E. coli* Aquaporin–Z (AqpZ) and the spinach plasma integral protein 2;1 (SoPIP2;1) were used as model membrane proteins in this study. Aquaporins are tetrameric α–helical membrane spanning proteins that function as highly selective water channels. The helicity and the oligomeric state of aquaporins make them a good general model for α-helical polytopic membrane proteins. To demonstrate folding and partitioning of membrane proteins during the formation of GPV using this new method, we created polarity–sensitive fluorescently labeled versions of SoPIP2;1 and AqpZ. An assay was established supporting visual quantifications of the degree of protein reconstitution in the established GPV, which was based on fluorescence generalized polarization ratio imaging.

In order to verify genuine membrane protein functionality in these GPV, Bacteriorhodopsin (BR), a light–activated proton–pumping protein, was reconstituted and a pH response assay established. Also, we found that the lipid membrane barrier properties could be modulated, while retaining the BR function of the GPV.

4

We suggest that this method of forming GPV may represent a general and versatile methodology that supports: i) vesicle formation in physiological ionic strength buffers; ii) controlled and functional reconstitution of membrane proteins and iii) modulation of membrane barrier properties by varying the solvent lipid bilayer partitioning propensity. This may open up for a general use of membrane protein reconstituted giant vesicles in biotechnological applications.

Results and discussion

The principle for formation of giant vesicles and GPV constitute an emulsion based self–assembly process, where giant vesicles are formed from fusion of large vesicles by using a lipid containing solvent phase as emulsifier. In this method, large vesicles were created with or without membrane proteins and subsequently mixed with the lipid containing solvent phase (1:3 vol/vol) by end–over–end rotation. This resulted in an emulsion consisting of an upper excess solvent phase (typically very low volume), a lower aqueous phase and a third intermediate phase containing the giant vesicles (Figure 1). High density vesicle solutions were created in this manner, which in principle could be diluted to create a solution of individually addressable giant vesicles (Figure 1). In this study we chose to perform characterization of high density vesicle solutions.

Although, giant vesicles typically formed within 30 min, the emulsification process was continued over night. From optical micrographs we observed that vesicle formations that were proceeded over night created considerably more stable vesicles (typically lifetimes > 1 week) and more well–defined vesicle (sizes 25–100 μm depending on lipid species) compared to shorter mixing times (<1 h).

Influence of solvents and lipids on giant vesicles formation

The solvents chosen for this study were the hydrocarbon–based oils squalene and *n*–decane. Squalene is naturally occurring unsaturated oil produced in all animals and plants, and is the precursor of cholesterol, steroid hormones and vitamin D. In relation to artificially made model membranes, squalene has been described as a suitable solvent for creating solventless bilayer lipid membranes because it does

5

not, or only to a very low extent, partition into the lipid bilayer.[23] On the other hand, n–decane is an alkane hydrocarbon often used in lipid model membranes to create solvent containing planar bilayer lipid membranes[24] and in contrast to squalene it has been suggested to readily partition into the lipid bilayer membrane.[25, 26] The physico-chemical properties of these oils were therefore of interest to compare with respect to giant vesicles and GPV formation.

First we created giant vesicles of DOPC (for full names of lipids, see figure caption of Figure 2) with either the lipid alone or reconstituted with the SoPIP2;1 or AqpZ aquaporins, respectively. With DOPC containing squalene as solvent, giant vesicles were formed in high densities in all instances (Figure 2). On the other hand, with DOPC containing n–decane as solvent, giant lipid vesicles were formed to a lesser extent and with considerably smaller sizes (Figure 3). DOPC giant SoPIP2;1 vesicles were formed with high densities, whereas DOPC giant AqpZ vesicles did not form (Figure 3). This indicated that the formation of giant lipid vesicles and GPV may be influenced not only by the solvent used, but also by the lipid species or the protein isoforms. The nature of the lipid species applied is likely an important factor that influences the giant vesicle formation processes. Difficulties of forming giant vesicles of solely negatively charged lipids (e.g. DOPS) as well as asolectin soybean mixture of phospholipids have previously been reported.[27] However with our methodology, negatively charged DOPS lipid was able to support GPV formations of both SoPIP2;1 and AqpZ using DOPS containing squalene or n–decane solvents (Figure 2 and 3). It is interesting to note that DOPS alone did not support giant lipid vesicles formation, whereas the same lipid species in the presence of proteins did create high density GPV solutions (Figure 2 and 3). This indicates that the membrane proteins themselves contribute significantly to the ability of forming giant vesicles. Also asolectin as well as *E. coli* total lipid extracts resulted in formation of giant lipid vesicles and GPV (Figure 2 and 3), demonstrating that our method may constitute a general methodology to create GPV, including lipid compositions that normally are not useful for forming giant vesicles. Encouraged by these findings we created giant lipid vesicles and GPV with a number of lipid species and lipid compositions, including DPhPC and DOPE (Figure 2 and 3). DPhPC was included because it has been extensively used for establishment of planar bilayer lipid

6

membranes and thus it would be interesting to see if this lipid also supports formation of GPV. Moreover, DPhPC is a methyl–branched phospholipid species and is for this reason a somewhat atypical lipid species for this purpose. Formation of DPhPC giant vesicles from DPhPC large vesicles using a mixture of DPhPC and squalene as solvent resulted in aggregated structures in all cases, albeit with some resembling vesicular structures (Figure 2). The created emulsions appeared macroscopically very turbid and adhered to the vial walls, indicating protein aggregation. We then created giant vesicles by mixing large DPhPC vesicles with DOPC in squalene as emulsifier. This resulted in formation of AqpZ GPV in high density, but not with lipid alone or with SoPIP2;1 (Figure 2). This is evidence for that the protein itself and the lipid species or combination of lipids directly have an influence on the giant vesicle formation processes. DPhPC or DOPC containing n–decane solvents together with DPhPC large vesicles led to high density giant vesicle solutions both with pure lipid and with the SoPIP2;1 or AqpZ aquaporins (Figure 3). We also evaluated the influence of DOPE on giant vesicle formations due to the inverted cone–shaped nature of this neutral lipid species, meaning that this lipid on its own has a non–bilayer propensity, and that this property is expected to affect the lipid membrane curvature. With large vesicles of DOPE:DOPC (1:1) mixed with solvents containing similar lipid composition, GPV were formed in all cases (Figure 2 and 3). However, vesicle densities of DOPE:DOPC giant vesicles formed using squalene as solvent were lower compared to the corresponding giant vesicles produced with pure DOPC lipids (Figure 2 and 3). We also observed large elongated vesicles and planar structures in the DOPE:DOPC emulsions, and especially giant AqpZ vesicles produced with n–decane exhibited almost exclusively elongated rod–shaped lipid structures (Figure 3). Yield and shape of produced giant vesicles may therefore also be influenced by the lipid species and protein.

Comparing the giant vesicles obtained from lipid containing squalene or n–decane, respectively, indicated that the partitioning of n–decane into the lipid bilayers may be able to contribute to a higher success rate in forming giant lipid vesicles or GPV. Combined the results show that GPV formation is influenced by the solvent, the lipid species and/or the aquaporin protein isoforms. It would be interesting to address how the lipid species and solvent partitioning into lipid bilayers influences protein

7

reconstitution into giant vesicles. We therefore created a method that directly visualized the degree of reconstitution of membrane proteins into GPV.

Membrane protein reconstitution into GPV

The generalized polarization (GP) technique has been applied to detect membrane phase properties and spatial lipid distributions of mixed lipid bilayers.[28-34] Lipid bilayer membranes are doped with the fluorescent naphthalene–derivative Laurdan, which is a polarity sensitive probe that shifts emission spectra upon polarity changes in the microenvironment around the Laurdan[35]. The Laurdan emission shifts can be measured by fluorescence spectroscopy or visualized by laser scanning confocal microscopy, and subsequently quantified by calculating the GP values.[35] Hansen *et al.* 2008 showed that GP microscopy could be adapted to quantify apo– and holo–forms of soluble fluorescently labeled acyl–CoA binding proteins microinjected into living mammalian cells, using Badan, another naphthalene-derivative, as a fluorescent polarity sensing probe.[36] In this work, we adapted the Badan methodology in order to establish a general method for quantification of membrane protein reconstitution into lipid bilayer membranes.

Aquaporins generally have cysteines naturally positioned in the hydrophobic segments of the protein, which is accessible for labeling reactions. Badan labeling of native SoPIP2;1 and AqpZ aquaporins resulted in fluorescently–labeled aquaporins with unique spectral fluorescent properties (Figure 4A and 4B). Solubilization of reconstituted membrane protein by detergent leads to increased polarity around the Badan probe, resulting in a concomitant change in the fluorescence emission spectrum.[37] The Badan–labeled SoPIP2;1 showed large emission shifts from being hydrophobically exposed in the lipid bilayer of large protein vesicles to being solubilized in aqueous solution by sodium dodecyl sulfate (SDS). Since the Badan–label of AqpZ is more hydrophilically exposed in the native protein environment (e.g. lipid bilayers) as compared to the Badan-SoPIP2;1, this results in lower spectral emission shifts upon polarity changes (e.g. by SDS) of the Badan group of AqpZ compared to SoPIP2;1 (Figure 4A and 4B).

8

GP measurements were carried out with large protein vesicle in solution by laser scanning confocal microscopy for the above mentioned lipid mixtures (Supplemental Figure S1). The GP values varied depending on the lipid species, but generally GP values were around +0.4 for Badan–SoPIP2;1 reconstituted in large vesicles, which shifted to around –0.4 to –0.5 for the SDS solubilized protein (Figure 4C). For Badan–AqpZ the GP values in large vesicles were around 0.0 to –0.1 depending on the lipid species, and shifted to –0.2 to –0.4 for Badan–AqpZ in the SDS solubilized state (Figure 4D, Supplemental Figure S1). In order to obtain further insights into protein reconstitution we conducted GP imaging of Badan–SoPIP2;1 and Badan–AqpZ reconstituted into GPV, consisting of various lipid compositions (as described in Figure 2 and 3). Since the GP measurements were lipid dependent, we decided to define the level of reconstitution for SoPIP2;1 and AqpZ on the basis of the GP measurements of large vesicles and the corresponding SDS solubilized solutions (Supplemental Figure S1). For aquaporin GPV with GP measurements correlating to the initial large protein vesicles were defined as good protein reconstitution, whereas GP measurements correlating to the corresponding SDS solubilized state were defined as poor protein reconstitution. GP values between these two situations deviating $\geq \pm 0.03$ GP units were defined as heterogeneous protein reconstitution.

Results obtained from fluorescence GP microscopy showed that distinct regions of positive and negative GP values could be observed in a single GP image, both for the SoPIP2;1 and AqpZ GPV, demonstrating that the degree of reconstitution could be differentiated in a single image (Figure 5A, 5B and 5E). For the complete set of obtained data we refer to Supplemental Figures S2 to S5).

Table 1 summarizes the degree of protein reconstitution obtained with GP measurements using the above mentioned definitions for the degree of protein reconstitution. Common for SoPIP2;1 and AqpZ GPV was good protein reconstitution in GPV with lipid compositions of DOPS and asolectin phospholipids from soybean (Table 1, Supplemental Figure S2–S5). This supported the notion that GPV could successfully be created from solely negatively charged lipids, or soybean lipid extracts. GPV produced using n–decane resulted in well–reconstituted protein in all cases for SoPIP2;1 (Table 1, Supplemental Figure S4), while AqpZ exhibited a more ambiguous reconstitution profile with

similarities to protein reconstitution in GPV formed using squalene (Table 1, Supplemental Figure S3 and S5).

Table 1. Degree of protein reconstitution in GPV determined by fluorescence GP measurements

GPV compositions	SoPIP2;1		AqpZ	
Solvent ⟍ Lipid	squalene	*n*–decane	squalene	*n*–decane
DOPC	🟨	🟩	🟥	🟥
DOPS	🟩	🟩	🟩	🟩
DPhPC	🟩 *	🟩	🟨	🟨
DPhPC/ DOPC-solvent	🟨	🟩	🟨	🟨
30% Chol:DOPC	🟩	🟩	🟩	🟨
DOPE:DOPC (1:1)	🟩	🟩	🟨	🟩
Asolectin	🟩	🟩	🟩	🟩
E.coli total lipids	🟩	🟩 **	🟩	🟩

Protein reconstitution degree are divided into: good reconstitution (green), heterogeneous reconstitution (yellow) and poor reconstitution (red). Definitions were based on GP measurements of large protein vesicles (we refer the text and Supplemental Figure S1). * SoPIP2;1 GPV created from DPhPC large vesicles mixed with DPhPC–squalene resulted in aggregated structures. ** SoPIP2;1 localization was confined within the apparent GPV created from *E. coli* total lipid mixed with *E. coli* total lipid containing *n*–decane (Supplemental Figure S4). The abbreviation Chol refers to cholesterol.

The mixtures of DOPE:DOPC (1:1) produced very interesting vesicular structures and protein distributions. AqpZ giant vesicles formed with squalene produced spherical vesicles with circumferential distribution of well–reconstituted protein (Figure 5B). AqpZ giant vesicles formed with *n*–decane exhibited elongated rod–shaped structures, but otherwise exhibited well–reconstituted protein (Figure 5F). SoPIP2;1 giant vesicles consisting of DOPE:DOPC formed with squalene as solvent exhibited spherical vesicular structures (Figure 5C), whereas the corresponding *n*–decane giant vesicles exhibited an almost hexagonal structural vesicular network with well defined circumferential protein distributions of well protein reconstitution. (Figure 5G). GP measurements of SoPIP2;1 giant vesicles of DPhPC vesicles formed with DOPC containing *n*–decane exhibited vesicle circumferential protein

10

correlating with well–reconstituted protein (Figure 5H, Supplemental Figure S). In contrast, AqpZ giant vesicles formed with the same conditions revealed heterogeneous protein reconstitution levels (Figure 5D, Supplemental Figure S5).

These results demonstrated that GP imaging as well as the corresponding GP measurements of Badan fluorescently labeled membrane proteins have the ability to give valuable details of protein distributions and degree of protein reconstitution of established GPV.

Protein functionality of established GPV

To study the protein functionality in GPV, we turned to the light–driven proton pump BR, in which proton transport is relatively straightforward to quantify. BR is a trimeric membrane protein with seven transmembrane α–helices, having a molecule of retinal covalently bound that is responsible for the light driven proton–pumping activity. Reconstitution of BR into vesicles results in a preferential protein orientation where the proton–pumping activity is from the outside to the interior of the vesicles ($H^+_{out} \rightarrow H^+_{in}$).[38] This results in a net proton flux into the vesicles upon illumination, leading to alkalization of the external bulk medium, which can be measured by a pH electrode. Turning off the illumination will inactivate the proton pump and the resulting passive proton diffusion ($H^+_{in} \rightarrow H^+_{out}$) will result in a decrease of the pH in the bulk medium.[38] Using this principle we reconstituted BR into large vesicles of asolectin and measured the light–activated proton–pumping activity and the subsequent adaptation to dark state conditions (Figure 6A). The same batch of BR vesicles was then used to form GPV using asolectin containing squalene as solvent. We measured the proton–pumping activity of the BR GPV and compared the protein function with the initial protein activity of the large BR vesicles (Figure 6A). In this manner we were able to demonstrate that BR was functionally reconstituted into GPV with an activity recovery of 66.7% compared to that of the BR large vesicles. In comparison, the proton pumping activity recovery of BR giant vesicles formed with *n*–decane was 58.3%. The light–driven net flux of proton transport across the membranes of BR reconstituted vesicles is modulated among other factors by vesicle size, and the proton pumping activity is diminished with increased vesicle sizes.[39] A

11

decrease in proton pumping activity was therefore expected for the BR GPV compared to the corresponding large BR vesicles.

Interestingly, BR GPV formed with n–decane exhibited an initial near similar rate of bulk solution alkalization upon illumination, but the pH decay in the dark state was slowed significantly compared to that of squalene formed GPV (Figure 6B). Returning of the pH to the baseline values took around 30 min for the BR GPV formed with n–decane compared to around 8 min for BR GPV formed with squalene. This is consistent with n–decane partitioning into the lipid membranes to a larger extent than squalene.[23] Biophysically it is very interesting that the membrane barrier properties (membrane solute permeability) could be modulated by the partitioning properties of solvents used. Modulation of membrane barrier properties could be a tool helping understanding how membrane protein function is modulated in the biological membrane. It may also be of importance in the development of membrane protein–based separation technologies where passive low ionic leaks are of importance for efficient solute separation across the membrane through functionally reconstituted proteins.

The use of solvents for formation of GPV from large vesicles could raise concerns about the general usefulness of this methodology to reconstitute α-helical bundle membrane proteins.[40, 41] However, GP ratio imaging of GPV reconstituted with Badan fluorescently labeled aquaporins combined with the functional measurements of BR demonstrated that membrane proteins could be properly and functionally reconstituted with the method of solvent formation of GPV. This could open up for the possibility of applying GPV in novel biotechnological applications. The biotechnological potential of proton pumps, alone or coupled with ATP–generating ATPases, has so far been poorly explored, however numerous applications have been suggested, ranging from targeted drug delivery to biocatalytic reactors, fuel cells and nano–machines.[42]

Conclusions

The formation of giant vesicles proceeded from mixing large vesicles with a lipid containing oil phase constitutes a new methodology to functionally reconstitute membrane proteins in controllable amounts

12

into giant vesicles. This method makes it possible to create GPV from a variety of lipid compositions, including lipids that previously may have posed difficulties for giant lipid vesicle formation, e.g. pure negatively charged lipids and total lipid extracts. Moreover, the method supports GPV formation in physiological ionic strength such as PBS, and does not require specialized equipment, specific lipids, synthetic peptides or dehydration/rehydration steps.

In this study we used a lipid–to–protein ratio (LPR) of 200 for aquaporin reconstitutions, whereas we used an LPR 1000 for BR. The amount of protein reconstituted into GPV may be controlled by defining the LPR of the large vesicles. Thus, the methodology allows for controlled reconstitution of membrane proteins including α-helical bundle membrane proteins, which compared to β-barrel proteins represent a delicate class of membrane protein structures.[43] The fluorescent labeling of membrane proteins with the environment sensitive probe Badan may provide a useful tool in studying membrane proteins in the cell–mimetic environment of giant vesicles. Polarity changes of the Badan probe of fluorescently labeled membrane proteins quantified by GP measurements may be used to address protein reconstitution and partitioning in bulk vesicle solutions as demonstrated in this study. The GP imaging methodology could also be envisaged to be refined to study membrane protein compartmentalization, spatial distribution in mixed lipid systems or may be applied to create sensitive receptor–ligand interaction assays for use in biosensor applications or drug discovery.

The biotechnological potentials of membrane proteins has so far been poorly explored, which to a large extent is related to the difficulties of reconstituting large amount of protein into artificially made membranes. The methodology for controlled reconstitution of membrane proteins to produce GPV as well as the ability to modulate membrane barrier properties may open up for the possibilities of a more general use of membrane proteins in biotechnological applications including membrane protein biosensors, drug discovery, bioreactors, nano–machines and novel separation technologies.

13

Supporting information available: Experimental Methods section, confocal microscopy GP measurements of Badan labeled SoPIP2;1 or AqpZ reconstituted in large vesicles and corresponding SDS solubilized states, GP images and histograms of Badan–SoPIP2;1 or Badan–AqpZ giant vesicles created by different solvents and with various lipid compositions.

14

References

1.   Merkle, D.; Kahya, N.; Schwille, P., Reconstitution and anchoring of cytoskeleton inside giant unilamellar vesicles. *Chembiochem* **2008,** 9, (16), 2673-81.

2.   Fidorra, M.; Duelund, L.; Leidy, C.; Simonsen, A. C.; Bagatolli, L. A., Absence of fluid-ordered/fluid-disordered phase coexistence in ceramide/POPC mixtures containing cholesterol. *Biophys J* **2006,** 90, (12), 4437-51.

3.   de Almeida, R. F.; Borst, J.; Fedorov, A.; Prieto, M.; Visser, A. J., Complexity of lipid domains and rafts in giant unilamellar vesicles revealed by combining imaging and microscopic and macroscopic time-resolved fluorescence. *Biophys J* **2007,** 93, (2), 539-53.

4.   Bagatolli, L. A., To see or not to see: lateral organization of biological membranes and fluorescence microscopy. *Biochim Biophys Acta* **2006,** 1758, (10), 1541-56.

5.   Wesolowska, O.; Michalak, K.; Maniewska, J.; Hendrich, A. B., Giant unilamellar vesicles - a perfect tool to visualize phase separation and lipid rafts in model systems. *Acta Biochim Pol* **2009,** 56, (1), 33-9.

6.   Kahya, N.; Scherfeld, D.; Bacia, K.; Schwille, P., Lipid domain formation and dynamics in giant unilamellar vesicles explored by fluorescence correlation spectroscopy. *J Struct Biol* **2004,** 147, (1), 77-89.

7.   Kahya, N.; Pecheur, E. I.; de Boeij, W. P.; Wiersma, D. A.; Hoekstra, D., Reconstitution of membrane proteins into giant unilamellar vesicles via peptide-induced fusion. *Biophys J* **2001,** 81, (3), 1464-74.

8.   Walde, P.; Cosentino, K.; Engel, H.; Stano, P., Giant vesicles: preparations and applications. *Chembiochem* **2010,** 11, (7), 848-65.

9.   Higashi, K.; Suzuki, S.; Fujii, H.; Kirino, Y., Preparation and some properties of giant liposomes and proteoliposomes. *J Biochem* **1987,** 101, (2), 433-40.

10.   Moscho, A.; Orwar, O.; Chiu, D. T.; Modi, B. P.; Zare, R. N., Rapid preparation of giant unilamellar vesicles. *Proc Natl Acad Sci U S A* **1996,** 93, (21), 11443-7.

11.   Horger, K. S.; Estes, D. J.; Capone, R.; Mayer, M., Films of agarose enable rapid formation of giant liposomes in solutions of physiologic ionic strength. *J Am Chem Soc* **2009,** 131, (5), 1810-9.

12.   Helm, C.; Lösche, M.; Möhwald, H.; Angelova, M.; Soléau, S.; Méléard, P.; Faucon, F.; Bothorel, P., Preparation of giant vesicles by external AC electric fields. Kinetics and applications. In *Trends in Colloid and Interface Science VI*, Springer Berlin / Heidelberg: 1992; Vol. 89, pp 127-131.

13.   Girard, P.; Pecreaux, J.; Lenoir, G.; Falson, P.; Rigaud, J. L.; Bassereau, P., A new method for the reconstitution of membrane proteins into giant unilamellar vesicles. *Biophys J* **2004,** 87, (1), 419-29.

14.   Montes, L. R.; Alonso, A.; Goni, F. M.; Bagatolli, L. A., Giant unilamellar vesicles electroformed from native membranes and organic lipid mixtures under physiological conditions. *Biophys J* **2007,** 93, (10), 3548-54.

15.   Akashi, K.; Miyata, H.; Itoh, H.; Kinosita, K., Jr., Preparation of giant liposomes in physiological conditions and their characterization under an optical microscope. *Biophys J* **1996,** 71, (6), 3242-50.

16.   Yamashita, Y.; Oka, M.; Tanaka, T.; Yamazaki, M., A new method for the preparation of giant liposomes in high salt concentrations and growth of protein microcrystals in them. *Biochim Biophys Acta* **2002,** 1561, (2), 129-34.

17.   Estes, D. J.; Mayer, M., Giant liposomes in physiological buffer using electroformation in a flow chamber. *Biochim Biophys Acta* **2005,** 1712, (2), 152-60.

18.   Pott, T.; Bouvrais, H.; Meleard, P., Giant unilamellar vesicle formation under physiologically relevant conditions. *Chem Phys Lipids* **2008,** 154, (2), 115-9.

19.   Bernardino de la Serna, J.; Perez-Gil, J.; Simonsen, A. C.; Bagatolli, L. A., Cholesterol rules: direct observation of the coexistence of two fluid phases in native pulmonary surfactant membranes at physiological temperatures. *J Biol Chem* **2004,** 279, (39), 40715-22.

20.   Noireaux, V.; Libchaber, A., A vesicle bioreactor as a step toward an artificial cell assembly. *Proc Natl Acad Sci U S A* **2004,** 101, (51), 17669-74.

21.   Renthal, R., An unfolding story of helical transmembrane proteins. *Biochemistry* **2006,** 45, (49), 14559-66.

22.   Doeven, M. K.; Folgering, J. H.; Krasnikov, V.; Geertsma, E. R.; van den Bogaart, G.; Poolman, B., Distribution, lateral mobility and function of membrane proteins incorporated into giant unilamellar vesicles. *Biophys J* **2005,** 88, (2), 1134-42.

23.   White, S. H., Formation of "solvent-free" black lipid bilayer membranes from glyceryl monooleate dispersed in squalene. *Biophys J* **1978,** 23, (3), 337-47.

24.   Mueller, P.; Rudin, D. O., Translocators in bimolecular lipid membranes: their role in dissipative and conservative bioenergetic transduction. *Curr Topics Bioenergetics* **1969,** 3, 157–249.

25.   White, S. H.; Thompson, T. E., Capacitance, area, and thickness variations in thin lipid films. *Biochim Biophys Acta* **1973,** 323, (1), 7-22.

26.   Hladky, S. B.; Gruen, D. W., Thickness fluctuations in black lipid membranes. *Biophys J* **1982,** 38, (3), 251-8.

27.   Estes, D. J.; Mayer, M., Electroformation of giant liposomes from spin-coated films of lipids. *Colloids and Surfaces B: Biointerfaces* **2005,** 42, (2), 115-123.

28.   Plasencia, I.; Norlen, L.; Bagatolli, L. A., Direct visualization of lipid domains in human skin stratum corneum's lipid membranes: effect of pH and temperature. *Biophys J* **2007,** 93, (9), 3142-55.

29.   Goni, F. M.; Alonso, A.; Bagatolli, L. A.; Brown, R. E.; Marsh, D.; Prieto, M.; Thewalt, J. L., Phase diagrams of lipid mixtures relevant to the study of membrane rafts. *Biochim Biophys Acta* **2008,** 1781, (11-12), 665-84.

30.   Fidorra, M.; Garcia, A.; Ipsen, J. H.; Hartel, S.; Bagatolli, L. A., Lipid domains in giant unilamellar vesicles and their correspondence with equilibrium thermodynamic phases: a quantitative fluorescence microscopy imaging approach. *Biochim Biophys Acta* **2009,** 1788, (10), 2142-9.

31.	Fidorra, M.; Heimburg, T.; Bagatolli, L. A., Direct visualization of the lateral structure of porcine brain cerebrosides/POPC mixtures in presence and absence of cholesterol. *Biophys J* **2009,** 97, (1), 142-54.

32.	Bagatolli, L. A.; Gratton, E., Two-photon fluorescence microscopy observation of shape changes at the phase transition in phospholipid giant unilamellar vesicles. *Biophys J* **1999,** 77, (4), 2090-101.

33.	Bagatolli, L. A.; Gratton, E., Two photon fluorescence microscopy of coexisting lipid domains in giant unilamellar vesicles of binary phospholipid mixtures. *Biophys J* **2000,** 78, (1), 290-305.

34.	Parasassi, T.; Gratton, E.; Yu, W. M.; Wilson, P.; Levi, M., Two-photon fluorescence microscopy of laurdan generalized polarization domains in model and natural membranes. *Biophys J* **1997,** 72, (6), 2413-29.

35.	Sanchez, S. A.; Tricerri, M. A.; Gunther, G.; Gratton, E., Laurdan Generalized Polarization: from cuvette to microscope. In *Modern Research and Educational Topics in Microscopy*, Méndez-Vilas, A.; Díaz, J., Eds. FORMATEX: 2007; Vol. 1, pp 1007-1014.

36.	Hansen, J. S.; Faergeman, N. J.; Kragelund, B. B.; Knudsen, J., Acyl-CoA-binding protein (ACBP) localizes to the endoplasmic reticulum and Golgi in a ligand-dependent manner in mammalian cells. *Biochem J* **2008,** 410, (3), 463-72.

37.	Valeva, A.; Siegel, I.; Wylenzek, M.; Wassenaar, T. M.; Weis, S.; Heinz, N.; Schmitt, R.; Fischer, C.; Reinartz, R.; Bhakdi, S.; Walev, I., Putative identification of an amphipathic alpha-helical sequence in hemolysin of Escherichia coli (HlyA) involved in transmembrane pore formation. *Biol Chem* **2008,** 389, (9), 1201-7.

38.	Huang, K. S.; Bayley, H.; Khorana, H. G., Delipidation of bacteriorhodopsin and reconstitution with exogenous phospholipid. *Proc Natl Acad Sci U S A* **1980,** 77, (1), 323-7.

39.	Hellingwerf, K. J.; Scholte, B. J.; van Dam, K., Bacteriorhodopsin vesicles. An outline of the requirements for light-dependent H+ pumping. *Biochim Biophys Acta* **1978,** 513, (1), 66-77.

40.	Ayala, G.; Nascimento, A.; Gomez-Puyou, A.; Darszon, A., Extraction of mitochondrial membrane proteins into organic solvents in a functional state. *Biochim Biophys Acta* **1985,** 810, (2), 115-22.

41.	Beddow, J. A.; Peterson, I. R.; Heptinstall, J.; Walton, D. J., Reconstitution of nicotinic acetylcholine receptors into gel-protected lipid membranes. *Anal Chem* **2004,** 76, (8), 2261-5.

42.	Lanyi, J. K.; Pohorille, A., Proton pumps: mechanism of action and applications. *Trends in Biotechnology* **2001,** 19, (4), 140-144.

43.	Bowie, J. U., Stabilizing membrane proteins. *Curr Opin Struct Biol* **2001,** 11, (4), 397-402.

44.	Beechem, J. M.; Gratton, E. In *Fluorescence Spectroscopy Data Analysis Environment A Second Generation Global Analysis Program*, Time-Resolved Laser Spectroscopy in Biochemistry, Proc. of SPIE, 1988; Lakowicz, J., Ed. 1988; pp 70-81

Figure legends

Figure 1　　　Images of the emulsion process for formation of giant vesicles. Large lipid vesicles or large protein vesicles are formed (200 nm) and added lipid containing solvent (e.g. squalene or n–decane) (A). Rotational mixing of the solutions results in an emulsion (B) consisting of an upper solvent phase, and intermediate phase containing the giant vesicles (C) and a lower aqueous phase. D) Shows 20× dilution of the giant vesicle solution of (C). Scale bars = 100 μm.

Figure 2　　　Brightfield images of giant vesicles and aquaporin SoPIP2;1 or AqpZ GPV created with lipid/squalene. Large vesicles or large protein vesicles were produced with the following lipid compositions (in mol%): pure 1,2-dioleoyl-*sn*-glycero-3-phosphocholine (DOPC), pure 1,2-dioleoyl-*sn*-glycero-3-phospho-L-serine (DOPS), pure　1,2-diphytanoyl-*sn*-glycero-3-phosphocholine (DPhPC), DPhPC/DOPC-sq refers to DPhPC giant vesicles formed with DOPC containing squalene mixture, mixture of 30% cholesterol (Chol) with 70% DOPC (30%Chol/DOPC), asolectin from soybean, *E coli* total lipid extract and mixture of 50% 1,2-dioleoyl-*sn*-glycero-3-phosphoethanolamine (DOPE)　with 50% DOPC (DOPE/DOPC 1:1). Giant vesicles were established by mixing large vesicles with squalene containing lipids matched to the lipid composition of the large vesicles. An exception was creation giant vesicles from mixing DPhPC large vesicles with DOPC in squalene. Scale bars = 100 μm.

Figure 3　　　Brightfield images of giant vesicles and GPV of aquaporin SoPIP2;1 or AqpZ formed from lipid containing decane solvents. Lipid compositions were as described in Figure legend 2. DPhPC/DOPC-dec refers to DPhPC giant vesicles formed with DOPC containing n–decane. Giant vesicles were established by mixing large vesicles with squalene containing lipids matched to the lipid composition of the large vesicles. In one case giant vesicles were formed from mixing DPhPC large vesicles with DOPC in n–decane. Scale bars = 100 μm.

18

Figure 4   Fluorescence emission spectra and GP histograms of aquaporin Badan labeled SoPIP2;1 and AqpZ. Badan labeled SoPIP2;1 (A) or AqpZ (B) were reconstituted into DOPC large vesicles and the fluorescence emission spectra with excitation 400 nm was measured for the Badan labeled aquaporins (blue lines). Sodium dodecyl sulfate (SDS) was added to a final concentration of 100 mM to the aquaporin reconstituted DOPC vesicles to bring the aquaporin proteins into an aqueous detergent solubilized state. The fluorescence spectra were recorded for the resulting SDS detergent solubilized Badan labeled aquaporins (green lines). The same protein samples was imaged using laser scanning confocal microscopy and the corresponding GP image histograms was obtained for SoPIP2;1 (C) and AqpZ (D), respectively. GP values were obtained using SimFCS software[44] by: $GP = I_b - I_g / I_b + I_g$, where I_b and I_g correspond to the intensities at the blue (band pass filter 420–480 nm) and green (band pass filter 505–550 nm) edges of the emission spectrum respectively.

Figure 5   GP images of vesicles structures and protein distribution of aquaporin giant vesicles. Images shown are SoPIP2;1 giant vesicles formed with A) DOPC and squalene; C) DOPE:DOPC (1:1) and squalene, G) DOPE:DOPC (1:1) and n–decane or H) DPhPC and DOPC containing n–decane. For AqpZ the giant vesicles were formed with E) DOPC and squalene; B) DOPE:DOPC (1:1) and squalene, F) DOPE:DOPC (1:1) and n–decane or D) DPhPC and DOPC containing n–decane.

Figure 6   Bacteriorhodopsin proton–pumping activities of large vesicles and GPV. A) Bacteriorhodopsin (BR) was reconstituted into asolectin large unilamellar vesicles (LUV) (100 nm) with a lipid–protein–ratio of 1000 (BR-LUV). The ΔpH of the bulk solution was measured before (180 s), with illumination (180 s) and during dark adaptation (420 s) (black, open diamonds). BR GPV were produced by mixing the BR large vesicles with asolectin containing squalene (BR GPV squalene) or n–decane solvents (BR GPV decane). The large vesicles were mixed 1:3 vol/vol with the oil phase. The pH activity assay of BR was repeated for the GPV formed with squalene (purple, open triangles) and n–decane (red, open squares). The pH was continuously sampled with 3 s recording intervals. B) Shows

19

ΔpH measurements of A) which was normalized and reduced to include measurements every 15 s to better resolve differences in rate of alkalization during illumination and proton efflux during BR dark adaption.

20

Figures

Figure 1

end-over-end rotation,
over night, cold room

Figure 2

Figure 3

23

Figure 4

24

Figure 5

25

A.

B.

C.

D.

E.

F.

G.

H.

Figure 6

A.

B.
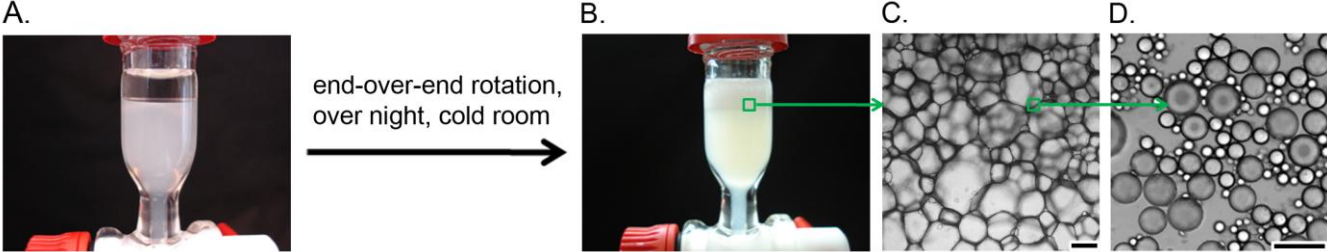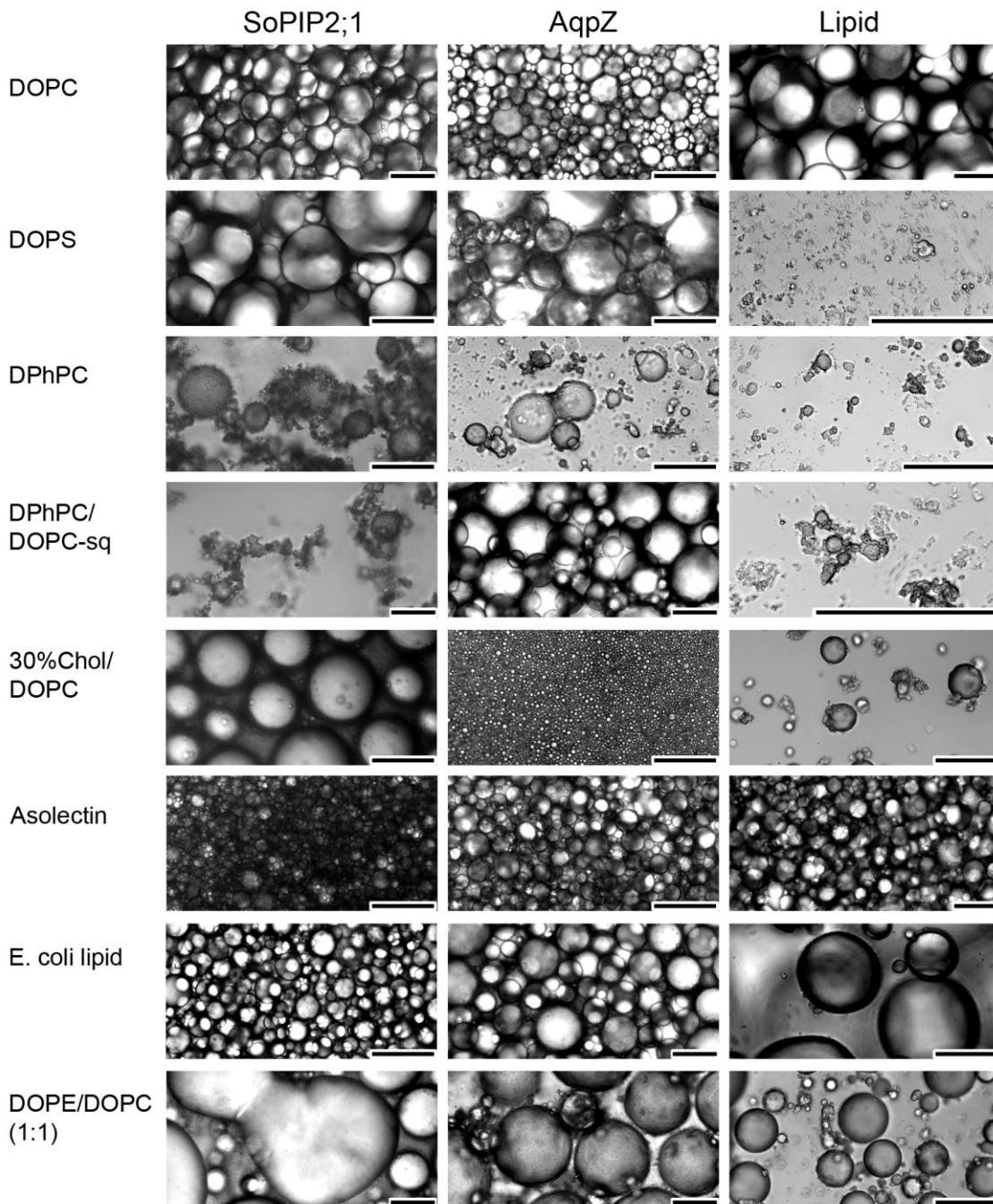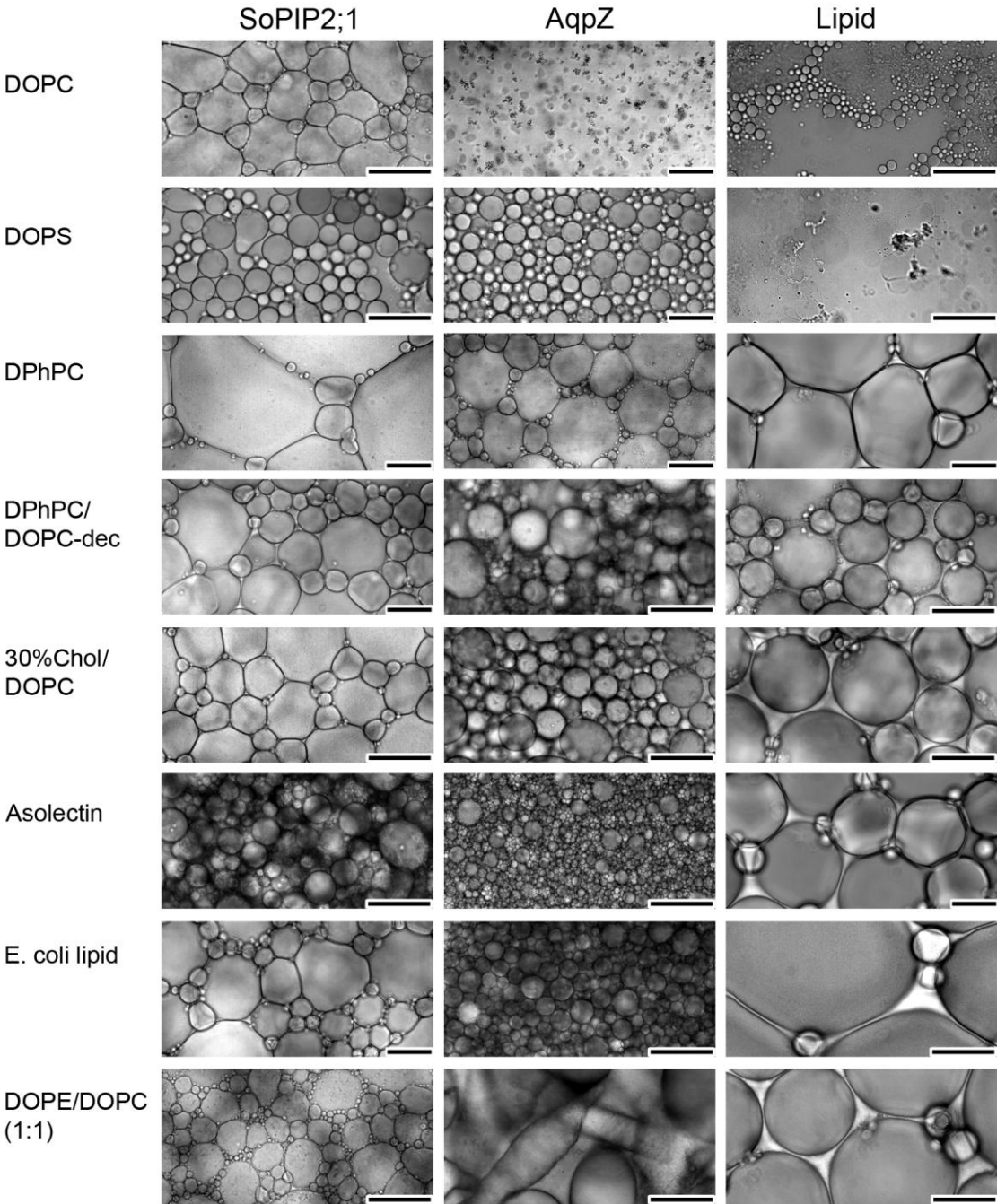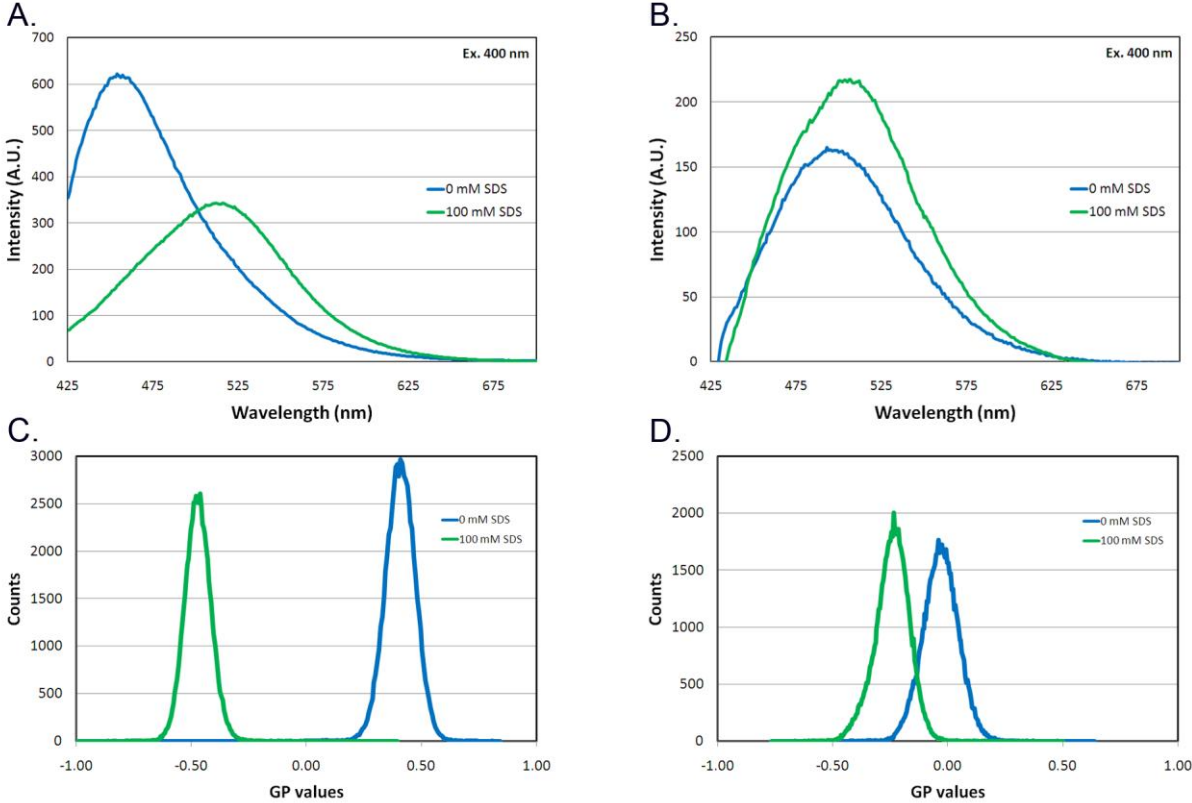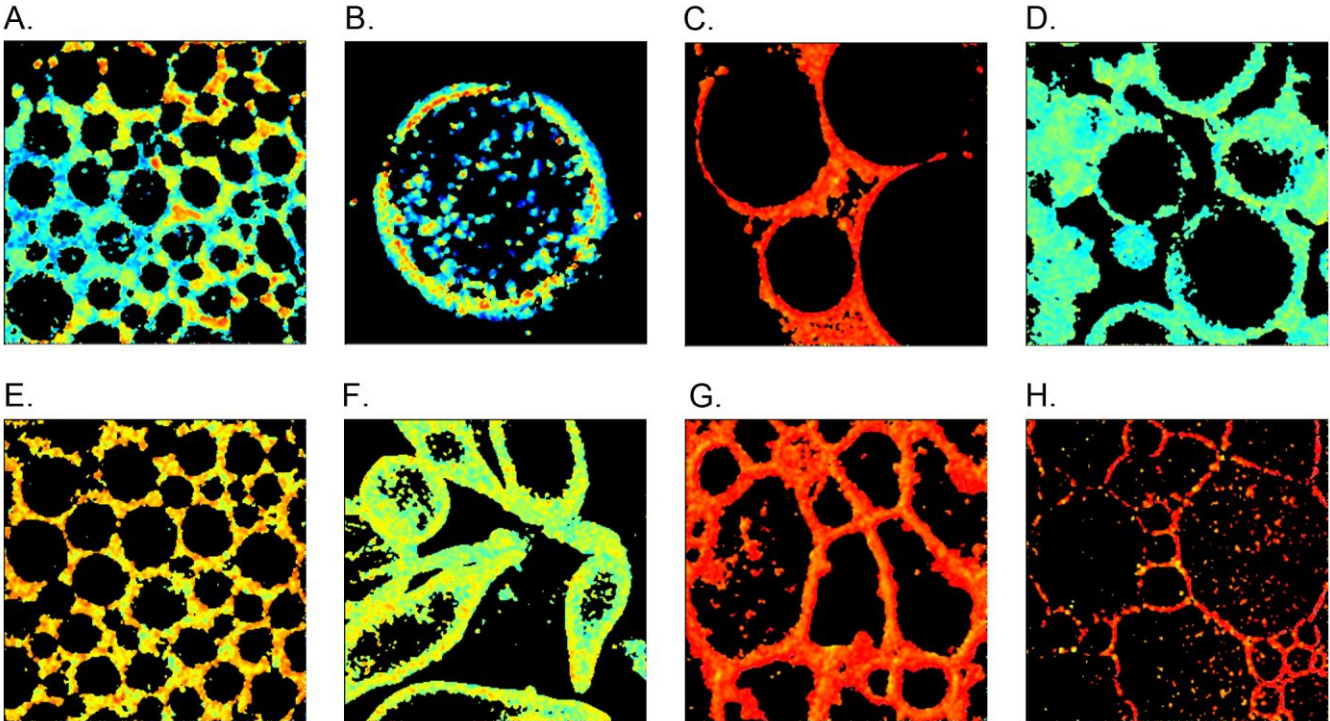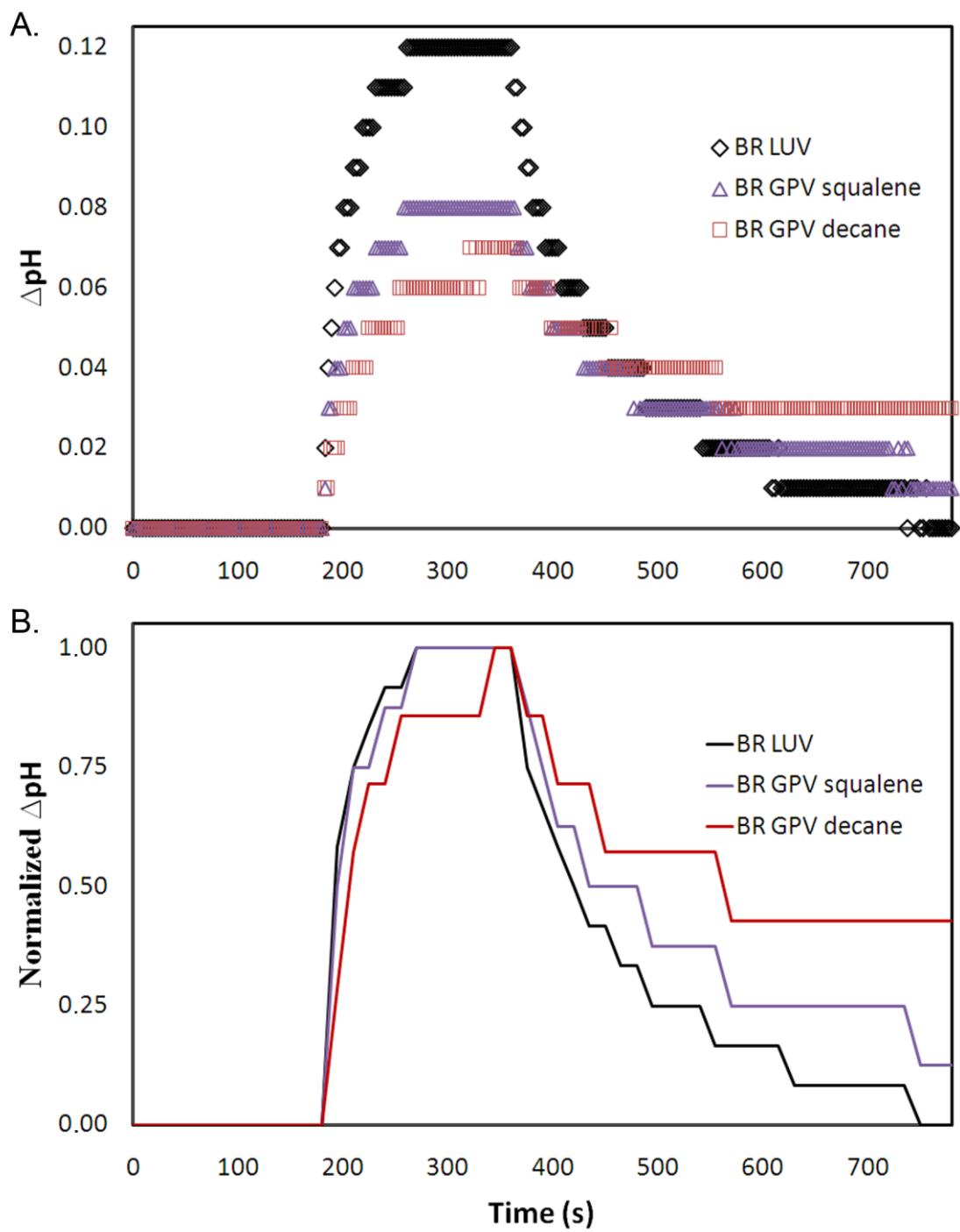
Supporting Information

Solvent formation of giant protein vesicles and visualization of membrane protein partitioning

Jesper S. Hansen[a, b], Ardcharaporn Vararattanavech[c], Thomas Vissing[b], Jaume Torres[c], Jenny Emnéus[a], Claus Helix-Nielsen[d,b,]*

[a]The Biomedical Microsystems Section (BIOMICS), DTU Nanotech, Technical University of Denmark, Kgs. Lyngby, Denmark. [b]Aquaporin A/S, Copenhagen Bio Science Park (COBIS), Copenhagen, Denmark. [c]Structural & Computational Biology, School of Biological Sciences, Nanyang Technological University, Singapore. [d]Quantum Protein Center, DTU Physics, Technical University of Denmark, Kgs. Lyngby, Denmark.

E-mail: claus.nielsen@dtu.fysik.dk

Experimental Methods

Reagents

Most lipids were from Avanti Polar Lipids Inc. (Alabaster, AL, USA). The fluorescent dye 6–bromoacetyl–2–dimethylaminonaphthalene (Badan) and polyacrylamide gel Econo–Pac 10DG desalting columns (Bio–Rad) for purification of dye-protein conjugations were obtained AnaSpec (Fremont, CA, USA). Octyl–β–D–glucopyranoside (OG) was purchased from Anatrace, Inc. (Maumee, OH, USA). Asolectin from soybean, cholesterol, sodium dodecyl sulfate (SDS), Tris, phosphate buffered saline (PBS), squalene, *n*–decane and 99.5% glycerol were obtained from Sigma Aldrich Denmark (Brøndby, Denmark). Uncoated 35 mm glass-bottom culture dishes for fluorescent microscopy were purchased from MatTek Corporation (Ashland, MA, U.S.A.). All other chemicals used were of analytical grade and purchased from commercial sources.

Heterologous protein overexpression of aquaporins SoPIP2;1 and AqpZ

Spinach aquaporin SoPIP2;1 was kindly provided by Professor Urban Johansson, Department of Biochemistry, Lund University, Sweden. The protein was overproduced in the methylotrophic yeast *Pichia pastoris* as His-tagged protein with a myc epitope, which was subsequently purified using Ni–affinity chromatography as previously published.[1] The protein was delivered solubilized in PBS (10 mM sodium phosphate, 138 mM sodium chloride, 2.7 mM potassium chloride, pH 7.4) supplemented with 1% OG and 10% glycerol. The SoPIP2;1 protein was stored at –80°C until use.

Bacterial aquaporin-Z (AqpZ) was overproduced in *E. coli* strain BL21(DE3) cultures as His–tagged protein with a tobacco etch virus cleavage site. The fusion protein has 264 amino acids and a M_w of 27,234 Da. Genomic DNA from *E. coli* DH5α was used as a source for amplifying the AqpZ gene. The AqpZ gene was amplified using gene specific primers with the addition of a tobacco etch virus cleavage site (TEV); ENLYFQSN at the N–terminus of AqpZ. The amplified AqpZ was digested with the enzyme *Nde*I and *BamH*I and then ligated to the similarly digested 6–His tagged expression pET28b

vector DNA. The positive clones were verified by PCR–screening. Then the authenticity of the constructs was confirmed by DNA sequencing.

The *E. coli* strain BL21(DE3) was used for expression of the protein. Luria Broth cultures containing 50 µg/ml Kanamycin were incubated for 13–16 hours at 37°C, diluted 100-fold into fresh LB broth and propagated to a density of about 1.2–1.5 (OD at 600 nm). Expression of recombinant protein was induced by addition of 1 mM IPTG for 3 hour at 35°C before centrifugation.

Harvested cells were resuspended in ice–cold binding buffer (20 mM Tris pH 8.0, 50 mM NaCl, 2 mM β–mercaptoethanol, 10% glycerol) in the presence of 0.4 mg/ml lysozyme, 50 units Bensonase and 3% OG. The sample was subjected to five times lysis cycles in a microfluidizer at 12,000 Pa. Insoluble material was pelleted by 30 minutes centrifugation at 40,000× g. The supernatant was passed through a Q–sepharose fast flow column (Amersham Pharmacia), and the flow through was collected. The flow though fraction was topped up with NaCl to 300 mM before loaded onto a pre–equilibrated Ni–NTA column. The column was washed with 100 column volumes of a wash buffer (20 mM Tris pH 8.0, 300 mM NaCl, 25 mM Imidazole, 2 mM β–mercaptoethanol, 10% glycerol) to remove non–specifically bound material. Ni–NTA agarose bound material was eluted with five bed volumes of elution buffer (20 mM Tris pH 8.0, 300 mM NaCl, 300 mM Imidazole, 2 mM β–mercaptoethanol, 10% glycerol, containing 30 mM n–octyl β–D–Glucopyranoside. AqpZ was further purified with anion exchange chromatography; monoQ column (GE healthcare). The mixture sample was diluted and concentrated to bring the salt and imidazole concentration to approximately 10 mM with Amicon concentrator, molecular weight cut off (MWCO) of 10,000 Da before loading to MonoQ column. The buffer used during anion exchange chromatography were (A) 20 mM Tris pH 8.0, 30 mM OG, 10% glycerol and (B) 20 mM Tris pH 8.0, 1 M NaCl, 30 mM OG, 10% glycerol. The eluted peak fractions containing AqpZ from the ion exchange column was pooled. The purified AqpZ was kept frozen at –80°C.

Fluorescent labeling of spinach SoPIP2;1 and E.Coli AqpZ aquaporins

Spinach aquaporin SoPIP2;1 and *E. coli* AqpZ were labeled with Badan. Synthesis and handling of Badan-derivatized proteins was carried out under dim light. To carry out the reaction, 10–fold molar excess of Badan to protein from a 20 mM stock solution of Badan (dissolved in dimethylformamide) was added to a 10 mg/ml protein solution. The reaction was allowed to take place for 20 h at 4 ℃ with end–over–end rotation. The reaction mixture was desalted for SoPIP2;1 into PBS, 1% OG, 1% glycerol, pH 7.4 and for AqpZ into 20 mM Tris, 30 mM OG, pH 8 on a polyacrylamide gel Econo–Pac 10DG desalting column (Bio–Rad). The resulting fluorescently labeled aquaporin was stored at 4 ℃ until use.

Preparation of large vesicles and protein vesicles

Large vesicles for protein reconstitution were prepared by evaporation of the chloroform by nitrogen gas, drying in under vacuum in a glass desiccator for 2 h followed by rehydration to a lipid concentration of 10 mg/ml. For Badan–SoPIP2;1 the lipid rehydration buffer consisted of PBS, 1.3% OG, pH 7.4, while for Badan–AqpZ the buffer was 20 mM Tris, 1.3% OG, pH 8.0. The vesicles were extruded 21 times through a 200 nm polycarbonate filter using a nitrogen pressurized LIPEX barrel extruder (Northern Lipids Inc., Burnaby, BC, Canada).

The SoPIP2;1 or AqpZ and the fluorescently labeled Badan–SoPIP2;1 or Badan–AqpZ were reconstituted by mixing with the vesicles at a lipid–to–protein ratio (LPR) of 200. Protein concentrations were determined by UV/Vis absorbance spectroscopy using the extinction coefficient at 280 nm of 46,660 M^{-1} cm^{-1} for SoPIP2;1 and 36,370 M^{-1} cm^{-1} for AqpZ. The mixed protein–vesicles solution was dialyzed for 24 h in a dynamic microdialyzer dialysis device (Spectrum Laboratories Europe, Breda, Netherlands) using a MWCO of 10,000 Daltons and a dialysate flow of 3 ml/min. Control vesicles were made in the same manner without protein. The resulting large protein vesicles (or vesicles alone) were stored at 4°C until use.

Solvent formation of giant protein vesicles and giant lipid vesicles

Giant protein vesicles or giant lipid vesicles were formed by mixing large lipid vesicles or large protein vesicles with a lipid containing oil solution consisting of either decane or squalene containing lipids matching that of the vesicles or protein vesicles used (10 mg/ml), except stated otherwise.

To form giant protein vesicles or giant vesicles, the lipid containing solvent solutions was gently added to large protein vesicles or lipid vesicles to a ratio of 1:3 vol/vol, and the oil/lipid/vesicles mixtures were emulsified with end–over–end rotation at 4 °C over night, resulting in the formation of giant protein vesicles or giant vesicles.

Generalized polarization measurements of Badan labeled aquaporins in giant protein vesicles

The fluorescence emission properties of Badan labeled aquaporin SoPIP2;1 and AqpZ are sensitive to the polarity of the local environment of the fluorescent probe Badan. The fluorescence maximum emission yield of Badan is blue shifted or red shifted if the local environment around the probe becomes more hydrophobic or hydrophilic, respectively. Saturating amounts of sodium dodecyl sulfate causes a red shift in the maximum emission yield. Emission spectral changes can be quantified comparing the generalized polarization (GP) values for shifted and unshifted fluorescence intensity peaks of Badan–labeled aquaporins. GP values were calculated by: $GP = I_b - I_g / I_b + I_g$, where I_b and I_g correspond to the intensities at the blue and green edges of the emission spectrum respectively.

Fluorescence spectroscopy was performed using a Varian Cary Eclipse fluorescence spectrometer (Varian Inc., Palo Alto, CA, USA) with a λ_{ex} (excitation wavelength) of 400 nm and emission recorded at 425 to 700 nm. I_b and I_g were calculated from the emission spectra corresponding to the band pass filter range applied for fluorescence confocal microscopy imaging.

GP images covering 420–480 and 505–550 nm fluorescence emission range, respectively, were obtained simultaneously in dual–channel setup on a confocal microscope (model LSM 510 META; Carl Zeiss MicroImaging).

The fluorescence data were analyzed using the Globals software package developed at the Laboratory for Fluorescence Dynamics at the University of Illinois at Urbana–Champaign to obtain the GP image and the associated GP histogram (distribution of the GP values per pixel).[2]

Bacteriorhodopsin photo induced pH-response assay

Bacteriorhodopsin (BR) has a light–driven proton–pump activity, which was utilized to create a functional protein reconstitution assay for giant protein vesicles. To reconstitute BR, lyophilized BR purple membranes were solubilized in a saline solution consisting of 0.15 M KCl with 1.3% OG. Large vesicles were created by dissolving soybean asolectin in 0.15 M KCl with 1.3% OG (6 mg/ml). The lipid solution was subsequently extruded 21× through a 100 nm polycarbonate filter. Lipid and protein was mixed in a LPR of 1000. The mixed protein–vesicles solution was dialyzed for 24 h in a dynamic microdialyzer dialysis device (Spectrum Laboratories Europe, Breda, The Netherlands) using a MWCO of 10,000 Daltons and a dialysate flow of 3 ml/min.

To assess the proton–pumping activity of the BR large protein vesicles, 2.5 ml of the large vesicles solution were transferred to a 3 ml UV–cuvette with magnetic stirring and placed in a dark cabinet. A glass micro pH electrode (Microelectrodes Inc., Bedford USA) was placed into the vesicle suspension. The glass micro electrode was connected with an ORION 3 STAR pH-meter (Fisher Scientific) operated through Star Plus navigator software (Fisher Scientific), which enabled automated sampling of pH measurements. Illumination was provided with a cold–light generator equipped with an incandescent halogen lamp of 200W with a light–guide (SCHOTT: model KL1500 LCD). The light produced was focused on the cuvette by means of a fiber optic cable. The resulting light intensity on the sample was about 80×10^3 Lux. Before illuminating the sample was equilibrated in the dark for 30 min to permit pH stabilization, and the pH baseline was subsequently recorded for 3 min. Illumination was carried out for 3 min followed by 7 min darkness, while the pH was continuously sampled throughout the experiment (3 sec recording intervals).

Upon illumination, the BR vesicle suspension produced an alkalinization (pH increase) of the external bulk medium. This indicated a preferred (but not necessarily a unique) protein orientation in the bilayers, causing a net proton translocation to the interior of the liposome. After the increase in pH during illumination, pH decay (an increase in proton concentration) was observed in all cases, being caused by passive proton diffusion from the internal aqueous space of the vesicles to the external bulk medium.

To produce BR giant protein vesicles, the BR large protein vesicles were mixed with 6 mg/ml asolectin in squalene or *n*–decane (1:3 oil phase: vesicles ratio) using end–over–end rotation, 4 °C, over night. The resulting BR giant protein vesicles were transferred to a UV–cuvette and the BR light–induced proton activity assay repeated a described for the BR large protein vesicles. The BR activity of the BR large protein vesicles and the BR giant protein vesicles were subsequently compared.

7

Supplemental results

Supplemental figure legends

Supplemental Figure S1   GP histograms of Badan SoPIP2;1 or AqpZ in different lipid compositions. Confocal laser scanning microscopy images were acquired of large protein vesicles in solution and of the vesicles solutions added 100 mM SDS to membrane solubilize the protein. Large protein vesicles were produced with the following lipid compositions (in mol%): pure 1,2-dioleoyl-*sn*-glycero-3-phosphocholine (DOPC), pure 1,2-dioleoyl-*sn*-glycero-3-phospho-L-serine (DOPS), pure 1,2-diphytanoyl-*sn*-glycero-3-phosphocholine (DPhPC), DOPC containing squalene mixture of 30% cholesterol (chol) with 70% DOPC (30%Chol/DOPC), asolectin from soybean, *E coli* total lipid extract and mixture of 50% 1,2-dioleoyl-*sn*-glycero-3-phosphoethanolamine (DOPE) with 50% DOPC (DOPE/DOPC 1:1). GP histograms were calculated by: $GP = I_b - I_g / I_b + I_g$, where I_b and I_g correspond to the intensities at the blue (band pass filter 420–480 nm) and green (band pass filter 505–550 nm) edges of the emission spectrum respectively.

Supplemental Figure S2   GP ratio images and corresponding GP histograms of Badan labeled SoPIP2;1 reconstituted into giant protein vesicles formed by squalene. DPhPC/DOPC-sq refers to DPhPC giant vesicles formed with DOPC containing squalene.

Supplemental Figure S3   GP ratio images and corresponding GP histograms of Badan labeled SoPIP2;1 reconstituted into giant protein vesicles formed by *n*–decane. DPhPC/DOPC-dec refers to DPhPC giant vesicles formed with DOPC containing *n*–decane.

Supplemental Figure S4   GP ratio images and corresponding GP histograms of Badan labeled AqpZ reconstituted into giant protein vesicles formed by squalene.

8

Supplemental Figure S5   GP ratio images and corresponding GP histograms of Badan labeled AqpZ

reconstituted into giant protein vesicles formed by *n*–decane.

Supplemental Figures

Supplementary Figure S1

SoPIP2;1   AqpZ

0 mM SDS   100 mM SDS   0 mM SDS   100 mM SDS

DOPC
av= 0.412 std= 0.069 n=65418 | av= -0.469 std= 0.062 n=65511 | av= -0.030 std= 0.080 n=65534 | av= -0.240 std= 0.078 n=65534

DOPS
av= 0.486 std= 0.050 n=65512 | av= -0.449 std= 0.057 n=65496 | av= -0.143 std= 0.050 n=65534 | av= -0.374 std= 0.047 n=65534

DPhPC
av= 0.429 std= 0.052 n=65524 | av= -0.396 std= 0.059 n=65516 | av= -0.079 std= 0.078 n=65534 | av= -0.357 std= 0.062 n=65528

30%Chol/DOPC
av= 0.459 std= 0.075 n=65405 | av= -0.488 std= 0.053 n=65525 | av= -0.064 std= 0.078 n=65534 | av= -0.390 std= 0.069 n=65475

Asolectin
av= 0.487 std= 0.049 n=65525 | av= -0.419 std= 0.059 n=65525 | av= -0.007 std= 0.082 n=65519 | av= -0.230 std= 0.079 n=65506

E coli lipid
av= 0.517 std= 0.060 n=65453 | av= -0.378 std= 0.060 n=65531 | av= -0.085 std= 0.079 n=65506 | av= -0.295 std= 0.091 n=65373

DOPE/DOPC (1:1)
av= 0.355 std= 0.057 n=65528 | av= -0.387 std= 0.060 n=65521 | av= -0.224 std= 0.094 n=65182 | av= -0.352 std= 0.058 n=65533

DOPC

A. av= 0.219 std= 0.123 n=20886
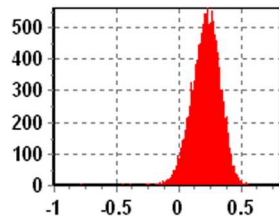
DOPS
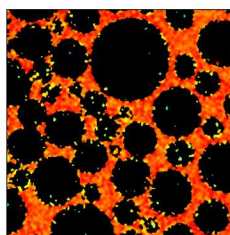
B. av= 0.442 std= 0.121 n=22519
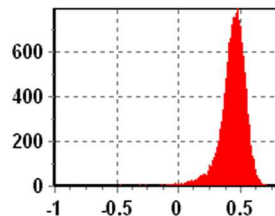
DPhPC
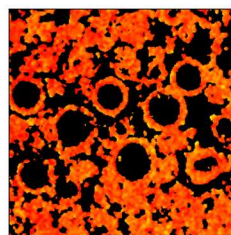
C. av= 0.444 std= 0.065 n=36822
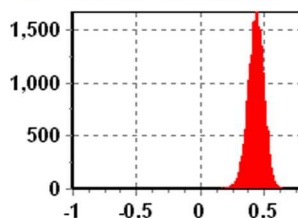
DPhPC / DOPC-sq
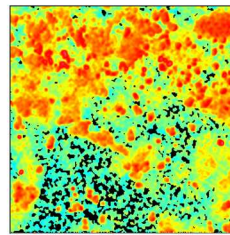
D. av= 0.027 std= 0.209 n=59425
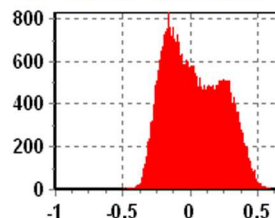
30%Chol/DOPC
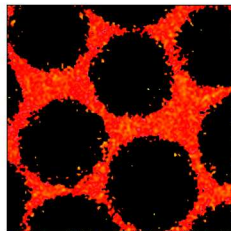
E. av= 0.493 std= 0.084 n=19997
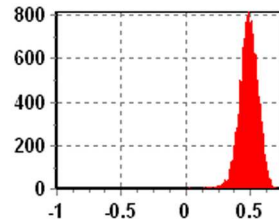
Asolectin
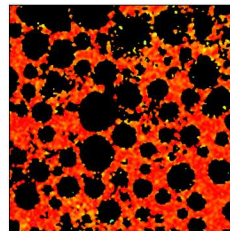
F. av= 0.481 std= 0.095 n=29761
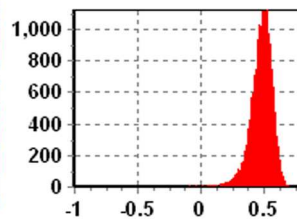
DOPE/DOPC (1:1)
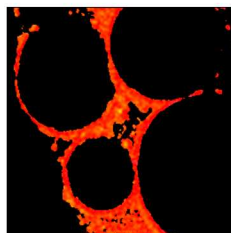
G. av= 0.322 std= 0.056 n=9567
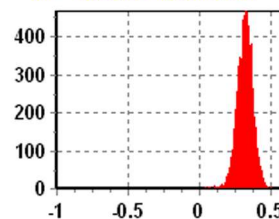
E. coli lipid extract
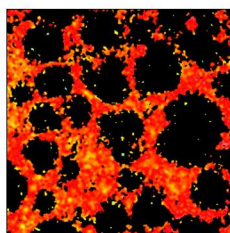
H. av= 0.511 std= 0.121 n=26912
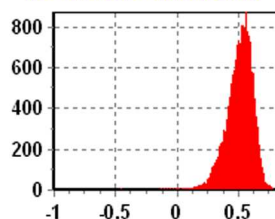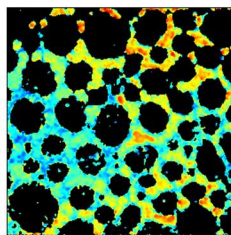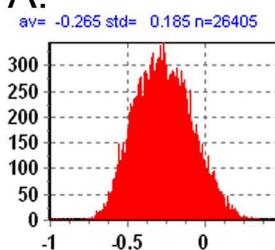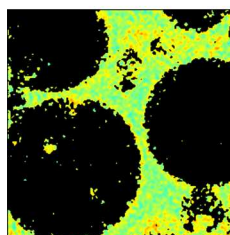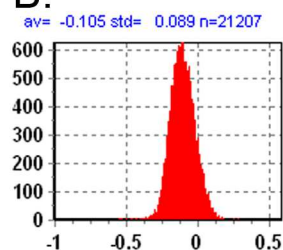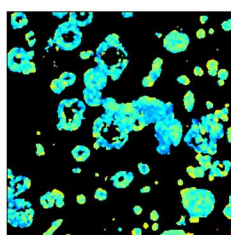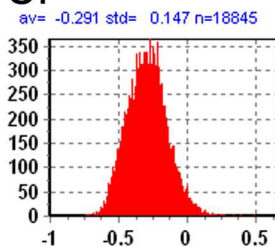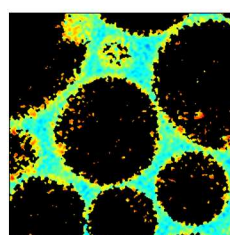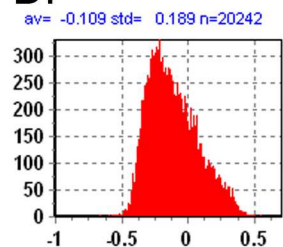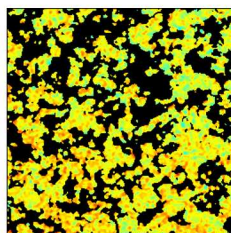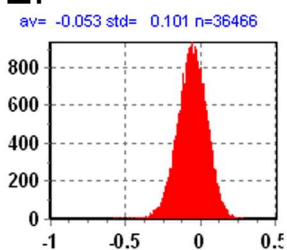
DOPC

A. av= 0.464 std= 0.096 n=26099

DOPS

B. av= 0.593 std= 0.080 n=51174

DPhPC

C. av= 0.586 std= 0.148 n=18281

DPhPC / DOPC-Dec

D. av= 0.501 std= 0.128 n=19479

30%Chol/DOPC

E. av= 0.494 std= 0.062 n=24703

Asolectin

F. av= 0.432 std= 0.106 n=38317

DOPE/DOPC (1:1)

G. av= 0.507 std= 0.083 n=28432

E. coli lipid extract

H. av= 0.592 std= 0.050 n=50347
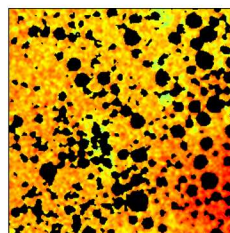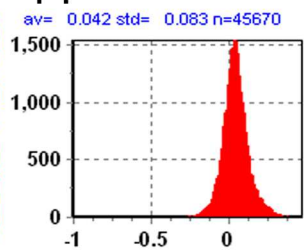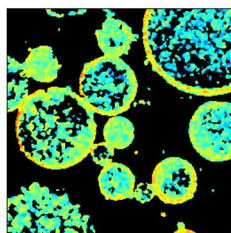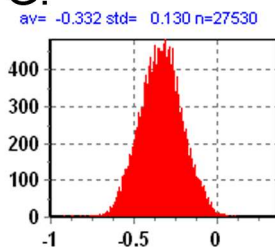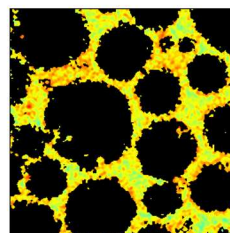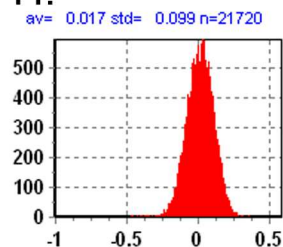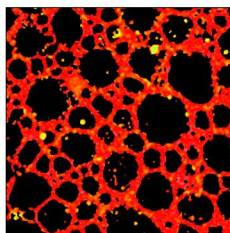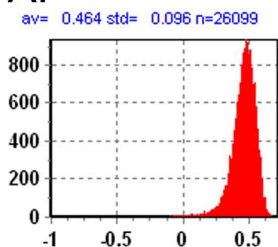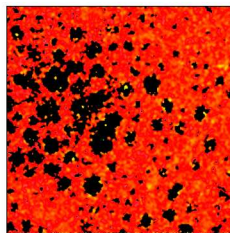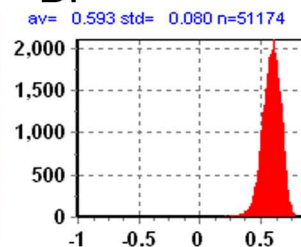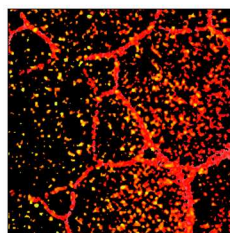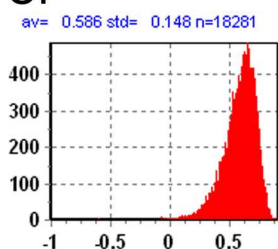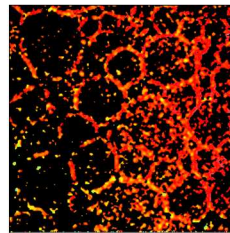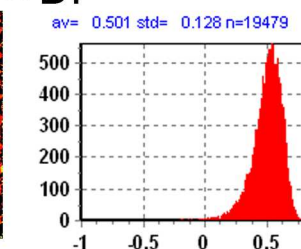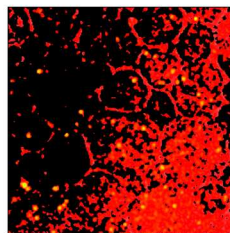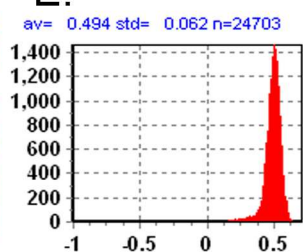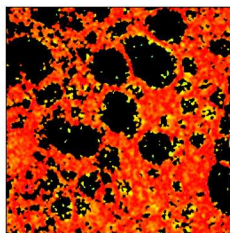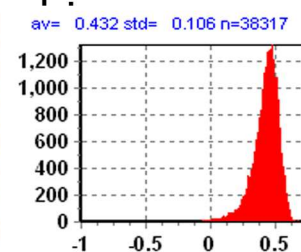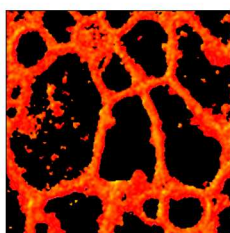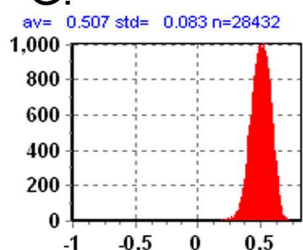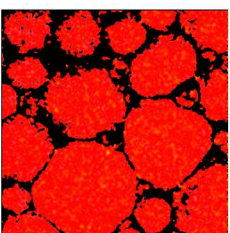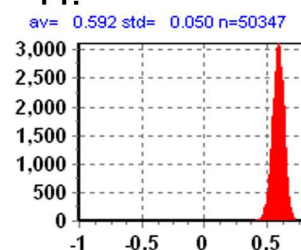
Supplemental Figure 5
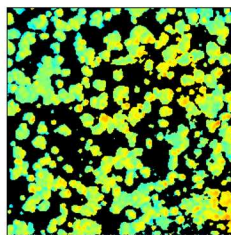
DOPC

A.
av= -0.295 std= 0.088 n=33826
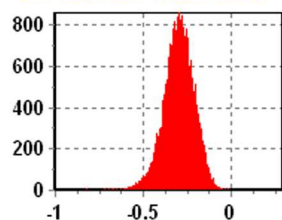
DOPS
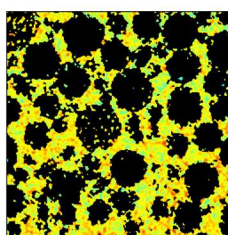
B.
av= -0.113 std= 0.094 n=27294
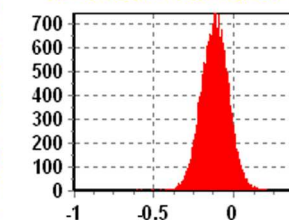
DPhPC
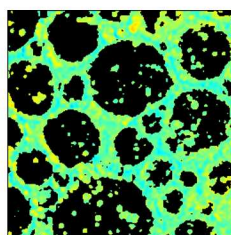
C.
av= -0.257 std= 0.077 n=30604
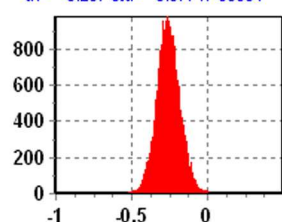
DPhPC / DOPC-Dec
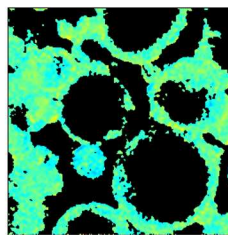
D.
av= -0.201 std= 0.080 n=29417
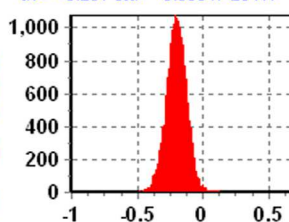
30%Chol/DOPC
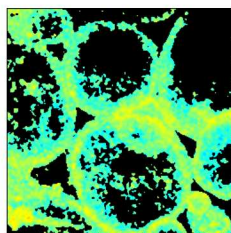
E.
av= -0.234 std= 0.090 n=35544
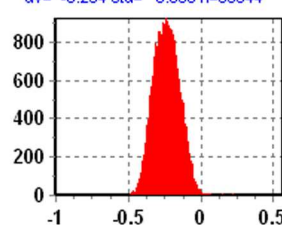
Asolectin
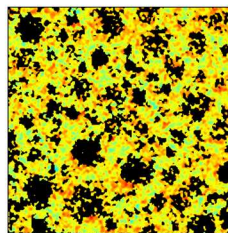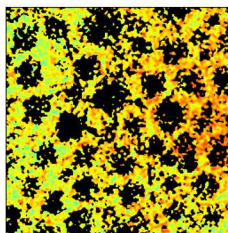
F.
av= 0.027 std= 0.110 n=44621
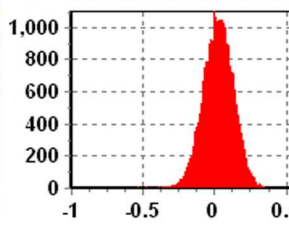
DOPE/DOPC (1:1)
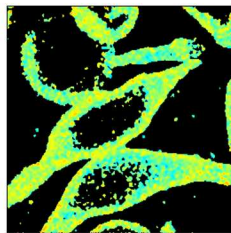
G.
av= -0,200 std= 0,097 n=23820
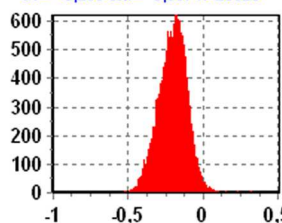
E. coli lipid extract

H.
av= 0.042 std= 0.111 n=38908

14
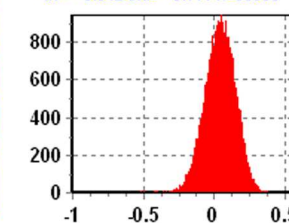
References

1.   Karlsson, M.; Fotiadis, D.; Sjovall, S.; Johansson, I.; Hedfalk, K.; Engel, A.; Kjellbom, P., Reconstitution of water channel function of an aquaporin overexpressed and purified from Pichia pastoris. *FEBS Lett* **2003,** 537, (1-3), 68-72.
2.   Beechem, J. M.; Gratton, E. In *Fluorescence Spectroscopy Data Analysis Environment A Second Generation Global Analysis Program*, Time-Resolved Laser Spectroscopy in Biochemistry, Proc. of SPIE, 1988; Lakowicz, J., Ed. 1988; pp 70-81

15

Chapter 5

Conclusion

This thesis has addressed novel ways of creating reproducible and scalable biomimetic membrane arrays and new strategies for incorporating correctly folded and fully functional membrane proteins into model membranes.

A prerequisite for implementing membrane proteins into a biomimetic membrane-based biotechnology is to construct an efficient platform to handle biomimetic membranes. In this study we developed a vertical automation technique for establishment of biomimetic membrane arrays and developed a complementary horizontal biomimetic chamber design that supported simultaneous optical-electrical measurements of established membranes. The developed automation technique for establishing artificially made membranes in arrays represent a new way of establishing biomimetic membranes. With the automation technique for establishment of biomimetic membranes reproducible bilayer experiments could be achieved by controlled deposition of precoating solution to the membrane aperture scaffold. This showed that sufficient interaction with the hydrophobic surface of the partition and the bilayer forming solution is a necessity in order to reproducibly establish biomimetic membranes.

Membrane area scalability was addressed in the horizontal chamber design, and we demonstrated that the effective membrane area could be scaled up from 64 membranes to comprise 576 membranes positioned in a rectangular aperture pattern and 648 membranes in a hexagonal aperture pattern. There is in principle no hindrance in further up scaling of the membrane area.

Fluorescently labelling of aquaporins SoPIP2;1 and AqpZ with the polarity sensitive fluorophore Badan was developed to allow visual inspection of aquaporin reconstituted into model membranes. The polarity sensitivity of the Badan probe was also used to address the effects of SDS acting on aquaporins reconstituted into large vesicles. CD spectroscopy combined with fluorescence

spectroscopy of Badan labelled aquaporins showed that SDS does not unfold SoPIP2;1 and AqpZ aquaporins.

Exploring strategies for controllable and reliable reconstitution of membrane proteins into artificially made membranes resulted in the development of a method to create giant protein vesicles (GPV). A unique feature of the GPV formation methodology is that it allows controllable amount of proteins to be reconstituted into GPV. The method of GPV formation was combined with fluorescence microscopy of Badan labelled aquaporin SoPIP2;1 and AqpZ. This led to the establishment of a visual assay to address reconstitution of aquaporins into artificially made model membranes. To demonstrate reconstitution of functionally active membrane proteins we established a functionality assay based on the light-driven proton-pump Bacteriorhodopsin.

The data presented in this thesis showing that membrane proteins can be correctly folded and functionally inserted in a controlled fashion into biomimetic membranes may open up for the possibility of a more general use of membrane proteins in biotechnological applications including novel aquaporin-based water filtration applications.

Chapter 6

Future perspectives

High-throughput screening (HTS) systems using biomimetic membrane protein arrays have a large potential as an alternative to cell-based screening of potential drug candidates acting on membrane proteins (e.g. receptors and ion channels). An advantage is that a lot of information can be achieved with low sample volumes, for example by designing biomimetic membrane platforms that support multiple read-outs (e.g. electrophysiological measurements combined with fluorescence assays). Although, recent advances in biomimetic membranes have led to biomimetic membrane arrays with increased stability in terms of lifetime, further developments are required to create a commercially available membrane protein-based HTS system. Challenges are among others to increase transportation robustness, develop general methods for reconstituting different types of membrane proteins into individual membranes of a membrane array and designing sensitive drug-protein interaction assays.

A strategy to establish sensitive drug-protein interaction assays could be to design membrane proteins conjugated with polarity sensitive fluorescent probes (e.g. Badan), where the fluorophore is, as an example, positioned close to the active site of the protein. Binding of a ligand/drug to the protein active site would preferably change the polarity around the probe, resulting in fluorescence emission changes that can be quantified. While designing fluorescent biosensors based on soluble proteins is a relatively well-established technique, the designing of membrane protein biosensors has so far been limited.

In this PhD project fluorescently labelled aquaporins were developed. Further developments of the Badan fluorescently labelled aquaporins could be to establish and validate a fluorescent assay to address how a potential drug candidate affects membrane barrier properties. Membrane polarity changes imposed by the presence of a pharmaceutical would result in a fluorescence emission response of Badan-Aquaporin (e.g. Badan-SoPIP2;1) due the positioning of the Badan fluorophore

in the protein TM region. A prerequisite for using Badan labelled aquaporins as reporter of membrane barrier properties in the presence of pharmaceuticals is that a potential drug candidate does not interact with the protein itself. A way to address this could be by combining electrophysiological measurements with fluorescence imaging (e.g. Badan generalized polarization imaging). Besides potential commercial interest in fluorescently labelled membrane proteins, fluorescence polarity sensitive probes conjugated to membrane proteins at strategic positions such as the TM region or active site may be used in biophysical studies to increase our understanding of the folding and function of membrane proteins.

The GPV formation methodology presented in this thesis offer a unique potential as a genuine cell-mimetic model membrane system, where controlled amounts of membrane proteins can be incorporated. We envisage that the GPV system may be used as a general model system to characterize membrane proteins. In this relation the generalized polarization imaging methodology developed in this PhD project may add a new dimension to the way of biophysically studying membrane proteins since, as demonstrated in this thesis, it is possible to visually address protein reconstitution, spatial distribution as well as protein-lipid interactions.

Besides the broad potential of GPV for studying membrane proteins, we envisage that implementation of aquaporin GPV into bulk liquid membrane systems may lead to a commercially available aquaporin-based water purification technology.

Appendix

Contents

A1: Patents and co-authored publications

Patents

(WO/2009/074155) SCAFFOLD FOR COMPOSITE BIOMIMETIC MEMBRANE. J. Vögel, M. Perry, C. Hélix-Nielsen, **J. S. Hansen**, P. H. Jensen, O. Geschke, P-Y. Bollinger. International filling date: 11.12.2008. Publication date: 18.06.2009.

Two additional patent applications have been filed, but still not published, with J.S. Hansen as inventor.

Co-authored publications

M. Perry, T. Vissing, T. P. Boesen, **J. S. Hansen**, J. Emnéus and C. H. Nielsen (2009). Automated sampling and data processing derived from biomimetic membranes. Bioinsp. Biomim. 4 044001 (6pp).

J. Vogel M. Perry, **J. S. Hansen**, P-Y. Bolinger, C. H. Nielsen and O. Geschke (2009). A support structure for biomimetic applications. J. Micromech. Microeng. 19 025026 (6pp).

I. Plasencia, S. Survery, S. Ibragimova, **J. S. Hansen**, C. Hélix-Nielsen, P. Kjellbom, U. Johanson, O.G. Mouritsen. Structure and Stability of the Spinach Aquaporin SoPIP2;1 in Detergent Micelles and Lipid Membranes. Submitted (2010) to PLosOne.

M. Perry, **J. S. Hansen**, K. Stibius, T. Vissing, K. Pszon-Bartosz, C. Rein, B. Eshtehardi, M. Benter and C. Hélix-Nielsen. Surface modifications of support partitions for stabilizing biomimetic membrane arrays. Submitted (2010) to BBA Biomembranes.

A2: Design protection (microscope accessories)

Alicante, 20/01/2009

INTERNATIONALT PATENT-BUREAU
A/S
Rigensgade 11
DK-1316 Copenhagen K
DINAMARCA

Certificate of Registration[1]

Registration No.:	**001059406**
Your reference:	406930
Applicant:	Aquaporin A/S
	Diplomvej 377
	DK-2800 Kgs. Lyngby
	DINAMARCA

Please find enclosed the certificate of registration for Community Design no. 001059406-0001 which was published in the Community Designs Bulletin no. 2009/011 on 20/01/2009 (see OHIM's website: http://oami.europa.eu).

This certificate contains information from the Community Designs Register at the date of entry into the Register (see code 15 on the certificate). If you have filed a request for modification of data on or after that date, no new certificate will be issued. You will be notified separately of the change after which an extract from our database may be requested to reflect the administrative status of the design.

For an explanation of the codes on the certificate please see consult the Vademecum on OHIM's website: http://oami.europa.eu/pdf/design/vademecum-rcd-en.pdf.

If you do not agree with the content of this certificate please do not send back the original. You should instead send the Office a letter indicating your objections, which will be dealt with separately.

Catherine DOBSON

---

[1] in accordance with Article 17(1) of Commission Regulation (EC) No 2245/02 of 21 October 2002 implementing Council Regulation (EC) No 6/02 on the Community design (http://oami.europa.eu)

Registrerede / Registered 19/12/2008

No 001059406-0001
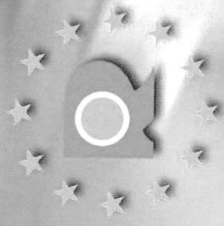
KHIM – KONTORET FOR
HARMONISERING I DET INDRE MARKED
VAREMÆRKER OG DESIGN

REGISTRERINGSBEVIS

Dette Registreringsbevis udstedes for det registrerede
EF-design, der er nærmere beskrevet nedenfor. De
tilsvarende indførelser er blevet Registreret i
EF-designregisteret.

OHIM – OFFICE FOR HARMONIZATION
IN THE INTERNAL MARKET
TRADE MARKS AND DESIGNS

CERTIFICATE OF REGISTRATION

This Certificate of Registration is hereby issued for the
Registered Community Design identified below. The
corresponding entries have been recorded in the
Register of Community Designs.
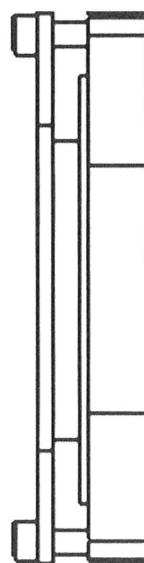
President / The President

Wubbo de Boer

21   001059406-0001
25   DA - EN
22   19/12/2008
15   19/12/2008
45   20/01/2009
11   001059406-0001
72   Jesper Søndergaard Hansen
73   Aquaporin A/S
      Diplomvej 377
      DK-2800 Kgs. Lyngby
      DINAMARCA
74   INTERNATIONALT PATENT-BUREAU A/S
      Rigensgade 11
      DK-1316 Copenhagen K
      DINAMARCA
51   16 - 06
54   BG - Микроскопи (Аксесоари за -)

      ES - Microscopios (Accesorios para -)

      CS - Mikroskopy (Příslušenství k -)

      DA - Mikroskoper (Tilbehør til -)

      DE - Mikroskope (Zubehöre für -)

      ET - Mikroskoobid (Lisaseadmed -)

      EL - Μικροσκόπια (Εξαρτήματα για -)

      EN - Microscopes (Accessories for -)

      FR - Microscopes (Accessoires pour -)

      IT - Microscopi (Accessori per -)

      LV - Mikroskopi (Piederumi -)

      LT - Mikroskopai (Priedai -)

      HU - Mikroszkópok (Kellékek -)

      MT - Mikroskopji (Aċċessorji għal -)

      NL - Microscopen (Accessoires voor -)

      PL - Mikroskopy (Akcesoria dla -)

      PT - Microscópios (Acessórios para -)

      RO - Microscoape (Accesorii pentru -)

      SK - Mikroskopy (Príslušenstvo k -)

      SL - Mikroskopi (Dodatna oprema za -)

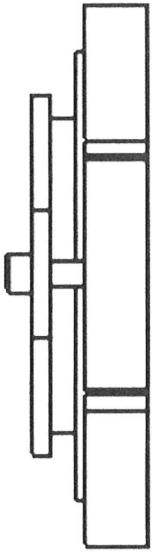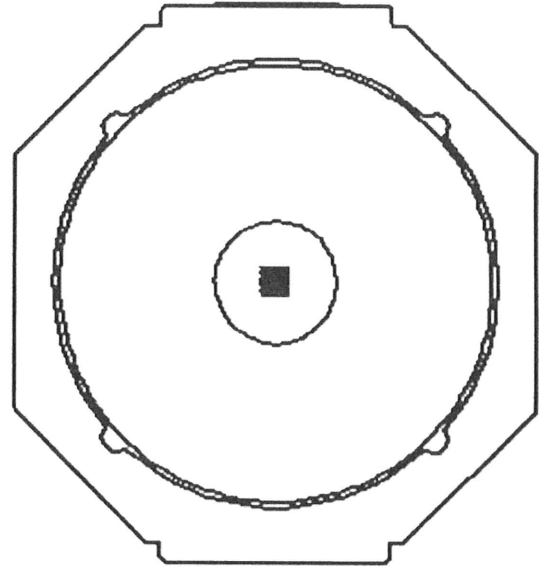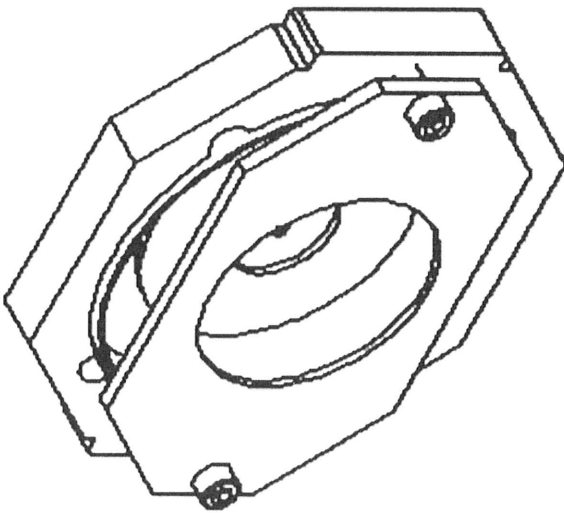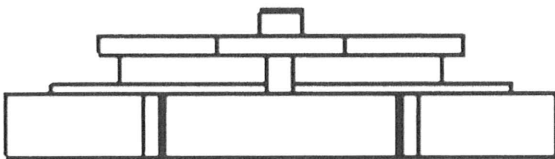   FI - Mikroskoopit (Tarvikkeet -)

      SV - Mikroskop (Tillbehör till -)

55
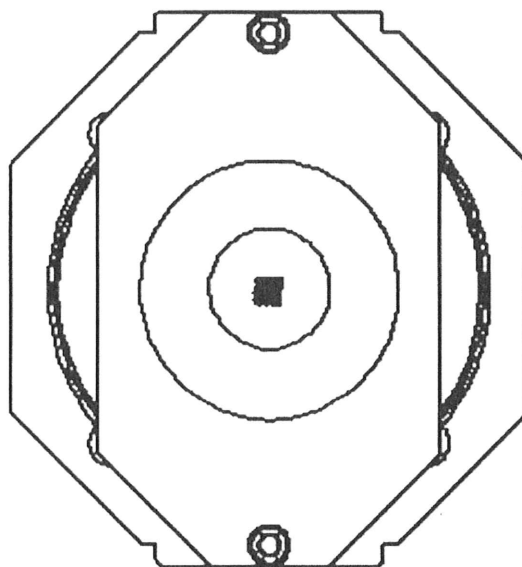
0001.1
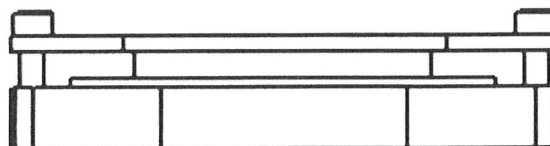
0001.2

0001.3

0001.4

0001.7

0001.5

0001.6